



UCGE Reports

Number 20307

Department of Geomatics Engineering

**Approaches for the Combined Tracking of GPS L1/L5
Signals**

(URL: <http://www.geomatics.ucalgary.ca/graduatetheses>)

by

Dina Reda Salem

April 2010



UNIVERSITY OF CALGARY

Approaches for the Combined Tracking of GPS L1/L5 Signals

by

Dina Reda Salem

A THESIS

SUBMITTED TO THE FACULTY OF GRADUATE STUDIES
IN PARTIAL FULFILMENT OF THE REQUIREMENTS FOR THE
DEGREE OF DOCTOR OF PHILOSOPHY

DEPARTMENT OF GEOMATICS ENGINEERING

CALGARY, ALBERTA

APRIL, 2010

© DINA REDA SALEM 2010

Abstract

The ever-increasing demand on GPS to enhance its performance is the main motivation behind this research. The modernization steps of GPS include the addition of new signals (L2C and L5 to the existing conventional L1 signal. Being transmitted from the same satellite through the same environment, the errors between these signals are correlated. Hence, an increase in tracking performance can be achieved by combining two or more of these signals.

The thesis proposes two approaches to combine the L1 and L5 signals in order to benefit from both signals' properties. The first approach is through aiding one signal with the tracking information of the other. The L5 signal was chosen to provide the aiding information to the L1 signal. The second approach is a novel method to combine both the L1 and L5 signals in a single Kalman filter based tracking module to estimate the tracking errors.

A detailed performance analysis of the two approaches is presented in scenarios suffering urban canyon multipath and a typical vehicle motion model. The aided L1 phase tracking loop outperforms the separate tracking loop both theoretically and experimentally. On the other hand, the combined Kalman filter shows an approximately 30% improvement in both the root mean square and standard deviations of the estimated carrier phase errors of the two signals over the separate Kalman filter.

Moreover, the thesis presents a methodology to compare different tracking approaches. Several methods are widely used for tracking the GPS signals, varying from the traditional code and phase tracking loops to the Kalman filter tracking loops. However,

few attempts have been made to compare the tracking capability of these two types. The thesis is focusing on comparing the standard phase tracking loop with the Kalman filter tracking loop. A method is shown for experimentally calculating the equivalent bandwidth of the Kalman filter and using it to evaluate the performance of the equivalent standard tracking loop. The Kalman filter shows an improvement over the standard PLL tracking loops in two main aspects: the transient response of the tracking loop and the adaptation to different signal dynamics.

Acknowledgements

It is a pleasure to thank those who made this thesis possible. First, I owe my deepest gratitude to prof. Gérard Lachapelle for his guidance, professional supervision and encouragement. He gave me the opportunity to pursue my PhD degree at our first meeting in Egypt in 2006. He believed in my capabilities, and provided me with all the support and flexibility which enabled me to finish my doctorate even with the birth of my child during my studies.

A hearty thanks to my co-supervisor Dr. Cillian O'Driscoll for his continuous support, proposed ideas, valuable discussions and constructive suggestions. His co-operation, positive attitude and understanding really deserve an everlasting appreciation. I could not wish for a better or friendlier supervisor.

I am thankful to my colleagues in the PLAN group for providing a comfortable and co-operative working environment. Their precious suggestions and discussions on my work are appreciated.

I would also like to acknowledge the financial support of General Motors of Canada, the Natural Science and Engineering Research Council of Canada, Alberta Advanced Education and Technology and the Western Economic Diversification Canada.

My mother, father and Amr, thanks for your support and unconditional love. Even though we are thousand of miles away, you were always there whenever I needed you. You can take all the credit for much of what I have achieved and what I will achieve in the future.

This thesis would have never been possible without my loving husband Ahmed. You were always around at times I thought that it is impossible to continue, you helped me to keep things in perspective. My son Tarek, I owe you lots and lots of fun hours. I couldn't imagine doing my PhD without you; you really gave me the reason to continue. Words would never say how grateful I am to both of you.

Dedication

“Say: Are those equal, those who know and those who do not know?”

Quran 39:9

To

My Loving Parents, My Dear Brother,

My Loving Husband, and My Son

“To all of you, I shall be forever indebted”

Table of Contents

Approval Page.....	ii
Abstract.....	iii
Acknowledgements.....	v
Dedication.....	vii
Table of Contents.....	viii
List of Tables.....	xii
List of Figures and Illustrations.....	xiii
List of Symbols.....	xix
List of Abbreviations.....	xxiv
CHAPTER ONE: INTRODUCTION.....	1
1.1 Background.....	2
1.2 GNSS Modernization.....	4
1.3 Limitations of Previous Work.....	6
1.4 Objectives.....	8
1.5 Contributions.....	9
1.6 Thesis Outline.....	11
CHAPTER TWO: GNSS SIGNALS AND TRACKING LOOPS.....	15
2.1 GPS Modernization.....	15
2.2 Signal Structures.....	17
2.2.1 GPS L1 C/A Code Signal Structure.....	17
2.2.2 GPS L5 Signal Structure.....	20
2.2.3 L1 and L5 Signals Differences.....	24
2.3 Standard Tracking Loops.....	25
2.3.1 L1 Signal Tracking.....	28
2.3.2 L5 Signal Tracking.....	29
2.3.2.1 L5 data and pilot combination.....	31
2.3.3 Carrier Tracking Loops.....	32
2.3.3.1 Frequency Tracking.....	33
2.3.3.2 Phase tracking.....	33
2.3.4 Code Tracking Loops.....	33
2.3.5 Standard Tracking Loops Parameters.....	34
2.3.5.1 Predetection integration time.....	34
2.3.5.2 Loop discriminators.....	34
2.3.5.3 Loop filter.....	35
2.3.5.4 Limitation on BT product.....	36
2.4 Kalman Filter Tracking.....	36
2.5 Tracking Performance Evaluation.....	38
2.5.1 Phase Lock Indicator.....	39
2.5.2 Frequency Lock Detector.....	39
2.6 Tracking Errors.....	40
2.7 Summary.....	41
CHAPTER THREE: SIMULATION TOOLS AND SOFTWARE RECEIVER.....	43

3.1 GPS Simulation Setup	43
3.2 Hardware Stage.....	44
3.2.1 Spirent GSS7700 Simulator	44
3.2.2 National Instrument Front-end	45
3.3 Software Stage.....	47
3.3.1 L1 and L5 Acquisition.....	49
3.3.2 L1 and L5 Bit Synchronization	51
3.3.3 L1 and L5 Tracking.....	53
3.4 GPS Errors Simulation.....	54
3.4.1 Propagation Errors.....	55
3.4.1.1 Ionospheric delay.....	56
3.4.1.2 Tropospheric delay	58
3.4.2 Receiver-based Errors	59
3.4.2.1 Oscillator stability.....	59
3.4.2.2 Multipath and shadowing.....	63
3.4.2.3 Signal power degradation	68
3.5 User Motion Simulation.....	68
3.6 Summary.....	69

CHAPTER FOUR: COMBINATION APPROACHES FOR TRACKING L1/L5

SIGNALS.....	71
4.1 Standard Tracking Loops.....	71
4.1.1 Separate Standard Tracking Loops.....	71
4.1.1.1 Loop parameters	72
4.1.2 Phase Tracking Loop Errors.....	75
4.1.2.1 Thermal noise	76
4.1.2.2 Vibration-induced oscillator phase noise.....	77
4.1.2.3 Allan deviation oscillator phase noise	77
4.1.2.4 Dynamic stress error	79
4.1.3 L1-Aided Tracking Loops	79
4.1.3.1 Comparison of L1 and L5 tracking errors	80
4.1.3.2 L1-aided carrier phase tracking loop	81
4.1.3.3 L1-aided code tracking loop	83
4.1.3.4 Loop parameters	84
4.2 Kalman Filter Tracking Loops.....	84
4.2.1 General Kalman Filter Structure	85
4.2.1.1 Dynamic model.....	85
4.2.1.2 Measurement model.....	85
4.2.1.3 Discretization	87
4.2.1.4 Linearization	87
4.2.2 Separate Kalman Filter.....	89
4.2.2.1 Dynamic model.....	90
4.2.2.2 Measurement model.....	92
4.2.3 Combined Kalman Filter	94
4.2.3.1 Dynamic model.....	95
4.2.3.2 Measurement model.....	98
4.2.4 Measurement Covariance R	99

4.2.5 Process Noise Q.....	100
4.3 Summary.....	102
CHAPTER FIVE: PERFORMANCE EVALUATION OF THE PROPOSED COMBINATION APPROACHES	103
5.1 Standard Tracking Loops.....	103
5.1.1 Aided Phase Tracking loop Errors	103
5.1.2 Theoretical Evaluation.....	108
5.1.3 Experimental Evaluation	111
5.1.3.1 Urban canyon multipath.....	112
5.1.3.2 Motion.....	117
5.2 Kalman Filter Tracking.....	121
5.2.1 Comparison with Separate Kalman Filter Tracking Loops	122
5.2.1.1 Urban canyon multipath.....	122
5.2.1.2 Motion.....	132
5.3 Standard Tracking Loops versus Kalman Filter Tracking Loop	140
5.3.1 Equivalent Bandwidth Calculation: Illustration using a Strong Signal.....	143
5.3.1.1 Separate EKF versus Separate Tracking Loops.....	143
5.3.1.2 Combined EKF versus Aided Tracking Loops.....	147
5.3.2 Equivalent Bandwidth Calculation Steps	149
5.3.3 Motion	150
5.3.3.1 Separate EKF versus Separate Tracking Loops.....	151
5.3.3.2 Combined EKF versus Aided Tracking Loops.....	153
5.3.4 Sensitivity Analysis.....	156
5.4 Summary.....	161
CHAPTER SIX: CONCLUSIONS AND RECOMMENDATIONS	163
6.1 Conclusions.....	163
6.1.1 Aiding Using Standard Tracking Loops.....	163
6.1.2 Combination Using Kalman-Filter Tracking.....	164
6.1.3 Combination of L1 Data, L5 Data and L5 Pilot Channels	165
6.1.4 Developing a Methodology to Compare the Standard PLL and Kalman Filter Based Tracking Loops.....	166
6.2 Recommendations for Future Work	166
REFERENCES	169
APPENDIX A: DSICRETE COVARIANCE MATRIX.....	175
A.1. Separate Kalman Filter Tracking Q Matrix	175
A.2. Combined Kalman Filter Tracking Q Matrix	176
APPENDIX B: INITIAL COMPARISON BETWEEN COMBINED KALMAN FILTER AND SEPARATE STANDARD TRACKING LOOPS.....	177
B.1. Sensitivity.....	178
B.2. Simulation Results	179
APPENDIX C: SVN 49	185

C.1. L5 Demonstration Payload on SVN 49.....185
 C.1.1. Problems186
 C.1.2. Causes and Solutions186
C.2. SVN 49 Real Data Example.....187

List of Tables

Table 2-1 L5 Improvements versus L1 Deficiencies	26
Table 3-1 Software initialization steps	48
Table 3-2 OCXO models	61
Table 4-1: Separate standard tracking loop parameters	74
Table 4-2: Aided tracking loop parameters	84
Table 4-3: Iterated EKF model	86
Table 4-4: Separate Kalman filter parameters	101
Table 4-5: Combined Kalman filter parameters	101
Table 5-1: Kalman filters statistics & improvements (pilot channel) - multipath	129
Table 5-2: Kalman filters statistics & improvements (data + pilot) - multipath.....	130
Table 5-3: Kalman filters statistics & improvements (pilot channel) - motion	137
Table 5-4: Kalman filters statistics & improvements (data + pilot) - motion.....	138
Table B-1: Standard tracking parameters	177

List of Figures and Illustrations

Figure 1-1: Error sources encountered by GPS signal.....	2
Figure 1-2: Different conditions facing GPS signal tracking	3
Figure 1-3: Power spectral density of the L5 demonstration signal (Los Angeles air force base 2009)	5
Figure 1-4: Elevation-dependant received power levels for L5 signal (Meurer et al 2009)	5
Figure 1-5: Positions suggested for combination in the tracking loops.....	8
Figure 2-1: GPS L1 C/A code signal structure	18
Figure 2-2: L1 C/A code normalized autocorrelation.....	19
Figure 2-3: L1 signal normalized power spectral density.....	20
Figure 2-4: GPS L5 signal structure	21
Figure 2-5: Normalized L5 data channel autocorrelation	22
Figure 2-6: Normalized L5 pilot channel autocorrelation	23
Figure 2-7: L5 data, pilot and total power spectral densities.....	23
Figure 2-8: L1 and L5 power spectral densities.....	25
Figure 2-9: Signal tracking loop	27
Figure 2-10: L5 pilot channel tracking loop	30
Figure 2-11: Data and pilot coherent combining	32
Figure 2-12 Kalman filter measurement model- option 1	38
Figure 2-13 Kalman filter measurement model- option 2	38
Figure 3-1: Experimental setup.....	43
Figure 3-2: GSS7700 Spirent signal simulator	44
Figure 3-3: NI Front-end.....	46
Figure 3-4: L1-L5 Tracking flow diagram.....	47
Figure 3-5: L1 signal acquisition	50

Figure 3-6: L5 signal acquisition	50
Figure 3-7: NH20 normalized correlation power.....	52
Figure 3-8: L1 bit synchronization	52
Figure 3-9: L5 bit synchronization	53
Figure 3-10: Flow chart for single channel tracking.....	54
Figure 3-11: Refraction of GPS signals in the earth’s atmosphere (Misra & Enge 2001)	56
Figure 3-12: Simulating atmospheric (ionospheric and tropospheric) errors	58
Figure 3-13: Allan deviation jitter for different OCXO models.....	61
Figure 3-14: OCXO models comparison: L5 FLI.....	62
Figure 3-15: OCXO models comparison: L5 PLI.....	63
Figure 3-16: Land mobile multipath categories.....	67
Figure 3-17: Signal power degradation – user action file.....	68
Figure 4-1: Schematic diagram for a standard tracking loop.....	72
Figure 4-2: Allan deviation and noise types (Physics Laboratory 2010).....	78
Figure 4-3: Comparison of total phase error for L1 and L5 signals	80
Figure 4-4: L5-aided L1 carrier tracking loop	81
Figure 4-5: L1 Aided Tracking Loop Flowchart	82
Figure 4-6: L1-aided code tracking loop	83
Figure 4-7: Flowchart of separate and combined Kalman filters	89
Figure 4-8: Separate Kalman filter tracking	91
Figure 4-9: Separate Kalman filter dynamic model.....	92
Figure 4-10: Combined Kalman filter tracking	95
Figure 4-11: Combined Kalman filter dynamic model.....	96
Figure 5-1: Aided L1 PLL tracking loop.....	104
Figure 5-2: Unaided L1 PLL tracking error.....	109

Figure 5-3: Aided L1 PLL tracking error	110
Figure 5-4: Comparison between L1-aided and unaided tracking loops	111
Figure 5-5: Multipath categories and satellites in view	112
Figure 5-6: L1 PLI of pilot aided PLL versus unaided PLL for multipath scenario	114
Figure 5-7: Aided L1 correlator outputs versus unaided correlator outputs for multipath scenario	115
Figure 5-8: L5 PLI using pilot only versus using data and pilot for multipath scenario	116
Figure 5-9: PLI of pilot aided L1 PLL versus data and pilot aided L1 PLL, for BW = 5 Hz, BW = 10 Hz, for multipath scenario.....	116
Figure 5-10: Dynamic vehicle model	117
Figure 5-11: L1 PLI for aided versus unaided tracking loops for moving vehicle scenario	118
Figure 5-12: L1 aided versus unaided correlator outputs for moving vehicle scenario..	119
Figure 5-13: L1 Doppler frequency for moving vehicle scenario	120
Figure 5-14: L1 PLI aided using pilot versus data and pilot for moving vehicle scenario	121
Figure 5-15: L1 FLI for separate versus combined Kalman filter for multipath scenario	123
Figure 5-16: L1 Doppler frequency for separate versus combined Kalman filter for multipath scenario	123
Figure 5-17: L1 PLI for separate versus combined Kalman filter for multipath scenario	124
Figure 5-18: L1 Correlator outputs for separate versus combined Kalman filter for multipath scenario	125
Figure 5-19: L5 Pilot PLI for separate versus combined Kalman filter for multipath scenario	125
Figure 5-20: L5 Pilot correlator outputs for separate versus combined Kalman filter for multipath scenario	126
Figure 5-21: Estimated states for separate versus combined Kalman filter for multipath scenario	127

Figure 5-22: Estimated standard deviations for separate versus combined Kalman filter for multipath scenario.....	128
Figure 5-23: Carrier phase RMS error comparison for multipath scenario	131
Figure 5-24: Carrier phase error standard deviations comparison for multipath scenario	131
Figure 5-25: L1 and scaled L5 Doppler frequencies for separate versus combined Kalman filter for moving vehicle scenario	132
Figure 5-26: L1 FLI for separate versus combined Kalman filter for moving vehicle scenario	133
Figure 5-27: L1 PLI for separate versus combined Kalman filter for moving vehicle scenario	133
Figure 5-28: L5 pilot FLI for separate versus combined Kalman filter for moving vehicle scenario.....	134
Figure 5-29: L5 pilot PLI for separate versus combined Kalman filter for moving vehicle scenario.....	135
Figure 5-30: Estimated carrier phase, frequency errors and acceleration states for separate versus combined Kalman filter for moving vehicle scenario	136
Figure 5-31: Estimated standard deviations for separate versus combined Kalman filter for moving vehicle scenario	136
Figure 5-32: Carrier phase RMS error comparison for moving vehicle scenario.....	139
Figure 5-33: Carrier phase error standard deviations comparison for moving vehicle scenario	140
Figure 5-34: Separate standard PLL tracking loop versus EKF tracking loop.....	141
Figure 5-35: Combined standard PLL tracking loop versus EKF tracking loop	142
Figure 5-36: PLL tracking errors for L1 and L5 signals: strong signal-separate tracking	144
Figure 5-37: Carrier phase error: strong signal-separate tracking	145
Figure 5-38: L1 PLI: strong signal-separate tracking.....	146
Figure 5-39: L5 PLI: strong signal-separate tracking.....	146
Figure 5-40: PLL tracking errors for L5 signal: strong signal-combined tracking.....	147

Figure 5-41: PLL tracking errors for L1 signal: strong signal-combined tracking.....	148
Figure 5-42: Carrier phase error: strong signal-combined tracking.....	148
Figure 5-43: L1 PLI: strong signal-combined tracking	149
Figure 5-44: EKF equivalent bandwidth calculation	150
Figure 5-45: PLL tracking errors for L1 and L5 signals: moving vehicle-separate tracking	151
Figure 5-46: Phase error: moving vehicle-separate tracking	151
Figure 5-47: L1 PLI and Doppler frequency: moving vehicle-separate tracking.....	152
Figure 5-48: L5 PLI and Doppler frequency: moving vehicle-separate tracking.....	153
Figure 5-49: L1 PLI and Doppler frequency: moving vehicle-combined tracking	154
Figure 5-50: PLL tracking errors for L5 signal: moving vehicle-combined tracking	155
Figure 5-51: PLL tracking errors for L1 signal: moving vehicle-combined tracking	155
Figure 5-52: Carrier phase error: moving vehicle-combined tracking	156
Figure 5-53: Carrier to noise ratio-sensitivity analysis.....	157
Figure 5-54: PLL tracking errors for L1 and L5 signals: sensitivity analysis-separate tracking	157
Figure 5-55: Phase error: sensitivity analysis-separate tracking.....	158
Figure 5-56: PLL tracking errors for L1 and L5 signals: sensitivity analysis-combined tracking	158
Figure 5-57 Phase error: sensitivity analysis-combined tracking.....	159
Figure 5-58: L1 Phase error versus carrier to noise ratio.....	159
Figure 5-59: L1 Phase error versus carrier to noise ratio.....	160
Figure B-1: Power level degradation	178
Figure B-2: Carrier to noise estimate.....	179
Figure B-5: L5 Doppler frequency, code Doppler.....	182
Figure B-6: L1 and L5 amplitudes.....	183

Figure B-7: L1 and L5 code phase errors	183
Figure B-8: L1 and L5 carrier phase errors	184
Figure B-9: L5 frequency and acceleration errors	184
Figure C-1: SVN 49 pseudorange residuals versus elevation (Langley 2009).....	186
Figure C-2: SVN 49 elevation	188
Figure C-3: SVN 49 received power versus elevation (Meurer et al 2009)	188
Figure C-4: Received C/N_0 for SVN 49	189
Figure C-5: PLI and FLI for L1 and L5 signals transmitted from SVN 49 using separate and combined KF	190

List of Symbols

Symbol	...	Definition
$1/T$...	Bandwidth of the measurements
A_{L1}	...	Effective amplitude of the L1 signal
A_{L5}	...	Effective amplitude of the subscripted channel
B_n	...	Loop filter noise bandwidth
C/N_0	...	Carrier to noise ratio
C_{data}, C_{pilot}	...	PN codes for the data and the pilot channels respectively
C_{Is}, C_{Qs}	...	Each represents a 3 x 3 covariance matrix of the in-phase and quadrature P/E/L correlator outputs on the subscripted signal s .
C_{L1}	...	L1 C/A code
<i>Coefficient</i>	...	Hz^2/n_e
40.3		
D_{L1}	...	L1 navigation data bits
D_{L5}	...	L5 navigation data bits
$F(t)$...	Coefficient matrix describing the dynamics of the system
$G(t)$...	Shaping matrix for the white noise input
H_k	...	Linearized Design matrix
IP	...	In-phase prompt correlator output
IP_{L1}	...	L1 in-phase prompt correlator output
IP_{L5}	...	L5 prompt in-phase correlator output
K_k	...	Kalman Gain
M	...	Coherent integration period
N	...	Number of multipaths
NBS_1	...	First bit synchronization threshold
NBS_2	...	Second bit synchronization threshold
NH_{10}, NH_{20}	...	10 and 20 bit Neuman-Hoffman codes applied to the data and the pilot channels respectively
N_I	...	the number of iterations
N_{L1}	...	Number of accumulated samples for the L1 signal

N_{L5}	...	Number of accumulated samples of the subscripted channel
$P(f_m)$...	Power curve of random vibration in g^2/Hz as a function of f_m
P_k	...	State Covariance Matrix
P_{L1}	...	L1 total received power
P_{L5}	...	L5 total received power
Q	...	Process noise covariance matrix
$Q(t)$...	Process noise spectral density matrix
QP	...	Quadrature prompt correlator output
QP_{L1}	...	L1 quadrature prompt correlator output
QP_{L5}	...	L5 quadrature correlator output
R	...	Measurement covariance matrix
$R(\tau)$...	Normalized autocorrelation function
$R(\delta\tau_{L1})$...	Correlation of the filtered incoming code with the local generated code for the L1 signal
$R(\delta\tau_{L5})$...	Correlation of the filtered incoming L5 code with the local generated code for the subscripted channel
R_k	...	Covariance matrix for the measurement noise
$S_v(f_m)$...	Oscillator vibration sensitivity of $\Delta f/f_L$ per g as a function of f_m
S_{am}	...	Amplitude power spectral density
S_{mp}	...	Code power spectral density
S_f	...	The spectral density of the white frequency noise, $S_f = (2\pi f_s) \cdot \sqrt{(h_0/2)}$
S_g	...	The spectral density of the random walk frequency noise, $S_g = (2\pi f_s) \cdot \sqrt{(2\pi^2 h_{-2})}$.
S_a	...	Carrier phase acceleration power spectral density
$S_y(\omega)$...	One sided spectral density of the fractional frequency fluctuation
T	...	Coherent integration time
T_c	...	Chip period
TEC	...	Total electron content in TEC units (TECU), where 1 TECU is defined as 10^{16} electrons/m ²

dR/dt	...	Maximum LOS velocity dynamics ($^{\circ}/s$)
d^2R/dt^2	...	Maximum LOS acceleration dynamics ($^{\circ}/s^2$)
d^3R/dt^3	...	Maximum LOS jerk dynamics ($^{\circ}/s^3$)
f	...	Nominal frequency of oscillator
$f_{carrier}$...	Carrier frequency
f_{code}	...	Code chipping rate of the subscribed channel
$f_{codeDoppler}$...	Code Doppler of the subscribed channel
f_{CR}	...	Code chipping rate
$f_{Doppler}$...	Doppler frequency
f_L	...	L-band input frequency in Hz
f_{L1}	...	L1 carrier frequency
f_{L5}	...	L5 carrier frequency
f_m	...	Random vibration modulation frequency in Hz
f_n	...	Frequencies of the multipath returns relative to the carrier frequency
g	...	Gravitational acceleration $\approx 9.8 \text{ m/s}^2$
h_0	...	White frequency noise
h_{-1}	...	Flicker frequency noise
h_{-2}	...	Random walk frequency noise
h_k	...	Nonlinear design matrix
n_e	...	Electron density (electrons/m ³) along LOS path dl
s	...	Subscript s refers to the signal of interest
v_k	...	Measurement noise
v_{rel}	...	Relative velocity between the satellite and the receiver
w	...	Random forcing function, zero-mean white Gaussian noise
x	...	States of dynamic system
$x(t)$...	Complex envelope of the transmitted signal
y	...	$\frac{\delta f}{f}$

z_k	...	Measurement vector
A_0	...	Direct signal's amplitude
A_n	...	Received amplitudes of the multipath returns
Δ	...	Early-late spacing
$\Delta S_{iono,g}$...	Group delay (m)
Δf_d	...	Filtered carrier discriminator output
Δf_{cd}	...	Filtered code discriminator output
Ψ	...	Correlator output for the subscripted channel
α_0	...	Phase acceleration in units of rad/s ² The subscript zero indicates the value at the start of the integration
β	...	Converts units of radians into units of chips for the subscripted signal
$\overline{\delta\phi_{L1}}$...	L1 average local carrier phase error over the integration interval in units of rad
$\overline{\delta\phi_{L5}}$...	L5 average local carrier phase error over the integration interval in units of rad for the subscripted channel
$\delta\phi$...	Carrier phase error
δf	...	Absolute frequency deviation
δf_{L1}	...	L1 local carrier frequency error in units of rad/s
δf_{L5}	...	L5 local carrier frequency error in units of rad/s, for the subscripted channel
$\delta\tau_L$...	L1 local code phase error in units of chips
$\delta\tau_{L5}$...	L5 local code phase error in units of chips, for the subscripted channel
θ_A^2	...	Allan variance induced oscillator jitter in degrees
θ_e	...	Dynamic stress error
ρ	...	Correlation coefficient between L1 and L5 errors

$\sigma_{\delta\phi}$...	1-sigma input tracking error (in degrees)
$\sigma_{\delta\phi,c}$...	Correlated sources of phase error
$\sigma_{L1-L5,aid}$...	1-sigma L1 phase error fed by the L5 signal
$\sigma_{L1-L5,aid,corr}$...	1-sigma L1 phase correlated errors fed by the L5 signal
$\sigma_{L1-L5,aid,uncorr}$...	1-sigma L1 phase uncorrelated errors fed by the L5 signal
σ_N^2	...	Noise variances
σ_{PLL}	...	1-sigma phase jitter from all sources (in degrees)
σ_t	...	1-sigma thermal noise (in degrees)
σ_v	...	1-sigma vibration-induced oscillator phase noise (in degrees)
τ_0	...	Propagation delay of the direct path
τ_n	...	Propagation delays of the multipath returns
ϕ_0	...	Carrier phase of the direct path
ϕ_n	...	Carrier phases of the multipath returns
ϕ_{L1}	...	L1 carrier phase
ϕ_{L5}	...	L5 carrier phase
Φ_k	...	State transition matrix
ω_L	...	Natural radian frequency

List of Abbreviations

Abbreviation	...	Definition
AGPS	...	Assisted Global Positioning System
ARNS	...	Aeronautical Radio Navigation Service
CRC	...	Cyclic Redundancy Check
DLL	...	Delay Lock Loop
EKF	...	Extended Kalman Filter
FEC	...	Forward Error Correction
FLI	...	Frequency Lock Indicator
FLL	...	Frequency Lock Loop
GPS	...	Global Positioning System
GSRx TM	...	GNSS Software Navigation Receiver
ICD	...	Interface Control Document
IF	...	Intermediate Frequency
ITU	...	International Telecommunications Union
L1 C/A	...	GPS Coarse/Acquisition Code
LOS	...	Line Of Sight
Mcps	...	Mega Chips Per Second
NCO	...	Numerically Controlled Oscillator
NH	...	Neuman-Hoffman
OCXO	...	Oven Controlled Crystal Oscillator
PLAN	...	Position, Location And Navigation
PLI	...	Phase Lock Indicator
PLL	...	Phase Lock Loop
PN code	...	Pseudo-Noise code
PRN	...	Pseudo-Random Noise
PSD	...	Power Spectral Density
QPSK	...	Quadrature Phase Shift Keying
RF	...	Radio Frequency
RMS	...	Root Mean Square

RNSS	...	Radio Navigation Satellite Services
SNR	...	Signal to Noise Ratio
SPS	...	Standard Positioning Service
sps	...	Symbol per second
STD	...	Standard Deviation
URA	...	User Range Accuracy

Chapter One: INTRODUCTION

The Global Positioning System (GPS) has been introduced as a means of positioning and navigation. GPS applications include, but are not limited to, high accuracy and high sensitivity applications, where each of them has its own specifications. The current thesis focuses on high sensitivity applications including weak signal environments, indoor environments suffering from multipath and fading, and urban canyon environments.

To overcome the severe performance degradations resulting from such environments, and also as a part of the GPS modernization, new signals are being designed to ensure enhanced GPS positioning performance, including the GPS L2 Civil (L2C) signal, the L5 signal and one military signal (the M code), to be added to both L1 and L2 signals.

The thesis deals with the L5 signal and the conventional L1 C/A code signal. Several works in the literature had attempted to combine the L1 C/A code signal with the new L2C signal, and that yielded encouraging results, e.g. Gernot (2009), Qaisar (2009) and Ioannides et al (2006). However, to the author's knowledge, no work was done to investigate the possibility of combining the L1 C/A with the new L5 signal. The L5 signal is designed with interesting characteristics, which motivates the current research to investigate the different possibilities of combining with the L1 C/A code signal. The L5 and L1 signals are both located in the Aeronautical Radio Navigation Service (ARNS) band, whereas the L2C signal is located in the Radio Navigation Satellite Services (RNSS) band, potentially subject to high power levels of interference, and thus cannot be used for the aviation applications. Different methods are proposed to combine

both to form one type of tracking loop capable of tracking the two signals in different challenging environments.

1.1 Background

This thesis focuses on combining the L1 and L5 signals for tracking purposes. As mentioned before, under normal circumstances, the GPS suffers from several conditions that make it challenging to keep tracking the already very weak GPS signal. These conditions introduce errors that highly affect the performance of GPS.

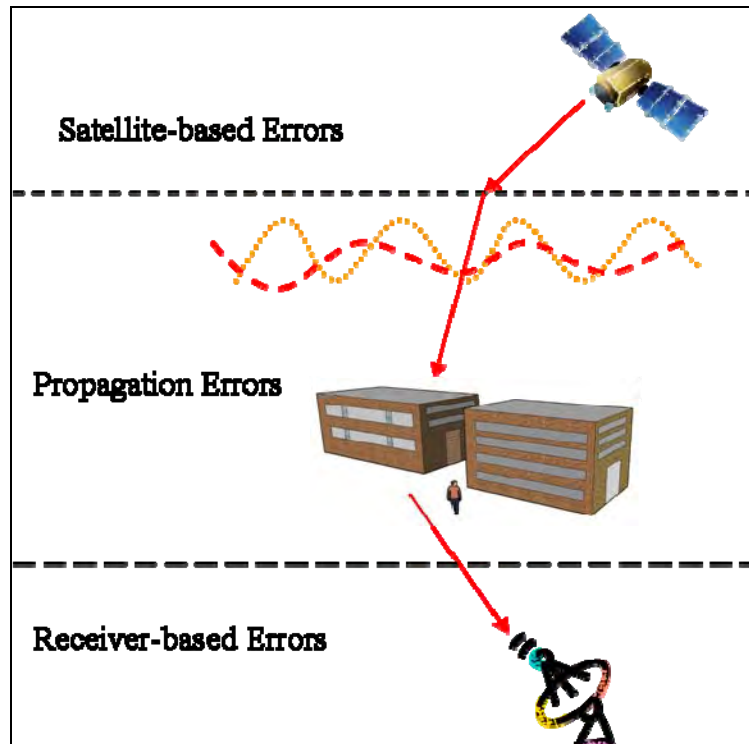


Figure 1-1: Error sources encountered by GPS signal

Figure 1-1 shows the different error sources that the GPS signal encounters throughout its journey. These errors are a) satellite-based, where they are introduced from the orbits and the satellite clocks, b) propagation errors, where the propagation medium and the

atmosphere introduce errors, c) receiver-based errors, where the receiver introduces antenna errors, clock errors, or timing and tracking errors. The received GPS L1 C/A code signal power is -158.5 dBW under nominal conditions, namely, open sky, no multipath, normal ionospheric activities (IS-GPS-200 2006). When the signal suffers a change in these conditions, a power degradation up to and, in many cases, in excess of 20 dB can occur which makes it difficult to acquire or track the signal.

Figure 1-2 illustrates the possible challenges that the GPS signal can encounter. Throughout its propagation, the GPS signal suffers from errors introduced by different atmospheric levels, the environments, and by the user himself.

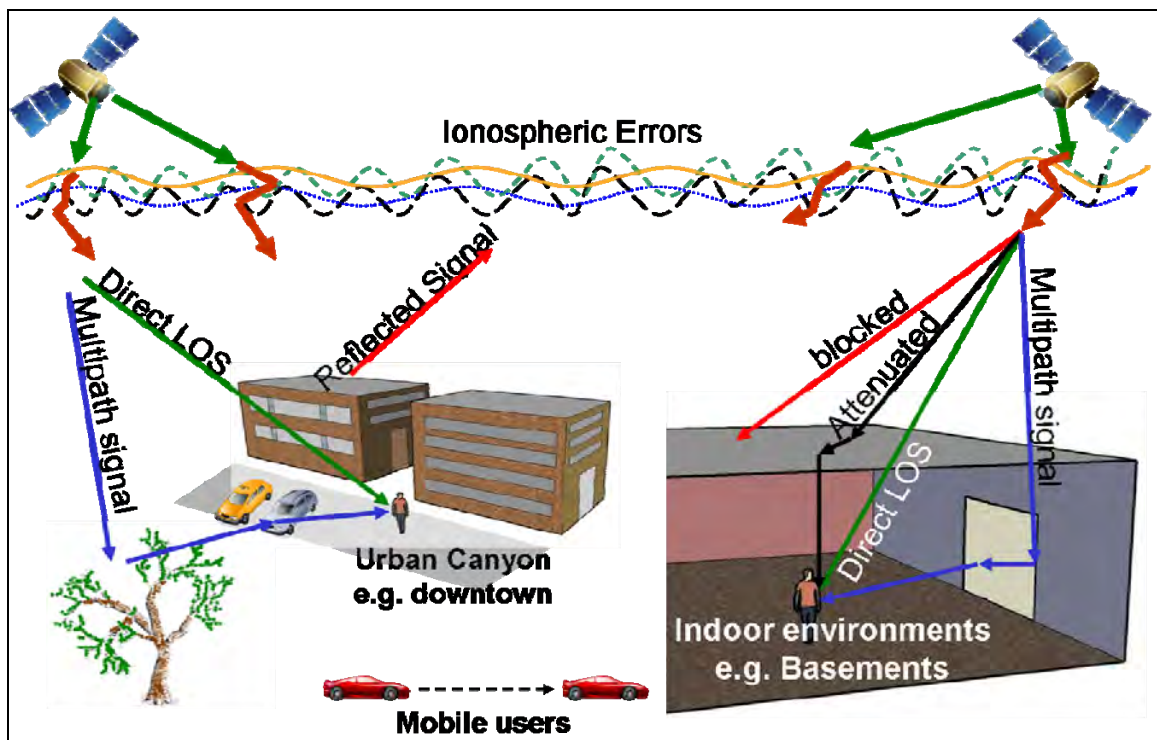


Figure 1-2: Different conditions facing GPS signal tracking

The GPS community is thus focusing on enhancing the current signals' characteristics, and developing new signals with new characteristics capable of better performance under these conditions. To fully illustrate this point, the next section discusses the GNSS modernization, followed by a literature review on the previous work related to both signals of interest and the tracking of weak signals.

1.2 GNSS Modernization

Three new signals are planned for future GPS satellites, namely two civil signals on two new frequencies: L2 Civil (L2C), which is modulated on the existing L2 carrier located at 1227.6 MHz and the L5 signal at 1176.45 MHz, and one military signal M code, to be added to the L1 and L2 signals (Ward et al 2006a). In addition to these two signals, a new civil signal is being developed, the L1C signal, which will be transmitted on the same L1 carrier frequency (Cahn et al 2007). The signal chosen for the current work is the L5 signal, designed for aviation safety of life applications. The first L5 demonstration payload was launched on the IIR(M)-20 satellite (SVN 49) on March 24th 2009, and began transmitting on April 10th 2009 (Los Angeles air force base 2009).

Figure 1-3 shows the power spectral density of the first L5 demonstration payload. However, up to the time of writing the thesis, the L5 signal transmitted is still for test purposes. Only the pilot channel is transmitted with no guarantee on the transmitted signal power, availability or quality. In fact, the received L5 pilot signal power from SVN 49 has shown, in addition to being 3 dB lower than the Interface Control Document (ICD) specifications, a clear dependency on the satellite elevation angle (Meurer et al 2009). Figure 1-4 shows the elevation-dependant received power levels.

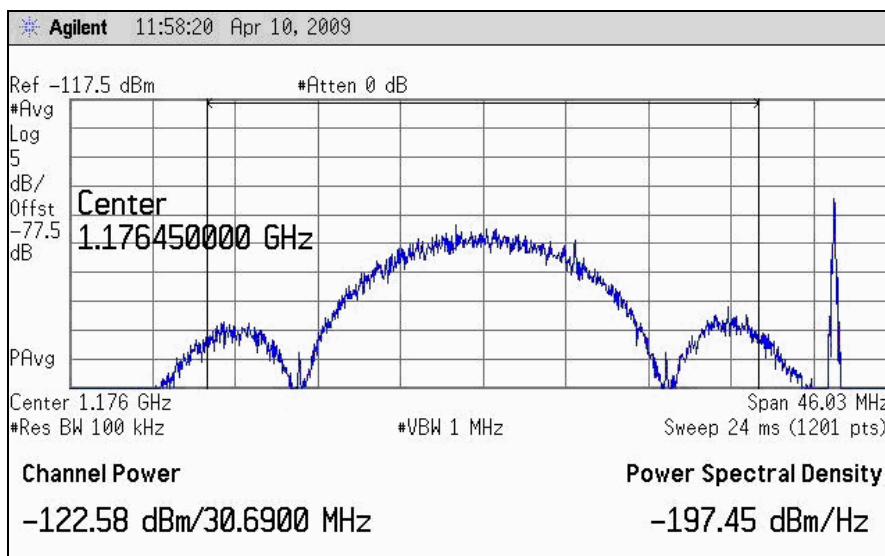


Figure 1-3: Power spectral density of the L5 demonstration signal (Los Angeles air force base 2009)

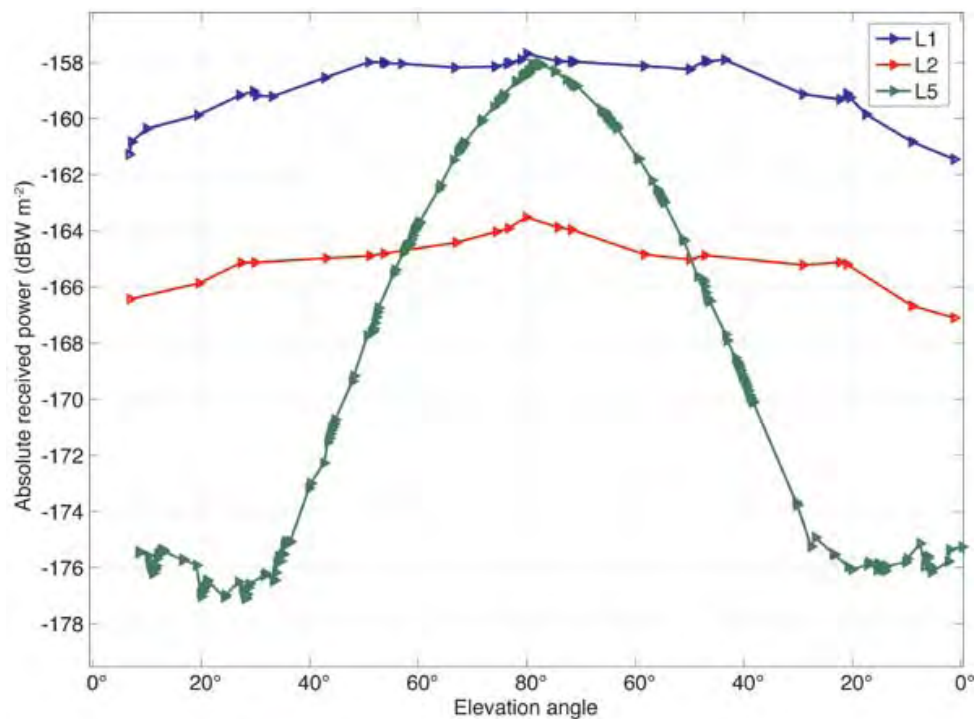


Figure 1-4: Elevation-dependant received power levels for L5 signal (Meurer et al 2009)

1.3 Limitations of Previous Work

The L5 signal has several characteristics that make it interesting to study. Only a highlight of these characteristics is presented herein. A detailed signal description is presented in Chapter 2. The L5 signal is allocated the carrier frequency of 1176.45 MHz, which is in the ARNS band authorized for use in emergency and safety of life applications (IS-GPS-705 2005). The L5 signal (and, indeed, all the modernized GPS signals) has implemented a dataless (pilot) channel, together with the data channel, to enable extended phase tracking without worrying about the data bits. This results in an increase of 6 dB in the minimum signal strength for which phase tracking is possible, relative to the conventional L1 C/A signal (Ward et al 2006a). It has a chipping rate 10 times that of the L1 with the same code period of 1 ms, resulting in a code length 10 times that of the L1 C/A signal. The L5 signal is also encoded with a Neuman-Hoffman (NH) code, 10 bits on the data channel and 20 bits on the pilot channel, to enhance the cross-correlation properties and data bit synchronization.

The L5 signal, having these properties, creates new research areas. Several papers study different receiver structures for the L5 signal from the acquisition to bit synchronization, tracking and navigation solution. Van Dierendonck & Spilker (1999) and Spilker & Van Dierendonck (1999) have first proposed the L5 signal and discussed a candidate receiver implementation. Both the non-coherent integration of the data and the pilot channel for acquisition purposes and the usage of the pilot channel only for tracking were presented. Bastide et al (2002) has analyzed the acquisition, tracking and data demodulation performance of the GPS L5 signal and the Galileo E5a/E5b signals. Several acquisition

schemes for the L5 signal including data and pilot combination and different NH code acquisition techniques have also been discussed (Hegarty & Tran 2003, Macabiau et al 2003 and Mongrédien 2008).

From the above, it is clear that the use of this new signal together with the L1 C/A signal to increase the tracking sensitivity of a software receiver presents an attractive possibility.

The idea of combining different signals is, by itself, not new. In the literature, several papers present the idea of combining two or more signals for acquisition purposes. Ioannides et al (2006) discussed the idea of combining two GPS signals in one acquisition scheme for indoor environments. It also outlined the issues and the benefits obtained from such combinations including the integration of the energies of different signals, the different chipping rates, different Doppler, and the relative code delays. Gernot (2009) also proposed combining the L1 and L2C signal for acquiring weak signals and verified the synchronization of the L1 and the L2C under normal ionospheric conditions.

For tracking purposes however, there is a lack of research dealing with combining the L1 and L5 signals. However, for other modern signals, the L1 and the L2C signal, Gernot (2009) discussed the idea of combining both signals at the discriminator level. It also presented the combination of the discriminators of both signals to estimate the ionosphere parameters using the least-squares method. Qaisar (2009) has also discussed the idea of Doppler aided tracking loops for the L1 and the L2C signals, where the L2C signal, the aiding source, is operated with a wide bandwidth loop to absorb any dynamic stress, and provides Doppler estimates to the L1 signal which operates at a narrow bandwidth.

Results from the two papers have shown that the joint usage of the L1 and the L2C signals for tracking purposes provides more robust tracking when compared to each of the two signals separately.

1.4 Objectives

Based on the aforementioned limitations, this thesis focuses on the idea of combining the L1 and the L5 signals in a single tracking loop. To accomplish this, two possibilities were suggested, as illustrated in Figure 1-5. The first one is after the loop filter, at the numerically controlled oscillator (NCO) level, and the second position is at the correlator output level.

The first position is actually a straightforward implementation, using standard tracking loops, where Doppler aiding can be achieved by scaling the Doppler frequency of one of the signals and providing it as assistance to the second signal. Thus, an L1 Doppler aided tracking loop is developed, where the L5 signal is the source of assistance. The advantages of this technique are analyzed in terms of the enhanced tracking sensitivity.



Figure 1-5: Positions suggested for combination in the tracking loops

The second position is to combine the L1 and the L5 signals at the correlator output level. To accomplish this, Kalman filter based tracking has been chosen. The Kalman filter has been investigated for tracking loop estimation for a single signal by, for example, Psiaki & Jung (2002), Petovello & Lachapelle (2006), and Mongrédien (2008) with different implementations. Psiaki & Jung (2002) proposed the estimation of the carrier phase error, in addition to the true value of the carrier frequency, the code phase and the carrier acceleration using the latter to propagate these values. The carrier phase error is computed as the difference between the estimated value and the value generated by the NCO. Petovello & Lachapelle (2006) have adopted a similar technique to that used by Psiaki & Jung (2002) in addition to estimating the errors instead of the true values. Both papers deal with the conventional L1 C/A signal. Mongrédien (2008) investigated the effect of Kalman filter based tracking loops on L5 signal performance from the tracking and the positioning accuracy point of view.

1.5 Contributions

In light of the objectives described before, the contributions of the thesis can be outlined as follows:

1) Analyzing the similarities and the differences between the L1 and the L5 signals, these differences are one of the main motivations to consider for such a combination. The differences in the two signal structures change the behaviour of each in different environmental challenges, thus combination becomes an advantage. These differences include the effect of the carrier frequency, code length, the NH code in the case of the L5 signal and all the other characteristics.

2) Analyzing and illustrating different ideas for combining the two signals, and that includes the Doppler aided tracking loops and the combined code and carrier tracking in general.

3) Implementing an L1/L5 combined software receiver, since it is required that both signals are received through one software receiver to implement and test different tracking methods. A modified version of the University of Calgary's GSNRxTM software receiver capable of acquiring and tracking the two signals was developed, providing a wide range of options for each signal on the sampling rates, tracking parameters, etc...

4) Implementing and testing the first method of combination using standard tracking loops, where the assistance data is provided from the L5 signal to the L1 signal in both the code and the carrier tracking loops. The results of such implementation are discussed.

5) Implementing and testing the second method of combination using the Kalman filter based tracking, for the tracking, the code and carrier phase errors of each of the two signals need to be estimated. The combination of the two signals includes the collaboration of the two signals' information in one adaptive filter, which helps in enhancing the performance of each. The L5 signal, with the existence of the pilot channel, and the NH codes, aids the L1 C/A signal in multipath environments, whereas the L1 has less sensitivity to the ionospheric errors, because of its higher frequency, and thus can aid the tracking of the L5 signal.

6) Investigating the different possibilities of the usage of the three available channels, namely the L1 data channel, L5 data channel, and L5 pilot channel. The data and pilot channels of the L5 signal constitute the total signal power; thus, it is important to consider using both of them, although in that case the benefit of the pilot channel will not be fully utilized.

7) Developing an experimental method to compare the standard tracking loop and the steady-state Kalman filter tracking loop, where the bandwidth and tracking thresholds of the steady-state Kalman filter are used to build the equivalent phase tracking loop. This helps in comparing the two techniques and in understanding the advantages of using the Kalman filter tracking.

As was discussed earlier in Section 1.2, the only satellite that transmits the L5 signal does not comply with the ICD characteristics. Thus, for evaluating the different proposed tracking schemes, simulated data from a GPS signal simulator is used. The different environments and simulation parameters are presented in Chapter 3. Moreover, Appendix C discusses the SVN 49 problems, and shows some of the results using the real data.

1.6 Thesis Outline

The thesis focuses on various combination techniques for L1 C/A code and L5 signals to enhance tracking. In order to provide a thorough view of the thesis contributions, the thesis is structured as follows:

Chapter 2 starts with a review of the L1 C/A code structure and the modern L5 signal structure. Since the thesis makes use of both signals, the improvements of each of them should be studied in light of the other's limitations. The second part of the chapter reviews the standard tracking loops in general including the frequency, phase and code tracking loops. The architecture and parameters affecting each are explained. The chapter also proceeds to a review on Kalman filter tracking, with the frequently used models in GPS signal tracking.

Chapter 3 discusses the simulation environment required to test the proposed methods. Throughout the work of the thesis, only one L5 GPS test signal was transmitted for the first time on April 10th 2009 for test purposes only, and with no guarantee on the signal power levels or the signal availability (GPS World 2009). For these reasons, an L1 and L5 signal generator and simulator was required to evaluate the methods proposed. The chapter discusses the capabilities of the simulator used (a Spirent GSS7700), the experiment setup and the different simulation environments. The chapter further illustrates the developed software receiver used for acquiring and tracking both the L1 and L5 signals which is one of the main contributions of the thesis.

Chapter 4 introduces two methods for combining data from the L1 and the L5 signals. The first is the aided L1 tracking loops, where the standard tracking loops are used. The concerns, limitations and methods of such a combination in the tracking loop are discussed. The second is the combined Kalman filter tracking loop, which is also one of the innovations of the thesis. A complete Kalman filter model is developed including the

state dynamic model and the observation model. The noise parameters are developed to allow a proper combination.

A detailed performance evaluation of the two methods is shown in Chapter 5. Both the combined standard and Kalman filter tracking are compared to the separate standard tracking of the L1 and L5 signals. Moreover, a new method of comparing the standard tracking to the Kalman filter tracking is presented. The evaluation criteria are discussed and the results are shown.

The thesis concludes with a summary and recommendations for future work in Chapter 6.

Appendix C provides a detailed discussion about SVN 49, the first satellite to transmit the L5 signal. The appendix discusses the different problems associated with the satellite and solutions adopted to make the signals transmitted from it usable. The appendix also shows results from a sample data collected from SVN 49.

Chapter Two: GNSS SIGNALS AND TRACKING LOOPS

The GNSS community has introduced new signals as a part of the ongoing modernization program. In order to make the best use of these new signals, the chapter provides a review on the characteristics of the conventional L1 C/A code and new L5 signals. As the title of the chapter suggests, it discusses two main topics, the GNSS signals of interest in the thesis and the different tracking loops. The chapter starts with a discussion on the modernization process of the GPS. Then it proceeds to illustrating the signal structures of L1 and L5. The second part of the chapter presents the tracking loops that are generally used for the GPS signal. That includes the standard code and carrier tracking loops, and the Kalman filter based tracking. The chapter also discusses the relation between the L1 and L5 signals' tracking errors.

2.1 GPS Modernization

The minimum specified performance GPS Standard Positioning Service (SPS) performance is 19.1 m for the 95 percent horizontal accuracy (GPS Navstar (1995), McDonald and Hegarty 2000). Although the GPS performance has exceeded what it was required to achieve by almost a factor of three, it was determined by the GPS community that new signals are required to enhance any deficiencies that were noticed in the GPS performance over the past decades. Actually, the modernization of the GPS is always an ongoing process, since the lifetime of the GPS space vehicles is from 7-11 years. The addition of new signals was a logical following step, when taking into consideration all the advantages of more GPS signals. The following discussion will consider only the civil signals.

In 2004, the GPS space vehicles transmitted only the L1 C/A code signal, which is the principal GPS signal. The L1 signal suffered from the group delay error introduced by the ionosphere. The ionospheric group delay (m) is given as (Equation 7.19 in Conley et al 2006)

$$\Delta S_{iono,g} = \frac{40.3 \cdot TEC}{f_{carrier}^2} \quad (2.1)$$

$$TEC = \int_{SV}^{User} n_e dl \quad (2.2)$$

where

- $\Delta S_{iono,g}$: Group delay (m)
- $f_{carrier}$: Carrier frequency (Hz)
- TEC : Total electron content in TEC units (TECU), where 1 TECU is defined as 10^{16} electrons/m²
- n_e : Electron density (electrons/m³) along LOS path dl
- Coefficient 40.3* : Hz^2/n_e

It is apparent from Equation 2.1 that the ionospheric errors are directly related to the square of the carrier frequency, and thus the use of two or more signals can help eliminate that error term. Considering this, there was a need for the availability of the L2C signal, whose primary purpose was to eliminate the slowly changing ionospheric delay. The first modernized Block IIR (Replenishment) satellite, PRN 17, was launched on 25 September 2005 carrying the new L2C signal, which became available on new satellites from 15 December 2005 (U.S. Air Force 2006). The L2C signal was allocated the carrier frequency of 1227.6 MHz, which is in the RNSS Band. Existing in this band,

the L2 signal is potentially subject to high power levels of interference, and thus cannot be used for the aviation applications.

From that point, the thought of having a new signal allocated in the ARNS band, to be used in safety of life applications, came into consideration. The L5 signal was first proposed in 1999, and was allocated the carrier frequency of 1176.45 MHz. Being designed specially for safety of life applications, the L5 signal has superior characteristics.

In addition to the L2C and L5 signals, a new L1C signal was proposed in 2006 (Betz et al 2006) for transmission on the L1 carrier frequency, 1575.42 MHz. This signal is designed to have superior performance, and to provide interoperability and capability with other signals in the L1 band.

2.2 Signal Structures

This section describes the models for the two signals in use: the conventional L1 C/A code signal and the L5 signal.

2.2.1 GPS L1 C/A Code Signal Structure

The L1 signal is the first and primary GPS signal. The navigation information is contained in the L1 data message, which is transmitted at 50 bps. This message is bi-phase modulated with the C/A code. The C/A code has a 1.023 Mcps rate, and 1023 chips length, resulting in 1 ms code period. The resulting code is further modulated by a carrier frequency of 1575.42 MHz. The L1 signal structure is shown in Figure 2-1.

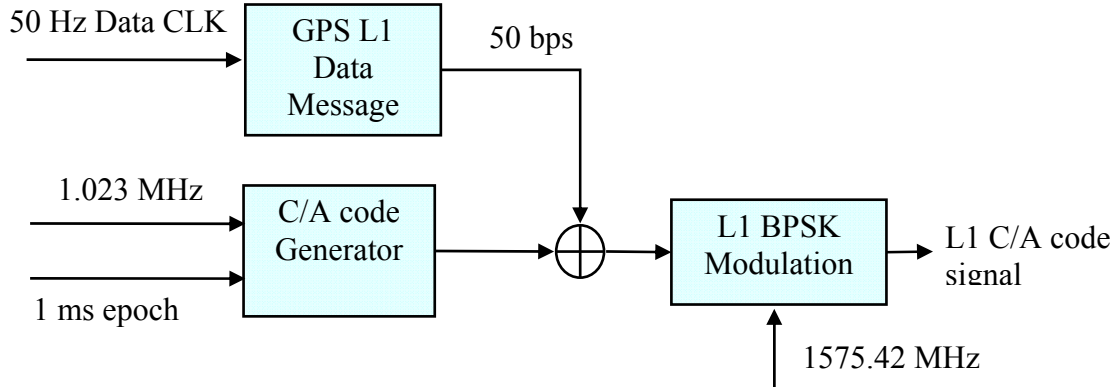


Figure 2-1: GPS L1 C/A code signal structure

In addition to the above characteristics, and for any satellite navigation application, two important characteristics have to be studied: the autocorrelation function and the power spectral density (PSD defines the distribution of power within the signal in the frequency domain).

Figure 2-2 shows the normalized autocorrelation function for PRN 12, with a zoomed version around the main peak. Neglecting the side peaks, the autocorrelation function has a perfect triangular shape. Thus, it can be approximated as (Ward & Betz 2006)

$$R(\tau) = \begin{cases} 1 - \frac{|\tau|}{T_c} & \text{for } |\tau| \leq T_c \\ 0 & \text{elsewhere} \end{cases} \quad (2.3)$$

where $R(\tau)$: Normalized autocorrelation function

T_c : Chip period

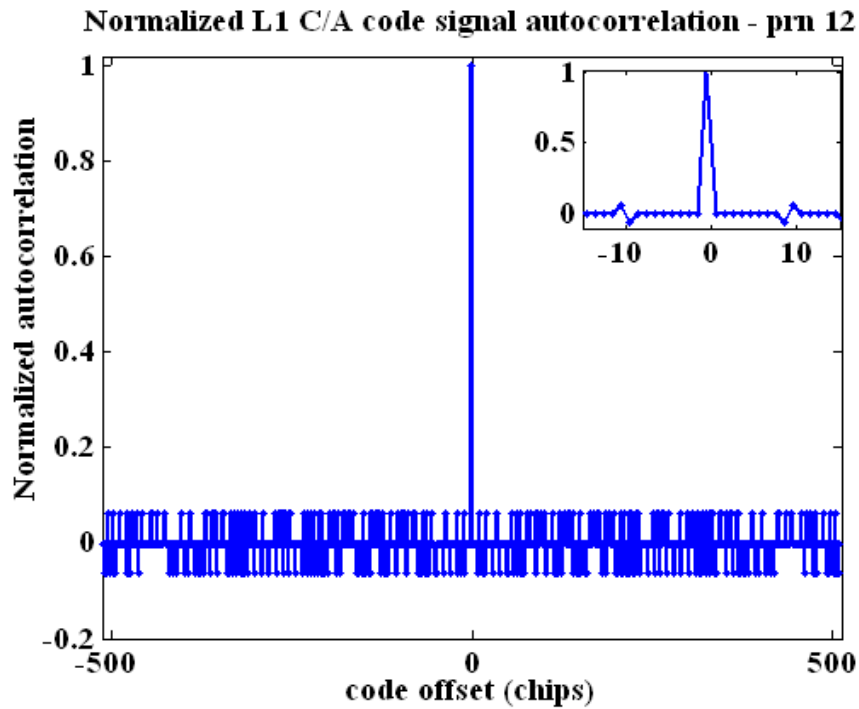


Figure 2-2: L1 C/A code normalized autocorrelation

Given that approximation of the autocorrelation function, the power spectral density can also be approximated as a sinc-squared function

$$S(f) = T_c \left(\frac{\sin(\pi f T_c)}{\pi f T_c} \right)^2 \quad (2.4)$$

where $S(f)$: Normalized power spectral density

Figure 2-3 shows the power spectral density of the L1 signal, which matches the sinc-squared shape.

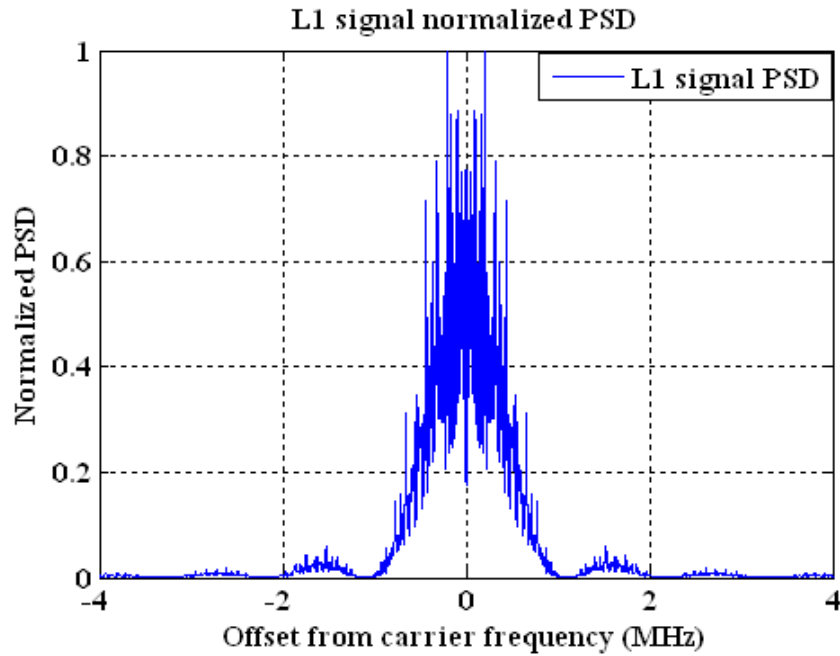


Figure 2-3: L1 signal normalized power spectral density

Given the aforementioned structure, the L1 C/A code signal model can be written as

$$S_{L1}(t) = \sqrt{P_{L1}} \cdot D_{L1}(t) \cdot C_{L1}(t) \cos(2\pi f_{L1}t + \varphi_{L1}) \quad (2.5)$$

where

- P_{L1} : L1 total power
- D_{L1} : L1 navigation data bits
- C_{L1} : L1 C/A code
- f_{L1} : L1 carrier frequency
- φ_{L1} : L1 carrier phase

2.2.2 GPS L5 Signal Structure

The new L5 signal is designed to eliminate most of the L1 C/A code deficiencies. The L5 signal has two channels: the in-phase data channel (I5) that carries the navigation message, and the quadrature dataless (pilot, Q5) channel which is used for enhancing

tracking, and carries no navigation message. The L5 signal has a minimum signal strength of -154.9 dBW equally shared between the data and pilot channel (IS-GPS-705 2005).

The data is transmitted at 50 bps. To enhance the error detection capability, a cyclic redundancy check (CRC) is added to the message, followed by a rate $\frac{1}{2}$, forward error correction convolution (FEC) code. The resulting code, transmitted at 100 symbols per seconds (sps), is then modulated by a 10 bit NH code [0000110101], which is clocked at 1 kHz. The output is bi-phase modulated with a pseudo-noise (PN) code (I5 code) having rate 10.23 Mcps, resulting in the I5 channel.

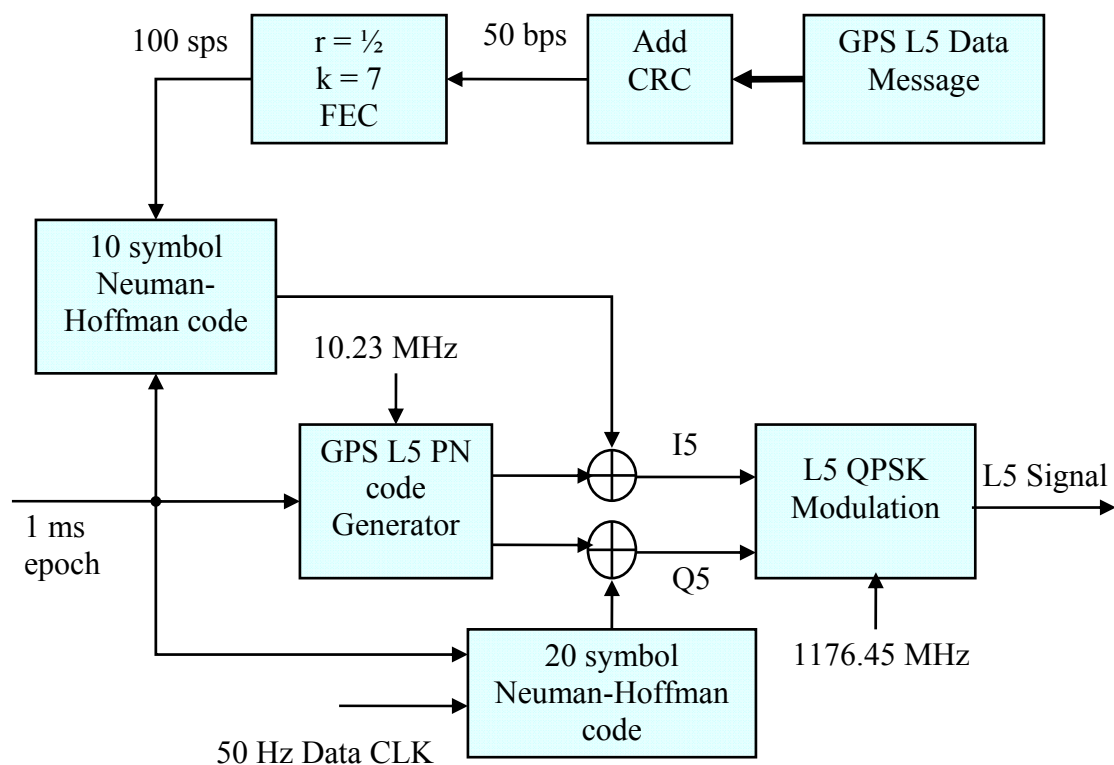


Figure 2-4: GPS L5 signal structure

On the other hand, the pilot channel is directly modulated with a 20 bits NH code [00000100110101001110], then bi-phase modulated by another PN code (Q5 code, different from that of the data channel, but with the same rate). The resulting code is the Q5 channel.

Finally, the I5 and Q5 channels are Quadrature Phase Shift Keying (QPSK) modulated by the L5 carrier frequency. Figure 2-4 shows the L5 signal structure.

Studying the autocorrelation and power spectral density of the L5 signal reveals more of its interesting characteristics. Figures 2-5 and 2-6 shows the autocorrelation function for PRN 12, both for the data and pilot channels. The secondary peaks created by the NH codes can reach up to -14 dB, which can create problems in the L5 acquisition, as mentioned by Ries et al (2002).

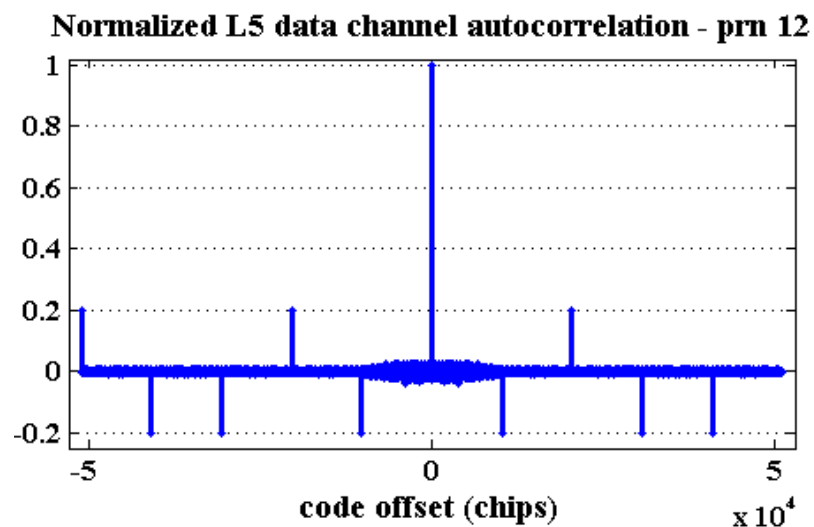


Figure 2-5: Normalized L5 data channel autocorrelation

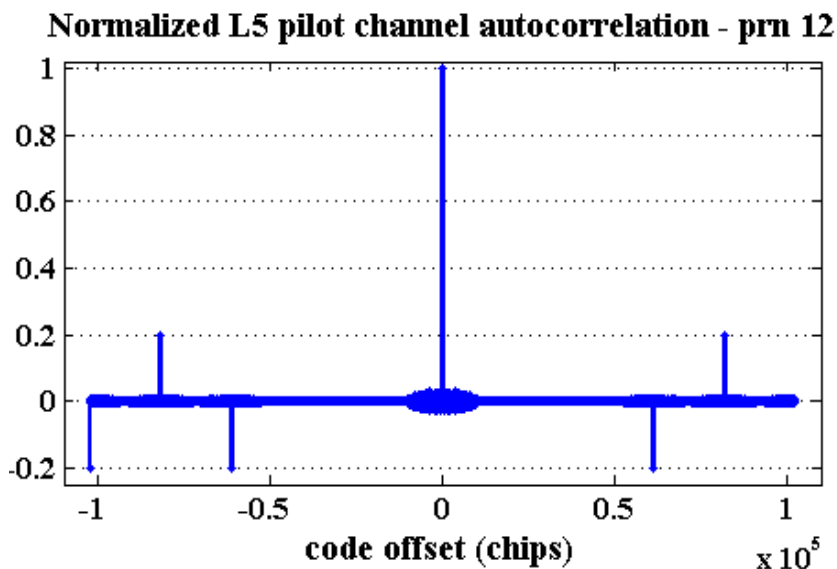


Figure 2-6: Normalized L5 pilot channel autocorrelation

As mentioned earlier, the L5 signal power is equally split between the data and pilot channels. Figure 2-7 shows the power spectral density of the L5 signal. More discussion on the L5 power spectral density is presented in the next section.

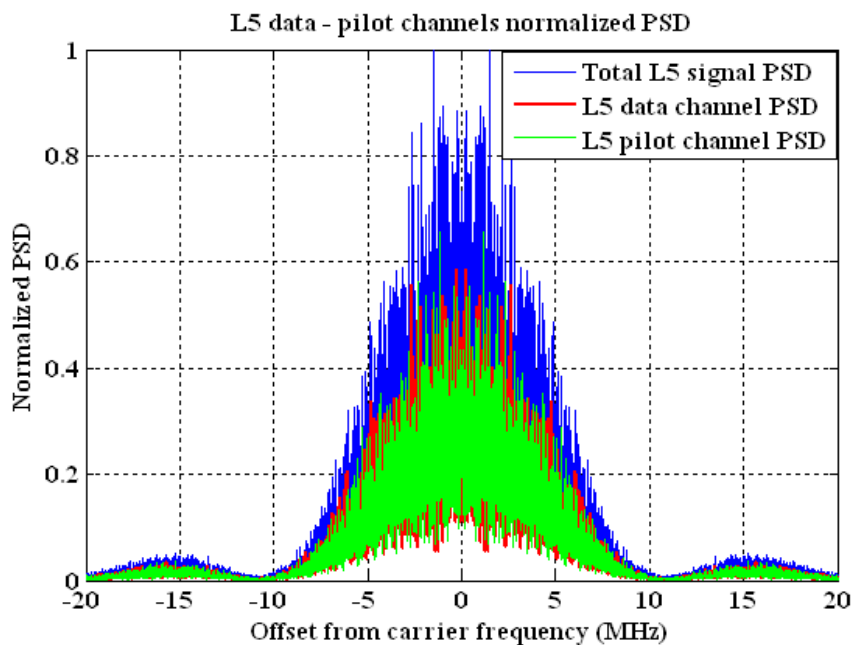


Figure 2-7: L5 data, pilot and total power spectral densities

The L5 signal model is finally written as

$$S_{L5}(t) = \sqrt{P_{L5}} \cdot \begin{bmatrix} D_{L5}(t) \cdot C_{data}(t) \cdot NH_{10}(t) \cdot \cos(2\pi f_{L5}t + \varphi_{L5}) \\ + C_{pilot}(t) \cdot NH_{20}(t) \cdot \sin(2\pi f_{L5}t + \varphi_{L5}) \end{bmatrix} \quad (2.6)$$

where

- P_{L5} : L5 total power
- D_{L5} : L5 navigation data bits
- C_{data}, C_{pilot} : PN codes for the data and the pilot channels respectively
- NH_{10}, NH_{20} : The 10 and 20 bit NH codes applied to the data and the pilot channels respectively
- f_{L5} : L5 carrier frequency
- φ_{L5} : L5 carrier phase

2.2.3 L1 and L5 Signals Differences

As discussed in the previous two sections, the L1 and L5 signals have different structures in general (Van Dierendonck & AJ Systems 2000). The L5 signal was designed to overcome all the deficiencies of the L1 signal. Intended for safety-of-life applications such as civil aviation, the L5 signal is located in the ARNS band and will bring significant benefits to high-precision users and those interested in increased integrity. The L1 signal has only a data channel, whereas the L5 signal has a pilot channel in addition, for more robust carrier phase tracking. The L5 signal has a minimum signal strength of -154.9 dBW, which is 3.6 dB higher than the minimum power of L1 signal. The L5 signal has a bandwidth that is 10 times larger, which provides the required accuracy in the

presence of multipath and noise. However, with the narrower bandwidth, the L1 C/A code signal requires lower sampling rate which consequently requires lower power at the receiver end, enabling the use of low-cost receivers. Figure 2-8 illustrates the differences in power spectral densities and bandwidth of the L1 and L5 signals.

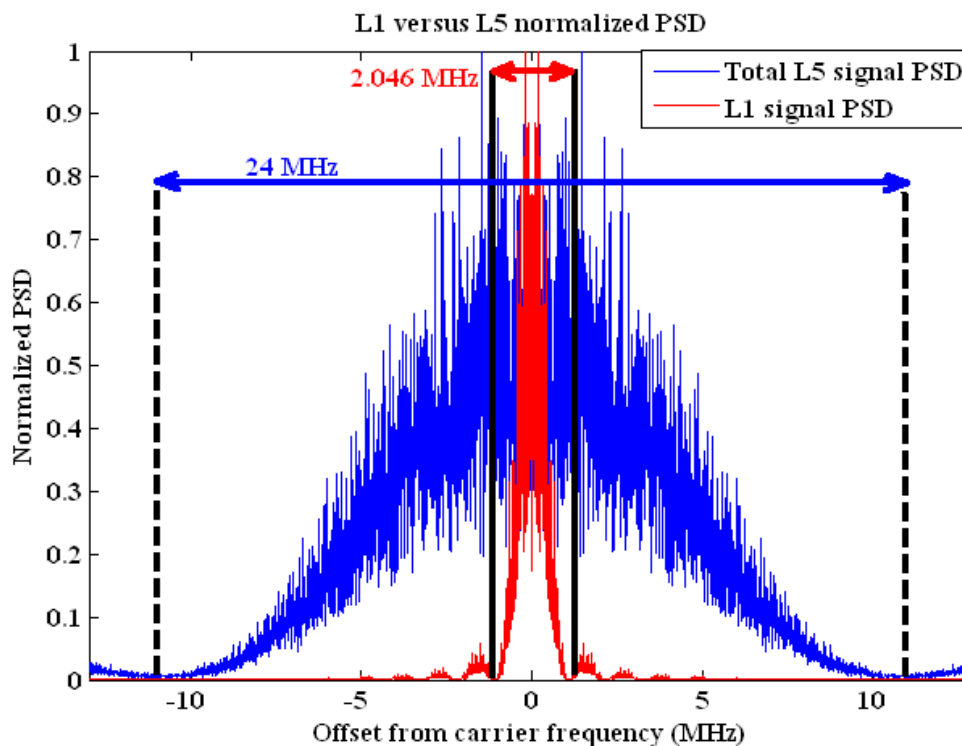


Figure 2-8: L1 and L5 power spectral densities

The L5 signal has improved its code cross-correlation properties by implementing ten times longer primary codes than that of the L1 signal, and by adding the secondary NH codes. Table 2-1 summarizes the main advantages of the L5 signal over the L1 signal.

2.3 Standard Tracking Loops

The thesis focuses on the tracking part in the software receiver. Assuming the acquisition and the bit synchronization of the GPS signal have been achieved, the receiver switches

to signal tracking. For tracking the signal, the receiver generates its local replica of the signal parameters: carrier frequency, and code phase, using the NCO.

Table 2-1 L5 Improvements versus L1 Deficiencies

L1 Deficiencies	L5 Improvements	Advantages
POWER LEVELS		
-158.5 dBW	3.6 dB Higher	Overcome higher interference levels
BANDWIDTH		
2 MHz	24 MHz	Provide required accuracy in presence of noise and multipath
CODE CROSS-CORRELATION PROPERTIES		
Marginal	Improved: •Long primary codes •Secondary Codes	1. Provide better signal integrity 2. Overcome false acquisition problems 3. Decrease susceptibility to interference
SECONDARY CODES		
N/A	NH codes	1. Spread 1 kHz to 50 Hz code spectral lines 2. Improve spectral line components spacing 3. Reduce effect of narrowband interference 4. Reduce space vehicle cross-correlation 5. Provide robust symbol/bit synchronization
CHIPPING RATE		
1.023 MHz	10.23 MHz	1. Provide higher bandwidth efficiency 2. Decrease susceptibility to waveform distortion 3. Provide better accuracy
DATA ENCODING		
N/A	Improved parity/CRC and data encoding	Provide better signal and data integrity

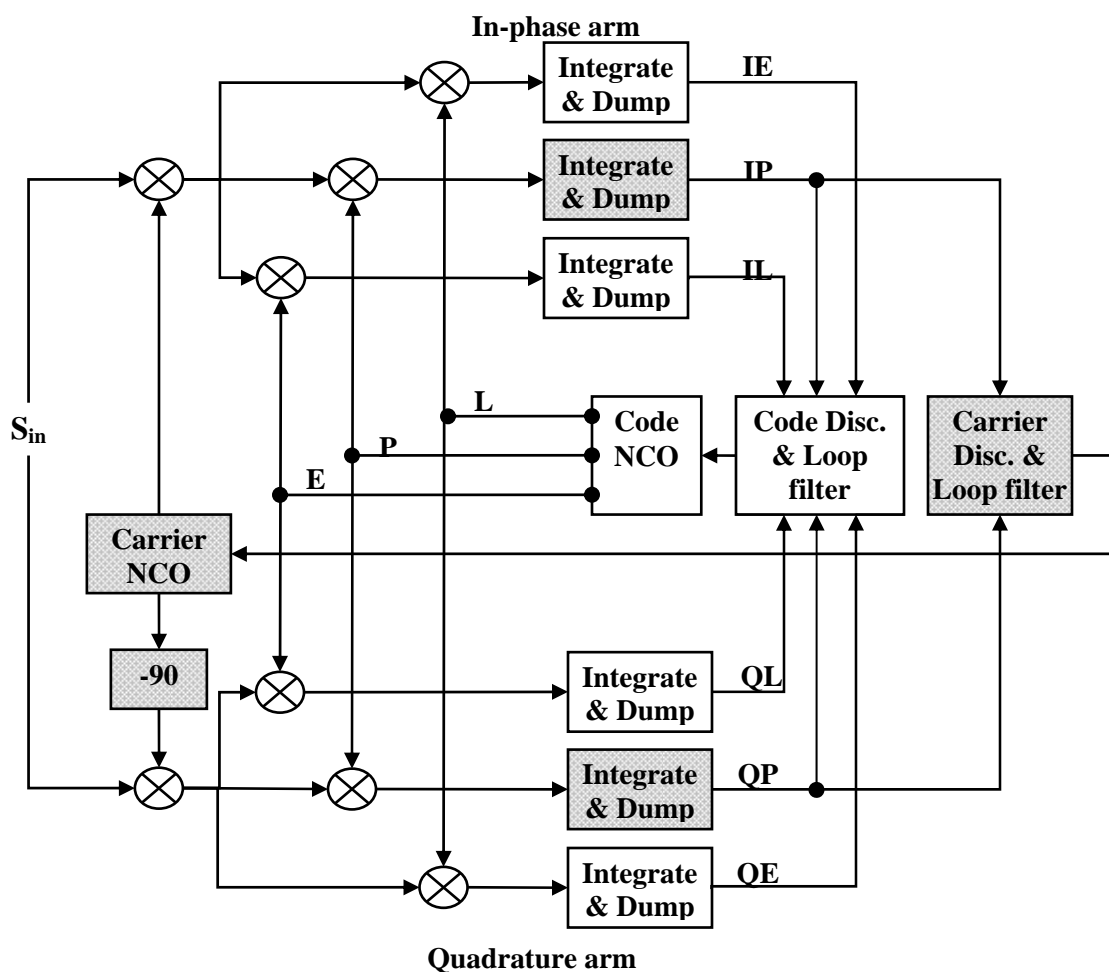


Figure 2-9: Signal tracking loop

Figure 2-9 illustrates the general structure of the tracking loop, including the code tracking (unshaded) and the carrier tracking (shaded). The tracking loop starts with wiping off the carrier frequency by multiplying the incoming signal with the locally generated carrier phase, the in-phase and 90° shifted. The result is then multiplied by the locally generated early, prompt and late code phase. The output is passed to integrate and dump blocks, creating the in-phase and quadrature early, prompt and late (IE, QE, IP, QP, IL, QL) correlator outputs. These correlator outputs pass through the appropriate

discriminator function, and a loop filter to generate the tracking errors. Finally, these tracking errors are applied to the NCO to update the locally generated code phase and carrier frequency.

The architecture described above and illustrated in Figure 2-9 assumes that signal dynamics, tracked by the loop, are of a deterministic nature. The order of the tracking loop comes from the assumption of the type of dynamics the signal is suffering, constant phase, constant frequency or constant acceleration.

Another valid architecture for signal tracking comes from assuming that the signal dynamics follows a linear stochastic model (O'Driscoll & Lachapelle 2009). Details on this type are given in Section 2.4.

2.3.1 L1 Signal Tracking

The L1 signal tracking follows exactly the same architecture as that shown in Figure 2-9. The tracking starts by the L1 carrier frequency wipe-off, followed by the C/A code wipe-off. The output is then integrated and dumped resulting in the correlator outputs. The in-phase and quadrature prompt correlator outputs can be written as

$$\begin{aligned} IP_{L1} &= A_{L1} \cdot N_{L1} \cdot D_{L1} \cdot R(\delta\tau_{L1}) \cdot \cos(\overline{\delta\varphi_{L1}}) \\ QP_{L1} &= A_{L1} \cdot N_{L1} \cdot D_{L1} \cdot R(\delta\tau_{L1}) \cdot \sin(\overline{\delta\varphi_{L1}}) \end{aligned} \quad (2.7)$$

$$A_{L1} = \frac{\sqrt{P_{L1}}}{2} \frac{\sin(\pi\delta f_{L1}T)}{\pi\delta f_{L1}T} \quad (2.8)$$

where IP_{L1} : L1 in-phase prompt correlator output

QP_{L1}	:	L1 quadrature prompt correlator output
A_{L1}	:	Effective amplitude of the L1 signal
N_{L1}	:	Number of accumulated samples for the L1 signal
$R(\delta\tau_{L1})$:	Correlation of the filtered incoming code with the locally generated code for the L1 signal
T	:	Coherent integration time
$\delta\tau_{L1}$:	L1 local code phase error in units of chips
δf_{L1}	:	L1 local carrier frequency error in units of rad/s
$\overline{\delta\varphi_{L1}}$:	L1 average local carrier phase error over the integration interval in units of rad

The average phase errors can be expanded as (Psiaki & Jung 2002)

$$\overline{\delta\varphi} = \delta\varphi_0 + \delta f_0 \frac{T}{2} + \alpha_0 \frac{T^2}{6} \quad (2.9)$$

where α_0 : Phase acceleration in units of rad/s^2

The subscript zero indicates the value at the start of the integration.

The early and late correlators for the two signals have the same parameters, each with early-late spacing (Δ) set to one chip.

2.3.2 L5 Signal Tracking

The L5 signal has two channels, namely the data and pilot channels. Each of the two channels has its own primary and secondary codes. Often the pilot channel is used for tracking the L5 signal, and provides information about the data channel.

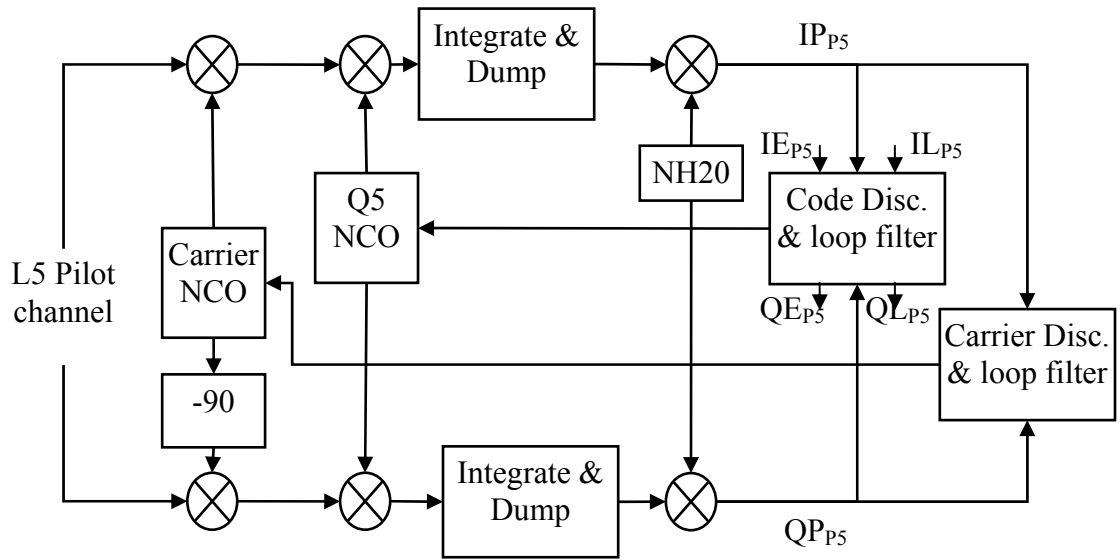


Figure 2-10: L5 pilot channel tracking loop

The pilot channel tracking loop follows a similar structure to that of the general tracking architecture shown before, but an additional step is required to wipe-off the secondary codes, NH20. Figure 2-10 shows the tracking loops for the pilot channel.

The data channel can also be used for tracking the L5 signal, although the advantage of the pilot channel will be lost in that case. The data channel tracking loop would follow the same structure shown in Figure 2-10, with NH10 wiped off instead of NH20.

The in-phase and quadrature prompt correlator outputs for the data and pilot channels are written respectively as

$$\begin{aligned}
 IP_{L5,D} &= A_{L5,D} \cdot D_{L5} \cdot N_{L5,D} \cdot R(\delta\tau_{L5,D}) \cdot \cos(\overline{\delta\phi_{L5,D}}) \\
 QP_{L5,D} &= A_{L5,D} \cdot D_{L5} \cdot N_{L5,D} \cdot R(\delta\tau_{L5,D}) \cdot \sin(\overline{\delta\phi_{L5,D}})
 \end{aligned}
 \tag{2.10}$$

$$\begin{aligned}
IP_{L5,P} &= A_{L5,P} \cdot N_{L5,P} \cdot R(\delta\tau_{L5,P}) \cdot \cos(\overline{\delta\varphi_{L5,P}}) \\
QP_{L5,P} &= A_{L5,P} \cdot N_{L5,P} \cdot R(\delta\tau_{L5,P}) \cdot \sin(\overline{\delta\varphi_{L5,P}})
\end{aligned} \tag{2.11}$$

$$A_{L5,D} = A_{L5,P} = \frac{\sqrt{P_{L5}}}{2} \frac{\sin(\pi\delta f_{L5}T)}{\pi\delta f_{L5}T} \tag{2.12}$$

- where
- IP_{L5} : L5 prompt in-phase correlator output
 - QP_{L5} : L5 quadrature correlator output
 - A_{L5} : Effective amplitude of the subscribed channel
 - N_{L5} : Number of accumulated samples of the subscribed channel
 - $R(\delta\tau_{L5})$: Correlation of the filtered incoming L5 code with the local generated code for the subscribed channel
 - $\delta\tau_{L5}$: L5 local code phase error in units of chips, for the subscribed channel
 - δf_{L5} : L5 local carrier frequency error in units of rad/s, for the subscribed channel
 - $\overline{\delta\varphi_{L5}}$: L5 average local carrier phase error over the integration interval in units of rad, for the subscribed channel

2.3.2.1 L5 data and pilot combination

Even though the pilot channel is designed for providing a reliable tracking performance, the idea of making use of the total signal power is still appealing. Several work in the literature have introduced the idea of combining the data and pilot at different stages of the tracking loop: the discriminator output, the loop filter output or the correlator output. The method used in the thesis, introduced by Mongrédien (2008), is to use both the combined data and pilot correlator outputs in order to produce the carrier phase error.

With the NH alignment performed at that point, the data and the pilot correlator outputs are either aligned or out of phase as shown in Figure 2-11.

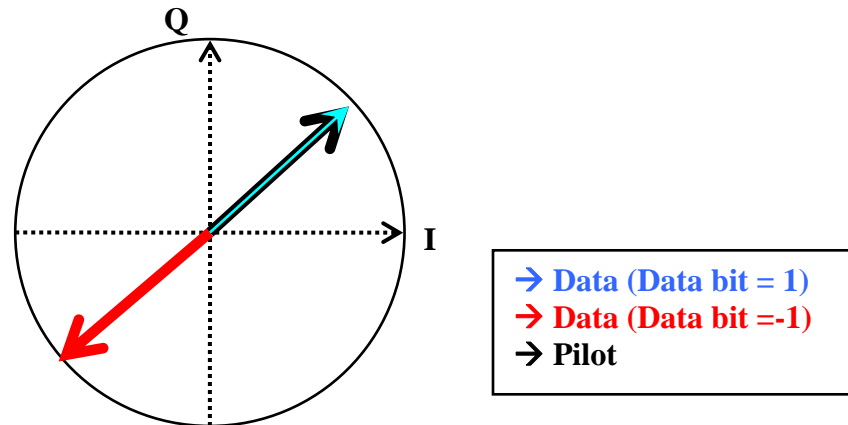


Figure 2-11: Data and pilot coherent combining

$$\Psi_{comb} = \Psi_{pilot} + \text{sign}(D_{L5})\Psi_{data} \quad (0.13)$$

where Ψ : Correlator output for the subscribed channel

2.3.3 Carrier Tracking Loops

The carrier tracking loop tracks the carrier frequency and phase. Depending on the discriminators, the loop can be a phase lock loop (PLL), a Costas PLL (PLL that tolerates the presence of data), or a frequency lock loop (FLL). Often in GPS signal tracking, the carrier tracking loop would start by frequency tracking, where an FLL is used. After frequency lock is achieved and ensured, the carrier tracking switches to phase tracking. A PLL is used in this case.

2.3.3.1 Frequency Tracking

An FLL is less sensitive to dynamic stress as compared to a PLL (Ward et al 2006a). The FLL generates the carrier frequency replica to wipe-off the incoming one. Therefore, the FLL discriminators have to be insensitive to the phase of the incoming signal. That is why the FLL is often used at the beginning, when the data transition boundaries are often unknown.

2.3.3.2 Phase tracking

The phase tracking loop wipes off both the carrier frequency and the carrier phase from the incoming signal, and produces phase error estimates at its output. Both kinds of phase tracking loops (PLL, Costas PLL) are more accurate (less noisy) compared to the FLL but far more sensitive to the dynamic stress. The phase tracking is of a special concern in the thesis, since it is one of the criteria used for analyzing the proposed Kalman filter performance. More details on the phase tracking loop is presented in Chapter 4.

2.3.4 Code Tracking Loops

The code tracking loops are often implemented using a delay lock loop (DLL). As illustrated in Figure 2-9, the DLL uses three correlators, namely the prompt, early and late, to estimate the code error. Although the carrier phase tracking loop is vulnerable to the phase changes in the signal, the code tracking loop thermal noise is larger than that of the carrier tracking loop (Ward et al 2006a). The code tracking loop is often aided by the carrier tracking loop, where the Doppler frequency estimate from the carrier tracking loop is scaled and used as external aiding to code tracking loop at the loop filter output.

2.3.5 Standard Tracking Loops Parameters

The tracking loops are characterized by three parameters: the predetection integration time, the loop discriminators and the loop filters.

2.3.5.1 Predetection integration time

The predetection integration time plays a critical role in the tracking loop. Increasing integration helps in gathering of more information and power of the signal, but there is always a risk that the signal dynamics might be changing during the integration interval.

The predetection integration time also determines the update rate of the loop.

Apart from the dynamics, the integration period of the L1 signal is limited due to the existence of the data bits. The duration of the data bits is 20 ms, which imposes a maximum limit over the integration period that can be used. The L5 signal does not always have this problem. Having implemented a pilot channel together with the data channel, this pilot channel can be used for tracking the L5 signal, without having to consider bit duration.

2.3.5.2 Loop discriminators

The loop discriminators define the type of the carrier tracking loops, whether FLL, PLL or Costas PLL. For the data channel, the discriminator sensitivity to any 180° phase jumps is of concern, whereas the pilot channel allows the use of a pure PLL.

In general, the loop discriminators are often characterized by their normalization requirements, as this may be significant in low signal power cases where the signal power

estimation may not be accurate. In addition, they are characterized by their computational burden and their response under Gaussian noise (Julien 2005). Ward et al (2006a) shows several FLL, PLL and DLL discriminators, and their associated characteristics.

2.3.5.3 Loop filter

The loop filter used in the tracking loops is one of the key factors in enhancing tracking loop performance. It reduces the noise in the loop in order to produce an accurate estimate. The loop filter is determined by the following parameters: **filter order and noise bandwidth** (Ward et al 2006a).

Filter order: It depends on the dynamics of the user, where the first order filter is sensitive to the velocity stress, second order is sensitive to acceleration stress, and third order is sensitive to jerk stress. In the case of a frequency tracking loop, the loop filter used is of a second degree, as a delay element has already been used to calculate the frequency of the signal. In the case of the phase tracking loop, the loop filter used is often of a third degree, in order to be capable of tracking the user dynamics, even if the user is accelerating. The dynamics taken into consideration also involve oscillator errors and ionospheric errors. On the other hand, in the code tracking loop, the loop filter is often of a first degree. Since it is aided by the carrier tracking loop, most of the dynamics are already absorbed, and the code tracking loop estimates only code errors due to ionospheric divergence.

Bandwidth (B): The loop filter bandwidth defines the permissible level of noise allowed in the tracking loop. It is a tradeoff between decreasing the bandwidth to decrease the

noise level and consequently decreasing the estimated errors, and increasing the bandwidth to decrease the convergence time and to be less sensitive to dynamic stress errors.

2.3.5.4 Limitation on BT product

The loop filters used in the tracking loops are a digital conversion of the traditional analog filters. This conversion is done under a condition that the multiplication of the bandwidth and the coherent integration time (BT) is much less than one ($BT \ll 1$). Increasing the integration time while keeping the bandwidth constant violates this condition and this imposes a limitation on the integration time. Due to the limitation of the BT multiplication discussed, Stephens & Thomas (1995) proposed a new loop filter design in the digital domain where the loop filter constants are determined for each value of the BT. This implementation allows a stable loop with a BT product less than 0.4 for the phase rate only feedback. Still for high sensitivity applications, longer coherent integration times are required. Kazemi (2008) has proposed complete implementation of the loop filters in the digital domain, thus the coherent integration time can be extended to reach a BT value up to three.

2.4 Kalman Filter Tracking

The Kalman filter tracking assumes the GPS signal dynamics follow a linear stochastic model. The Kalman filter will be discussed in detail in Chapter 4; only an overview of how the tracking works in this case is given here.

The Kalman filter is used to estimate a set of states. It undergoes two major steps: the prediction step, where the states are propagated and the update step, where the states are updated using the new available information from measurements. It uses two models: the state space model, which includes the dynamic models of the states to be estimated, and the measurement model, which carries the new information to be used in the update (Gelb 1974).

In the state space model, the states to be estimated for GPS signal tracking can include the amplitude of the signal and the tracking errors: the code phase error, the carrier phase error, and the frequency error. In order to develop the dynamic model of these states, the process noise is used. The process noise models the errors in the assumed dynamics model. These errors include the line of sight signal dynamics, the signal level variations, the code and carrier ionospheric error divergence, the multipath, and the receiver oscillator jitter effects.

The measurement model, on the other hand, includes the information used to update these states. Two possible measurement models can be used in the context of GPS Kalman filter tracking. The first option is to use the code and carrier discriminators as measurements, where the Kalman filter replaces the loop filters (Figure 2-12). The second option is to use directly the correlator outputs, where the Kalman filter replaces both the code and carrier discriminators and loop filters. In the first case, the Kalman filter is linear, and no more modifications are required, whereas in the second step the Kalman filter is nonlinear and has to be adapted as shown in Figure 2-13.

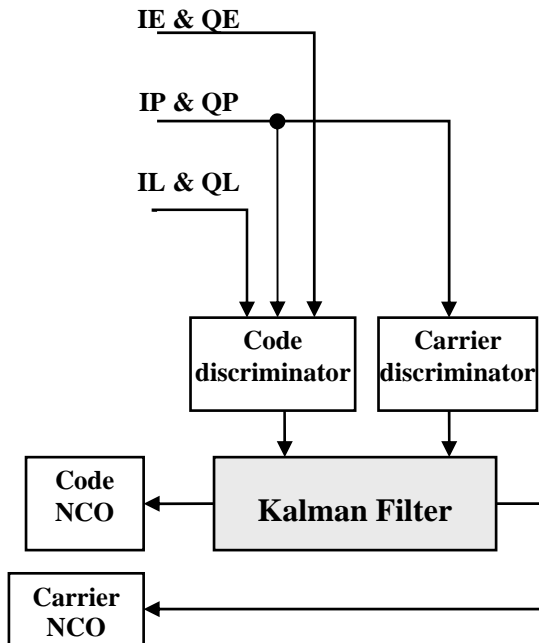


Figure 2-12 Kalman filter measurement model- option 1

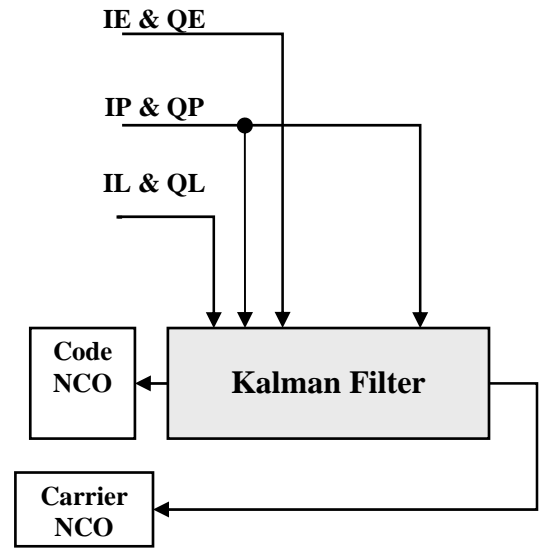


Figure 2-13 Kalman filter measurement model- option 2

In order to tune a Kalman filter, two parameters have to be adjusted: the measurements covariance matrix R and the process noise covariance matrix Q . The measurement covariance matrix reflects the quality of the new information, whereas the process noise covariance matrix reflects the expected dynamics in each of the corresponding states.

2.5 Tracking Performance Evaluation

In order to evaluate any signal tracking performance, the lock indicators are used. They are implemented to determine code, phase or frequency lock. The phase and frequency lock indicators inherently contain the code lock information, thus more focus is given to them as follows.

2.5.1 Phase Lock Indicator

The phase lock can be detected using the normalized estimate of the cosine of twice the carrier phase. The phase lock indicator (PLI) can be written as (Van Dierendonck 1996)

$$PLI = \frac{NBD_k}{NBP_k} \quad (2.14)$$

Assuming no external disturbance, the PLI can be approximated as

$$PLI \approx \cos(2\delta\phi) \quad (2.15)$$

and

$$NBD_k = \left(\sum_{i=1}^M IP_i \right)_k^2 - \left(\sum_{i=1}^M QP_i \right)_k^2 \quad (2.16)$$

$$NBP_k = \left(\sum_{i=1}^M IP_i \right)_k^2 + \left(\sum_{i=1}^M QP_i \right)_k^2 \quad (2.17)$$

where M : Coherent integration period

The values of the lock indicator will range from -1, where the locally generated signal is completely out of phase with the incoming signal, and 1 that indicates perfect match.

2.5.2 Frequency Lock Detector

The frequency lock can be determined using two consecutive samples of both the in-phase and quadrature correlator outputs. The frequency lock indicator (FLI) used is given as (Mongrédien 2008)

$$FLI = \frac{cross^2 - dot^2}{cross^2 + dot^2} \quad (2.18)$$

Assuming no external disturbance, the FLI can be approximated as

$$FLI \approx \cos(4\pi\delta f_k T) \quad (2.19)$$

and

$$\begin{aligned} \dot{dot} &= IP_{k-1}IP_K + QP_{k-1}QP_K \\ \dot{cross} &= IP_{k-1}QP_K - IP_kQP_{K-1} \end{aligned} \quad (2.20)$$

Similar to the PLI, the values of this lock indicator ranges from -1 to 1. Note that both indicators are often averaged to reduce their variances.

2.6 Tracking Errors

Before attempting to combine the two signals, the relationship between their tracking parameters has to be found. Two important parameters in a tracking loop are the code and carrier Doppler frequencies. The carrier Doppler frequency is defined as the frequency offset due to relative motion between the satellite and the receiver. It is a function of both the relative velocity and the carrier frequency (Ioannides et al 2006)

$$f_{Doppler} = f_{carrier} \left(\frac{c}{c + v_{rel}} \right) \quad (2.21)$$

where $f_{Doppler}$ $\dot{}$ Doppler frequency
 c $\dot{}$ Speed of light ($c=299,792,485$ m/s)
 v_{rel} $\dot{}$ Relative velocity between the satellite and the receiver

Thus, the ratio of the Doppler frequencies of the L1 and L5 signals is the same as the ratio between their carrier frequencies. The same applies to the code Doppler as follows:

$$\frac{f_{Doppler,L1}}{f_{Doppler,L5}} = \frac{f_{carrier,L1}}{f_{carrier,L5}} = \frac{1575.42 \text{ MHz}}{1176.45 \text{ MHz}} \quad (2.22)$$

$$\frac{f_{codeDoppler,L1}}{f_{codeDoppler,L5}} = \frac{f_{code,L1}}{f_{code,L5}} = \frac{1.023 \text{ MHz}}{10.23 \text{ MHz}} \quad (2.23)$$

where $f_{codeDoppler}$: Code Doppler of the subscribed channel

f_{code} : Code chipping rate of the subscribed channel

This ratio is valid under the following two conditions:

- 1) The same satellite is transmitting both signals to guarantee the same relative velocity
- 2) The same oscillator is used at the receiver to generate the local frequencies.

This ratio is maintained even given the fact that each of the two signals is affected by the ionosphere in a different manner if low ionospheric activity is available (Ioannides et al 2006 and Ries et al 2002). Throughout the thesis work, it is assumed that the ionospheric Doppler drift is lower than 50 Hz, the minimum predetection bandwidth of L1.

2.7 Summary

The chapter gave an overview of the L1 and L5 signal structures. These were presented and the main differences between the two signals were outlined. In addition, two different techniques of signal tracking, the standard tracking loops and the Kalman filter tracking, were presented.

The next chapter describes the software developed and simulation tools used for analyzing and testing the proposed models in the thesis. Moreover, the different error

sources that can affect the GPS tracking, and the methods by which they are simulated will be discussed.

Chapter Three: SIMULATION TOOLS AND SOFTWARE RECEIVER

On April 10th 2009, the first L5 demonstration payload was transmitted from the IIR(M)-20 satellite (SVN 49). As discussed in the introduction, this signal is just for demonstration purposes, and thus there is no guarantee on its quality. Taking this into consideration, and in order to test the proposed tracking methods, a GPS signal simulator is required. This chapter discusses the general simulation setup, and then goes into the details of both the hardware and software stages of the receiver. The second part of the chapter presents an overview of the GPS error sources, and methods of their simulation or modelling.

3.1 GPS Simulation Setup

Given the fact that only one GPS satellite is currently transmitting the L5 signal in testing mode, usage of an L5 signal simulator is required to collect the raw data samples required as input to the software receiver. The test setup is divided into two major stages: hardware and software. The hardware component consists of a Spirent GSS7700 signal simulator, and a National Instruments front-end. The output of this stage is a pair of streams of intermediate frequency (IF) samples, which are subsequently passed to the software receiver for acquisition and tracking. Figure 3-1 shows the setup of the experiment used.

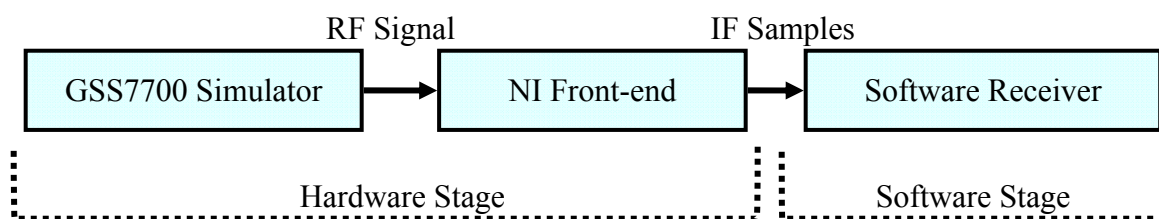


Figure 3-1: Experimental setup

3.2 Hardware Stage

The hardware stage starts by simulating the two signals using the Spirent GSS7700 simulator whose output is then passed to the National Instrument front-end.

3.2.1 Spirent GSS7700 Simulator

The Spirent GSS7700 simulator (Spirent 2006), shown in Figure 3-2, was used to generate both L1 and L5 signals under the same conditions. The various simulation parameters are discussed later in Section 3.4. The radio frequency (RF) output of the simulator is passed to the front-end.



Figure 3-2: GSS7700 Spirent signal simulator

3.2.2 National Instrument Front-end

The front-end consists of two National Instruments PXI-5661 RF vector signal analyzers (VSAs) that can be synchronized to acquire two different signals. Each VSA has an internal Oven Controlled Crystal Oscillator (OCXO) onboard, or can be driven by an external oscillator. For the tests described herein, both VSAs were driven by a common oscillator, leading to synchronous samples. However, each VSA uses a separate PLL to drive the down-converters and, hence, there is an unknown but constant phase offset between the two data streams. This phase offset introduces an extra step in the software receiver to allow for the alignment of the samples. The output of the front-end is a pair of IF data sample streams, which are then processed by the software receiver.

Figure 3-3 shows the hardware configuration of the NI (top) and the software developed in the Position, Location And Navigation (*PLAN*) group to acquire the IF samples (bottom).

Different sampling frequencies are required for both L1 and L5 signals to account for the difference in their bandwidths. Since the L5 signal bandwidth is 10 times that of the L1 chosen and a higher sampling frequency is required for the L5 signal. This difference in the sampling frequencies introduces a phase offset between the two signals and has to be compensated in the software stage of the receiver.

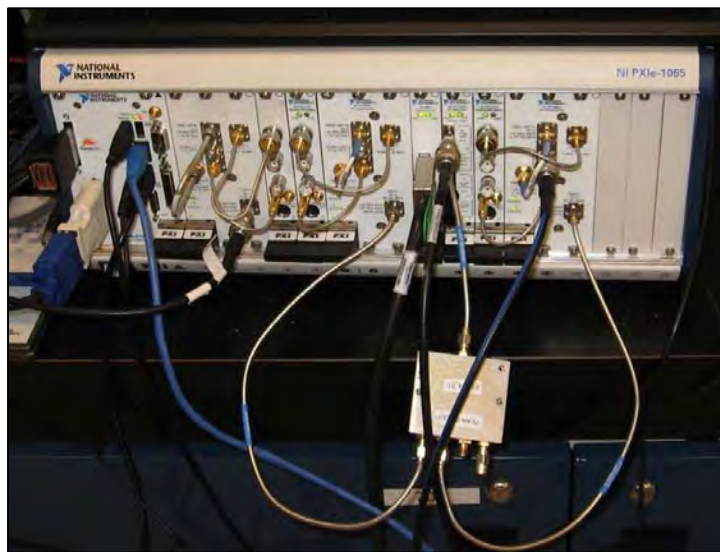


Figure 3-3: NI Front-end

3.3 Software Stage

The proposed algorithms are implemented in a software receiver, thereby enabling rapid prototyping and debugging. Figure 3-4 shows the flowchart of a one-channel software receiver.

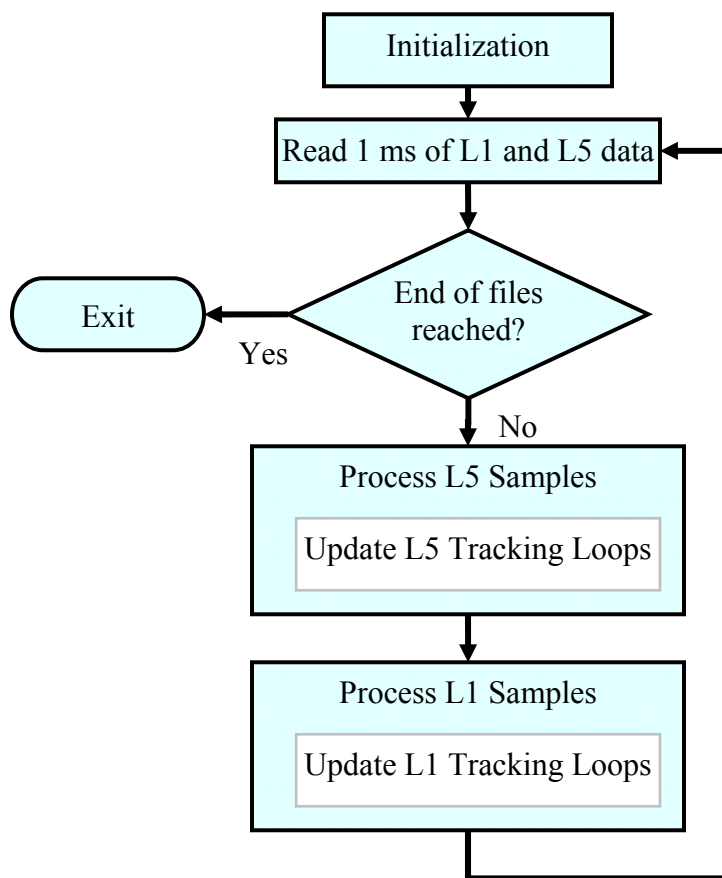


Figure 3-4: L1-L5 Tracking flow diagram

First, an initialization step is done to put the L1 and the L5 data in a usable format and to acquire the L1 signal. The data of both signals are loaded from the data files in 1 ms sets. The next step is the processing of the L5 channels, and that includes a call to the loop update function when appropriate. The following step is the processing of the L1 channel, which includes a call to the L1 loop update functions.

Table 3-1 shows the software initialization steps. The two columns of the table correspond to the initialization of the L1 and the L5 signals respectively.

Table 3-1 Software initialization steps

L1 Initialization	L5 Initialization
DATA PREPARATION	
1.Read L1 Data Samples 2.Convert into two separate I and Q files	1.Read L5 Data Samples 2.Convert into two separate I and Q files
ACQUISITION	
1.Acquire L1 signal 2.FLL tracking for carrier frequency 3.Set status to Bit synchronization	1.Acquire L5 signal 2.PRN-only tracking step using FLL tracking for carrier frequency 3.Set status to Bit synchronization
Align the two signals using information from the acquisition step	
BIT SYNCHRONIZATION	
1.Do Bit synchronization (Histogram method) 2.Set status to Tracking	1.Do a fine acquisition step (NH20 correlation) 2.Set status to Tracking
By this step	
1.Both signals are aligned 2.Both signals are bit-synchronized	

For both signals, the data is first converted to a usable format by the software receiver. It is converted to two separate in-phase samples and quadrature samples files for each signal.

For the L1 signal, an acquisition step is done to get a rough estimate of the Doppler frequency and the code shift in samples. On the other hand, a course acquisition step is first performed to acquire the primary codes of the L5 signal. Based on the acquisition

step, an alignment of the samples of the two signals is carefully done to allow for the combination.

The status of the L1 channel is then set to bit synchronization. The histogram method is used to perform the bit synchronization on L1 (Van Dierendonck 1996). To that end, the L1 signal is acquired and bit-synchronized. The status is then set to tracking.

For the L5 signals, an intermediate step (PRN-only tracking) is included to track the primary codes (PRN) before acquiring the secondary codes. The details of that step are discussed later in the following sections. Then a fine acquisition step is performed to acquire the NH codes. When the primary and the secondary codes are successfully acquired, the status is set to tracking.

Each of the acquisition, bit synchronization and tracking stages are described in the following sections.

3.3.1 L1 and L5 Acquisition

The second step in the initialization procedure shown in Table 3-1 is the acquisition of both signals. The Fast Fourier Transform (FFT) method is used to acquire both signals. Since the acquisition is not the main objective of the thesis, a strong signal is often simulated at the beginning to speed up both the acquisition and bit synchronization steps. Figure 3-5 shows the L1 acquisition for PRN 12, with carrier to noise ratio (C/N_0) of 46 dB-Hz. The integration interval is 10 ms.

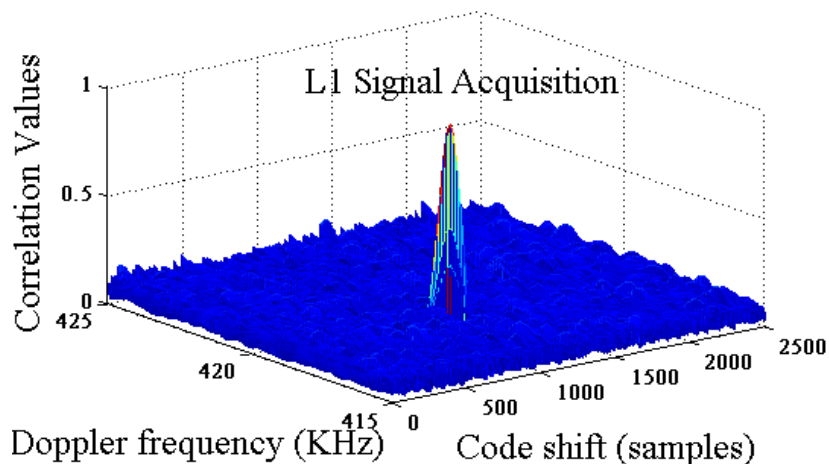


Figure 3-5: L1 signal acquisition

For the L5 signal, the acquisition step aims at acquiring only the primary codes, where the pilot channel is used. This part is often referred to as the coarse-acquisition. The NH code acquisition comes later in the context of bit synchronization.

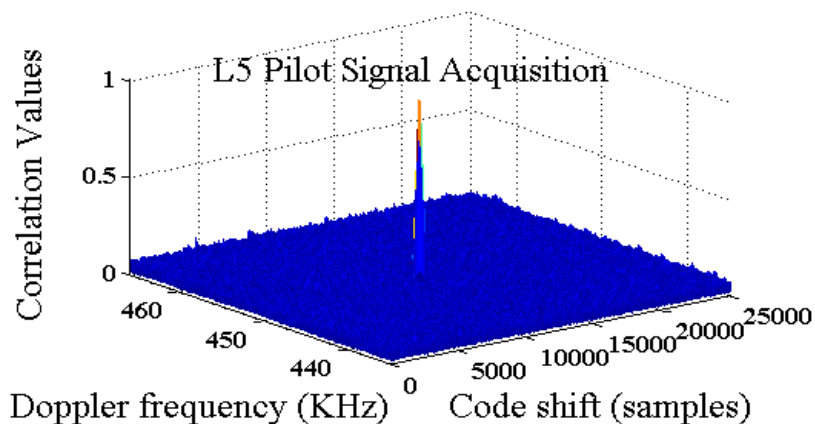


Figure 3-6: L5 signal acquisition

Figure 3-6 shows the L5 pilot signal acquisition for PRN 12, with C/N_0 of 49 dB-Hz, and the same integration interval. Note that in that figure, a 1 ms coherent integration and

10 ms non-coherent integration times were used which justified the non existence of the NH transitions.

3.3.2 L1 and L5 Bit Synchronization

Both signals require different approaches when dealing with the bit synchronization. In case of the L1 signal, prior to the bit synchronization, a PRN tracking is performed using 10 ms FLL tracking to minimize the frequency errors. When the frequency tracking loop locks on the L1 frequency, the bit synchronization is initialized. A histogram approach is used (Van Dierendonck 1996):

1. A cell counter K_{cell} runs from 0 to 19
2. Each sensed sign change is recorded by adding one to the corresponding K_{cell}
3. The process continues till:
 - i. Two cell counts exceed threshold NBS_2
 - ii. One cell count exceeds threshold NBS_1

Threshold NBS_1 and NBS_2 are calculated as in *ibid* depending on the Signal to Noise Ratio (SNR) and the bit synchronization time interval.

For the L5 signal, the direct combined acquisition of both L5 PRN and NH codes is not efficient when the Doppler residual is larger than 30 Hz. In order to minimize frequency errors, a PRN tracking step, suggested by Macabiau et al (2003), is implemented using 1 ms FLL tracking prior to the NH acquisition. After this PRN tracking, the NH acquisition is performed. The NH acquisition, or fine acquisition, determines the bit edge

based on correlating the incoming signal with the locally generated NH code at the receiver. The pilot channel is chosen for this step in order to avoid any unknown bit transitions on the data channel. A good 13.5 dB isolation between the main peak and the secondary peak can be obtained as shown in Figure 3-7.

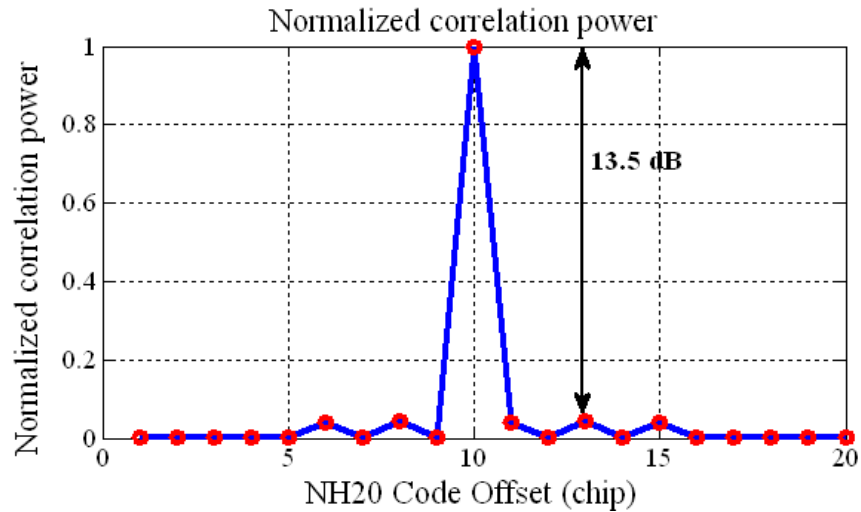


Figure 3-7: NH20 normalized correlation power

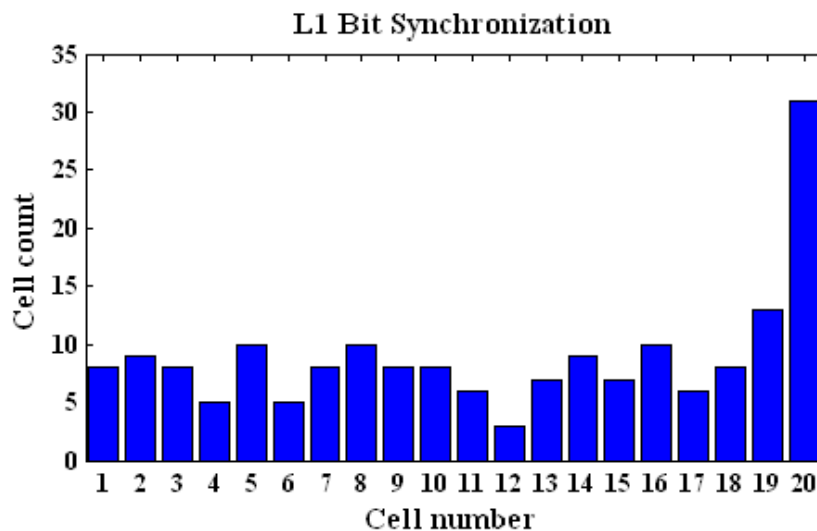


Figure 3-8: L1 bit synchronization

The results of the L1 bit synchronization is shown Figure 3-8 and L5 bit synchronization in Figure 3-9.

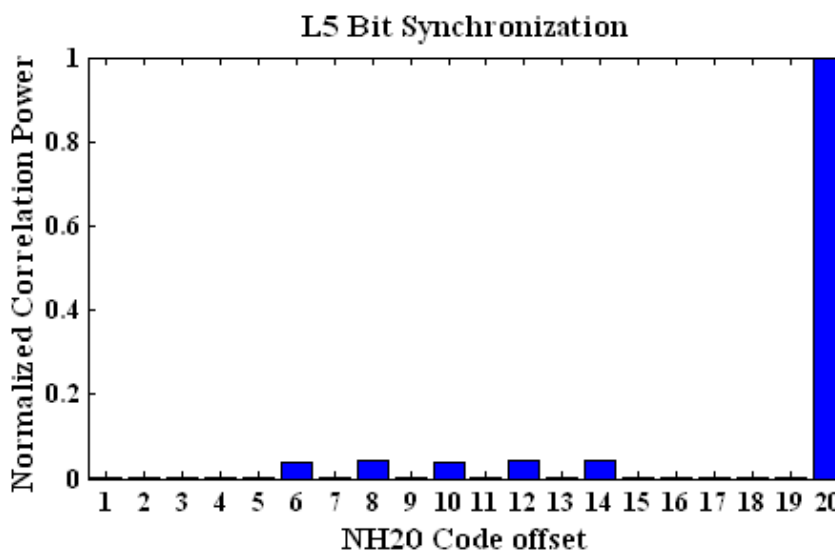


Figure 3-9: L5 bit synchronization

3.3.3 L1 and L5 Tracking

The theoretical steps for tracking the two signals were discussed in Chapter 2. However, in order to understand how tracking works in the software receiver, a description of the software flowchart is presented hereafter. The L1 tracking part falls in the “Process L1 Samples” box, including the “Update Tracking Loops”, shown in Figure 3-4, and similarly for L5. Figure 3-10 zooms into this box, and shows how the samples are really processed. The receiver starts by computing the next code rollover. The channel processes the samples up to the next code rollover or to the end of the remaining samples. If it is the time for the rollover, a Doppler removal and correlation update is performed. A check is also performed to see whether it is time for the loop update or not, this is configured by setting the coherent integration number in the initialization of the software.

When the accumulation period equals to the tracking loop update period, the tracking loops are updated.

The difference between the L1 and L5 processing is in both the correlator update function and the loop update function, L5 having primary and secondary codes that have to be taken into consideration in this update, and L1 having only the C/A code.

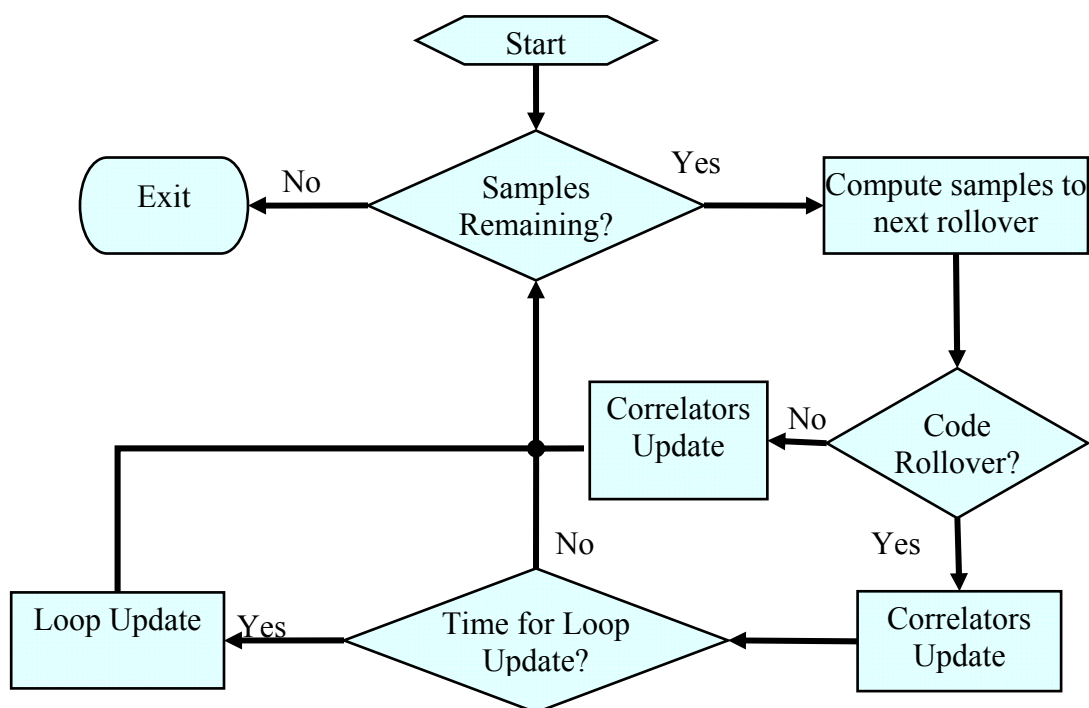


Figure 3-10: Flow chart for single channel tracking

3.4 GPS Errors Simulation

In order to evaluate the proposed models, the error sources encountered by the simulated GPS signals have to be studied and taken into consideration. The error sources, as discussed before, can be grouped as follows:

a) Satellite-based errors: Errors in the parameter values broadcast by the satellite in the navigation message. These parameters can be set in the GSS7700 simulator.

- Ephemeris (orbital errors)
- Satellite clock

b) Propagation errors: The medium through which the GPS signal travels from the satellite to the receiver

- Ionospheric and tropospheric delay
- Ionospheric scintillation

c) Receiver-based errors: Errors resulting from signal power, code structure and receiver design

- Multipath and shadowing
- Receiver noise induced by the tracking loops (e.g. thermal noise jitter)
- Signal power degradation
- Oscillator stability

Typically, the propagation-induced errors have the highest impact on the positioning performance, followed by the receiver-induced errors (Misra & Enge 2001). A comprehensive description of these errors can be found in the literature (Misra & Enge 2001, Conley et al 2006 and Watson 2005). For the current work, a brief review of some of these errors is given below with a focus on the simulations needed.

3.4.1 Propagation Errors

GPS signals are affected by the medium through which they travel. In free space, the signal travel with the constant speed of light. However, closer to the surface of the Earth,

at a height of 1000 km, the signal travels through an electrically charged atmosphere, called the *ionosphere*. Later, at a height of 60 km, the signal again experiences an electrically neutral atmosphere, namely the *troposphere*. Due to the medium change, the signal undergoes a corresponding change in its propagation velocity, namely *refraction*, which in turn affects the signal's transit time. Figure 3-11 shows the refraction of the GPS signal when it enters the atmosphere.

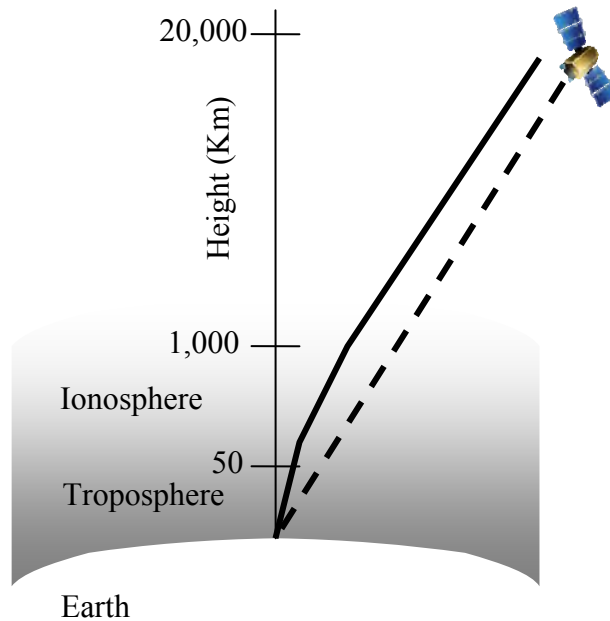


Figure 3-11: Refraction of GPS signals in the earth's atmosphere (Misra & Enge 2001)

3.4.1.1 Ionospheric delay

The ionosphere is a dispersive medium located in the region of atmosphere between 70 km and 1000 km above the Earth's surface. It consists of ionized gases (free electrons and ions). The electron density changes by one or two order of magnitudes between day

and night, where it peaks at 2 p.m. The delay introduced by the ionosphere depends on the number of the free electrons in the signal's path, defined as the *total electron content* (TEC), as given in Equation 2.1. The presence of these free electrons is related to the solar radiation, and thus the ionospheric errors vary according to the solar cycle by a factor of 3. The typical undifferenced measurement error due to the ionosphere is averaging about 15 m for a zenith satellite and can increase by a factor of 3 near the horizon (Lachapelle 2007).

The GSS7700 simulator has several options for modelling of the ionospheric delay:

1. **Modelled:** Either GPS ionospheric model area is enabled, terrestrial, spacecraft or a switched model.
 - a. **Terrestrial:** uses the Klobuchar ionospheric model to determine the ionospheric delay.
 - b. **Spacecraft:** uses an ionospheric model that takes account of the reduction in the ionization level with increasing height in the ionospheric layer.
 - c. **Switched:** Enables switching from the terrestrial model to the spacecraft model automatically on transition through a defined height. This height is the altitude you switch from using the terrestrial model to using the spacecraft model. This altitude is nominally the lower edge of the ionospheric layer.
2. **Fixed:** Ionospheric delay is set to a fixed number.
3. **Off:** Sets the Ionospheric delay to zero.

Throughout the thesis simulations, ionospheric activity is modelled using the default terrestrial Klobuchar model, i.e. a normal ionospheric activity is assumed.

3.4.1.2 Tropospheric delay

The troposphere is an electrically neutral gaseous atmosphere. It consists of two components: dry and wet. The dry component extends to a height of 40 km above the Earth, whereas the wet component extends to a height of 10 km (Conley et al 2006). The typical undifferenced measurement error due to the tropospheric effect is approximately 2.4 m for a zenith satellite and can increase to 19.3 m for a satellite at a 15° elevation (Lachapelle 2007). The tropospheric errors are proportioned approximately 80-90% for the dry term and 10-20% for the wet term, however the dry term can be predicted using the troposphere models by accuracy better than only 1%, whereas the wet term can be predicted by accuracy of 10-20%.

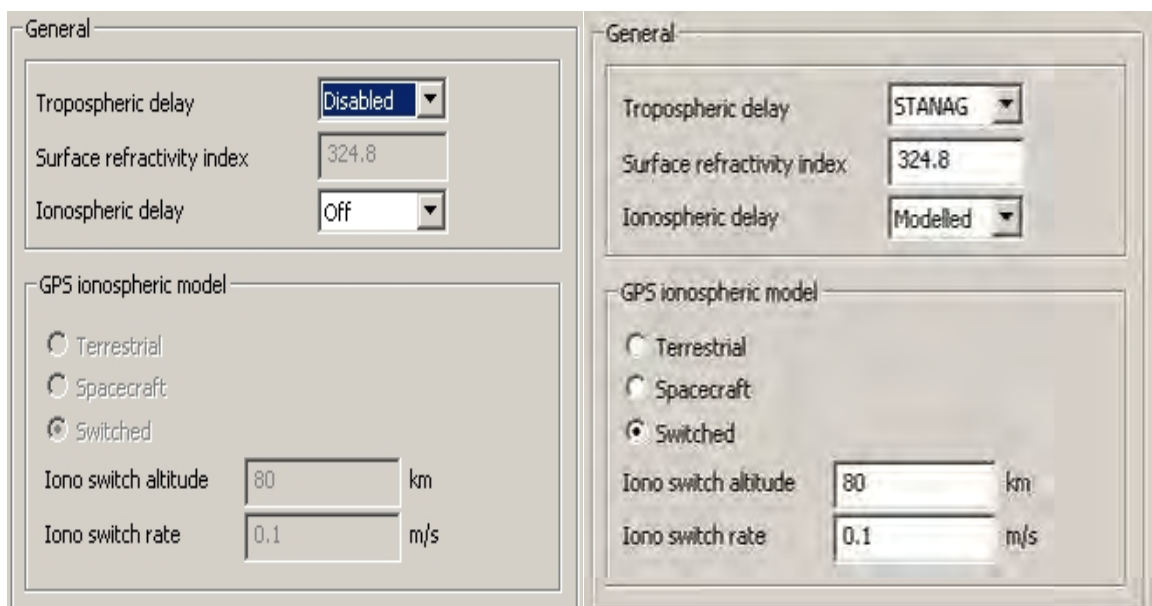


Figure 3-12: Simulating atmospheric (ionospheric and tropospheric) errors

For the tropospheric delay, the options in the GSS7700 simulator are:

1. **STANAG:** It enables surface refractivity index (at Mean Sea Level).
2. **Disabled:** The model sets tropospheric delay to zero.

Figure 3-12 shows the setup required for simulating the ionospheric and tropospheric errors, where the left shows the atmospheric errors disabled and the right figure shows the atmospheric errors simulated.

3.4.2 Receiver-based Errors

These errors are grouped to include those incurred in the receiver measurement process. The first set is the receiver-induced errors, and these depend on the design of the receiver's tracking loops, the oscillator stability, the antenna design, etc. The tracking loops induced errors will be discussed in detail in the next chapters. The antenna design is out of the scope of this thesis. The second set includes the multipath errors and the degraded signal power.

3.4.2.1 Oscillator stability

The receiver oscillator instabilities can cause errors on the phase as well as the code measurements, causing a range of dynamics that should be tracked by the tracking loops. Thus, an adequate model for the receiver oscillator used should be used to account for these instabilities. The oscillator models have been studied extensively in the literature, e.g. Brown & Hwang (1992), Winkel (2000) and Watson (2005). The one-sided spectral density of the fractional frequency fluctuation is defined as (Winkel 2000)

$$S_y(\omega) = \frac{2\pi^2 h_{-2}}{\omega^2} + \frac{\pi^2 h_{-1}}{\omega} + \frac{h_0}{2} \quad (3.24)$$

- where
- $S_y(\omega)$: One sided spectral density of the fractional frequency fluctuation
 - y : $\frac{\delta f}{f}$
 - δf : Absolute frequency deviation
 - f : Nominal frequency of oscillator
 - h_0 : White frequency noise
 - h_{-1} : Flicker frequency noise
 - h_{-2} : Random walk frequency noise

The spectral density formula shown in Equation 3.24 consists of three distinct segments, the white frequency noise, flicker noise and integrated frequency noise. In modelling the oscillator error in the receiver software tracking loops, only the white frequency noise and integrated frequency noise are taken into consideration. The flicker noise, however, cannot be modelled exactly with a finite-order state model, and thus it is completely ignored (Brown & Hwang 1992).

The Allan variance deviation θ_A is a common measure of oscillator stability. It is based on the instantaneous fractional frequency deviation, and is expressed in terms of the clock parameters h_0, h_{-1}, h_{-2} (Irsigler & Eissfeller 2002).

An OCXO is used for NI synchronized front-end (NI PXI-5661 2006). Three different OCXO models, from Brown & Hwang (1992), Mongrédien (2008) and Winkel (2000) respectively, were tested to determine the differences between the Doppler frequency tracking.

Table 3-2 shows the models tested. The Allan deviation oscillator jitters for these models are also calculated for the third order PLL using the same parameters as shown in Equation 3.25 (Irsigler & Eissfeller 2002) and plotted in Figure 3-13:

$$\theta_A^2 = \frac{180}{\pi} \left[2\pi^2 f_{carrier}^2 \left(\frac{\pi^2 h_{-2}}{3\omega_L^3} + \frac{\pi h_{-1}}{3\sqrt{3}\omega_L^2} + \frac{h_0}{6\omega_L} \right) \right] \quad (\text{degrees}) \quad (3.25)$$

where θ_A^2 : Allan variance induced oscillator jitter in degrees

ω_L : L-band input frequency = $2\pi f_L$ (rad/s)

Table 3-2 OCXO models

Oscillator	White (h_0)	Flicker (h_{-1})	Random walk (h_{-2})
OCXO ¹	8e-20 s	2e-21	4e-23 Hz
OCXO ²	1e-21 s	1e-20	2e-20 Hz
OCXO ³	2.51e-26 s	2.51e-23	2.51e-22 Hz

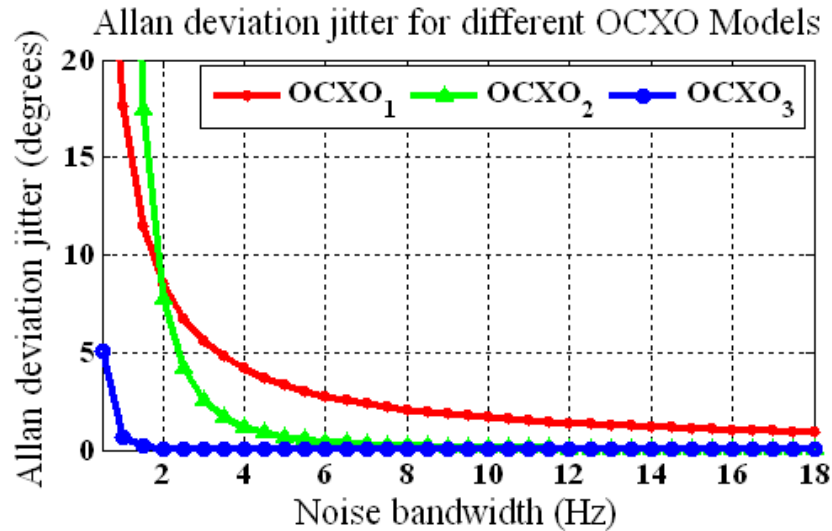


Figure 3-13: Allan deviation jitter for different OCXO models

In order to verify the oscillator model, the error sources that can contribute to phase jitters, including the user's dynamics and the atmospheric errors, have to be mitigated, leaving the OCXO model as the only variable. The following test scenario is conducted:

1. A stationary user is simulated to mitigate errors due to user motions
2. The L5 pilot channel is chosen to eliminate errors due to data bits
3. The atmospheric errors are not simulated, to mitigate any uncertainties due to the ionospheric delay
4. A strong signal power (Carrier to noise ratio (C/N_0) = 45 dB-Hz) is simulated.

Figure 3-14 shows the L5 signal FLI, followed by the PLI in Figure 3-15. The two figures show a marginally higher indicators when the third OCXO model is used. Thus, the third model is used to model the NI OCXO oscillator in the software receiver.

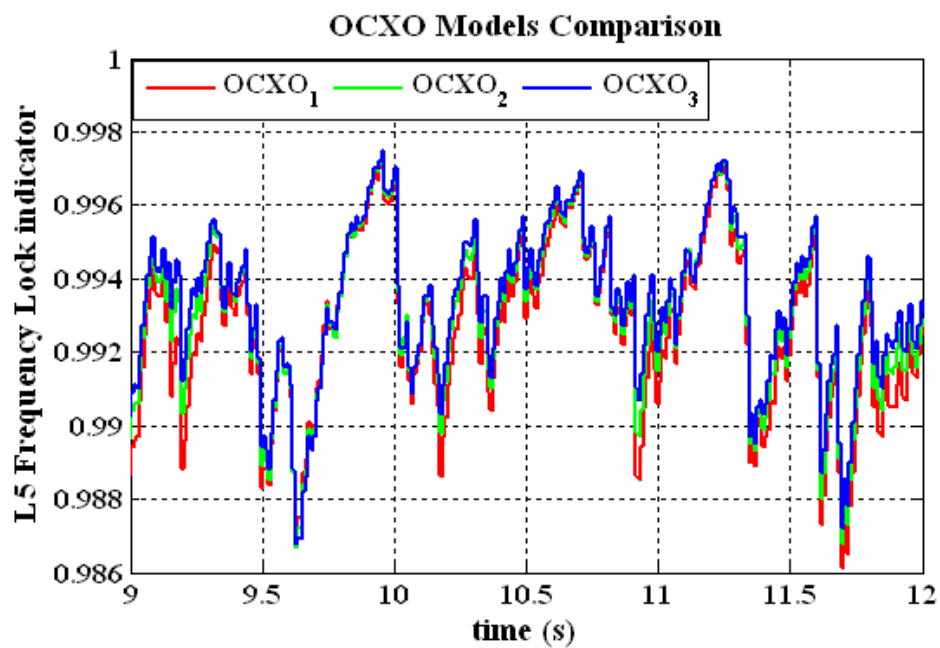


Figure 3-14: OCXO models comparison: L5 FLI

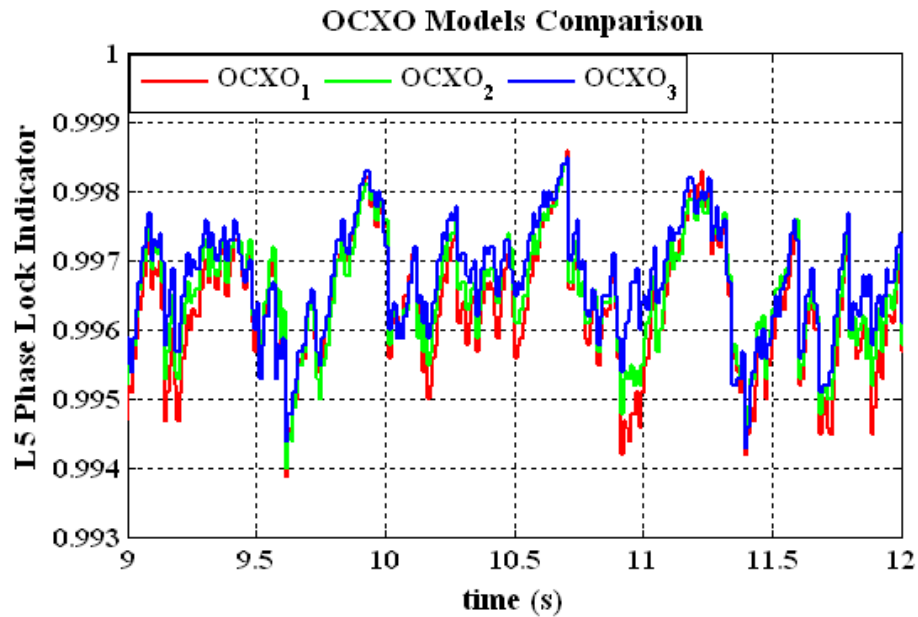


Figure 3-15: OCXO models comparison: L5 PLI

3.4.2.2 Multipath and shadowing

One of the most significant errors encountered by the GPS signal is multipath. Multipath refers to the distortion of the line of sight (LOS) GPS signal, by its reflected or diffracted replicas of the signal. The multipath delay depends on the path traveled by the reflected signal, which is longer than the direct signal's path.

Large delay multipath, greater than twice the spreading code symbol period, can be resolved by the receiver. However, short delay multipath, those reflected from nearby objects, results in a composite signal (direct plus multipath). That kind of multipath distorts the correlation function between the received signal and the locally generated signal in the receiver.

Shadowing, on the other hand, is an extra attenuation introduced when the direct path propagates through an obstacle, foliage or a structure, whereas the multipath does not suffer from the same attenuation (Misra & Enge 2001) .

The multipath errors vary significantly in magnitude depending on the environment, the satellite elevation angle, the receiver and the antenna design and the signal characteristics.

The error introduced by the multipath depends on the relative parameters of the multipath signal, compared to the direct signal, including the code delay, power and carrier phase.

If the direct signal is described as (Ward et al 2006b)

$$s(t) = A_0 x(t - \tau_0) e^{-j(-2\pi f_c(t - \tau_0) + \phi_0)} \quad (3.26)$$

where

A_0	:	Direct signal's amplitude
$x(t)$:	Complex envelope of the transmitted signal
τ_0	:	Propagation delay of the direct path
ϕ_0	:	Carrier phase of the direct path

A simple model for the received signal with multipath after down conversion is

$$r(t) = A_0 e^{-j\phi_0} x(t - \tau_0) e^{-j2\pi f_c \tau_0} + \sum_{n=1}^N A_n e^{-j\phi_n} x(t - \tau_n) e^{-j2\pi f_n t} \quad (3.27)$$

where

N	:	Number of multipaths
A_n	:	Received amplitudes of the multipath returns
τ_n	:	Propagation delays of the multipath returns
ϕ_n	:	Carrier phases of the multipath returns

f_n : Frequencies of the multipath returns relative to the carrier frequency

In general each parameter in Equation 3.27 is time varying. Ward et al (2006b) discusses several models that can be used for multipath. The most common model used is a parametric one that groups the arrivals into three components the LOS signal, the near echoes and the far echoes. Shadowing on the LOS path is modelled using a Rician distribution, where Rayleigh distribution is used when no LOS exists.

Simpler models can also be applied by setting the different parameters of the reflected signals, i.e. number of reflected signal, amplitudes, Doppler frequency, and propagation delay.

The GSS7700 simulator enables the simulation of multipath using either manual multipath, where the different parameters are set by the user, or the land mobile multipath, where only the environment is set by the user.

3.4.2.2.1 Manual multipath

A manual multipath simulation sets some of the parameters shown in Equation 3.27.

Various manual multipath kinds can be modelled as follows:

- **Ground reflection:** This model assumes a flat plane Earth surface below the vehicle and calculates the range and arrival angle (at the antenna) of the satellite signal bouncing off this plane. The user sets the number of reflected signals, and the corresponding attenuation.

- ***Fixed offset:*** This model creates a simple multipath signal having constant user specified range and power offsets with respect to the normal LOS signal. The user sets the number of reflected signals, and the corresponding attenuation and range offset (m).
- ***Doppler offset:*** This model has been introduced in response to the testing requirements of the Assisted GGS (A-GPS) mobile phone test community. The user sets the same parameters as the fixed offset in addition to the initial delay, Doppler offset and the initial phase.
- ***Vertical plane:*** This model allows geometric representation of satellite signal reflection from buildings. It differs from the land mobile multipath model, as the latter applies statistical signal modification. The buildings are modelled as vertical planes with specific heights and distance from the LOS user. The user sets action time, and the geometry appearing around the receiver.

3.4.2.2.2 Land Mobile multipath

This model currently only applies to the static vehicle type. It can be modified via a user action file. This model has been specially developed to simulate the effects of multipath signals on a mobile phone incorporating GPS positioning (Boulton et al 2002). The user sets the type of surrounding environment, whether it is rural, sub-urban, or urban canyon. For each type, a corresponding category mask editor is defined. The signals determined by their arrival angles, fall in one of four categories, which are modified according the environment set by the user (shown in Figure 3-16):

- **Category A:** Obstruction, that represents a visibility mask where all the signals below 5 degree of elevation are excluded.
- **Category B:** LOS only, signals that are unobstructed and not subject to any reflections. These signals suffer Rician fading only.
- **Category C:** LOS & Echoes, signals that are unobstructed but subject to reflections. The LOS signal suffers Rician fading, where the echoes suffer modified Rayleigh fading.
- **Category D:** Echoes only, these represent obstructed LOS signals that are present as reflections only, and they suffer modified Rayleigh fading.

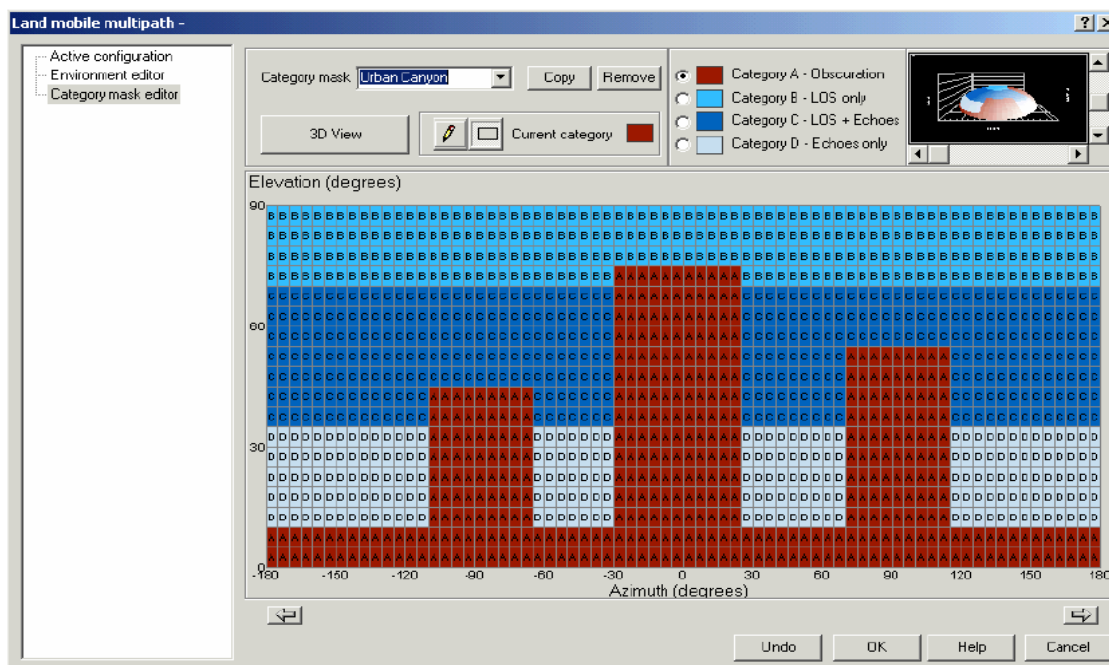


Figure 3-16: Land mobile multipath categories

Note that a Rician model is used to describe the fading on LOS signals, whereas a Rayleigh model is used to describe the fading on echo channels.

3.4.2.3 Signal power degradation

The receiver's sensitivity is an important metric when it comes to comparing different acquisition or tracking algorithms. In order to test the receiver sensitivity, a simulated GPS signal power degradation is required. The GPS signal power received can be varied using the user action file. This variation helps in studying the limiting power for the proposed tracking algorithms. Figure 3-17 shows the user action file used to decrease the L1 and L5 signals power by 24 dB using a rate of 0.5 dB per 2 s.

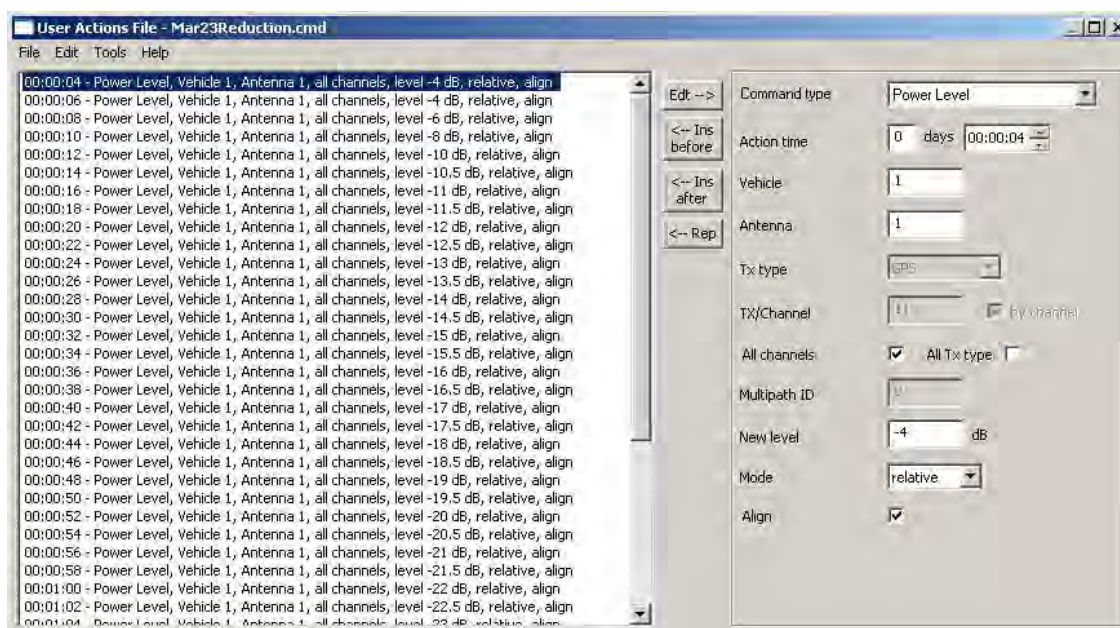


Figure 3-17: Signal power degradation – user action file

3.5 User Motion Simulation

The previous section discussed the different error sources that can be encountered by the GPS signal during its journey. At the receiver side though, any motion introduced by the user can cause a change in the Doppler frequency calculated. A method was required to simulate user motion to test the combined tracking scheme. The GSS7700 simulator

again provides different models of user motion. The motion models vary from the simple rectangular racetrack, circular motion up to the advanced aircraft motion.

For this thesis, the interest was to be able to simulate several variations in the velocities and directions of the user. For that purpose, the rectangular racetrack model fits perfectly. The details on the simulated motion are discussed in Chapter 5.

3.6 Summary

The chapter discussed the simulation tools and the software required to test the proposed models. The different simulation parameters used on the GSS7700 hardware simulator are illustrated, followed by a description of the developed software receiver for the L1 and the L5 signals. The chapter also reviews the different error sources encountered by a GPS signal, and how they are simulated using the hardware simulator.

The next chapter discusses the combination of the two signals using the standard tracking loops, and comparing it to the separate tracking.

Chapter Four: COMBINATION APPROACHES FOR TRACKING L1/L5 SIGNALS

The chapter introduces two methods for combining data from the L1 and the L5 signals. The first is through the direct use of the standard tracking loops, called aided tracking loops. This is achieved through the scaling of the L5 Doppler frequency estimate and applying it as an external aiding to the L1 tracking loops. The separate standard tracking loops are first reviewed followed by a discussion on the different phase tracking loops error sources. The chapter then proceeds to the aided tracking loops, where the architecture and the different loop parameters are presented. In addition, the reason for choosing the L5 signal as an aiding source is justified.

The second method shown in the chapter is the combined Kalman filter tracking loop, one of the main innovations of the thesis. The general architecture of the Kalman filter is shown, followed by the Kalman filter model used for the separate tracking. The combined Kalman filter model is then illustrated, with the associated state dynamic model, observation model and the modified noise parameters.

4.1 Standard Tracking Loops

4.1.1 Separate Standard Tracking Loops

The structure of the standard tracking loops was shown in detail in Chapter 2. This section concentrates on the actual loop parameters that were used for tracking the two signals separately.

Figure 4-1 shows a schematic diagram for the standard tracking loop. The loop depends entirely on three parameters: coherent integration interval, loop discriminator and loop filter.

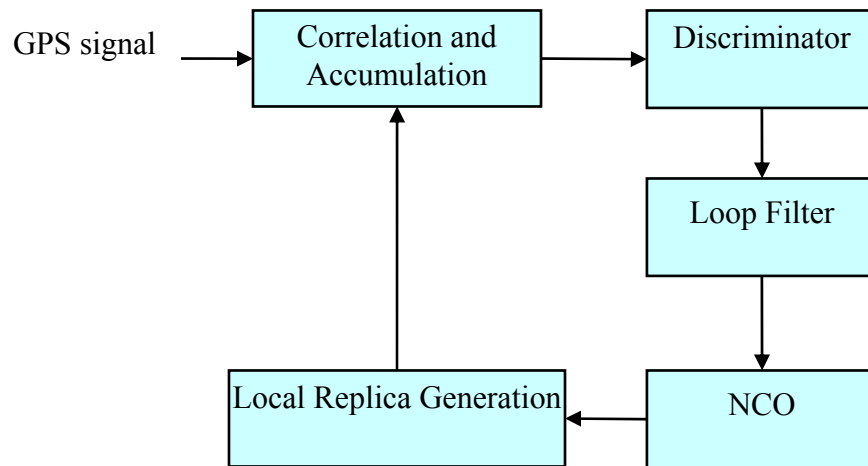


Figure 4-1: Schematic diagram for a standard tracking loop

4.1.1.1 Loop parameters

Though the combination is done at the phase tracking part using a standard tracking loops, it is important to discuss the carrier frequency discriminators as only the frequency tracking loop is used initially in the Kalman filter tracking. The carrier frequency discriminator is used during initial signal acquisition, when the data boundaries are unknown. This requires smaller predetection integration times, compared to the data bit transition intervals. The carrier frequency discriminators are discussed in detail in the literature, e.g. Ward et al (2006a). The discriminator chosen for the thesis is the four-quadrant arctangent. Finally, a second order filter is usually used in the FLL because it has the same steady-state tracking error performance as a third order PLL.

For the phase lock loop, the problem of the data bit appears on the L1 signal, which prohibits the use of a pure PLL discriminator. A Costas PLL, which is insensitive to the presence of data modulation, is thus required. Several Costas PLL discriminators are discussed in Ward et al (2006a). The two-quadrant arctangent discriminator is chosen for tracking the L1 data channel.

To overcome the drawback due to the data bits, all modernized signals are provided with a dataless channel to enable pure PLL tracking. This dataless channel shares the total signal power with the data channel. Although this sharing technique loses 3 dB, when the dataless channel is used for tracking, it still provides a net gain of 3 dB in tracking sensitivity (Ward et al 2006a). In addition, it also enables longer coherent integration intervals without worrying about the data bit transitions. The L5 pilot channel is an example of the new signals. The pilot channel is used for tracking the L5 signal using the four-quadrant arctangent discriminator.

For the code tracking loop, usually an aided DLL is used. The DLL discriminator used for the L1 and L5 signals is the Dot-Product discriminator with an Early-Plus-Late normalization (Mongrédien 2008). The normalization removes the signal amplitude dependency, and thus improves the performance under changing SNR; however, the performance degrades under low SNR. Considering an aided code tracking loop, a first order loop filter is used with the same coherent integration interval to be consistent with the carrier tracking loop's update rate.

The last parameter is the coherent integration interval. The L1 signal has only a data channel, thus is limited by the bit duration of 20 ms as its maximum coherent integration

interval, with no external data bit aiding provided. Although the L5 signal has a pilot channel that enables longer coherent integration intervals, a 20 ms coherent integration interval is used in this work, in order to be consistent with the L1 signal update rate. A summary of the used parameters are shown in Table 4-1.

Table 4-1: Separate standard tracking loop parameters

Discriminator Algorithm	Loop Order	Noise Bandwidth (Hz)	Coherent Integration Time (T)
DLL			
Normalized Dot-Product: $D = (IE - IL).IP + (QE - QL).QP$ $N = (IE + IL).IP + (QE + QL).QP$ $D_{\tau} = \frac{(2 - \Delta)}{2N} D$	First	$B_n = 0.25\omega_0$ $B_n = 0.05 \text{ Hz}$	$T = 20 \text{ ms}$
FLL			
Extended Arctangent Hz: $D_f = \frac{\text{atan2}(\text{dot}, \text{cross})}{T}$	Second	$B_n = 0.53\omega_0$ $B_n = 10 \text{ Hz}$	$T = 20 \text{ ms}$
Pure PLL			
Extended Quadrant Arctangent: $D_{\phi} = \text{atan2}(QP, IP)$	Third	$B_n = 0.7845\omega_0$ $B_n = 10 \text{ Hz}$	$T = 20 \text{ ms}$
Costas PLL			
Two-quadrant Arctangent: $D_{\phi} = \text{atan}(QP, IP)$	Third	$B_n = 0.7845\omega_0$ $B_n = 10 \text{ Hz}$	$T = 20 \text{ ms}$
where the dot and cross are the operations on the correlators shown earlier in Equation 2.20			

4.1.2 Phase Tracking Loop Errors

The performance of the PLL is measured by the variance of the total phase jitter σ_{PLL}^2 . It is defined as

$$\sigma_{PLL}^2 = \sigma_t^2 + \sigma_{\delta\phi}^2 \quad (4.1)$$

where σ_{PLL} : 1-sigma phase jitter from all sources (in degrees)

σ_t : 1-sigma thermal noise (in degrees)

$\sigma_{\delta\phi}$: 1-sigma input tracking error (in degrees)

Often the thermal noise σ_t is treated as the only source of carrier tracking error. The input tracking error $\sigma_{\delta\phi}$, on the other hand, can be classified into correlated sources and the dynamic stress error as shown below (Egziabher et al 2003)

$$\sigma_{\delta\phi} = \sqrt{\sigma_{\delta\phi,c}^2} + \frac{\theta_e}{3} \quad (4.2)$$

$$\sigma_{\delta\phi,c}^2 = \sigma_v^2 + \theta_A^2 \quad (4.3)$$

where $\sigma_{\delta\phi,c}$: Correlated sources of phase error

θ_e : Dynamic stress error

σ_v : 1-sigma vibration-induced oscillator phase noise (in degrees)

The correlated sources include the vibration-induced oscillator noise and Allan deviation (Section 3.4.2.1). These errors constitute the total phase jitter, which follows the PLL rule thresholds given as (Ward et al 2006a)

$$\sigma_{PLL} = \sqrt{(\sigma_t^2 + \sigma_v^2 + \theta_A^2)} + \frac{\theta_e}{3} \leq 15^\circ \quad (\text{data present})$$

$$\leq 30^\circ \quad (\text{dataless}) \quad (4.4)$$

The following sections provide a review of each of these error sources in detail.

4.1.2.1 Thermal noise

The thermal noise characterizes the noise on the PLL's estimated phase output. The thermal noise jitter for an arctangent PLL is computed as (Ward et al 2006a)

$$\sigma_t = \frac{180}{\pi} \sqrt{\frac{B_n}{C/N_0} \left(1 + \frac{1}{2.T.C/N_0} \right)} \quad (\text{degrees}) \quad (4.5)$$

The carrier thermal noise error is independent of the carrier frequency when it is expressed in degrees. However, it is strictly dependent on both the carrier to noise ratio, the noise bandwidth and the coherent integration time. The C/N_0 is measured at the correlator output at the input to the tracking loop. The lower the C/N_0 , the higher the thermal noise jitter, whereas minimizing the noise bandwidth results in less thermal noise jitter. On the other hand, increasing the coherent integration time lowers the resulting standard deviation.

4.1.2.2 Vibration-induced oscillator phase noise

In some cases, the oscillator is installed in environments where it is subjected to mechanical vibrations. The equation for the vibration-induced oscillator jitter is given in *ibid* as

$$\sigma_v = \frac{360 f_L}{2\pi} \sqrt{\int_{f_{min}}^{f_{max}} S_v^2(f_m) \frac{P(f_m)}{f_m^2} df_m} \quad (\text{degrees}) \quad (4.6)$$

where f_L : L-band input frequency in Hz

$S_v(f_m)$: Oscillator vibration sensitivity of $\Delta f/f_L$ per g as a function of f_m

f_m : Random vibration modulation frequency in Hz

$P(f_m)$: Power curve of random vibration in g^2/Hz as a function of f_m

g : Gravitational acceleration $\approx 9.8 \text{ m/s}^2$

4.1.2.3 Allan deviation oscillator phase noise

The Allan deviation oscillator phase jitter for the third order PLL has been discussed in detail in Chapter 3. It consists of three distinct segments, the white frequency noise, flicker noise and integrated frequency noise, as shown in Figure 4-2.

For a third order PLL, the Allan deviation phase jitter is given by

$$\theta_A^2 = \frac{180}{\pi} \left[2\pi^2 f_{carrier}^2 \left(\frac{\pi^2 h_{-2}}{3\omega_L^3} + \frac{\pi h_{-1}}{3\sqrt{3}\omega_L^2} + \frac{h_0}{6\omega_L} \right) \right] \quad (\text{degrees}). \quad (4.7)$$

For a second order PLL the Allan deviation oscillator phase jitter is derived as (Irsigler & Eissfeller 2002)

$$\theta_A^2 = \frac{180}{\pi} \left[2\pi^2 f_{carrier}^2 \left(\frac{\pi^2 h_{-2}}{\sqrt{2}\omega_L^3} + \frac{\pi h_{-1}}{4\omega_L^2} + \frac{h_0}{4\sqrt{2}\omega_L} \right) \right] \quad (\text{degrees}). \quad (4.8)$$

Both expressions account for the three types of noise shown in Figure 4-2. On the other hand, for a first order PLL, although it can never be used as a standalone method for the phase tracking, it can be used in case of the aided carrier phase tracking loop. The Allan deviation oscillator phase jitter, in that case, only accounts for the white frequency noise (Lee 2002), and is given as

$$\theta_A^2 = \frac{180}{\pi} \left[2\pi^2 f_{carrier}^2 \left(\frac{h_0}{4\omega_L} \right) \right] \quad (\text{degrees}). \quad (4.9)$$

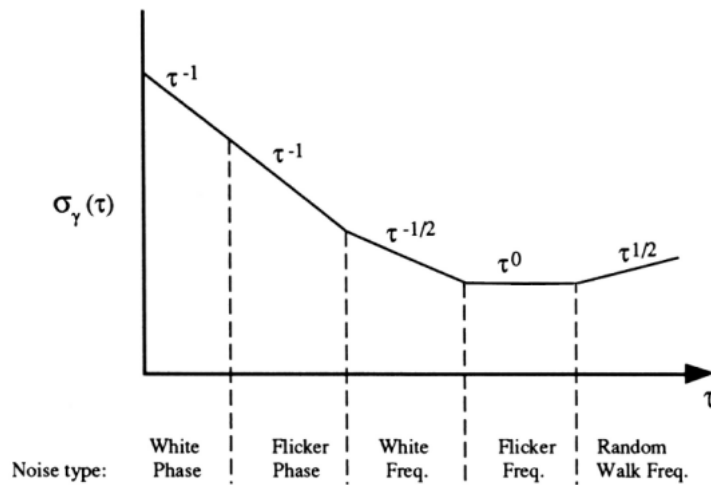


Figure 4-2: Allan deviation and noise types (Physics Laboratory 2010)

4.1.2.4 Dynamic stress error

The dynamic stress characterizes the transient response of the PLL to a non-continuous input signal, e.g. a step, acceleration or jerk input phase. It can be obtained from the following steady-state errors:

$$\begin{aligned}
 \theta_e &= 0.25 \frac{dR / dt}{B_n} && \text{(First order)} \\
 &= 0.2809 \frac{d^2 R / dt^2}{B_n^2} && \text{(Second order)} \\
 &= 0.4828 \frac{d^3 R / dt^3}{B_n^3} && \text{(Third order)}
 \end{aligned} \tag{4.10}$$

where dR/dt : Maximum LOS velocity dynamics ($^\circ/s$)

d^2R/dt^2 : Maximum LOS acceleration dynamics ($^\circ/s^2$)

d^3R/dt^3 : Maximum LOS jerk dynamics ($^\circ/s^3$)

As shown in Equation (4.10), the dynamic stress error depends on both the loop order and the noise bandwidth. Increasing the bandwidth decreases the total dynamic stress error.

4.1.3 L1-Aided Tracking Loops

Doppler aided tracking loops have been used in the literature (Egziabher et al 2003) to enhance the phase tracking performance, where an external source was used to provide that assistance. However, using the fact that more than one GPS signal are transmitted from the same space vehicle, Doppler aiding could now be provided from one signal to another. Qaisar (2009) shows the theoretical results of applying L2C Doppler aiding to the L1 signal under an assumed interference scenario affecting only the L1 signal, however it fails to provide an experimental verification and performance analysis in cases

where both signals undergo the same power changes. A similar approach is used in this thesis, with the L5 pilot channel chosen as the source of the aiding presented as follows.

4.1.3.1 Comparison of L1 and L5 tracking errors

In order to decide which signal is going to be the source of the aiding information, a comparison is made between the L1 signal and L5 pilot signal tracking errors. Figure 4-3 shows the total phase tracking error of both L1 and L5 signals using Equation (4.4). The total phase standard deviation for the L5 signal is smaller than that of the L1 signal, allowing the receiver to track lower C/N_0 given the same bandwidth and dynamic rate.

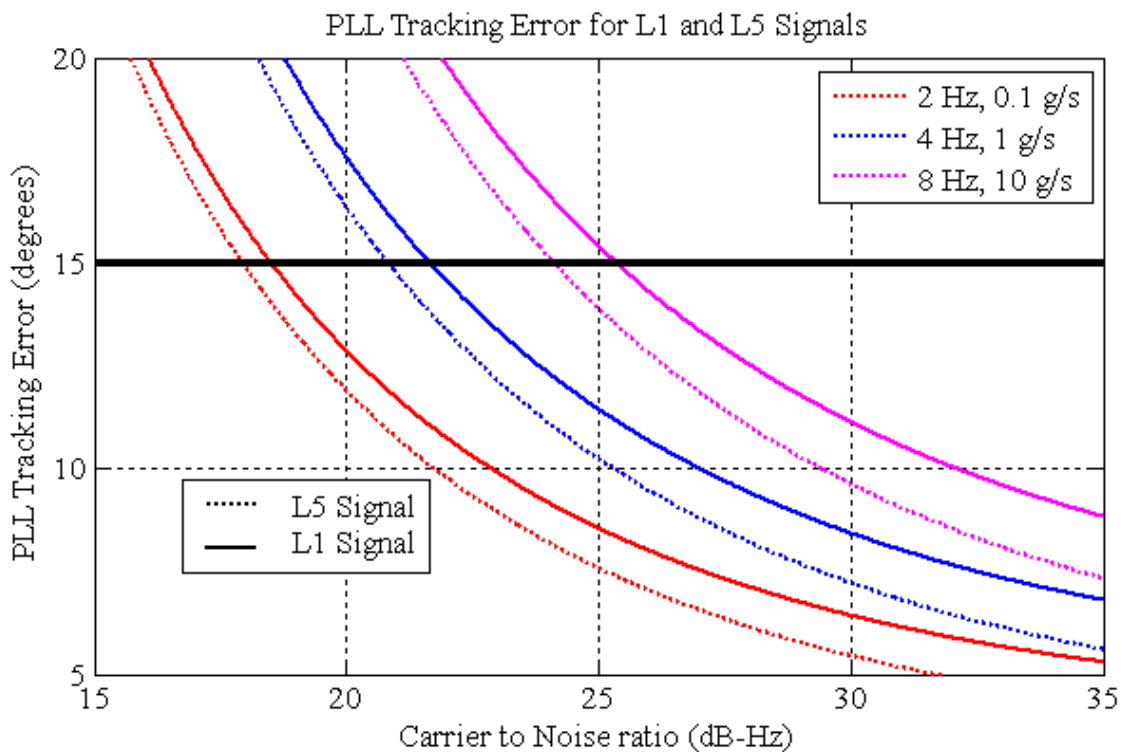


Figure 4-3: Comparison of total phase error for L1 and L5 signals

Given these results, the L5 signal is chosen to provide the aiding information for the L1 signal.

4.1.3.2 L1-aided carrier phase tracking loop

With the source of aiding determined as discussed above, the architecture of the aided L1 tracking loop is shown in Figure 4-4.

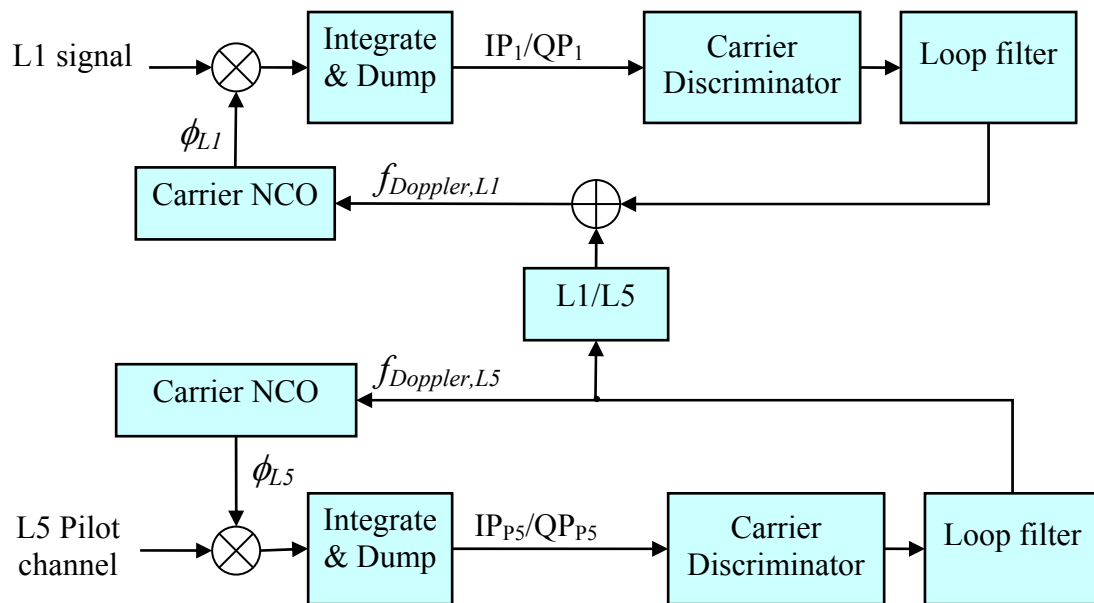


Figure 4-4: L5-aided L1 carrier tracking loop

Note that the combination is done in the phase tracking stage, where the two signals are phase-locked. The sequence is shown in Figure 4-5. After locking to the frequency, the L1 carrier tracking switches to the Costas PLL tracking mode. However, before beginning the standalone PLL tracking, a check is done to determine if the L5 pilot signal is in a PLL tracking mode. If the L5 signal is in the PLL tracking mode, the L5 Doppler

frequency is passed to the L1 loop update function as an external aiding (shown in Section 3.3.3). The L5 Doppler frequency is scaled and added to the phase corrections provided by the L1 Costas PLL discriminator as

$$f_{Doppler,L1} = f_{Doppler,L5} \frac{f_{L1}}{f_{L5}} + \Delta f_d \quad (4.11)$$

where Δf_d : Filtered carrier discriminator output.

If the L5 is not in the PLL tracking mode, then the L1 Doppler frequency is simply updated by the corrections provided by the discriminator.

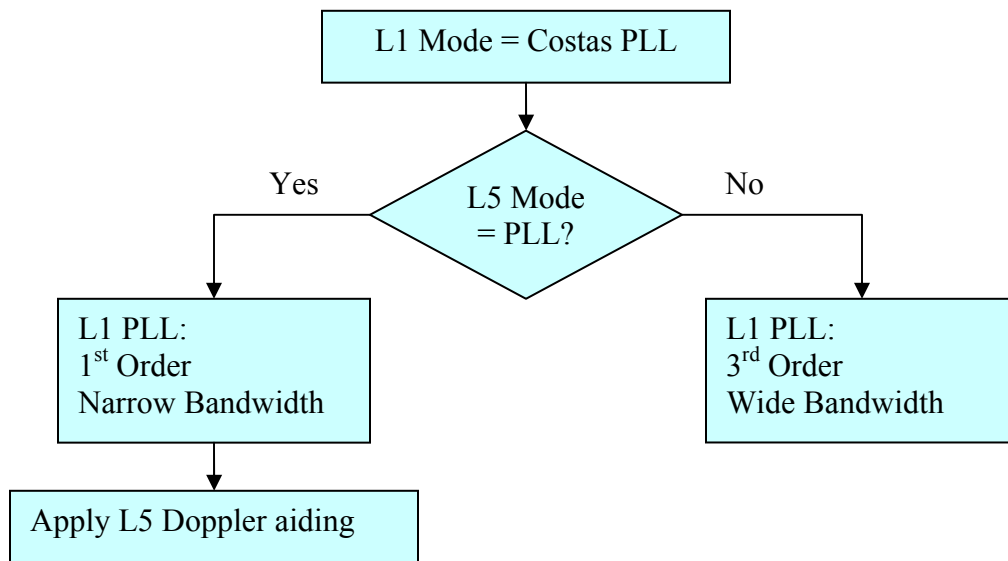


Figure 4-5: L1 Aided Tracking Loop Flowchart

The two tracking loops are fully operational. However, with the aiding information provided, the L5 tracking loop becomes responsible for tracking the signal dynamics. It is set to operate at a wider loop bandwidth, with a third order PLL. On the other hand, the

L1 tracking loop operates at a narrower bandwidth, using a first order PLL, aiming only at tracking any divergence from the L5 signal.

4.1.3.3 L1-aided code tracking loop

The combination in the code tracking loops is done similarly by scaling the code Doppler of the L5 signal and adding it to the code corrections provided by the L1 tracking loop as shown below:

$$f_{codeDoppler,L1} = f_{codeDoppler,L5} \frac{f_{CR1}}{f_{CR5}} + \Delta f_{cd} \quad (4.12)$$

where f_{CR} : Code chipping rate

Δf_{cd} : Filtered code discriminator output

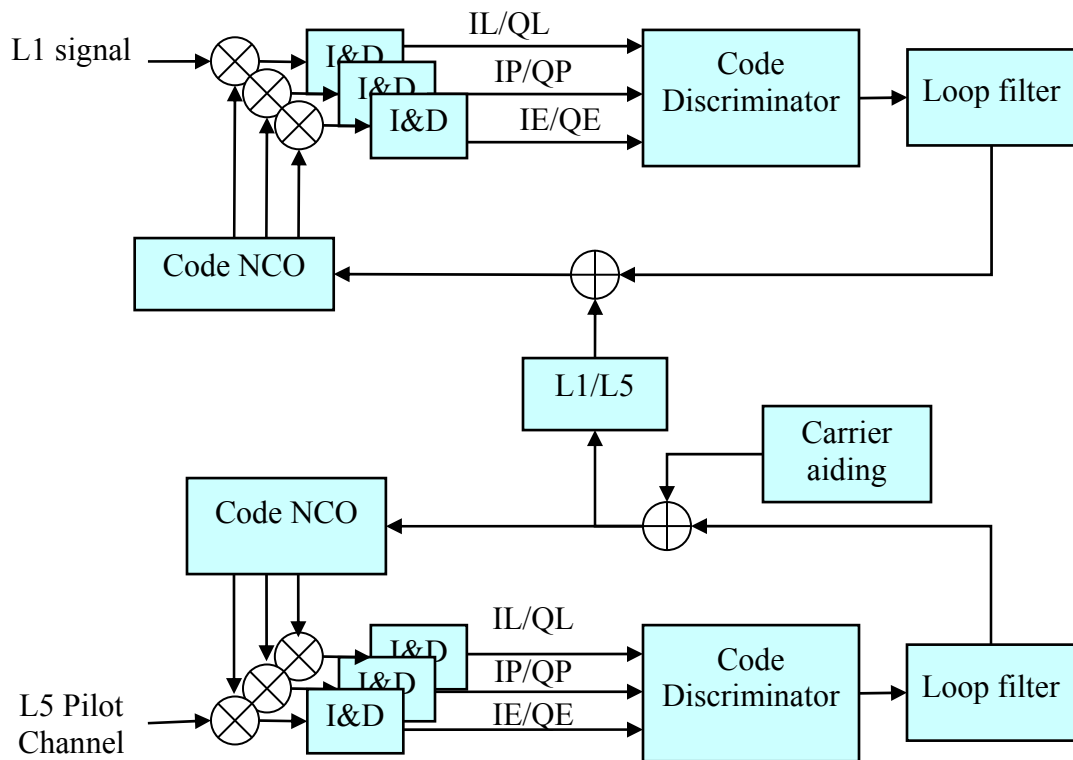


Figure 4-6: L1-aided code tracking loop

Note that the L5 code tracking loop itself is a carrier-aided one that uses the scaled L5 Doppler information as an external aiding to the loop. The aided code tracking loop architecture is shown in Figure 4-6.

4.1.3.4 Loop parameters

Following with the discussion in the above two sections, the loop parameters used for the two signals are summarized in Table 4-2.

Table 4-2: Aided tracking loop parameters

L1 Signal	PLL	DLL
	1 st Order $B_n = 1-5$ Hz L5-aided PLL	1 st Order $B_n = 0.05$ Hz L5-aided DLL
L5 Signal	PLL	DLL
	3 rd Order $B_n = 10$ Hz	1 st Order $B_n = 0.05$ Hz Carrier-aided DLL

One further point to note on the aided tracking loops is that the L5 aiding to the L1 tracking loop introduces some additional errors to those discussed in Section 4.1.2. However, the details and the derivation of the total phase error are described later in Chapter 5 after all the required background is described.

4.2 Kalman Filter Tracking Loops

The second approach for combining the L1 and L5 signals is through an Extended Kalman Filter (EKF). This section explains the detailed general filter structure used, including the dynamic model, measurement model, and the required processing for each.

Then two Kalman filter models are presented: the separate Kalman filter model, where each of the two signals is tracked separately, and the combined Kalman filter model, which is one of the main contributions of the thesis.

4.2.1 General Kalman Filter Structure

Each of the two Kalman filter models that will be discussed in the thesis follows the general Kalman filter structure that has been used extensively in the literature (Petovello & Lachapelle 2006, Psiaki & Jung 2002). The Kalman filter generally consists of two models, namely the system dynamic model and measurement model.

4.2.1.1 Dynamic model

The system dynamic model that describes the dynamics of a continuous time system can be written as

$$\dot{x}(t) = F(t)x(t) + G(t)w(t) \quad (4.13)$$

where x : States of dynamic system
 $F(t)$: Coefficient matrix describing the dynamics of the system
 $G(t)$: Shaping matrix for the white noise input
 w : Random forcing function, zero-mean white Gaussian noise.

The states will vary depending on the tracking approach, whether it is separate or combined as discussed later.

4.2.1.2 Measurement model

The measurement model includes the set of observations z available to estimate the states x . The state vector x is known to relate to the observation vector z as

$$z_k = H_k x_k + v_k \quad (4.14)$$

where z_k : Measurement vector
 H_k : Linearized Design matrix
 v_k : Measurement noise vector.

Each of the two filters under comparison are iterated EKFs (Table 4-3) due to the nonlinear nature of the measurement models used. The table includes two steps that must be performed: 1) discretization of the dynamic matrix, 2) linearization of the measurement model. The details of these two steps are described in Table 4-3.

Table 4-3: Iterated EKF model	
Continuous Time System Model	$\dot{x}(t) = F(t)x(t) + G(t)w(t)$ $w(t) \sim N(0, Q(t))$
Nonlinear Measurement Model	$z_k = h_k(x_k(t)) + v_k$ $v_k \sim N(0, R_k)$
Discrete Time System Model	$x_k = \Phi_{k-1}x_{k-1} + w_{k-1}$ $w_k \sim N(0, Q_k)$
Linearized Measurement Model	$z_k = H_k x_k + v_k$ $v_k \sim N(0, R_k)$
Prediction Step	$\hat{x}_k(-) = \Phi_{k-1}\hat{x}_{k-1}(+)$ $P_k(-) = \Phi_{k-1}P_{k-1}(+)\Phi_{k-1}^T + Q_{k-1}$
Kalman Gain Matrix	$\bar{K}_k = P_k(-)H_k^T [H_k P_k(-)H_k^T + R_k]^{-1}$
Update Step	$\hat{x}_k(+) = \hat{x}_k(-) + \bar{K}_k [z_k - H_k \hat{x}_k(-)]$ $P_k(+) = [I - \bar{K}_k H_k] P_k(-)$

where Φ_k : State transition matrix
 h_k : Nonlinear design matrix
 $Q(t)$: Process noise spectral density matrix
 R_k : Covariance matrix for the measurement noise

P_k : State Covariance Matrix
 K_k : Kalman Gain

4.2.1.3 Discretization

The state space model above is a continuous time model, which needs to be discretized.

The discretization process is done in two steps:

1) Discretization of the dynamic matrix to get the transition matrix: Since F is a time invariant matrix, the transition matrix can be calculated as

$$\Phi_k = \exp(FT) = 1 + FT + \frac{(FT)^2}{2!}. \quad (4.15)$$

The results of the discretization step are shown in the description of each of the two models later.

2) Calculation of the discrete covariance matrix of the process noise. This can be done as follows (Gelb 1974):

$$Q_k = \int_k^{k+1} \Phi(t, t+\tau) G(\tau) Q_c(\tau) G^T(\tau) \Phi^T(t, t+\tau) d\tau. \quad (4.16)$$

The discretized Q matrix for both the separate and combined Kalman filters is shown in Appendix A.

4.2.1.4 Linearization

Linearization of the design matrix is obtained by expanding the measurement equation in a power series about the previous state estimate as

$$H_k(\hat{x}_k(-)) = \left. \frac{\partial h_k(x(t_k))}{\partial x(t_k)} \right|_{x(t_k)=\hat{x}_k(-)} \quad (4.17)$$

To obtain better estimate of the states, an iterated calculation of $\hat{x}_k(+)$, $P_k(+)$ and K_k is performed, each time linearizing about the most recent estimate to form the iterated Kalman filter (Gelb 1974). Denote the i^{th} estimate of $x_k(+)$ by $\hat{x}_{k,i}(+)$, $i = 0, 1, \dots, N_I$, where N_I is the number of iterations. The update step is then repeated for N_I times, or until the estimate converges.

One further observation regarding the L1 correlators output is that the data bit has to be taken into consideration in the Kalman filter model; otherwise it would be absorbed in the estimated states and cause unpredictable performance. This is taken into consideration in the design matrix H_k , where the data bit is estimated as the sign of the accumulated in-phase prompt arm, and again in the update step when computing the innovations from the new correlator outputs.

This structure of the Kalman filter is used for the two cases under consideration: the separate Kalman filter and the combined Kalman filter tracking. To enable a fair comparison between the two filters, they are required to follow exactly the same steps in the software receiver.

Figure 4-7 shows the flowchart of the software receiver developed herein. It starts with the L1 and L5 acquisition and bit synchronization and then proceeds to the frequency tracking, and then to the phase tracking of each signal. Up to that point, each of the two signals is dealt with separately. After phase lock is achieved, the receiver either proceeds

to the separate Kalman filter tracking for each of the two signals, or the combined Kalman filter tracking.

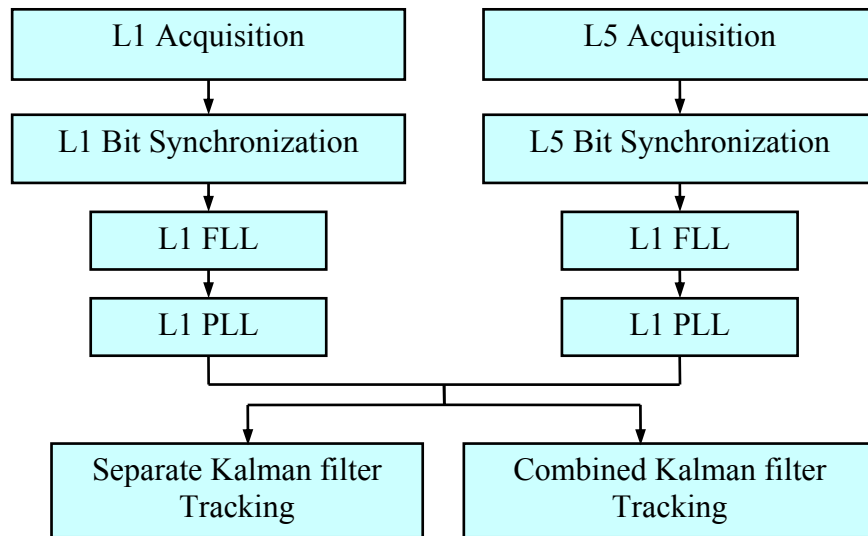


Figure 4-7: Flowchart of separate and combined Kalman filters

The next two sections will describe the two elements of comparison:

- 1) The separate Kalman filter tracking, in which each of the two signals is tracked separately.
- 2) The combined Kalman filter tracking.

To ensure a fair comparison, the dynamic model for the states is the same for the two filters. Further details will be presented in the following sections.

4.2.2 Separate Kalman Filter

The separate Kalman filter tracking model follows the general structure introduced above. Figure 4-8 shows the steps for tracking each of the L1 and the L5 signals. For the

L1 signal, the incoming signal undergoes a carrier wipe-off followed by a code wipe-off. The output of this stage is then applied to the Kalman filter to extract the tracking errors, and use these to update the NCOs.

The L5 signal undergoes the exact same steps, namely a carrier wipe-off followed by a code wipe-off. An extra step is required to wipe-off the NH codes. Since the pilot L5 signal only is used, wipe-off of the NH20 codes is required. Then the steps proceed similar to those for the L1 signal.

4.2.2.1 Dynamic model

The states to be estimated in single signal tracking are the amplitude of the signal, the code phase error, the carrier phase error, the frequency error and the carrier acceleration error.

The amplitude is modelled as a random walk and its process noise accounts for the signal level variations. The code phase error is estimated from the carrier frequency error, with two process noise components, w_{τ_1} and $\beta_1 w_{\phi_1}$. The random walk component w_{τ_1} accounts for any ionospheric error divergence and multipath. The carrier frequency and phase process noises account for the oscillator jitter effects. The carrier acceleration process noise accounts for the signal dynamics. The model is shown in Figure 4-9.

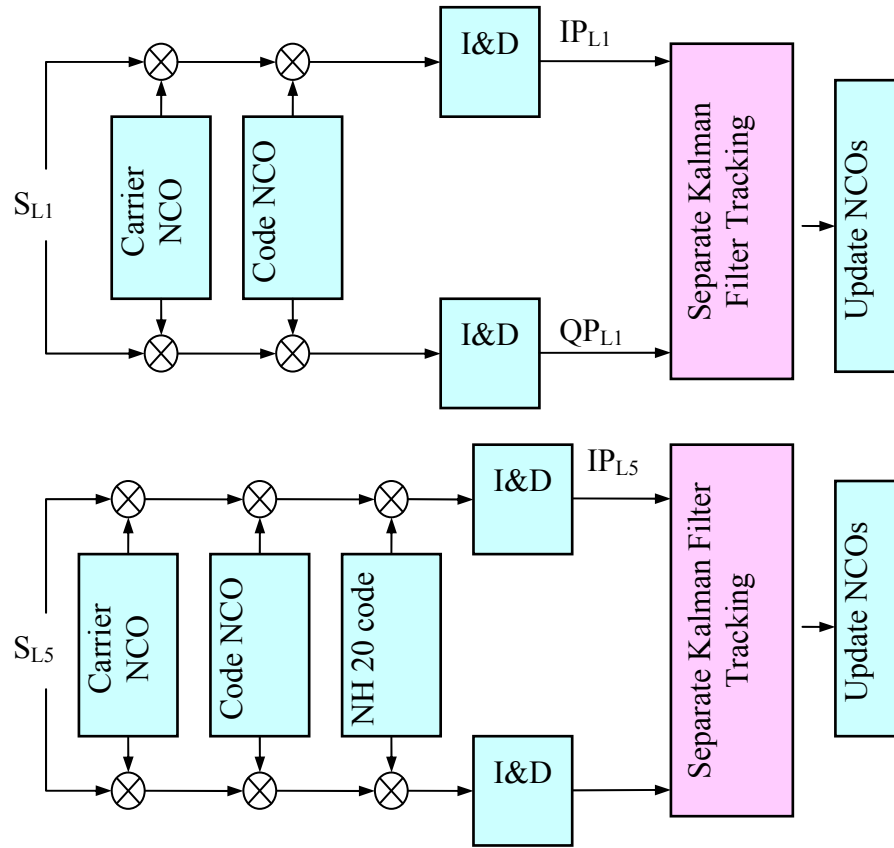


Figure 4-8: Separate Kalman filter tracking

The states to be estimated and the corresponding state space equations can be written as

$$\begin{aligned} x_{L1} &= (A_1 \quad \delta\tau_1 \quad \delta\phi_{01} \quad \delta f_{01} \quad \alpha_{01})^T \\ x_{L5} &= (A_5 \quad \delta\tau_5 \quad \delta\phi_{05} \quad \delta f_{05} \quad \alpha_{05})^T \end{aligned} \quad (4.18)$$

where the states are those defined in sections 2.3.1 and 2.3.2 for each signal.

$$\frac{d}{dt} \begin{pmatrix} A_1 \\ \delta\tau_1 \\ \delta\phi_{01} \\ \delta f_{01} \\ \alpha_{01} \end{pmatrix} = \begin{pmatrix} 0 & 0 & 0 & 0 & 0 \\ 0 & 0 & 0 & \beta_1 & 0 \\ 0 & 0 & 0 & 1 & 0 \\ 0 & 0 & 0 & 0 & 1 \\ 0 & 0 & 0 & 0 & 0 \end{pmatrix} \begin{pmatrix} A_1 \\ \delta\tau_1 \\ \delta\phi_{01} \\ \delta f_{01} \\ \alpha_{01} \end{pmatrix} + \begin{pmatrix} 1 & 0 & 0 & 0 & 0 \\ 0 & 1 & \beta_1 & 0 & 0 \\ 0 & 0 & 1 & 0 & 0 \\ 0 & 0 & 0 & 1 & 0 \\ 0 & 0 & 0 & 0 & 1 \end{pmatrix} \begin{pmatrix} w_{A_1} \\ w_{\tau_1} \\ w_{\phi_{01}} \\ w_{f_{01}} \\ w_{\alpha_{01}} \end{pmatrix} \quad (4.19)$$

where β : Converts units of radians into units of chips for the subscripted signal

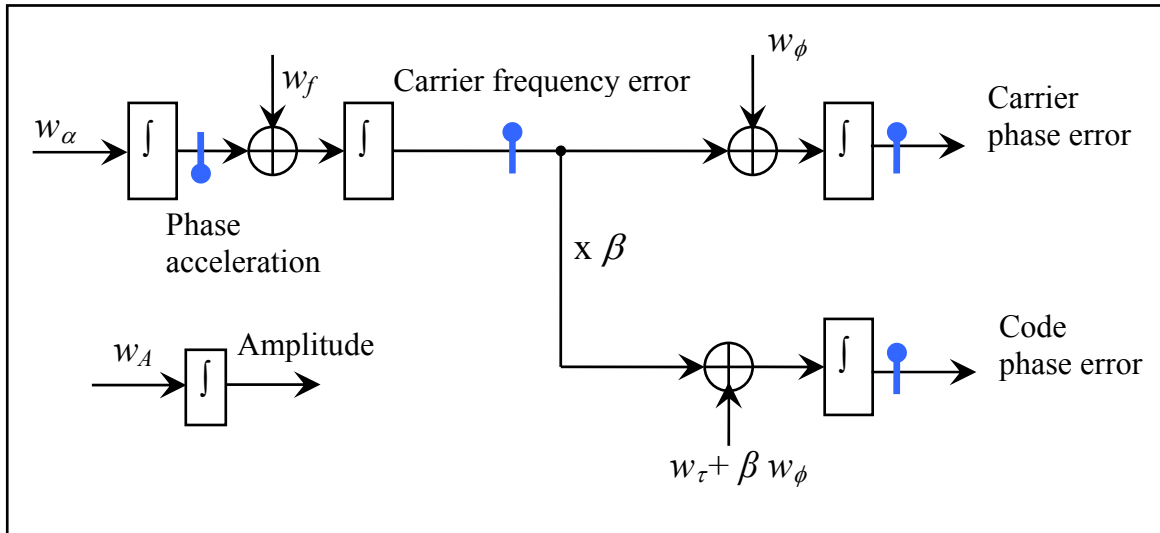


Figure 4-9: Separate Kalman filter dynamic model

The corresponding transition matrix resulting from the discretization step discussed in Section 4.2.1.3 is:

$$\Phi_k = \begin{pmatrix} 1 & 0 & 0 & 0 & 0 \\ 0 & 1 & 0 & \beta T & \beta \frac{T^2}{2} \\ 0 & 0 & 1 & T & \frac{T^2}{2} \\ 0 & 0 & 0 & 1 & T \\ 0 & 0 & 0 & 0 & 1 \end{pmatrix}_k \quad (4.20)$$

4.2.2.2 Measurement model

For each signal, the observations are formed from the six correlator outputs available, namely the in-phase and quadra-phase prompt, early, and late (IP, QP, IE, QE, IL, QL)

correlators. These correlator outputs are then used to estimate the state parameters shown in Equation (4.18).

The z vector can thus be written as

$$\begin{aligned} z_{L1} &= (IP_{L1} \quad IE_{L1} \quad IL_{L1} \quad QP_{L1} \quad QE_{L1} \quad QL_{L1})^T \\ z_{L5} &= (IP_{L5} \quad IE_{L5} \quad IL_{L5} \quad QP_{L5} \quad QE_{L5} \quad QL_{L5})^T \end{aligned} \quad (4.21)$$

Where for each signal, the observations z can be related to the states x through the linearized design matrix H as follows:

$$\begin{pmatrix} IP \\ IE \\ IL \\ QP \\ QE \\ QL \end{pmatrix} = \begin{pmatrix} \frac{\partial IP}{\partial A} & \frac{\partial IP}{\partial \delta\tau} & \frac{\partial IP}{\partial \delta\phi} & \frac{\partial IP}{\partial \delta f} & \frac{\partial IP}{\partial \alpha} \\ \frac{\partial IE}{\partial A} & \frac{\partial IE}{\partial \delta\tau} & \frac{\partial IE}{\partial \delta\phi} & \frac{\partial IE}{\partial \delta f} & \frac{\partial IE}{\partial \alpha} \\ \frac{\partial IL}{\partial A} & \frac{\partial IL}{\partial \delta\tau} & \frac{\partial IL}{\partial \delta\phi} & \frac{\partial IL}{\partial \delta f} & \frac{\partial IL}{\partial \alpha} \\ \frac{\partial QP}{\partial A} & \frac{\partial QP}{\partial \delta\tau} & \frac{\partial QP}{\partial \delta\phi} & \frac{\partial QP}{\partial \delta f} & \frac{\partial QP}{\partial \alpha} \\ \frac{\partial QE}{\partial A} & \frac{\partial QE}{\partial \delta\tau} & \frac{\partial QE}{\partial \delta\phi} & \frac{\partial QE}{\partial \delta f} & \frac{\partial QE}{\partial \alpha} \\ \frac{\partial QL}{\partial A} & \frac{\partial QL}{\partial \delta\tau} & \frac{\partial QL}{\partial \delta\phi} & \frac{\partial QL}{\partial \delta f} & \frac{\partial QL}{\partial \alpha} \end{pmatrix} \begin{pmatrix} A \\ \delta\tau \\ \delta\phi \\ \delta f \\ \alpha \end{pmatrix}. \quad (4.22)$$

Where the correlator outputs contain the states required to be estimated as was shown in Equations 2.7 to 2.12.

4.2.3 Combined Kalman Filter

To enable the combined tracking of the L1 and the L5 signals in one Kalman filter, a new model has to be designed. The combined Kalman filter makes use of the correlator outputs of both the L1 and the pilot L5 signals to extract the tracking errors of each.

The software receiver follows similar steps to that of the separate Kalman filter tracking. However, for the dual frequency case, a new state space model is developed to handle these two signals. A straight forward implementation is to directly duplicate the previous states, resulting in a ten state filter. This, however, would prohibit the combination of the two signals and furthermore, the increased number of states can lead to a decrease in the system observability. The proposed Kalman filter implementation overcomes this problem by reducing the number of states. The new state space representation contains the L1 and the L5 amplitudes, carrier phases and code phases. In addition it includes the frequency and acceleration errors of only one of the signals, chosen to be the L5 pilot signal. Then the same concept of scaling shown in Section 2.6 can be used to scale the measured frequency and acceleration errors of the measured signal, L5, to obtain the L1 signal errors, resulting in eight states instead of ten. In this case the L5 carrier frequency and acceleration errors are the driving force of the entire model. They are used to propagate the L1 and the L5 code and carrier phase errors.

As shown in Figure 4-10, first each of the two signals undergoes carrier and code wipe-off. The output of this stage, both the L1 and the L5 correlator outputs, is then applied to one Kalman filter instead of two separate Kalman filters.

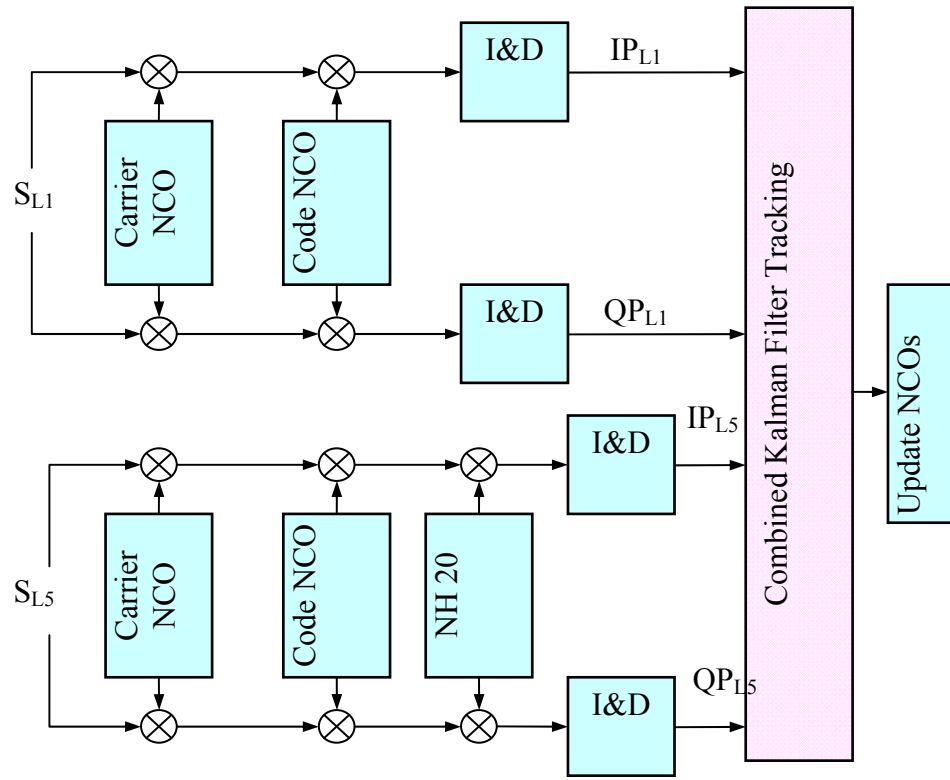


Figure 4-10: Combined Kalman filter tracking

4.2.3.1 Dynamic model

The states to be estimated, which are discussed in the previous section, can be written as

$$x = (A_1 \quad \delta\tau_1 \quad \delta\phi_{01} \quad A_5 \quad \delta\tau_5 \quad \delta\phi_{05} \quad \delta f_{05} \quad \alpha_{05})^T. \quad (4.23)$$

where the states are those defined in sections 2.3.1 and 2.3.2 for each signal.

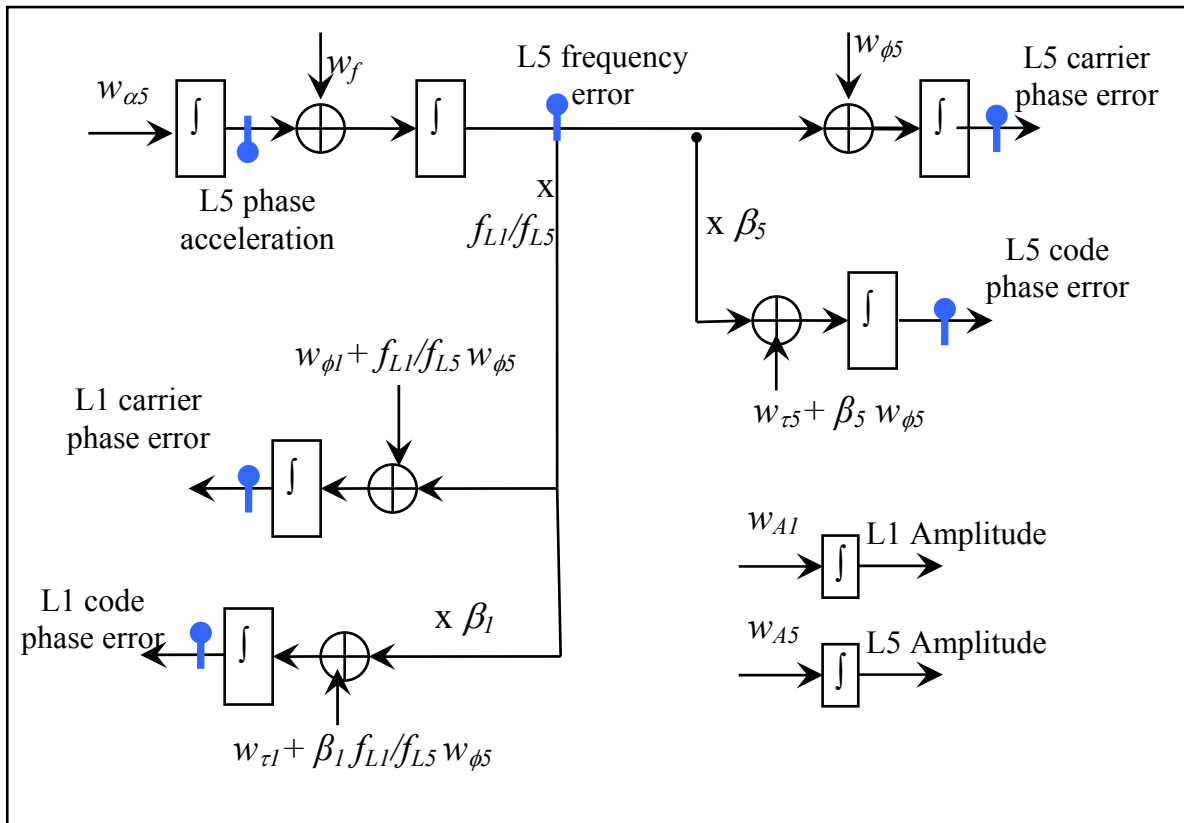


Figure 4-11: Combined Kalman filter dynamic model

To ensure a fair comparison, the same dynamic model assumption of the separate KF is used for the combined filter. The L5 carrier phase acceleration noise is the driving force for the filter. It accounts for the L5 signal dynamics. The L5 carrier frequency and phase errors accounts for the oscillator jitters. The L1 carrier phase error is estimated from the L5 carrier frequency error. Note that a random walk noise was also added to the L1 carrier phase model as a tuning parameter to account for the divergence from the L5 carrier. The value of this tuning parameter is determined by simulations. The L1 code phase error is estimated from the scaled L5 carrier frequency. A random walk component

is added to the L1 code phase error to account for the L1 code and L5 carrier divergence.

The state space model, illustrated in Figure 4-11, is given as

$$\begin{aligned}
 \frac{d}{dt} \begin{pmatrix} A_1 \\ \delta\tau_1 \\ \delta\phi_{01} \\ A_5 \\ \delta\tau_5 \\ \delta\phi_{05} \\ \delta f_{05} \\ \alpha_{05} \end{pmatrix} &= \begin{pmatrix} 0 & 0 & 0 & 0 & 0 & 0 & 0 & 0 \\ 0 & 0 & 0 & 0 & 0 & 0 & \beta_1 \frac{f_{L1}}{f_{L5}} & 0 \\ 0 & 0 & 0 & 0 & 0 & 0 & \frac{f_{L1}}{f_{L5}} & 0 \\ \hline 0 & 0 & 0 & 0 & 0 & 0 & 0 & 0 \\ 0 & 0 & 0 & 0 & 0 & 0 & \beta_5 & 0 \\ 0 & 0 & 0 & 0 & 0 & 0 & 1 & 0 \\ 0 & 0 & 0 & 0 & 0 & 0 & 0 & 1 \\ 0 & 0 & 0 & 0 & 0 & 0 & 0 & 0 \end{pmatrix} \begin{pmatrix} A_1 \\ \delta\tau_1 \\ \delta\phi_{01} \\ A_5 \\ \delta\tau_5 \\ \delta\phi_{05} \\ \delta f_{05} \\ \alpha_{05} \end{pmatrix} \\
 + \begin{pmatrix} 1 & 0 & 0 & 0 & 0 & 0 & 0 & 0 \\ 0 & 1 & 0 & 0 & 0 & \beta_1 \frac{f_{L1}}{f_{L5}} & 0 & 0 \\ 0 & 0 & 1 & 0 & 0 & \frac{f_{L1}}{f_{L5}} & 0 & 0 \\ \hline 0 & 0 & 0 & 1 & 0 & 0 & 0 & 0 \\ 0 & 0 & 0 & 0 & 1 & \beta_5 & 0 & 0 \\ 0 & 0 & 0 & 0 & 0 & 1 & 0 & 0 \\ 0 & 0 & 0 & 0 & 0 & 0 & 1 & 0 \\ 0 & 0 & 0 & 0 & 0 & 0 & 0 & 1 \end{pmatrix} \begin{pmatrix} w_{A_1} \\ w_{\tau_1} \\ w_{\phi_{01}} \\ w_{A_5} \\ w_{\tau_5} \\ w_{\phi_{05}} \\ w_{f_{05}} \\ w_{\alpha_{05}} \end{pmatrix} \tag{4.24}
 \end{aligned}$$

The corresponding transition matrix resulting from the discretization step, discussed in Section 4.2.1.3, is

$$\Phi_k = \begin{pmatrix} 1 & 0 & 0 & 0 & 0 & 0 & 0 & 0 \\ 0 & 1 & 0 & 0 & 0 & 0 & \beta_1 \frac{f_{c,L1}}{f_{c,L5}} T & \beta_1 \frac{f_{c,L1}}{f_{c,L5}} \frac{T^2}{2} \\ 0 & 0 & 1 & 0 & 0 & 0 & \frac{f_{c,L1}}{f_{c,L5}} T & \frac{f_{c,L1}}{f_{c,L5}} \frac{T^2}{2} \\ \hline 0 & 0 & 0 & 1 & 0 & 0 & 0 & 0 \\ 0 & 0 & 0 & 0 & 1 & 0 & \beta_5 T & \beta_5 \frac{T^2}{2} \\ 0 & 0 & 0 & 0 & 0 & 1 & T & \frac{T^2}{2} \\ 0 & 0 & 0 & 0 & 0 & 0 & 1 & T \\ 0 & 0 & 0 & 0 & 0 & 0 & 0 & 1 \end{pmatrix}_k. \quad (4.25)$$

4.2.3.2 Measurement model

The observations are formed from the six correlator outputs available for each signal, namely the in-phase and quadra-phase prompt, early, and late (IP, QP, IE, QE, IL, QL) correlators for each of the L1 and L5 pilot channels. These correlators are used to estimate the state parameters shown in Equation (4.23). The z vector can be written as

$$z = \begin{pmatrix} IP_{L1} & IE_{L1} & IL_{L1} & QP_{L1} & QE_{L1} & QL_{L1} \\ IP_{L5} & IE_{L5} & IL_{L5} & QP_{L5} & QE_{L5} & QL_{L5} \end{pmatrix}^T. \quad (4.26)$$

In order to obtain the design matrix of the combined Kalman filter, the $\overline{\delta\phi_{L1}}$ has to be re-expanded in terms of the L5 frequency and phase acceleration as

$$\begin{aligned} \overline{\delta\phi_{L1}} &= \frac{1}{T} \int_0^T \delta\phi_{L1}(t) dt \\ &= \delta\phi_{0,L1} + \delta f_{0,L5} \frac{T}{2} \times \frac{f_{L1}}{f_{L5}} + \alpha_{0,L5} \frac{T^2}{6} \times \frac{f_{L1}}{f_{L5}} \end{aligned} \quad (4.27)$$

The relation between the measurements vector z and the states can be derived similar to the separate KF case, shown in Equation (4.22).

4.2.4 Measurement Covariance R

To fully evaluate the quality of the measurements, an adequate measure of their noise variances is required.

For the separate Kalman filter, the measurement covariance matrix is represented by:

$$R_z = \begin{pmatrix} C_{I_s} & 0 \\ 0 & C_{Q_s} \end{pmatrix} \quad (4.28)$$

where C_{I_s}, C_{Q_s} : Each represents a 3 x 3 covariance matrix of the in-phase and quadrature P/E/L correlator outputs on the subscripted signal s .

$$C_{correlator, signal} = \sigma_N^2 \cdot \begin{pmatrix} R(0) & R(\Delta) & R(\Delta) \\ R(\Delta) & R(0) & 0 \\ R(\Delta) & 0 & R(0) \end{pmatrix}. \quad (4.29)$$

For the combined Kalman filter, the measurement covariance matrix is expanded to give a measurement for both signals as follows:

$$R_z = \begin{pmatrix} C_{I1} & 0 & 0 & 0 \\ 0 & C_{Q1} & 0 & 0 \\ 0 & 0 & C_{I5} & 0 \\ 0 & 0 & 0 & C_{Q5} \end{pmatrix} \quad (4.30)$$

In order to obtain a reasonable estimate of the noise variances σ_N^2 of each correlator, an unused PRN, in this case PRN 35, is simulated and tracked. The noise variance is then

estimated from the squared magnitude of the prompt correlator output. This operation is performed separately on the L1 and L5:

$$\sigma_N^2 = \frac{1}{T} \cdot \sum_T |IP_{35}|^2 \quad (4.31)$$

where $1/T$: Bandwidth of the measurements

4.2.5 Process Noise Q

The process noise is an important tuning factor that has to be adjusted fairly in the two elements of comparison. For the separate Kalman filter tracking, five process noise spectral densities occurs for each of the L1 and the L5 signals, whereas for the combined Kalman filter eight process noise spectral densities occur.

Three main tuning parameters taken into consideration are:

1. Amplitude standard deviation: accounts for the signal level variations
2. Code Carrier Divergence: accounts for the code carrier divergence due to ionospheric errors and multipath
3. LOS Spectral Density: that is the driving force for the filter

The other two process noises are the carrier phase and frequency; these are tuned according to the oscillator used in the receiver front-end.

The combined Kalman filter tuning parameters are similar to those of the separate Kalman filter with five tuning parameters are dealt with, namely the amplitude standard deviation of both the L1 and the L5 signals, the code carrier divergence of both, and the LOS spectral density. To ensure a fair comparison between the filters, the values of the

L5 spectral densities used are the same, since the dynamic model for them is unchanged. However, the L1 code and carrier phase process noises have to be tuned in case of the combined Kalman filter to account for the divergence from the L5 carrier. Table 4-4 and Table 4-5 show the process noise spectral densities for both separate and the combined Kalman filter, respectively. These parameters were tuned experimentally for various conditions, e.g. static/dynamic user, multipath and modelled/unmodeled atmospheric conditions.

Table 4-4: Separate Kalman filter parameters	
Process noise	Spectral density
A_s (dB/s/ $\sqrt{\text{Hz}}$)	1
$\delta\tau_s$ (m/s/ $\sqrt{\text{Hz}}$)	0.1
$\delta\phi_s$ (cycles/s/ $\sqrt{\text{Hz}}$)	$(2\pi f_s) \cdot \sqrt{(h_0/2)}$
δf_s (Hz/s/ $\sqrt{\text{Hz}}$)	$(2\pi f_s) \cdot \sqrt{(2\pi^2 h_{-2})}$
α_s (m/s ³ / $\sqrt{\text{Hz}}$)	5
where subscript s refers to the signal of interest	

Table 4-5: Combined Kalman filter parameters	
Process noise	Spectral density
A_{L1} (dB/s/ $\sqrt{\text{Hz}}$)	1
$\delta\tau_{L1}$ (m/s/ $\sqrt{\text{Hz}}$)	1
$\delta\phi_{L1}$ (cycles/s/ $\sqrt{\text{Hz}}$)	0.6
A_{L5} (dB/s/ $\sqrt{\text{Hz}}$)	1
$\delta\tau_{L5}$ (m/s/ $\sqrt{\text{Hz}}$)	0.1
$\delta\phi_{L5}$ (cycles/s/ $\sqrt{\text{Hz}}$)	$(2\pi f_s) \cdot \sqrt{(h_0/2)}$
δf_{L5} (Hz/s/ $\sqrt{\text{Hz}}$)	$(2\pi f_s) \cdot \sqrt{(2\pi^2 h_{-2})}$
α_{L5} (m/s ³ / $\sqrt{\text{Hz}}$)	5

4.3 Summary

The chapter presented two major approaches for combining the conventional L1 signal and the new L5 signal. The first approach is through aiding the L1 signal with the L5 tracking information. That is achieved by scaling both the L5 Doppler frequency and the code Doppler and adding them to the corrections calculated by the L1 tracking loop. In this approach, only one signal, the L1 signal, benefits from the aiding.

The second approach is through the use of Kalman filter. In order to achieve this a complete combined Kalman filter model is designed and implemented to collaborate the tracking information of the two signals. The two signals benefit in that case from the combination.

The next chapter provides a detailed performance evaluation of these two approaches.

Chapter Five: PERFORMANCE EVALUATION OF THE PROPOSED COMBINATION APPROACHES

This chapter provides a performance evaluation of both the aided standard tracking loops and the combined Kalman filter tracking loops. The chapter starts with a derivation for the phase tracking loops in case of aided standard tracking loops, followed by a theoretical and experimental evaluation of the proposed approach compared to the separate standard tracking loops. The second part of the chapter evaluates the combined Kalman filter tracking, compared to the separate Kalman filter tracking in two sets of environments.

The last part in the evaluation is comparing the standard tracking loops with the Kalman filter tracking loop. A method for experimentally deriving the equivalent bandwidth of the Kalman filter's tracking loop is presented. Results are shown for comparing the separate Kalman filter tracking with the equivalent standard tracking loops, and the combined Kalman filter tracking with the aided standard tracking loops.

5.1 Standard Tracking Loops

In order to get an adequate evaluation for the aided tracking loop, the error contribution of the L5 signal to the L1 tracking loops have to be accounted for. This section provides a derivation for the total phase error encountered by the aided L1 tracking loop, followed by both theoretical and experimental evaluation.

5.1.1 Aided Phase Tracking loop Errors

In Chapter 4, the total phase error standard deviation for the PLL tracking loop was shown. For the L1 and L5 signals it is given by

$$\begin{aligned}\sigma_{L1} &= \sqrt{(\sigma_{t1}^2 + \sigma_{v1}^2 + \theta_{A1}^2)} + \frac{\theta_{e1}}{3} \quad (\text{degrees}) \\ \sigma_{L5} &= \sqrt{(\sigma_{t5}^2 + \sigma_{v5}^2 + \theta_{A5}^2)} + \frac{\theta_{e5}}{3} \quad (\text{degrees})\end{aligned}\tag{5.1}$$

Equation (5.1) shows the standard deviation for the case of separate phase tracking. However, when aiding the L1 signal with the L5 Doppler frequency, as shown in Figure 5-1, the errors fed by the L5 signal have to be accounted for.

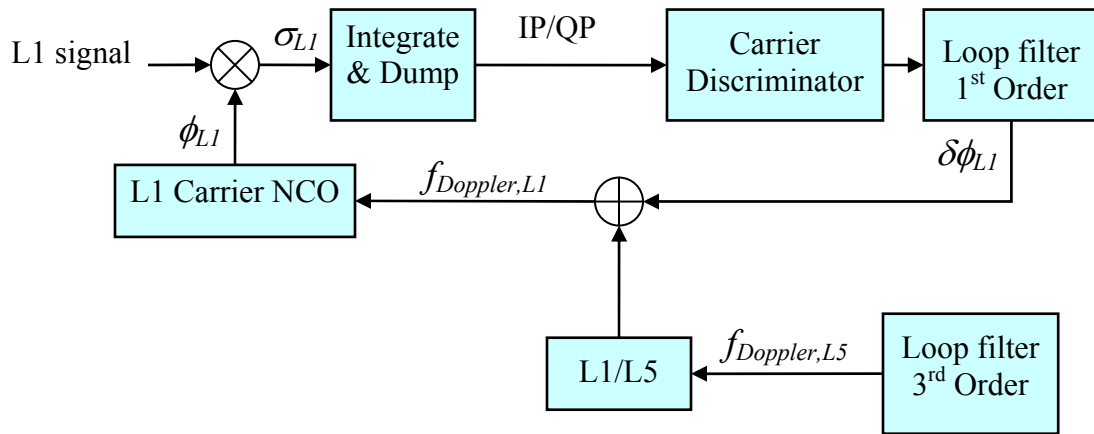


Figure 5-1: Aided L1 PLL tracking loop

To get the L5 contribution to the L1 tracking loop, the following relation shown by Egziabher et al (2003) for the 1-sigma standard deviation of the phase error between the L1 and L5 signals is used:

$$\sigma_{L1} = \frac{f_{L1}}{f_{L5}} \sigma_{L5}.\tag{5.2}$$

Equation (5.2) states that the ratio of the standard deviation of the two signals is the same as the ratio between their carrier frequencies, which is a reasonable and expected relation. Applying this to the errors fed to the L1 loop due to the L5 signal yields (Qaisar 2009)

$$\sigma_{L1-L5,aid} = \frac{f_{L1}}{f_{L5}} \sigma_{L5} \quad (5.3)$$

where $\sigma_{L1-L5,aid}$: 1-sigma L1 phase error fed by the L5 signal.

This error $\sigma_{L1-L5,aid}$ can be classified into correlated sources and uncorrelated sources. The correlated sources include the vibration-induced oscillator noise, Allan deviation and the dynamic stress error. The uncorrelated sources include only the thermal noise. The error can be written as

$$\sigma_{L1-L5,aid} = \begin{cases} \sigma_{L1-L5,aid,corr} = \theta_A, \sigma_v, \theta_e \\ \sigma_{L1-L5,aid,uncorr} = \sigma_{t5} \end{cases} \quad (5.4)$$

where $\sigma_{L1-L5,aid,corr}$: 1-sigma L1 phase correlated errors fed by the L5 signal

$\sigma_{L1-L5,aid,uncorr}$: 1-sigma L1 phase uncorrelated errors fed by the L5 signal.

The vibration-induced noise is ignored in the simulations, as the oscillator is firmly mounted in the NI front-end, and due to the lack of adequate information on the oscillator vibration sensitivity. On the other hand, the total Allan deviation is a combination of those of the L1 and L5 signals. It consists of the errors due to the L1 signal, the scaled errors due to the L5 signal and a term that depends on the correlation between the two signals as follows:

$$\theta_{Total}^2 = \theta_{A1}^2 + 2 \cdot \rho \cdot \theta_{A1} \left(\frac{f_{L1}}{f_{L5}} \cdot \theta_{A5} \right) + \left(\frac{f_{L1}}{f_{L5}} \theta_{A5} \right)^2 \quad (5.5)$$

where ρ : Correlation coefficient between L1 and L5 errors

In order to get the accurate correlation factor between the L1 and L5 Allan variances, the results of the combined Kalman filter are used, where the process noise covariance matrix Q is used to relate the standard deviation of the L1 and scaled L5 phase errors to the clock parameters. Eliminating all the other sources, the resulting covariance matrix is

$$\begin{aligned} Q_k &= \begin{pmatrix} \sigma_{\delta\phi_{01}}^2 & \left(\frac{f_{L1}}{f_{L5}} \right) \cdot \sigma_{\delta\phi_{01}, \delta\phi_{05}} \\ \left(\frac{f_{L1}}{f_{L5}} \right) \cdot \sigma_{\delta\phi_{01}, \delta\phi_{05}} & \left(\frac{f_{L1}}{f_{L5}} \right)^2 \cdot \sigma_{\delta\phi_{05}}^2 \end{pmatrix} \\ &= \begin{pmatrix} \left(\frac{f_{L1}}{f_{L5}} \right)^2 \cdot \left(S_{f5} \cdot T + \frac{1}{3} \cdot T^3 \cdot S_{g5} \right) & \left(\frac{f_{L1}}{f_{L5}} \right)^2 \cdot \left(S_{f5} \cdot T + \frac{1}{3} \cdot T^3 \cdot S_{g5} \right) \\ \left(\frac{f_{L1}}{f_{L5}} \right)^2 \cdot \left(S_{f5} \cdot T + \frac{1}{3} \cdot T^3 \cdot S_{g5} \right) & \left(\frac{f_{L1}}{f_{L5}} \right)^2 \cdot \left(S_{f5} \cdot T + \frac{1}{3} \cdot T^3 \cdot S_{g5} \right) \end{pmatrix} \end{aligned} \quad (5.6)$$

where S_{f5} : The spectral density of the white frequency noise, $S_{f5} = (2\pi f_s) \cdot \sqrt{(h_0/2)}$

S_{g5} : The spectral density of the random walk frequency noise,
 $S_{g5} = (2\pi f_s) \cdot \sqrt{(2\pi^2 h_{-2})}$.

Equation (5.6) shows the covariance matrix of both the L1 and scaled L5 phase errors due to the clock parameters. The correlation coefficient is calculated as:

$$\rho = \frac{\sigma_{xy}}{\sigma_x \sigma_y} = \frac{\left(\frac{f_{L1}}{f_{L5}}\right) \cdot \sigma_{\delta\phi_{01}, \delta\phi_{05}}}{\left(\frac{f_{L1}}{f_{L5}}\right) \cdot \sigma_{\delta\phi_{01}} \sigma_{\delta\phi_{05}}} \quad (5.7)$$

Substituting in Equation (5.6) yields

$$\rho = \frac{\left(\frac{f_{L1}}{f_{L5}}\right)^2 \cdot \left(S_{f5} \cdot T + \frac{1}{3} \cdot T^3 \cdot S_{g5}\right)}{\sqrt{\left(\frac{f_{L1}}{f_{L5}}\right)^2 \cdot \left(S_{f5} \cdot T + \frac{1}{3} \cdot T^3 \cdot S_{g5}\right)} \cdot \sqrt{\left(\frac{f_{L1}}{f_{L5}}\right)^2 \cdot \left(S_{f5} \cdot T + \frac{1}{3} \cdot T^3 \cdot S_{g5}\right)}} = 1 \quad (5.8)$$

Equation (5.8) shows that the variance of the L1 and the L5 signals are correlated, with a correlation coefficient equal to 1, as they are both driven by the same oscillator.

Substituting that correlation coefficient into Equation (5.5) gives the total expression of the Allan deviation as

$$\theta_{Total}^2 = \theta_{A1}^2 + 2 \cdot \theta_{A1} \left(\frac{f_{L1}}{f_{L5}} \cdot \theta_{A5}\right) + \left(\frac{f_{L1}}{f_{L5}} \theta_{A5}\right)^2. \quad (5.9)$$

Returning to the discussion in Chapter 4, the L1 loop filter is set to be of a 1st order, only tracking the divergence between itself and the L5 signal, with a low noise bandwidth. The L5 signal is responsible for tracking the signal dynamics and the oscillator jitters, and uses a 3rd order loop filter. Thus, the Allan deviation expression for the L5 signal is that of a 3rd order PLL, whereas for the L1 signal is that of a 1st order PLL.

The third correlated error is the dynamic stress. Given that the L5 signal is the one responsible for tracking any dynamics, the total dynamic error can be expressed as (Qaisar 2009)

$$\theta_{total} = \frac{f_{L1}}{f_{L5}} \theta_{e5}. \quad (5.10)$$

Note that a quick analysis shows that a steady state error in the L5 tracking loop yields a zero steady state error in the L1 tracking loop, which requires further investigation. Nonetheless, the approximation presented in Equation (5.10), as proposed by Qaisar (2009), works well in practice as shown in the following sections.

The only uncorrelated source is the thermal noise, which is fed to the L1 tracking loop using the relation shown in Equation (5.3).

Summing up, the total 1-sigma total phase error of the L1 signal is calculated as

$$\sigma_{L1} = \sqrt{\left(\sigma_{i1}^2 + \left(\frac{f_{L1}}{f_{L5}} \right)^2 \sigma_{i5}^2 + \sigma_{vtotal}^2 + \theta_{Atotal}^2 \right)} + \frac{f_{L1}}{f_{L5}} \cdot \frac{\theta_{e5}}{3} \leq 15^\circ \quad (\text{data present}). \quad (5.11)$$

5.1.2 Theoretical Evaluation

In order to evaluate the tracking performance of the L1-aided tracking loops in terms of the 1-sigma phase error, it is compared to the L1 standard tracking loop. In the aided case, the L5 PLL is set to operate as a 3rd order loop using a bandwidth of 10 Hz, whereas the L1 PLL is set to operate using a 1st order PLL. For the separate case, the L1 PLL is set to operate as a 3rd order PLL.

For the first test, the assumed dynamic stress experienced by the two signals is 0.2 g/s. The L1 signal C/N_0 is 25 dB-Hz, and the L5 pilot channel C/N_0 is 27 dB-Hz. Figure 5-2 shows the total tracking error for the unaided L1, with the contribution of the different errors sources to it. The unaided PLL can track the signal with a bandwidth of 8.2 Hz.

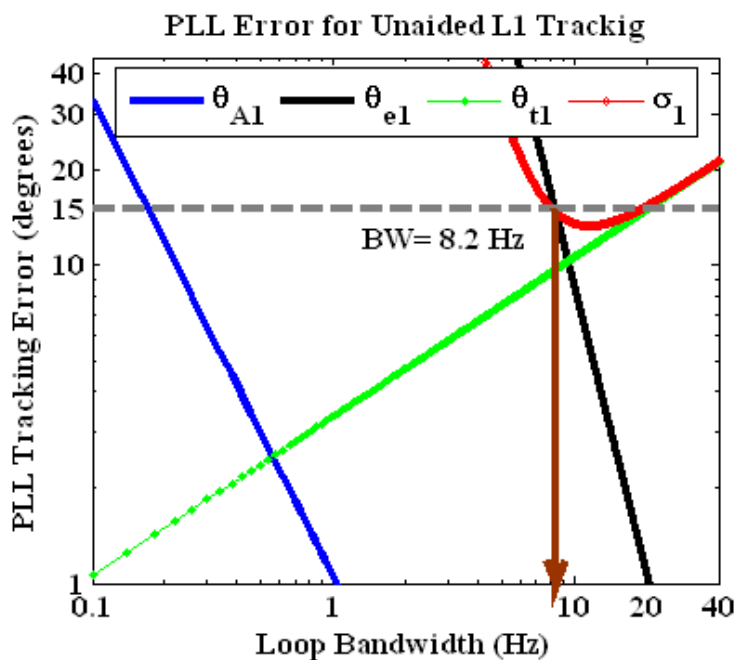


Figure 5-2: Unaided L1 PLL tracking error

Figure 5-3 shows the total tracking error for the aided L1 case for the same scenario. Since the dynamics are tracked using the L5 PLL, the L1 PLL can track the signal with a bandwidth less than 4.2 Hz. That verifies the assumption of the lower bandwidth used in the aided PLL case.

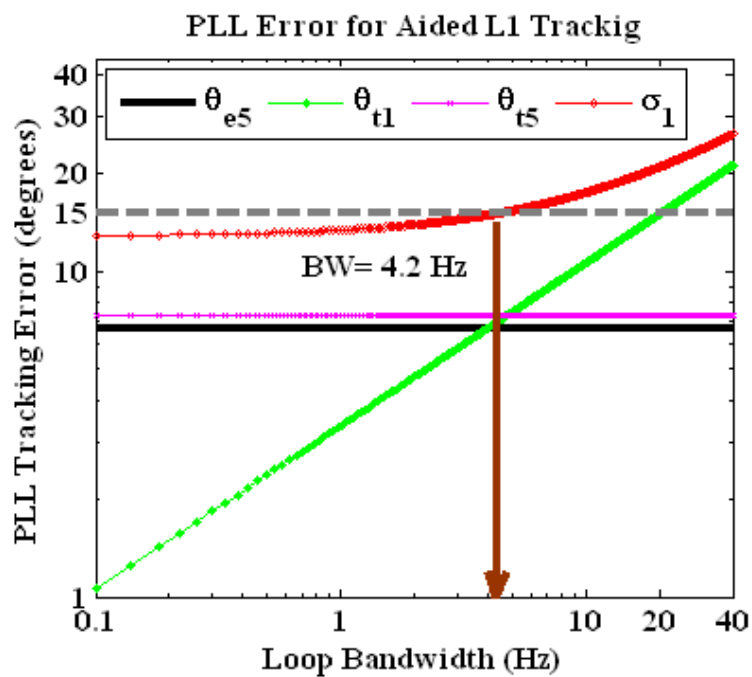


Figure 5-3: Aided L1 PLL tracking error

The second part of the evaluation is intended to show the gain achieved when using the aided L1 PLL in terms of the minimum C/N_0 it can track compared to the unaided case. Figure 5-4 shows the results for two dynamic stresses, namely 0.01 g/s and 1 g/s. For the 1 g/s case, the aided L1 PLL could track the signal down to a C/N_0 of 23 dB-Hz, using loop bandwidth of 0.1 Hz. For the same dynamics, the unaided L1 PLL could track down to 23.8 dB-Hz using loop bandwidth of 10 Hz. That is an increase of sensitivity of only 0.8 dB; however the reduction in the noise bandwidth is significant.

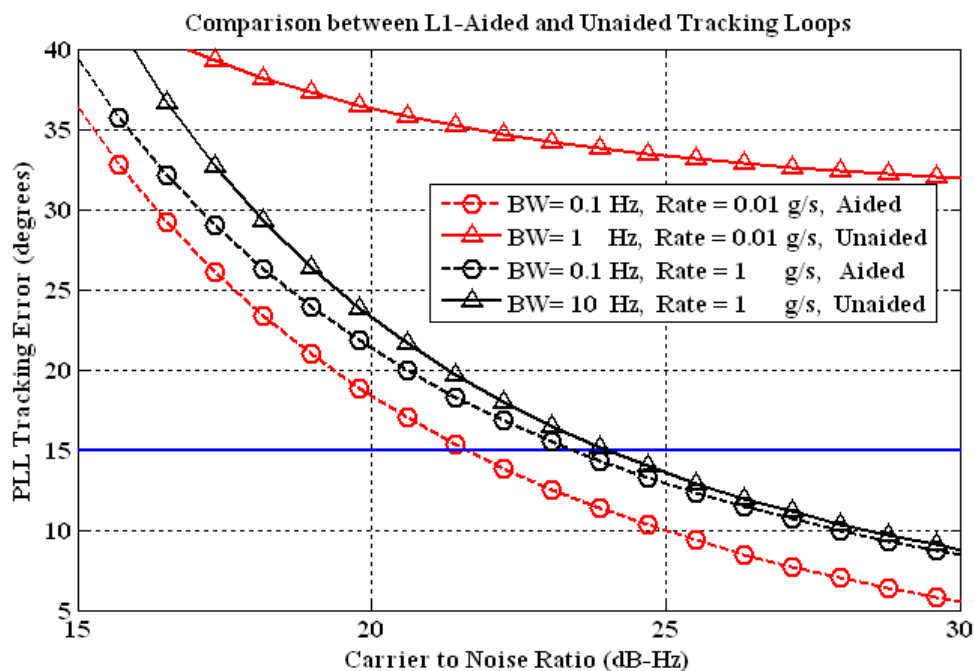


Figure 5-4: Comparison between L1-aided and unaided tracking loops

The gain achieved is more obvious in the case of 0.01 g/s dynamic stress. The aided L1 PLL could track the signal down to a C/N_0 of 21.5 dB-Hz using a loop bandwidth of 0.1 Hz, whereas the unaided L1 could not track the signal using 10 times larger bandwidth. However it should be noted that the unaided L1 PLL would be able to track that signal with a 10 Hz bandwidth which is 100 times that of the aided L1 PLL, however that would increase the thermal noise in the loop.

5.1.3 Experimental Evaluation

Following the theoretical evaluation, an experimental evaluation is conducted to verify the results. Two different environments are simulated using a Spirent GSS7700 simulator (Spirent 2006): The first is a land mobile multipath with an urban canyon multipath

environment on a static vehicle, and the second is a dynamic vehicular user moving with a high acceleration and sudden turns. The details of each simulation setup are as follows.

5.1.3.1 Urban canyon multipath

The first test is on a static vehicle operating in an urban canyon multipath environment.

The following conditions are chosen:

1. Static vehicle
2. Land mobile multipath
3. Urban canyon multipath environment

Several studies in the literature (e.g. Lachapelle et al 2003, Hu et al 2005) have studied the matching of the simulated multipath environments using the Spirent signal simulator to actual multipath environments.

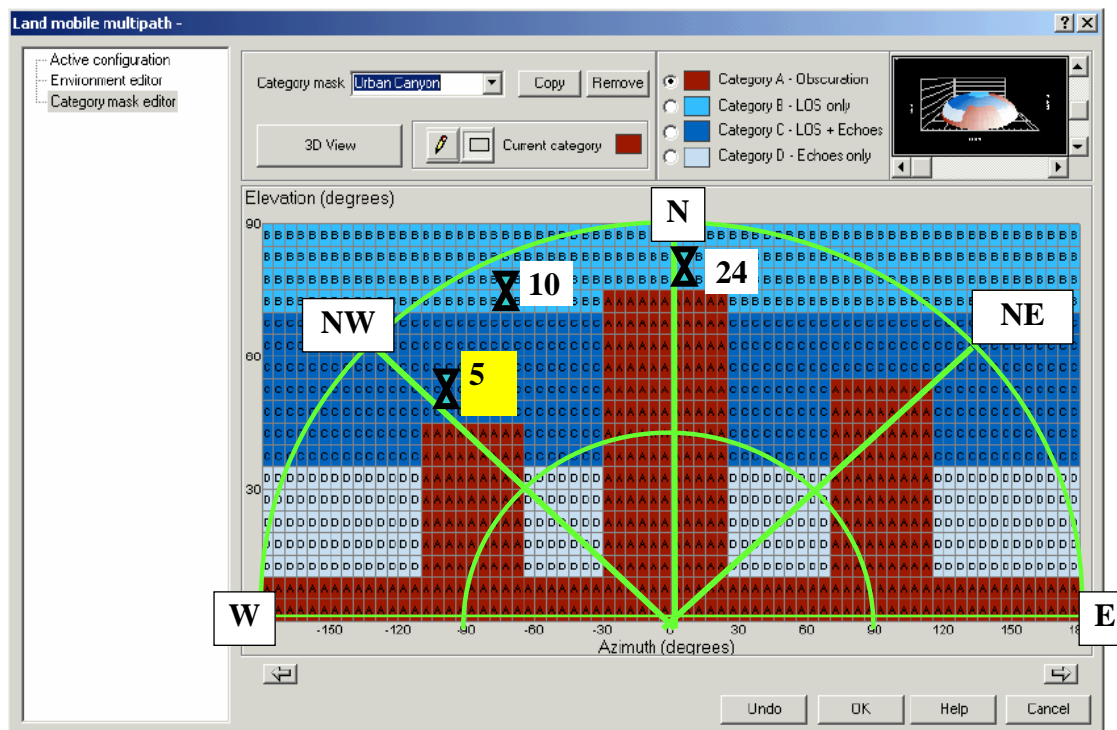


Figure 5-5: Multipath categories and satellites in view

The land mobile multipath model allows four categories for the signals determined by their arriving angles discussed in Chapter 3. For the test conducted, the satellite chosen must have both LOS and echoes. The signal being tracked during this test is that for PRN 5 (highlighted in Figure 5-5). From the elevation and the azimuth angle of the satellite, it lies in category C, where it is simulated as LOS and echoes.

5.1.3.1.1 Pilot only

The first approach is implemented using only the pilot channel of the L5 signal to aid the L1 signal. The tracking performance is analyzed by the PLI (Section 2.5), and the correlator outputs of the aided PLL versus the unaided PLL. Figure 5-6 shows the L1 PLI for the aided PLL and the unaided PLL for two values of the noise bandwidth, namely 5 Hz and 10 Hz. The unaided PLL, with the 10 Hz bandwidth, allowed more noise in the loop, which caused it to lose lock with the experienced multipath. The 5 Hz unaided loop was able to continue tracking with low PLI. The aided PLL, on the other hand, had higher PLI in both cases, as the PLL is tracking only the divergence from the pilot channel in that case.

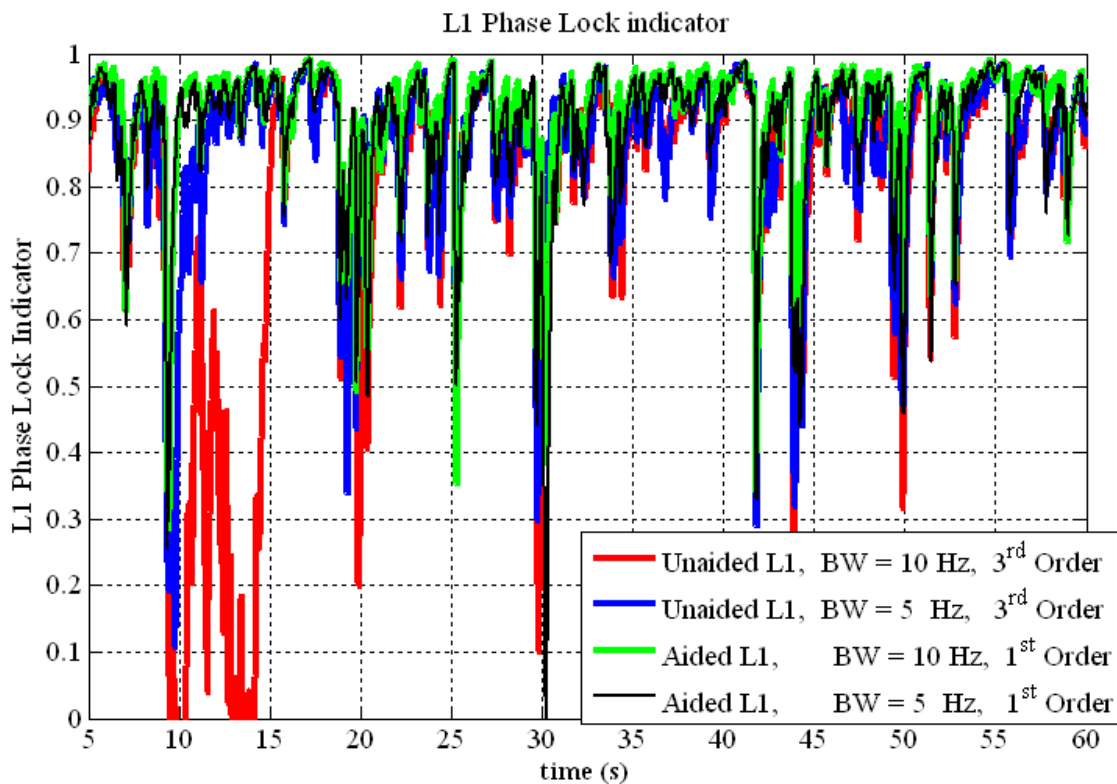


Figure 5-6: L1 PLI of pilot aided PLL versus unaided PLL for multipath scenario

Figure 5-7 shows the correlator outputs for the aided versus the unaided PLL, using a 5 Hz bandwidth. Zooming into the period where the signal was suffering from multipath reveals that the unaided PLL has totally lost track of the signal, as indicated by the in-phase correlator output. The aided PLL continued tracking with its in-phase correlator output reflecting the signal power variations due to the multipath.

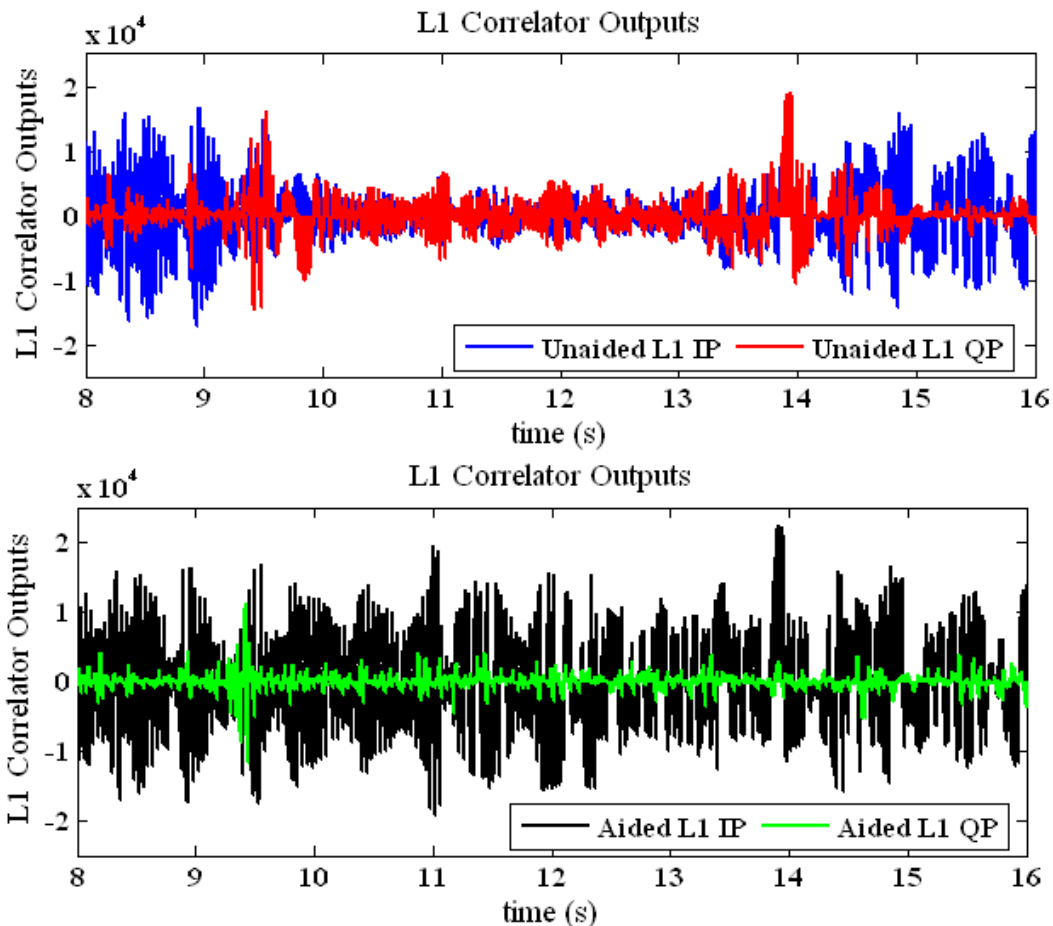


Figure 5-7: Aided L1 correlator outputs versus unaided correlator outputs for multipath scenario

5.1.3.1.2 Data and pilot

The second aiding approach is implemented using the total signal power of the L5 signal. In order to confirm the advantages of such combination, Figure 5-8 shows the L5 PLI when tracking using the pilot channel only versus using the total signal power. It shows that there is a marginal benefit in the PLI under the simulated urban canyon multipath environment, as the combined data and pilot tracking are giving higher values for the PLI.

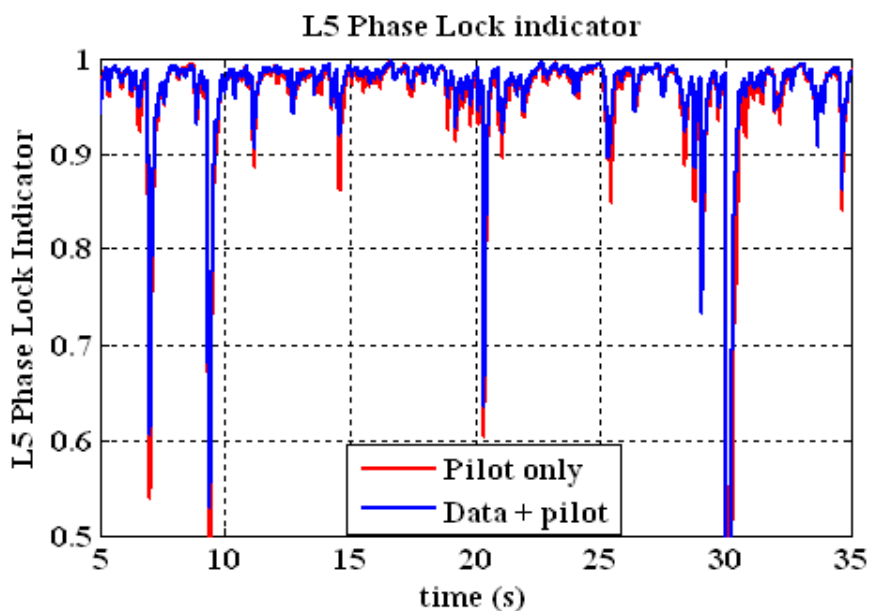


Figure 5-8: L5 PLI using pilot only versus using data and pilot for multipath scenario

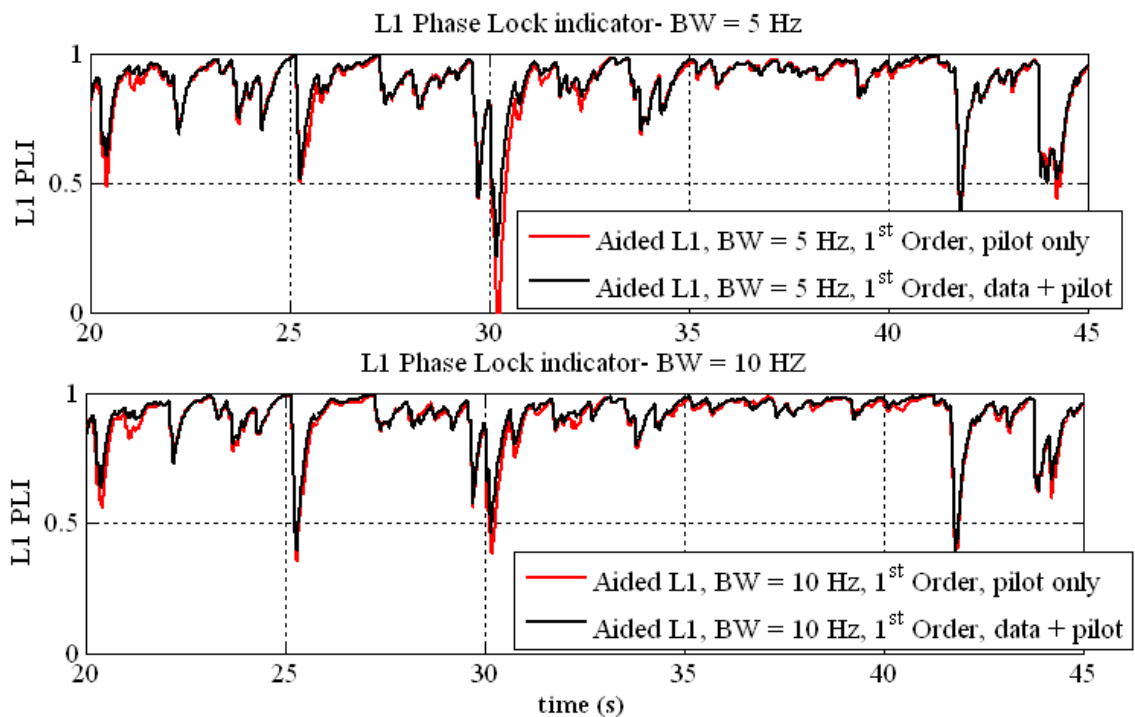


Figure 5-9: PLI of pilot aided L1 PLL versus data and pilot aided L1 PLL, for BW = 5 Hz, BW = 10 Hz, for multipath scenario

Figure 5-9 shows the L1 PLI for the aided tracking loops, for two bandwidth values. Although the combined data and pilot tracking show marginal improvements in the L5 PLI, when used for aiding the L1 PLL, it enhances the overall tracking performance by increasing the PLI, especially at the periods where the signal suffers from higher power variations.

5.1.3.2 Motion

The second scenario simulated is for the dynamic vehicle, with the following parameters:

1. Dynamic vehicle, with a velocity ranging between 25 km/hr and 100 km/hr, moving in the rectangular path shown in Figure 5-10 and accelerating within a distance of 100 m.
2. Moderate signal power levels (The received L1 C/N_0 is 36 dB-Hz).

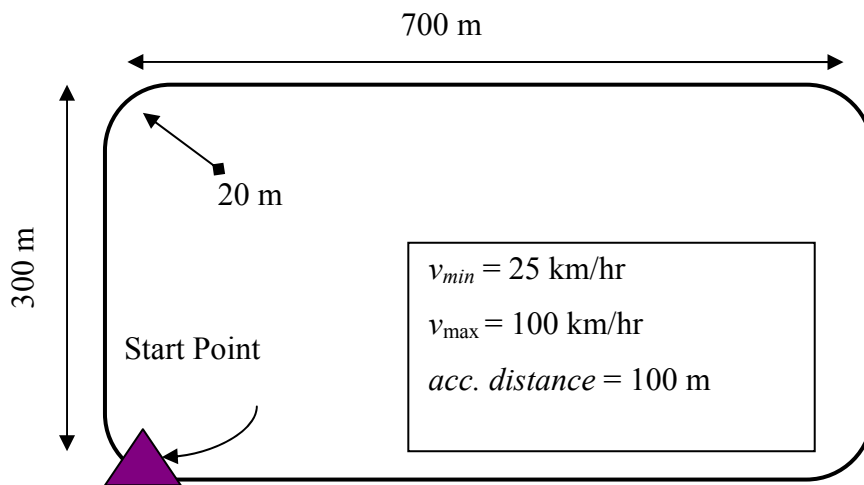


Figure 5-10: Dynamic vehicle model

The results are shown for aiding using the pilot channel and using both the data and pilot channels.

5.1.3.2.1 Pilot only

Three different values of the noise bandwidth, namely 1 Hz, 5 Hz and 10 Hz, are used in the L1 PLL for the two cases of the aided and the unaided approaches. Figure 5-11 shows the L1 PLI for the two cases. The unaided PLL failed to keep track of the signal using the two low bandwidth values, while it was successful using the 10 Hz bandwidth. Thus, contrary to the multipath case, increasing the bandwidth actually helped the PLL to keep track of the signal's dynamics. Comparing to the aided case, it kept track of the signal whatever value of noise bandwidth used. However increasing the noise bandwidth shows higher values of PLI.

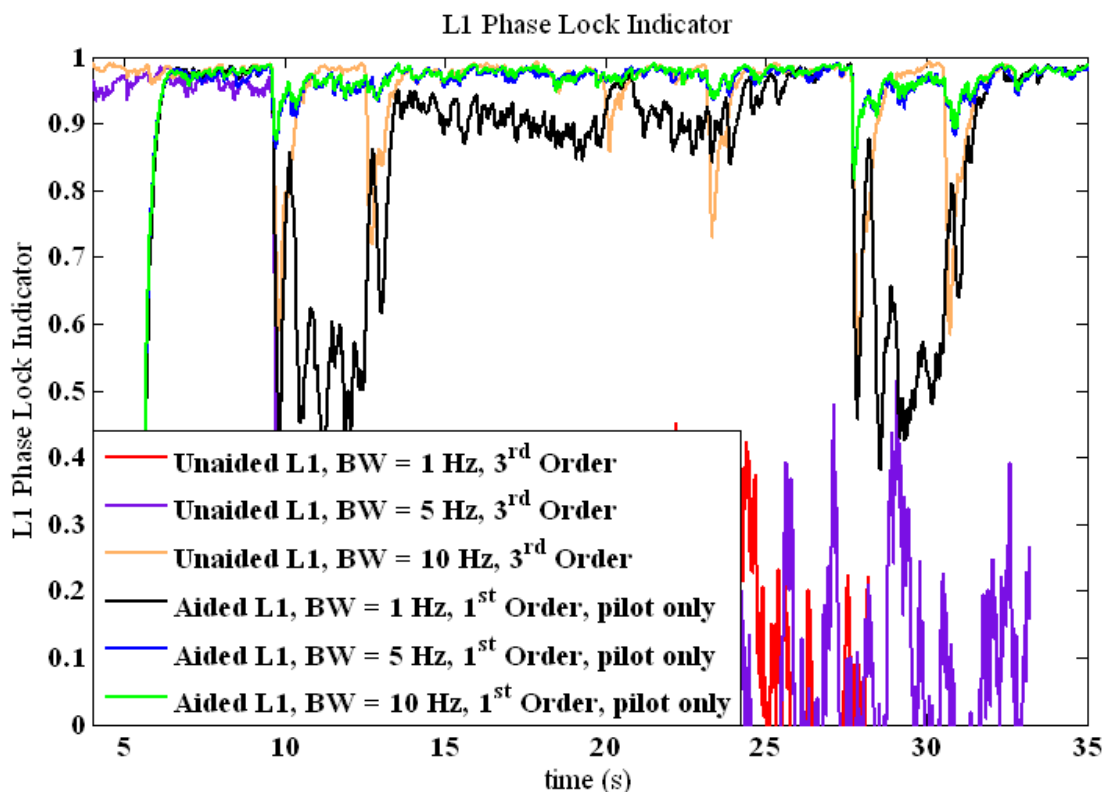


Figure 5-11: L1 PLI for aided versus unaided tracking loops for moving vehicle scenario

Figure 5-12 shows the correlator outputs of the aided and the unaided PLL using a 10 Hz bandwidth, where the unaided in-phase correlator shows lower signal power, and the quadrature correlator shows higher noise, compared to the aided case.

Figure 5-13 shows the Doppler frequency calculated using the aided and unaided PLL. Even though the unaided L1 PLL continued to track the signal, with the 10 Hz bandwidth throughout the entire simulation period, it is showing a larger error which is reflected in the correlator outputs shown in Figure 5-12. With the 5 Hz bandwidth however, the unaided PLL could not track the signal.

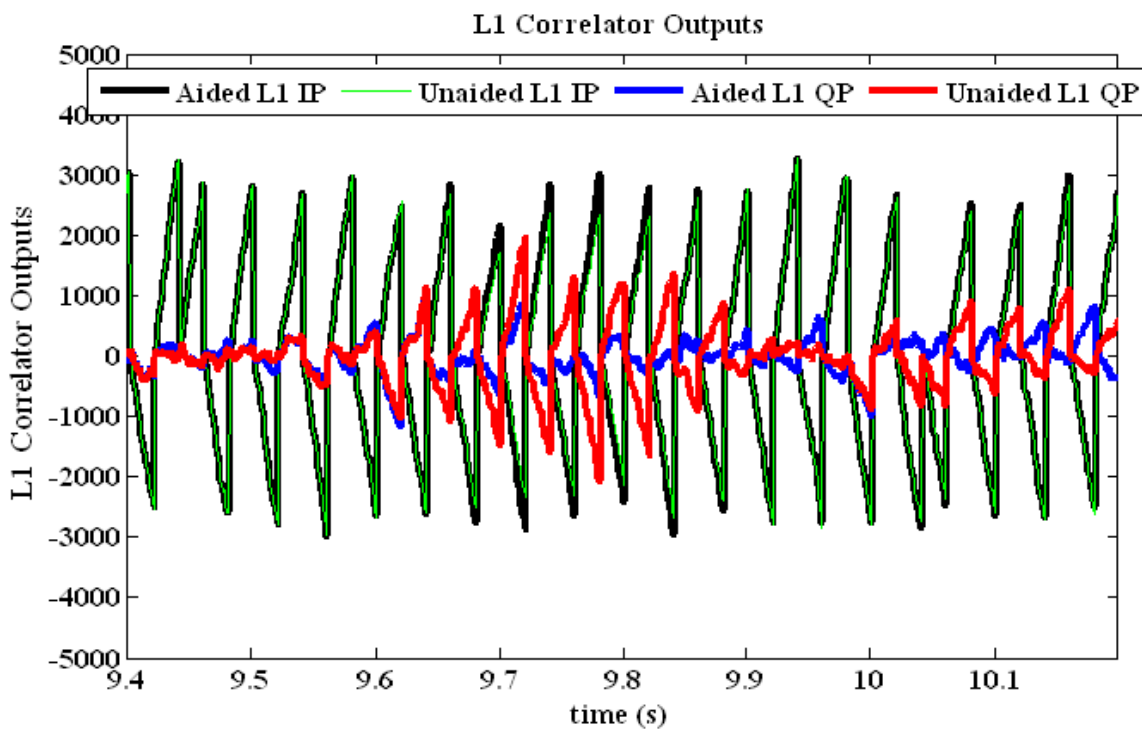


Figure 5-12: L1 aided versus unaided correlator outputs for moving vehicle scenario

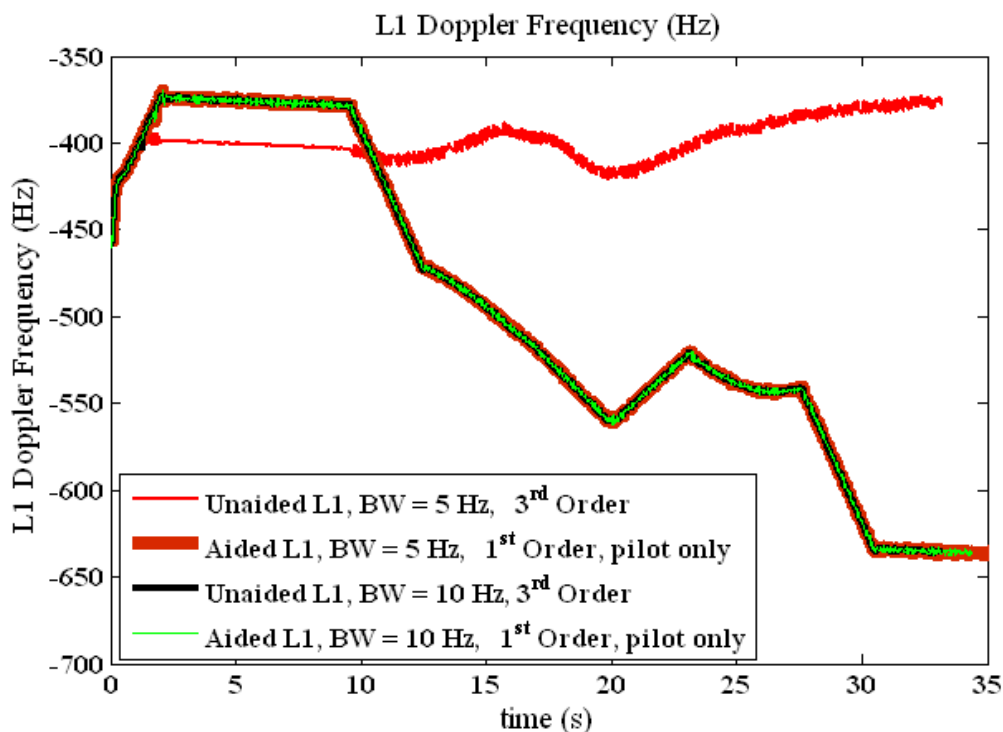


Figure 5-13: L1 Doppler frequency for moving vehicle scenario

Note that both the frequency and phase lock indicators show that the four scenarios of the tracking loops, shown in Figure 5-12, tracked the correct frequency.

5.1.3.2.2 Data and pilot

The second set of results is generated by using the combined data and pilot channel to track the moving vehicle's signal. Figure 5-14 shows the L1 PLI for the pilot aided versus the data and the pilot aided PLL. The data and pilot aided PLL shows higher PLI compared to the pilot only aided PLL. Combining the total signal power of the L5 signal has helped the L1 to enhance its tracking performance in these dynamic conditions.

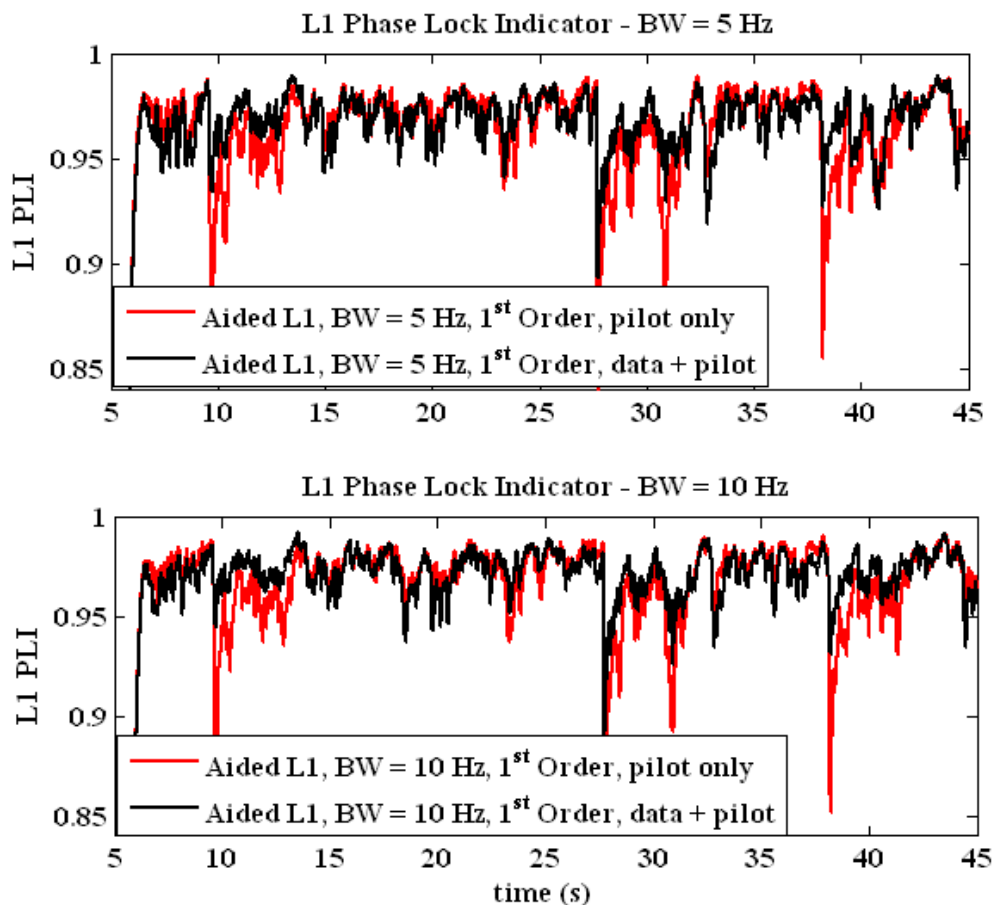


Figure 5-14: L1 PLI aided using pilot versus data and pilot for moving vehicle scenario

5.2 Kalman Filter Tracking

The second tracking approach considered in the thesis is through the Kalman filter. Several steps were done to evaluate the Kalman filter model presented in Chapter 4. First, a rough comparison was made with the separate standard tracking loops to verify the applicability of the model; the results are shown in Appendix B. Second, a thorough comparison is done with the separate Kalman filter tracking loops to identify the benefits of the combination scheme.

5.2.1 Comparison with Separate Kalman Filter Tracking Loops

The results shown in this section are categorized into two parts as follows (Salem 2009):

- a) The tracking performance analyzed by the phase lock indicators, the frequency lock indicators, the Doppler frequency and the correlator outputs of both signals using each of the two methods under comparison.
- b) The Kalman filter states and their corresponding standard deviations for each of the two filters.

5.2.1.1 Urban canyon multipath

The scenario used is the same urban canyon multipath described in Section 5.1.3.1. The Kalman filter parameters used are discussed in sections 4.2.4 and 4.2.5.

5.2.1.1.1 Tracking errors

Examining the tracking errors in the urban multipath case, Figure 5-15 shows the FLI of the L1 frequency for the separate Kalman filter, combined Kalman filter using the L5 pilot channel and the combined Kalman filter using both the data and pilot channels.

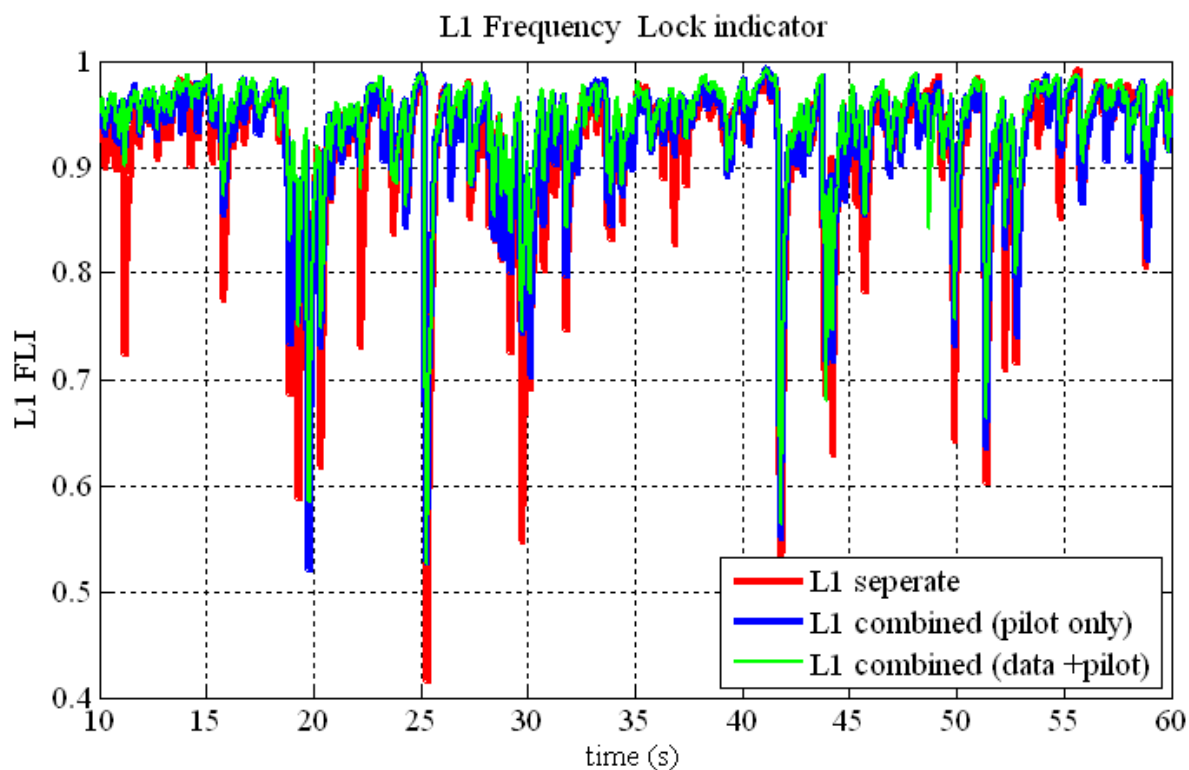


Figure 5-15: L1 FLI for separate versus combined Kalman filter for multipath scenario

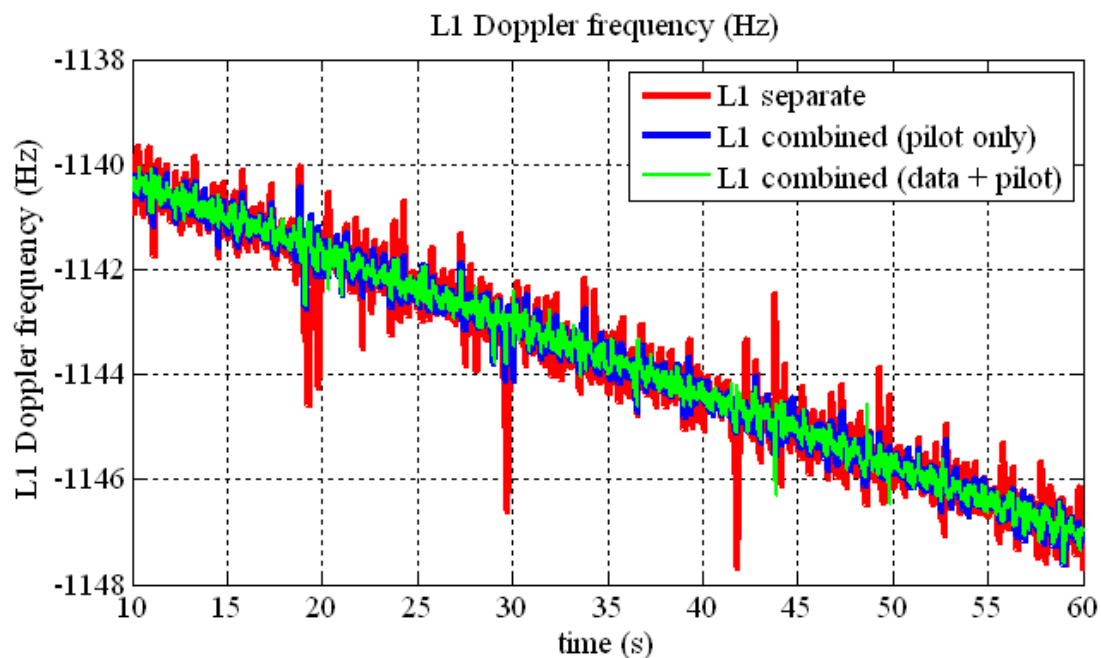


Figure 5-16: L1 Doppler frequency for separate versus combined Kalman filter for multipath scenario

The combined Kalman filter has helped in general in enhancing the FLI in the urban canyon multipath environment and this is reflected in the less noisy Doppler frequency estimate shown in Figure 5-16. The use of the combined L5 signal power has helped in further raising the L1 FLI, compared to the pilot only case.

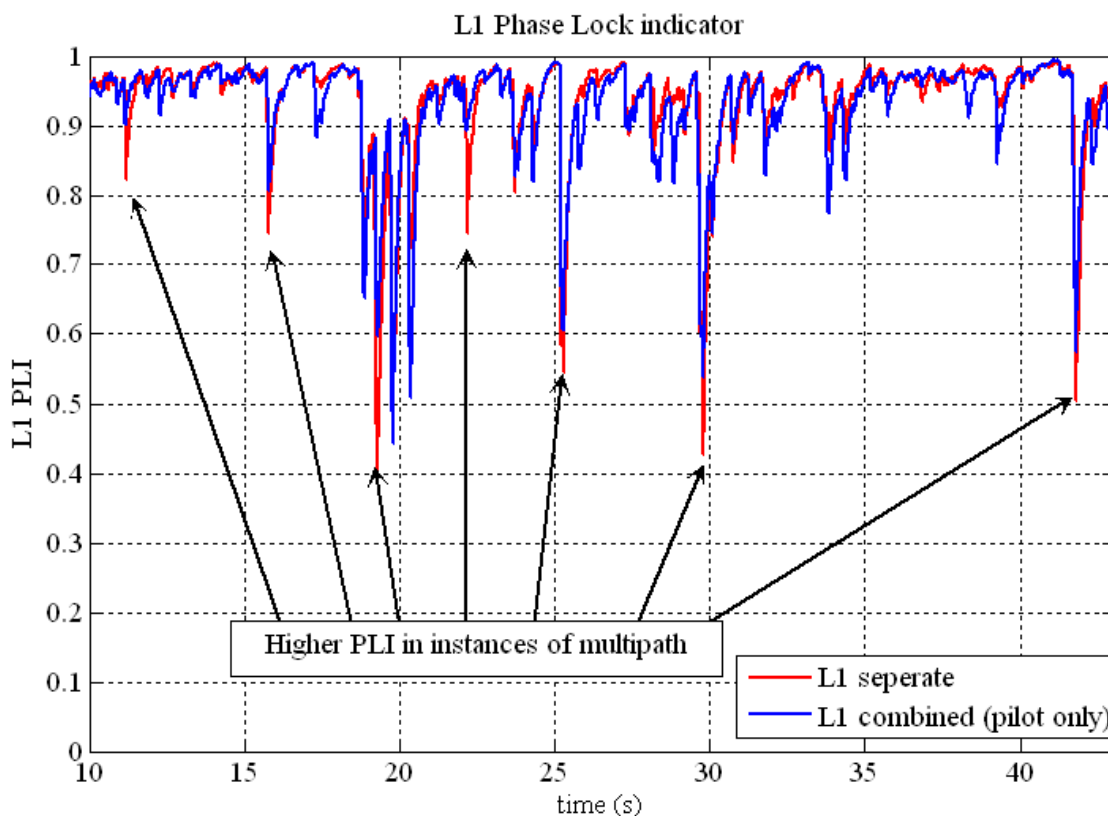


Figure 5-17: L1 PLI for separate versus combined Kalman filter for multipath scenario

For the combined Kalman filter using the pilot channel, Figure 5-17 zooms on the PLI of L1 in an interval where it suffers more power variations, with the corresponding correlator outputs being shown in Figure 5-18. Though both the separate and the combined Kalman filter follow almost the same trend in the PLI and the correlator output plots, Figure 5-18 shows that the separate Kalman filter failed to maintain the phase lock

and suffered half-cycle slips as seen by the black lines which shows the inphase correlator outputs of the separate KF and green lines which shows the inphase correlator outputs of the combined KF.

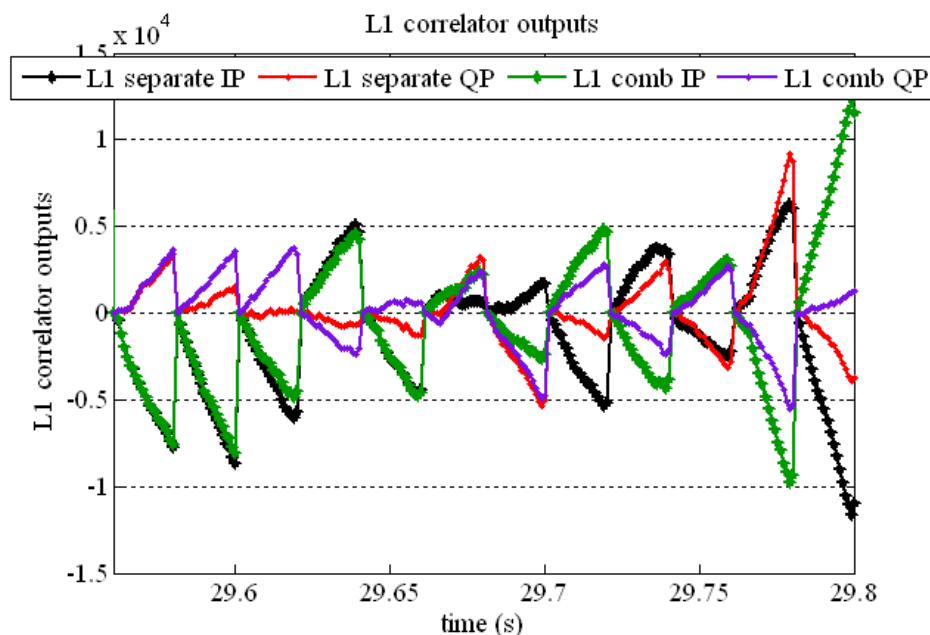


Figure 5-18: L1 Correlator outputs for separate versus combined Kalman filter for multipath scenario

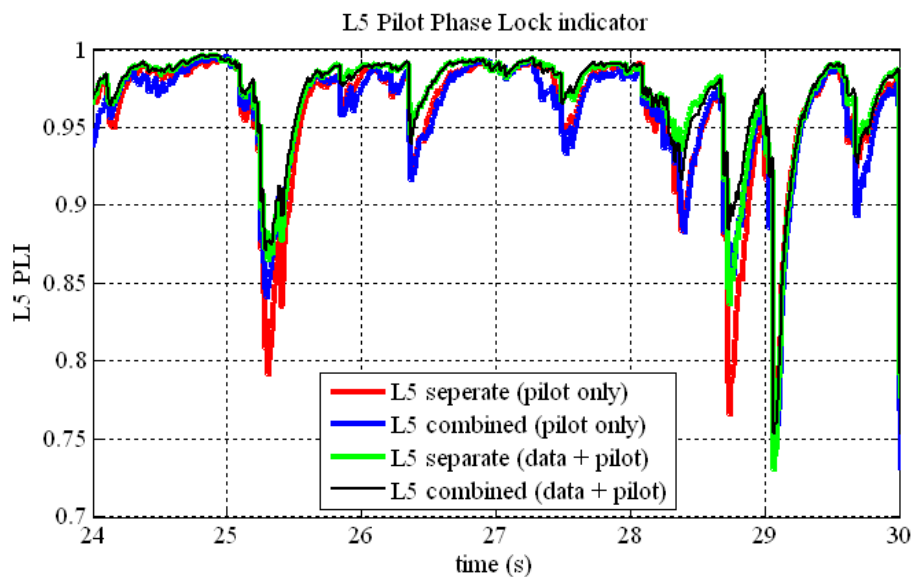


Figure 5-19: L5 Pilot PLI for separate versus combined Kalman filter for multipath scenario

The L5 pilot signal shows similar results when comparing the separate and combined Kalman filter. Figure 5-19 shows the PLI zoomed in the interval of higher signal variations and the corresponding correlator outputs in Figure 5-20. The combined Kalman filter clearly helps to decrease the level of noise in the PLI and the correlator outputs. Furthermore the use of the total signal power has raised the L5 PLI compared to the usage of only the pilot channel.

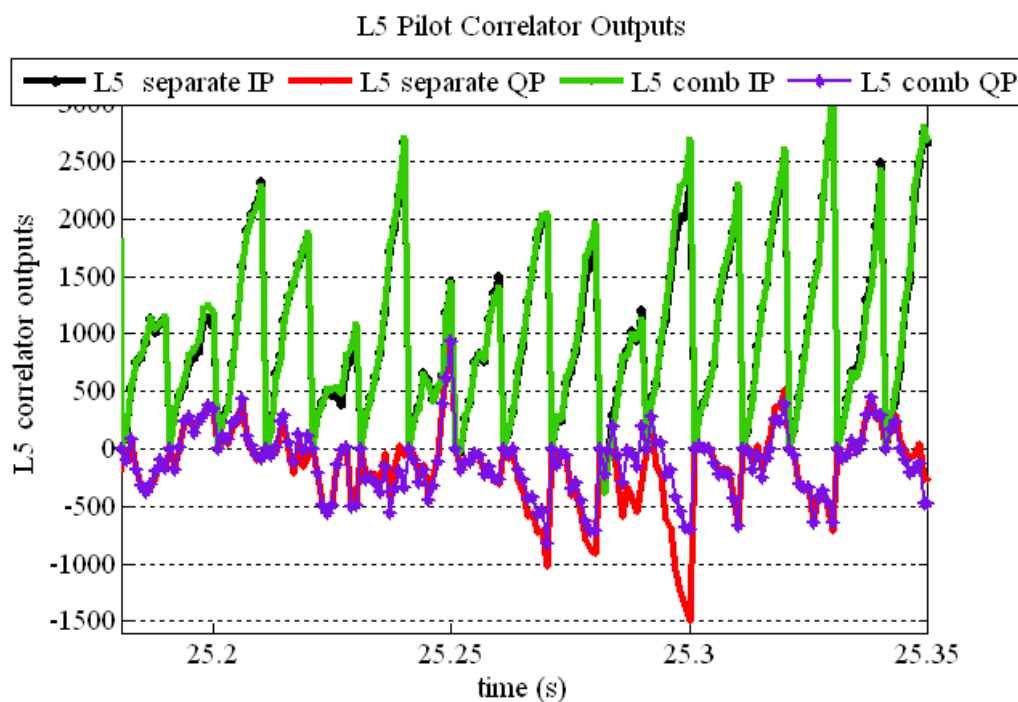


Figure 5-20: L5 Pilot correlator outputs for separate versus combined Kalman filter for multipath scenario

5.2.1.1.2 Kalman filter Analysis

The second category of results for this test is the Kalman filter states analysis. The figures shown are for the separate Kalman filter tracking versus the combined Kalman filter tracking using the pilot channel only to enable a clearer illustration of the performance. A

table will be shown later summarizing the results of using the pilot channel only versus using the data and pilot channels.

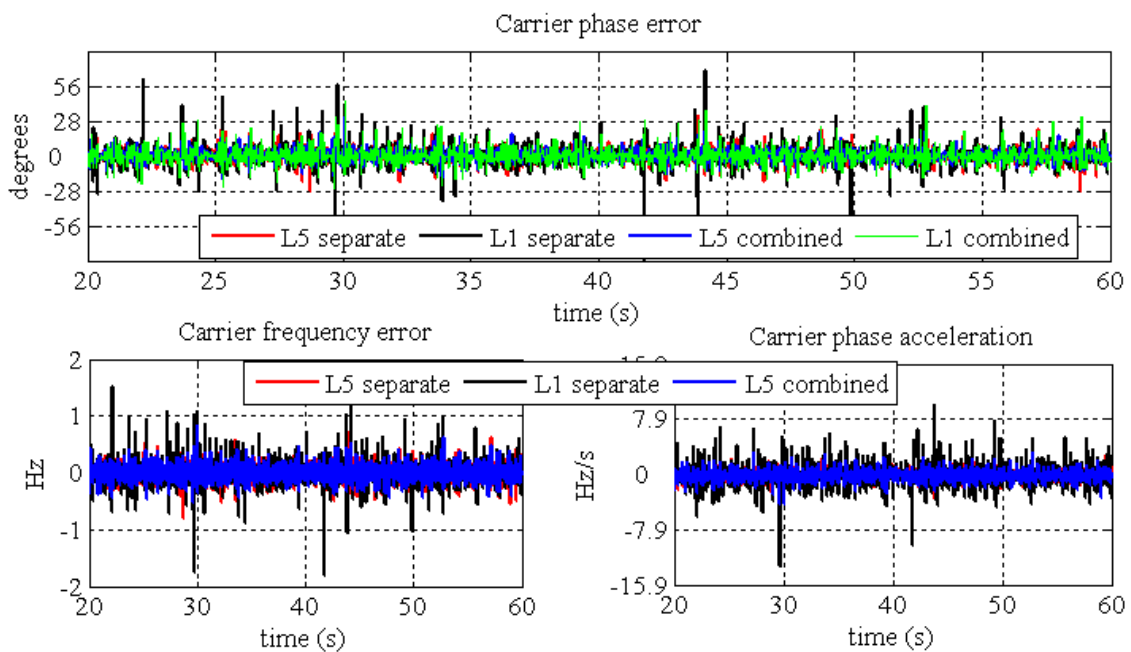


Figure 5-21: Estimated states for separate versus combined Kalman filter for multipath scenario

Figure 5-21 shows the estimated carrier tracking errors followed by the corresponding estimated standard deviations in Figure 5-22 for both the L5 separate and combined cases and the L1 separate and combined cases.

Note that in the lower plots in each of the two figures, only the separate L1 is shown, as the carrier frequency and the carrier phase acceleration of the L1 are not estimated in the combined Kalman filter case. In addition, the states estimates and deviations are unscaled to show the real values for the two cases.

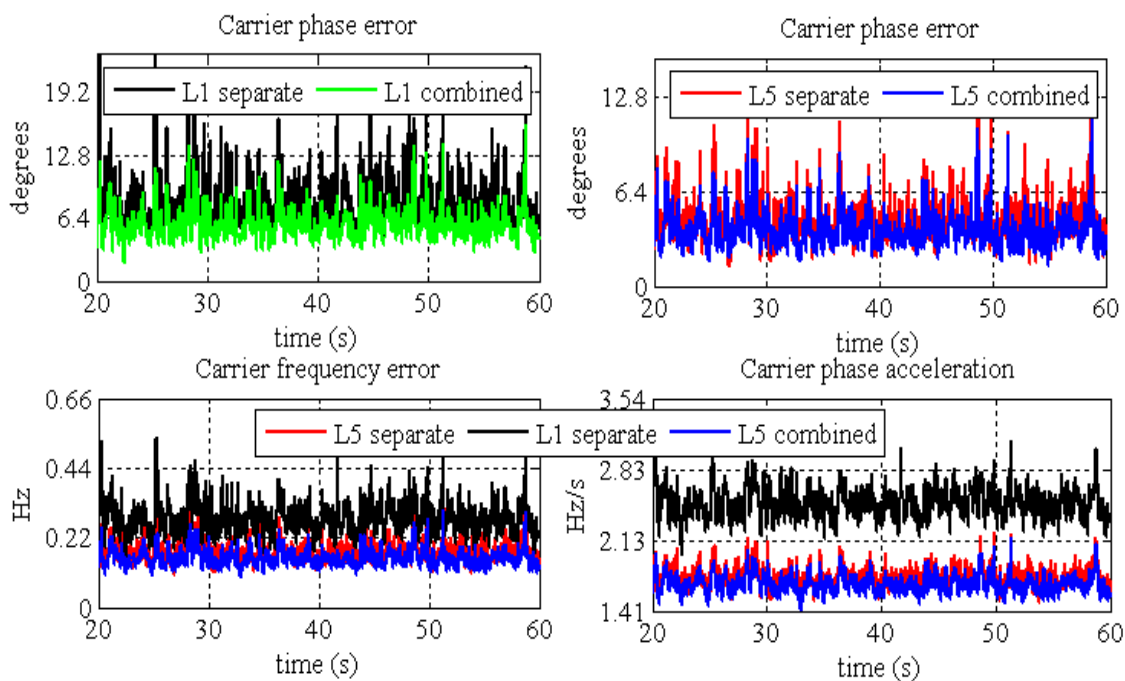


Figure 5-22: Estimated standard deviations for separate versus combined Kalman filter for multipath scenario

Figure 5-22 illustrates how the combined Kalman filter helped to reduce the standard deviations by comparing the separate and the combined L1 standard deviations in the upper plots, and the separate and combined L5 standard deviations in the lower plots.

To further clarify the improvements when using the combined Kalman filter, Table 5-1 summarizes the root mean square (RMS) of the actual error and the standard deviations (STD) as calculated from the KF of each of the estimated states in both cases and the corresponding improvements in percentile. Table 5-2 shows the improvements in percentile when the total L5 signal power is used in the KF.

Table 5-1: Kalman filters statistics & improvements (pilot channel) - multipath			
State		RMS	Average Std
$\delta\tau_s$ (chips)	L1 separate	0.00029	0.0022
	L1 combined	0.00029	0.0022
	<i>Improvement (%)</i>	0	0
	L5 separate	0.002	0.002
	L5 combined	0.0013	0.002
	<i>Improvement (%)</i>	35	0
$\delta\phi_s$ (rad)	L1 separate	0.16	0.14
	L1 combined	0.12	0.1
	<i>Improvement (%)</i>	25	28
	L5 separate	0.095	0.079
	L5 combined	0.089	0.067
	<i>Improvement (%)</i>	6.3	15
δf_s (Hz)	L5 separate	0.14	0.18
	L5 combined	0.14	0.159
	<i>Improvement (%)</i>	0	11

Since the main focus is on the carrier phase estimates, Figure 5-23 shows the RMS of the carrier phase error, for both the L1 and L5 signals. The L1 signal is showing a lower RMS error when using the combined Kalman filter with the pilot channel only, compared to the separate case. A lower error is obtained on the L1 signal using the combined data and pilot channels.

Table 5-2: Kalman filters statistics & improvements (data + pilot) - multipath			
State		RMS	Average Std
$\delta\tau_s$ (chips)	L1 separate	0.00029	0.0022
	L1 combined	0.00026	0.002
	<i>Improvement (%)</i>	10.3	9
	L5 separate	0.0042	0.0015
	L5 combined	0.0035	0.0014
	<i>Improvement (%)</i>	16.6	6.6
$\delta\phi_s$ (rad)	L1 separate	0.16	0.14
	L1 combined	0.1	0.07
	<i>Improvement (%)</i>	37.5	50
	L5 separate	0.064	0.03
	L5 combined	0.063	0.03
	<i>Improvement (%)</i>	1.5	0
δf_s (Hz)	L5 separate	0.13	0.1
	L5 combined	0.128	0.1
	<i>Improvement (%)</i>	1.5	0

For the L5 signal, comparing the separate Kalman filter tracking with the combined Kalman filter tracking using the pilot channel only, shows better carrier phase error results. However, when comparing the separate Kalman filter tracking using both the data and pilot channels, with the combined Kalman filter tracking using both, the same results are obtained, which shows that the L5 signal is benefiting from the data and pilot combination more than the noisy L1 estimates in this case. The results are confirmed with the standard deviations shown in Figure 5-24.

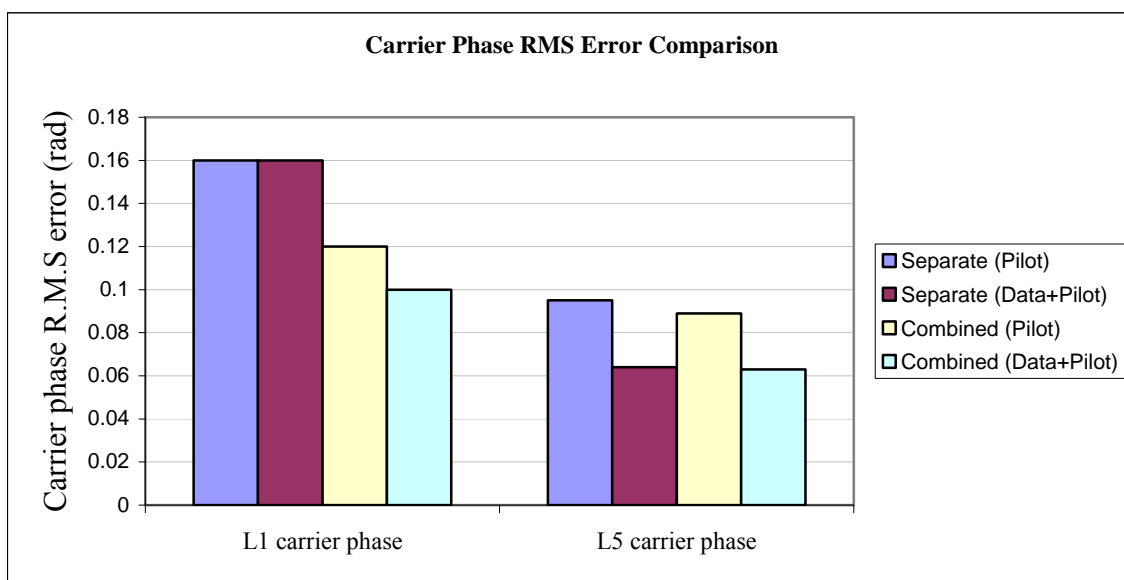


Figure 5-23: Carrier phase RMS error comparison for multipath scenario

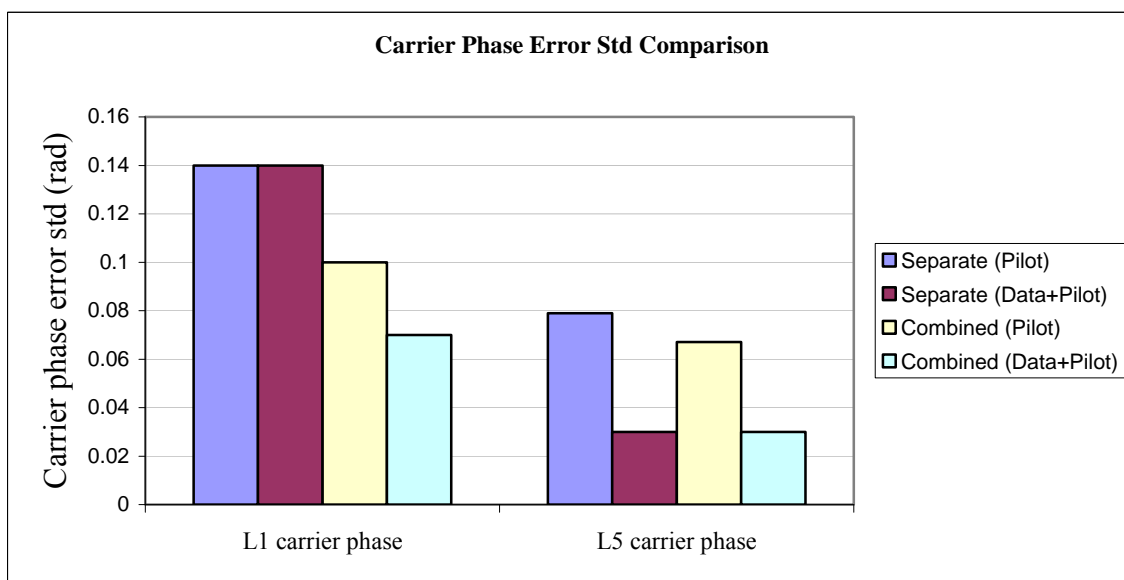


Figure 5-24: Carrier phase error standard deviations comparison for multipath scenario

5.2.1.2 Motion

The scenario uses the dynamic vehicle model presented in Section 5.1.3.2.

5.2.1.2.1 Tracking errors

The second test conducted is the dynamic user. Figure 5-25 first shows the Doppler frequencies of both the L1 and the scaled pilot L5 using the two kinds of filters. The separate and the combined Kalman filters both succeeded in tracking the signals under the tested velocity and acceleration.

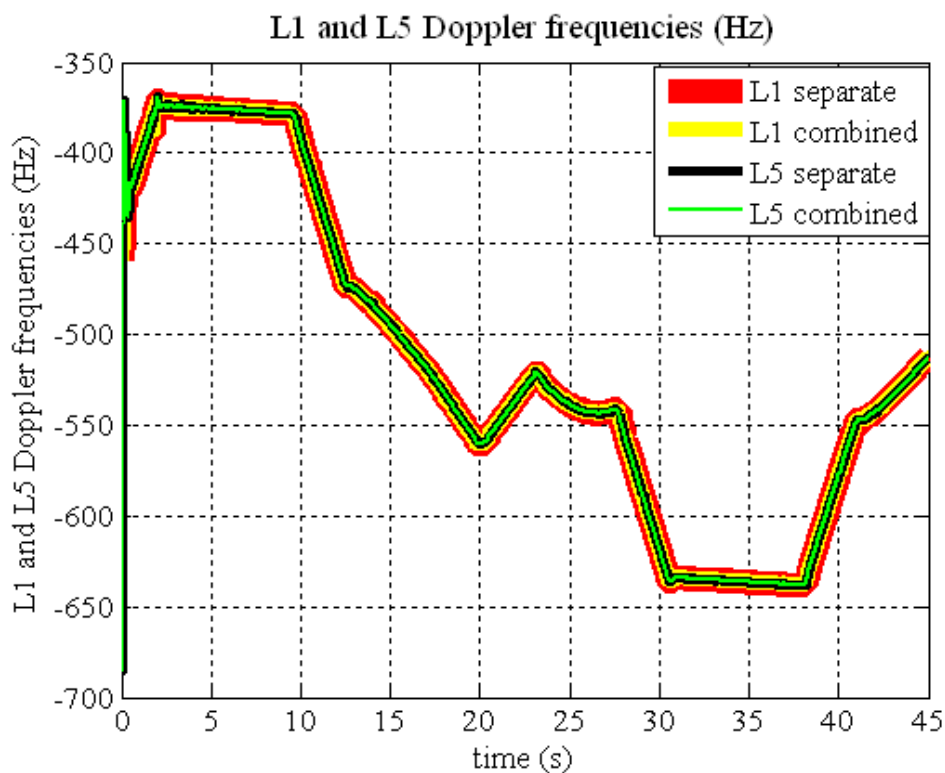


Figure 5-25: L1 and scaled L5 Doppler frequencies for separate versus combined Kalman filter for moving vehicle scenario

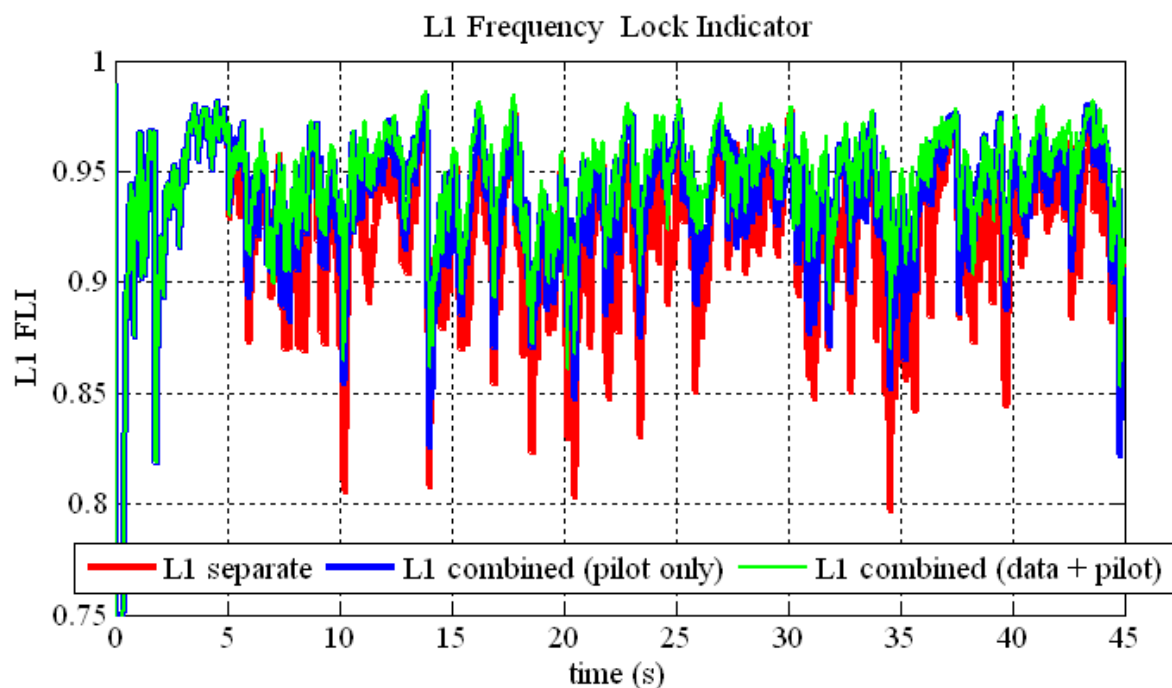


Figure 5-26: L1 FLI for separate versus combined Kalman filter for moving vehicle scenario

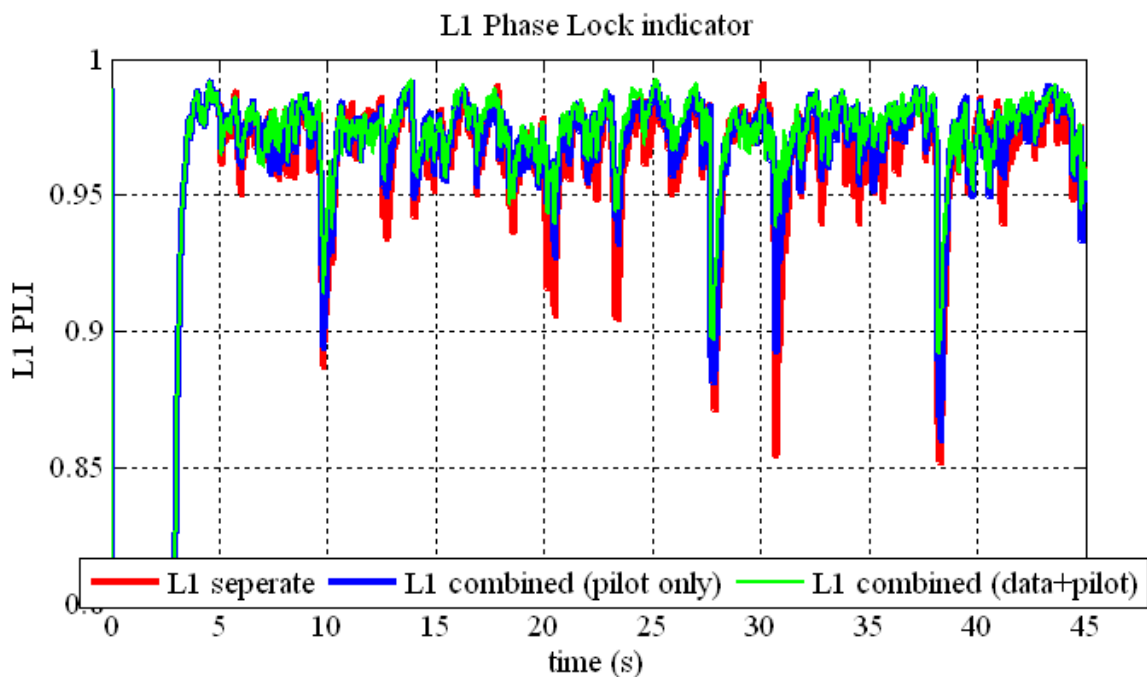


Figure 5-27: L1 PLI for separate versus combined Kalman filter for moving vehicle scenario

By further examining the frequency and the phase lock indicators for the L1 signal in Figure 5-26 and Figure 5-27, it becomes clear that there is a significant advantage when using the combined Kalman filter in the dynamic user case. The two indicators become higher and less noisy in the combined Kalman filter case.

Similarly, for the L5 signal results shown in Figure 5-28 and Figure 5-29, the combined Kalman filter again shows much higher phase and frequency lock indicators when compared to the separate case.

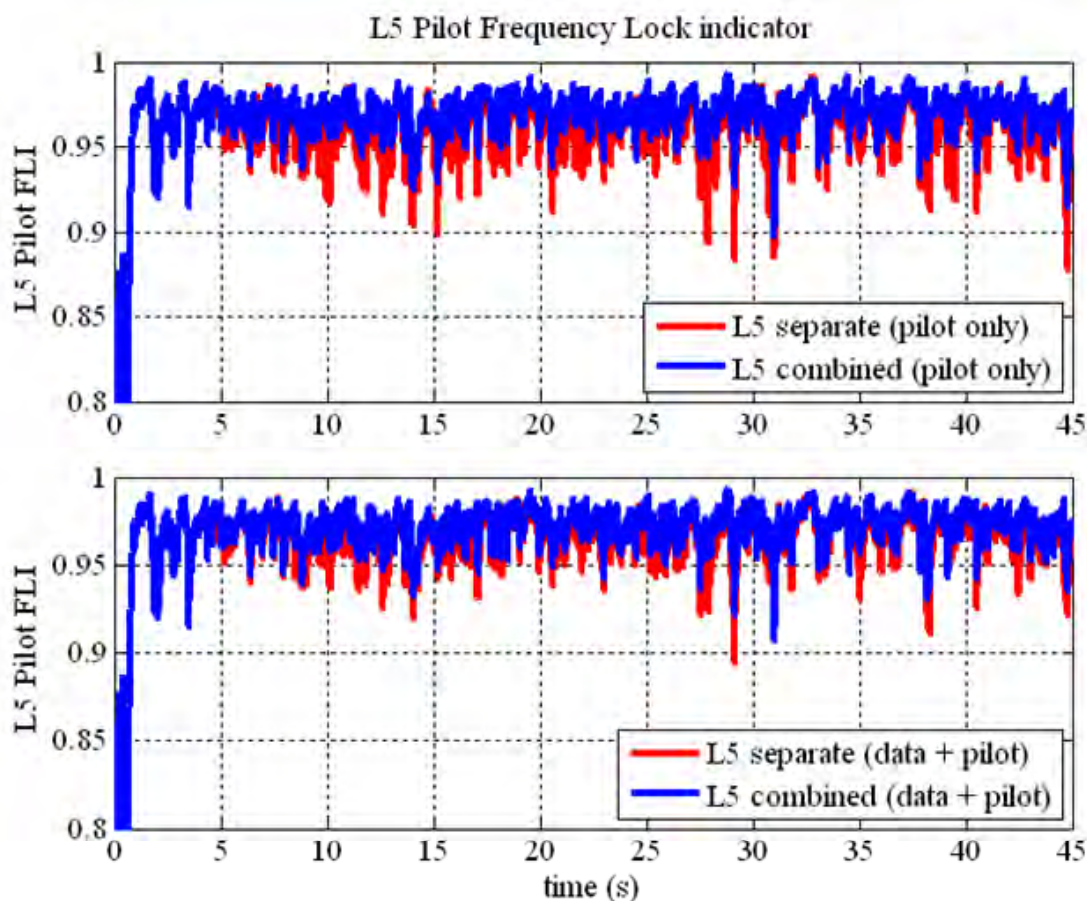


Figure 5-28: L5 pilot FLI for separate versus combined Kalman filter for moving vehicle scenario

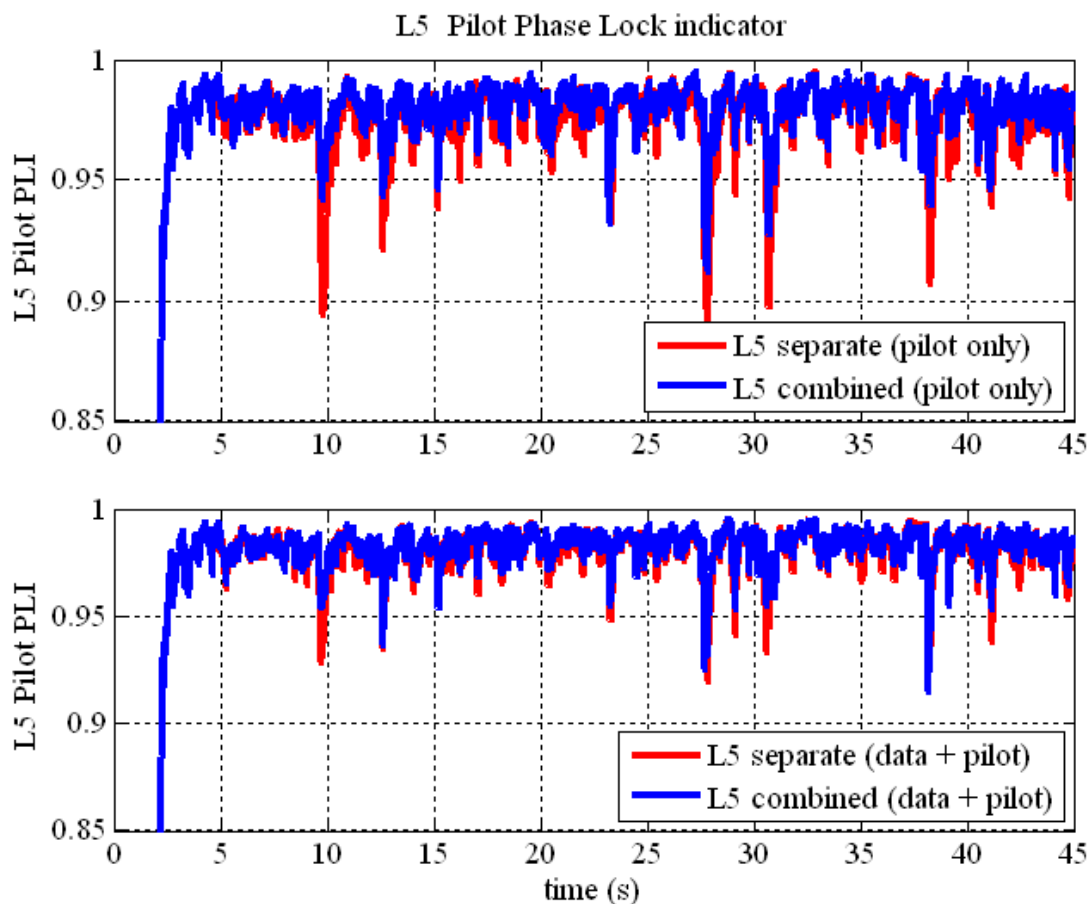


Figure 5-29: L5 pilot PLI for separate versus combined Kalman filter for moving vehicle scenario

5.2.1.2.2 Kalman filters Analysis

The figures shown herein are for the separate Kalman filter tracking versus the combined Kalman filter tracking using the pilot channel only to enable a clearer illustration. A table will be shown later summarizing the results of using the pilot channel only versus using the data and pilot channels.

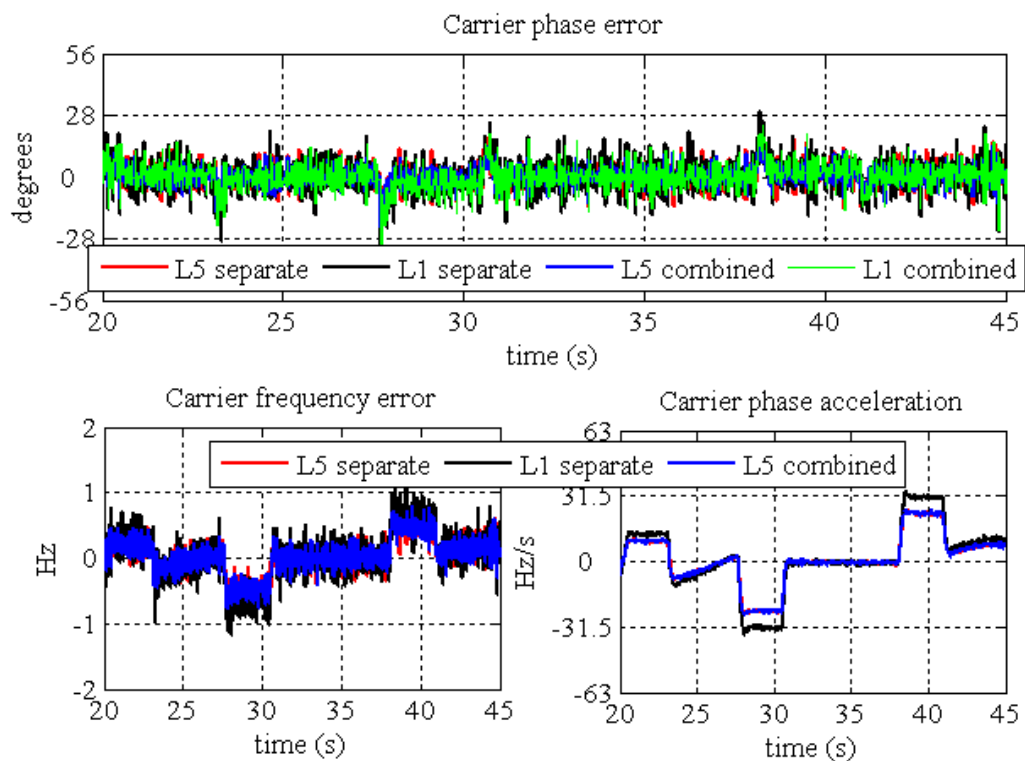


Figure 5-30: Estimated carrier phase, frequency errors and acceleration states for separate versus combined Kalman filter for moving vehicle scenario

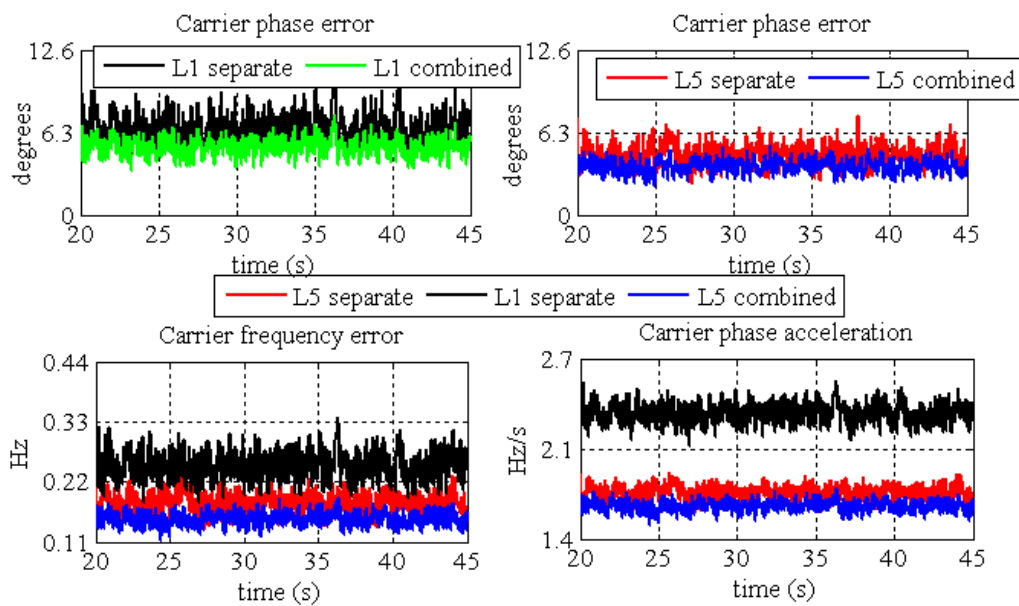


Figure 5-31: Estimated standard deviations for separate versus combined Kalman filter for moving vehicle scenario

Proceeding to the Kalman filter states analysis, Figure 5-30 and Figure 5-31 show the estimated states and the corresponding standard deviations for the carrier tracking part. Examining the states standard deviations in Figure 5-31, the upper figure shows a significant improvement in the L1 carrier phase errors as illustrated by the black and the green lines, whereas the lower plots shows improvements in the L5 frequency errors as per the red and the blue lines. Also the L5 carrier phase acceleration shows a lower deviation for the combined Kalman filter case.

Table 5-3: Kalman filters statistics & improvements (pilot channel) - motion			
State		RMS	Average Std
τ_s (chips)	L1 separate	0.0004	0.002
	L1 combined	0.0005	0.002
	<i>Improvement (%)</i>	-25	0
	L5 separate	0.0005	0.0026
	L5 combined	0.0004	0.0024
	<i>Improvement (%)</i>	20	1.85
ϕ_s (rad)	L1 separate	0.135	0.114
	L1 combined	0.113	0.092
	<i>Improvement (%)</i>	16.3	4.4
	L5 separate	0.09	0.08
	L5 combined	0.079	0.06
	<i>Improvement (%)</i>	12.2	4.3
f_s (Hz)	L5 separate	0.28	0.183
	L5 combined	0.27	0.154
	<i>Improvement (%)</i>	3.5	3.53

Table 5-3 summarizes the statistics of the estimated states for both the separate and the combined Kalman filters using the L5 pilot channel only with the corresponding improvements in percentile, followed by Table 5-4 using both the data and pilot channels. Note that in case of the L1 code phase error, there is actually a degradation in the RMS calculated, but this is because both values are actually very low.

As expected, using the total signal power for the dynamic user case enhances the statistics of the Kalman filter, which matches the results from the phase and frequency lock indicators shown before.

Table 5-4: Kalman filters statistics & improvements (data + pilot) - motion			
State		RMS	Average Std
τ_s (chips)	L1 separate	0.0004	0.0022
	L1 combined	0.0004	0.0012
	<i>Improvement (%)</i>	0	46
	L5 separate	0.0015	0.0022
	L5 combined	0.00073	0.0018
	<i>Improvement (%)</i>	51	18
ϕ_s (rad)	L1 separate	0.135	0.114
	L1 combined	0.099	0.075
	<i>Improvement (%)</i>	26.6	34
	L5 separate	0.075	0.044
	L5 combined	0.067	0.041
	<i>Improvement (%)</i>	10.6	6.8
f_s (Hz)	L5 separate	0.27	0.128
	L5 combined	0.27	0.119
	<i>Improvement (%)</i>	0	7

Figure 5-32 shows the RMS of the carrier phase error, for both the L1 and L5 signals. The L1 signal is showing the least RMS errors when using the combined Kalman filter with both data and pilot channels. Contrary to the multipath case where the L1 estimates were noisy, the L5 signal is now making use of the L1 signal where the combined Kalman filter with both the data and pilot channels is resulting in a lower carrier phase error compared to the separate case, using also both the data and pilot channels. The results are confirmed with the standard deviations shown in Figure 5-33.

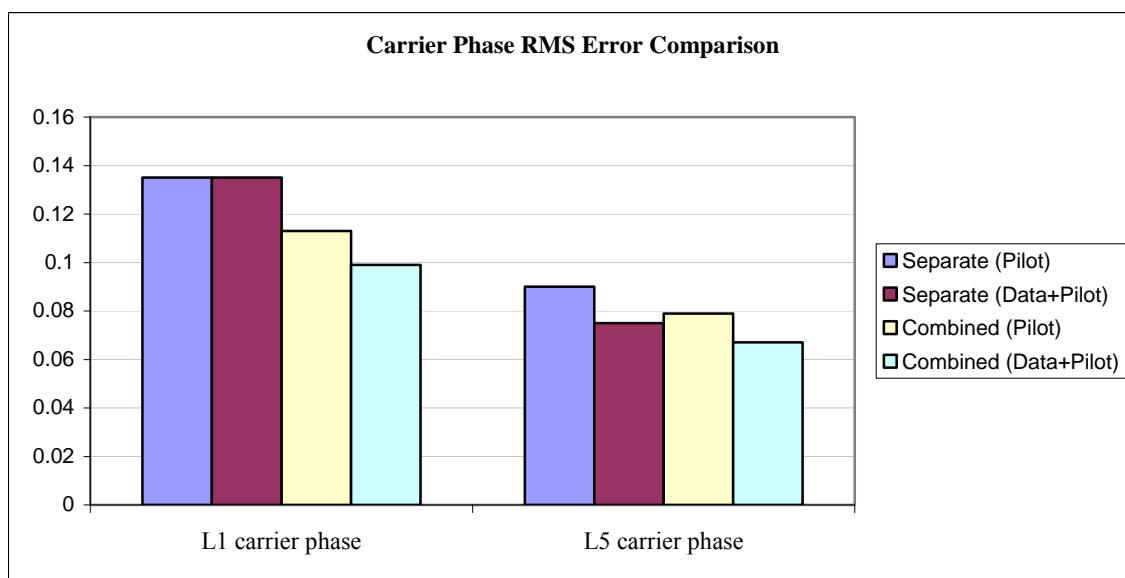


Figure 5-32: Carrier phase RMS error comparison for moving vehicle scenario

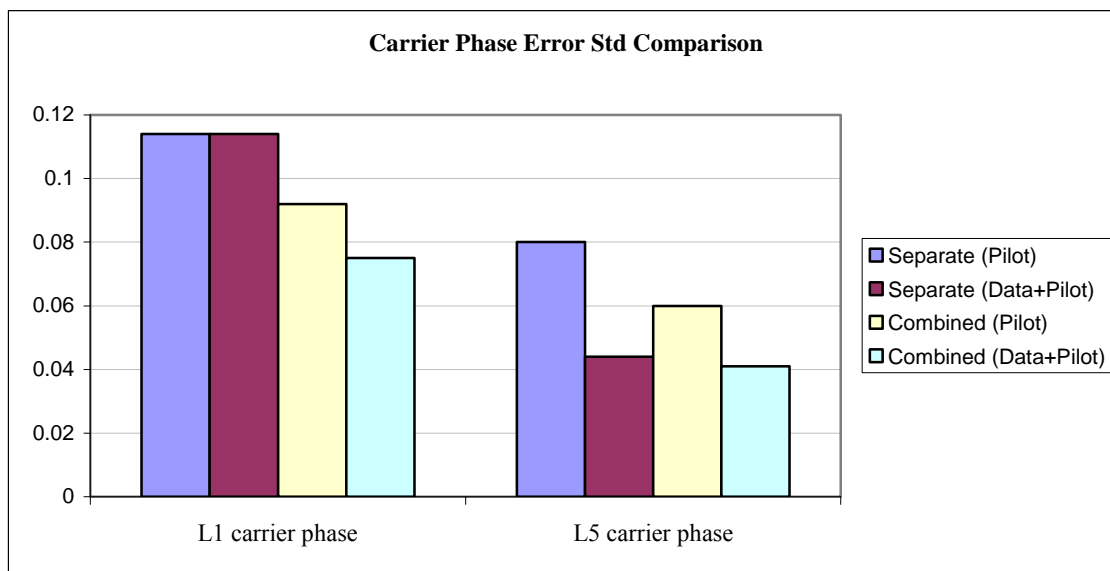


Figure 5-33: Carrier phase error standard deviations comparison for moving vehicle scenario

5.3 Standard Tracking Loops versus Kalman Filter Tracking Loop

The final step in the evaluation is to compare the two tracking methods, namely the Kalman filter and the standard tracking loops. Focusing on the carrier phase tracking, the normal approach is to find the equivalent PLL that gives the same performance as the steady-state EKF. Several works in the literature have attempted to find the steady-state model of the Kalman filter, e.g. O’Driscoll & Lachapelle (2009), Yi et al (2009). Their idea is to obtain the steady-state Kalman gain and derive the equivalent loop bandwidth. By getting the noise equivalent bandwidth, the equivalent PLL should give the same phase jitter and steady-state response of the Kalman filter.

However, there is no work in the literature, to the author’s knowledge, that attempted to get the equivalent PLL of an EKF. That is due to the nonlinearity introduced by the

nature of the models used in the EKF. That called for an experimental method to get an equivalent PLL.

The equivalent model has to take into account the different signal model assumptions and parameters dealt with. The EKF assumes a linear stochastic model for the signal dynamics, whereas the standard tracking loops assumes a deterministic model for the signal dynamics.

The equivalent model is thus derived based on the 1-sigma carrier phase error estimates obtained from each of the two models. Note that the 1-sigma carrier phase error is the one expressed in Equation (4.1), which includes both the thermal error and the steady-state error.

For the separate tracking, the comparison is directly performed for each of the two signals between the 1-sigma carrier phase errors as shown in Figure 5-34.

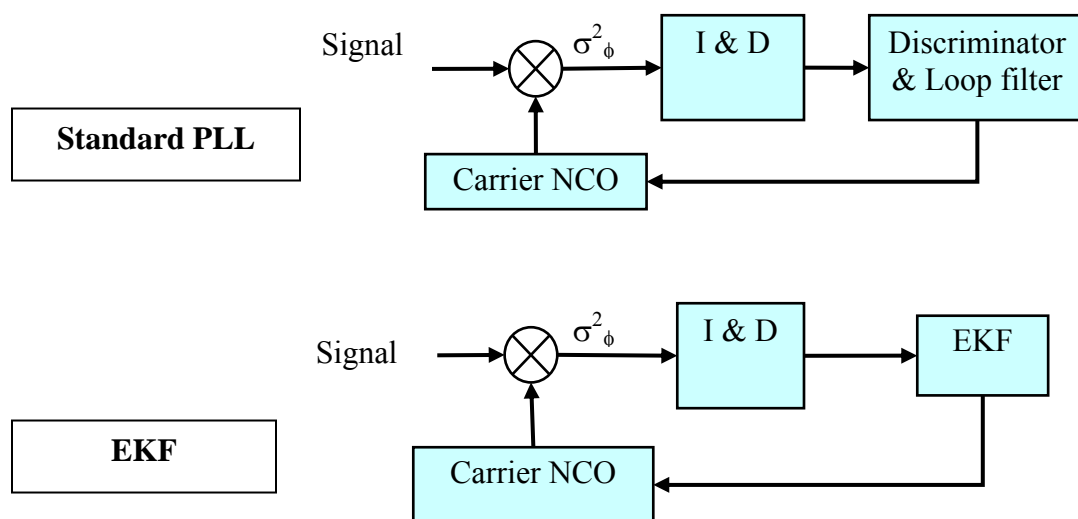


Figure 5-34: Separate standard PLL tracking loop versus EKF tracking loop

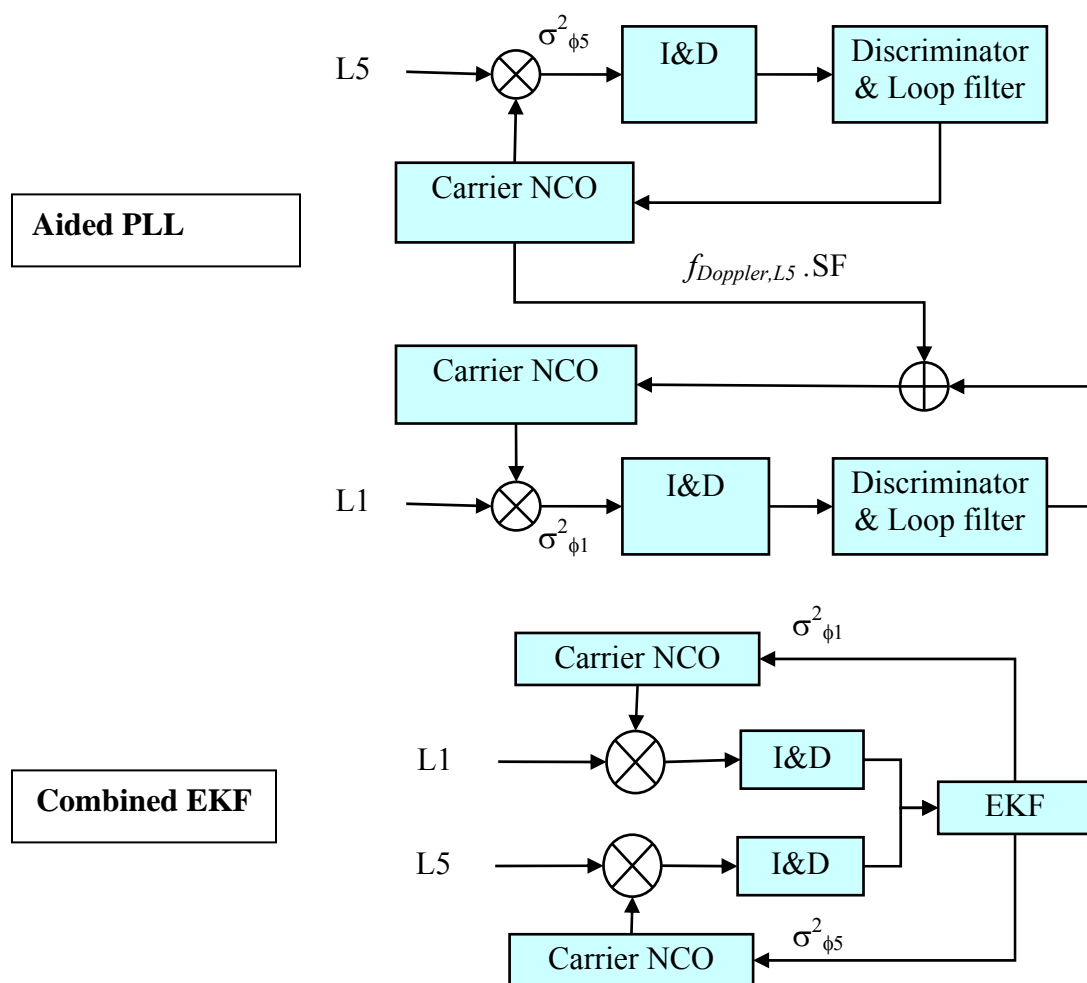


Figure 5-35: Combined standard PLL tracking loop versus EKF tracking loop

However, for the combined case shown in Figure 5-35, the aided PLL is compared to the combined EKF. Both tracking loops use the L5 pilot signal as the driving force. For the aided PLL, the L5 pilot PLL provides its Doppler frequency as an aiding to the L1 PLL and is responsible for tracking most of the two signals' dynamics, whereas for the combined EKF, the L5 acceleration PSD is the driving force for the filter, which accounts for the LOS dynamics encountered by the two signals. So the comparison will be mainly based on the 1-sigma carrier phase error of the L5 signal. For all the equivalent

bandwidth calculations that follow, only the pilot channel of the L5 signal is used to simplify calculations.

The steps of calculating the EKF equivalent bandwidth are illustrated with an applied example on a strong stationary signal.

5.3.1 Equivalent Bandwidth Calculation: Illustration using a Strong Signal

For illustrating the methodology used, the equivalent bandwidth of the EKF is calculated first for a strong signal. A strong signal for a static user is simulated, with an L1 C/N_0 of 42 dB-Hz.

5.3.1.1 Separate EKF versus Separate Tracking Loops

First, set the acceleration PSD in the EKF to $0.01 \text{ g/s}/\sqrt{\text{Hz}}$, and calculate the average value of the estimated phase standard deviation of both the L1 and L5 signals. Note that the estimated phase standard deviation is extracted from the appropriate element of the estimated state covariance matrix. **Second**, set the dynamic stress to the same value of the acceleration PSD, 0.01 g/s. It is found by experiment that setting the dynamic stress in the PLL and the acceleration PSD in the EKF results in the same response to a certain level of dynamics. The PLL tracking error is plotted as a function of the loop bandwidth using Equation (4.4). The next step is to use the calculated mean of the L1 and L5 1-sigma carrier phase error from step 1 as the thresholds for the PLL as shown in Figure 5-36. Using these thresholds, the equivalent bandwidth for each EKF can be found, as marked in the figure.

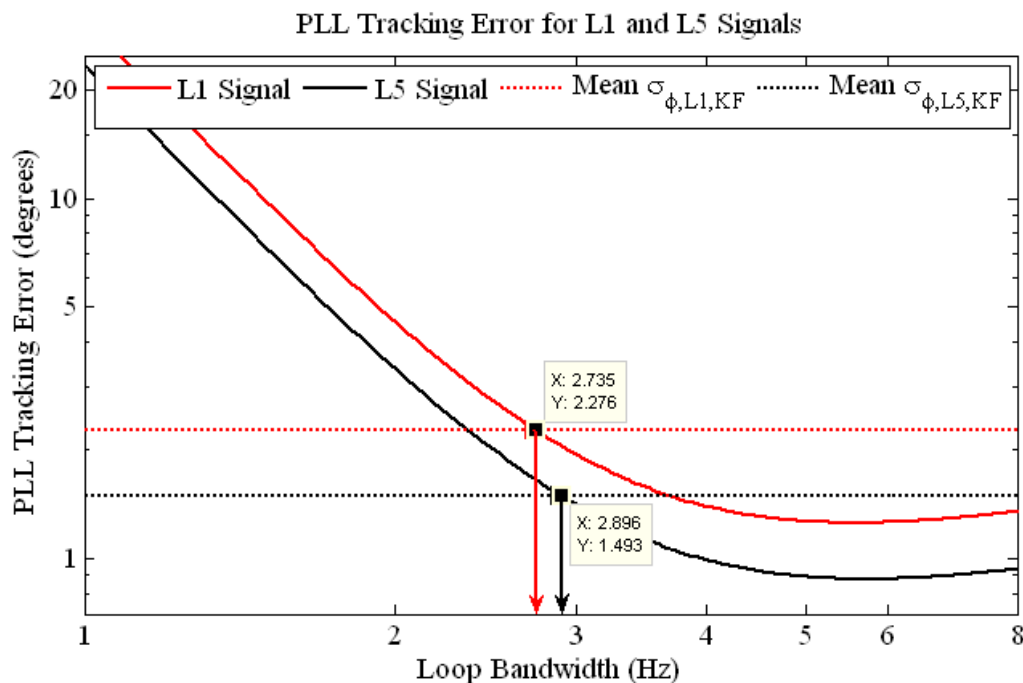


Figure 5-36: PLL tracking errors for L1 and L5 signals: strong signal-separate tracking

Finally, using the equivalent bandwidth in the standard PLL, the actual 1-sigma phase error is calculated. Figure 5-37 shows the results from both the EKF and standard PLL, where it is observed that the two tracking loops give the same standard deviations for each signal separately. For the EKF, the estimated standard deviations are obtained from the appropriate element of the state covariance matrix from the Kalman filter, whereas the PLL standard deviations are the theoretical standard deviations given in Equation (4.4) with the C/N_0 estimated and averaged over one second period using the software receiver. The smoothing of the C/N_0 estimate is what leads to smoother estimates of the phase error standard deviation for the standard tracking case, when compared to the EKF. To that end, the equivalent PLL for each Kalman filter has been calculated.

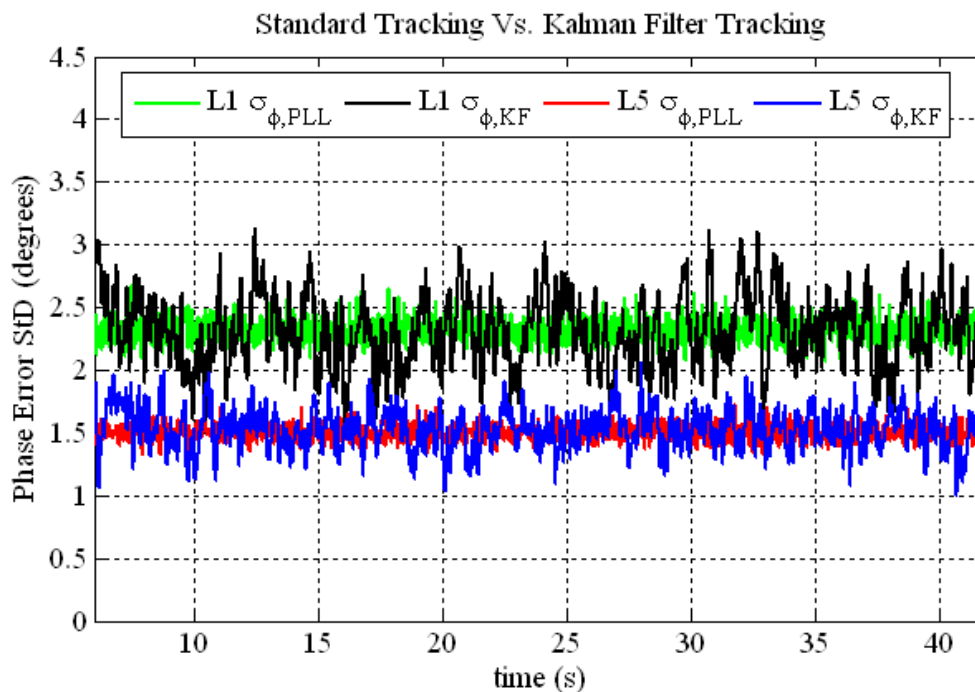


Figure 5-37: Carrier phase error: strong signal-separate tracking

The tracking performance of the EKF and the standard PLL can now be compared in a fairer manner as shown in the next figures. Figure 5-38 shows the L1 PLI calculated using each method. It shows an important advantage of the EKF, namely the faster transient response noticed in faster adaptation to the change of bandwidth when switching from the FLL, compared to the PLL. Moreover, once the two loops settle, they both have similar PLI. Similar results for the L5 pilot channel are shown in Figure 5-39.

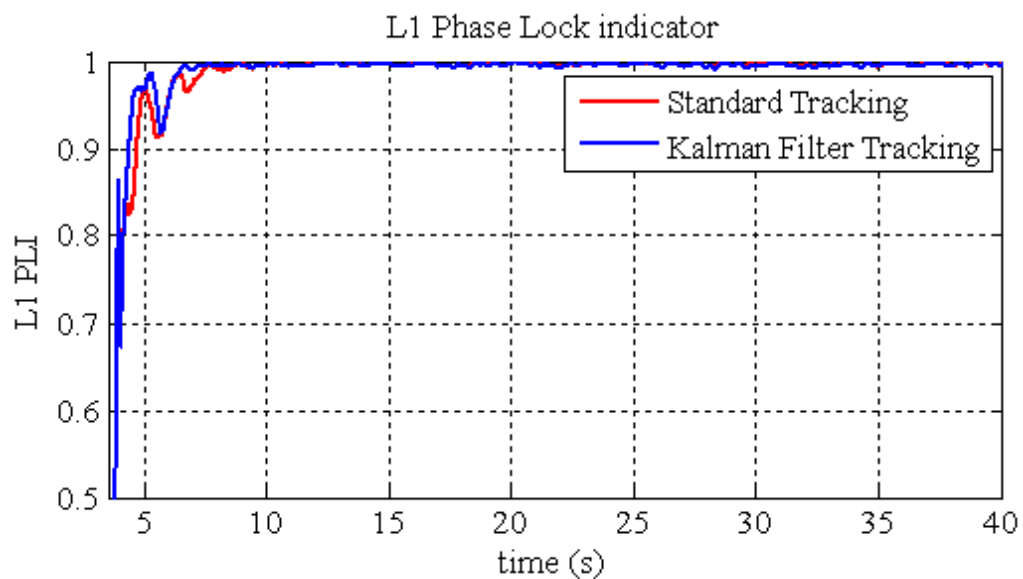


Figure 5-38: L1 PLI: strong signal-separate tracking

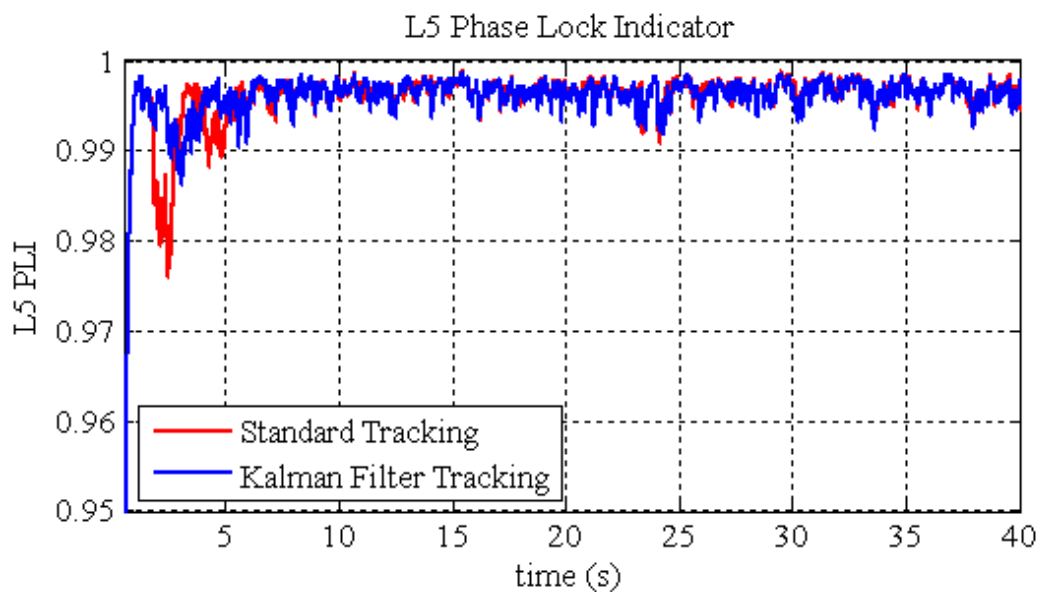


Figure 5-39: L5 PLI: strong signal-separate tracking

5.3.1.2 Combined EKF versus Aided Tracking Loops

For the combined case, the 1-sigma carrier phase error of the L5 pilot channel is the basis of the comparison. The L5 PLL tracking error is plotted as a function of the loop bandwidth using Equation (4.4). Using the same calculations as in the separate case, the 1-sigma carrier phase error mean of the Kalman filter is set as the threshold as shown in Figure 5-40, and the equivalent bandwidth is found.

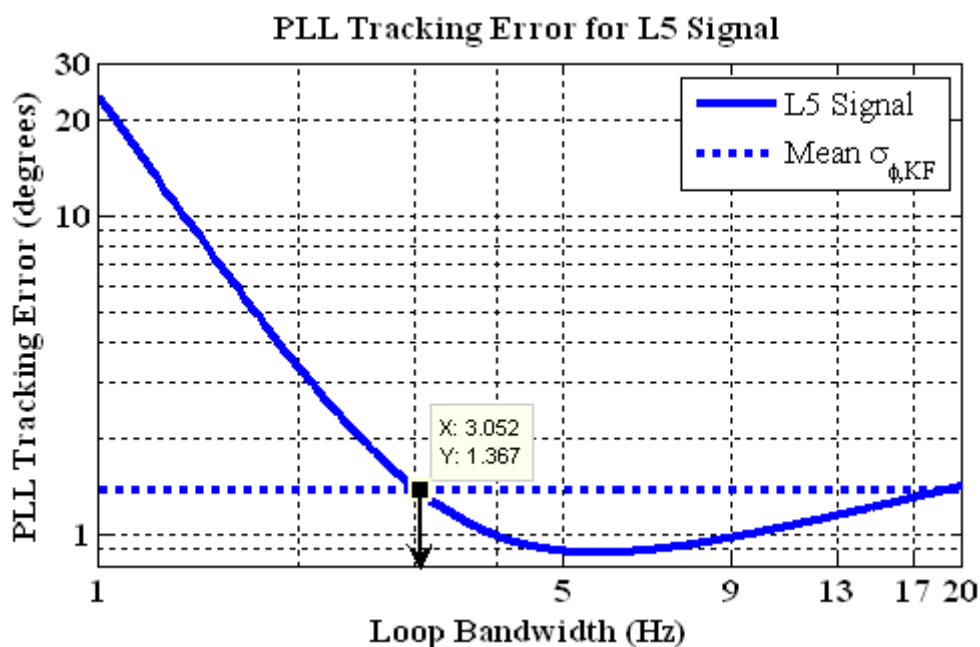


Figure 5-40: PLL tracking errors for L5 signal: strong signal-combined tracking

The same steps are followed for the L1 signal; however the PLL tracking error has to account for the aiding from the L5 pilot channel using Equation (5.11). Figure 5-41 shows the equivalent bandwidth of the combined L1 Kalman filter tracking.

The L5 bandwidth is then used in the standard PLL tracking loop, and the L1 bandwidth is used in the aided PLL. The 1-sigma carrier phase errors calculated are shown in Figure 5-42, showing agreement with those of the Kalman filter.

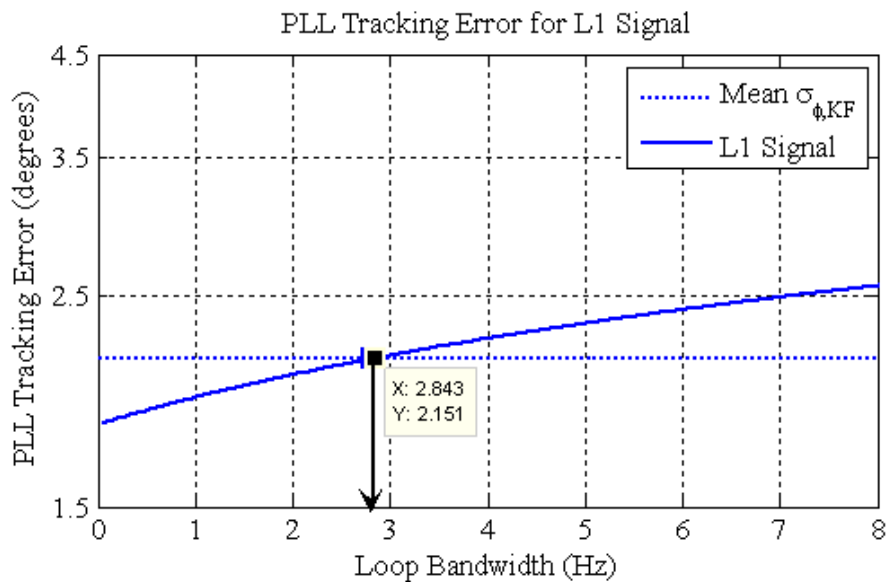


Figure 5-41: PLL tracking errors for L1 signal: strong signal-combined tracking

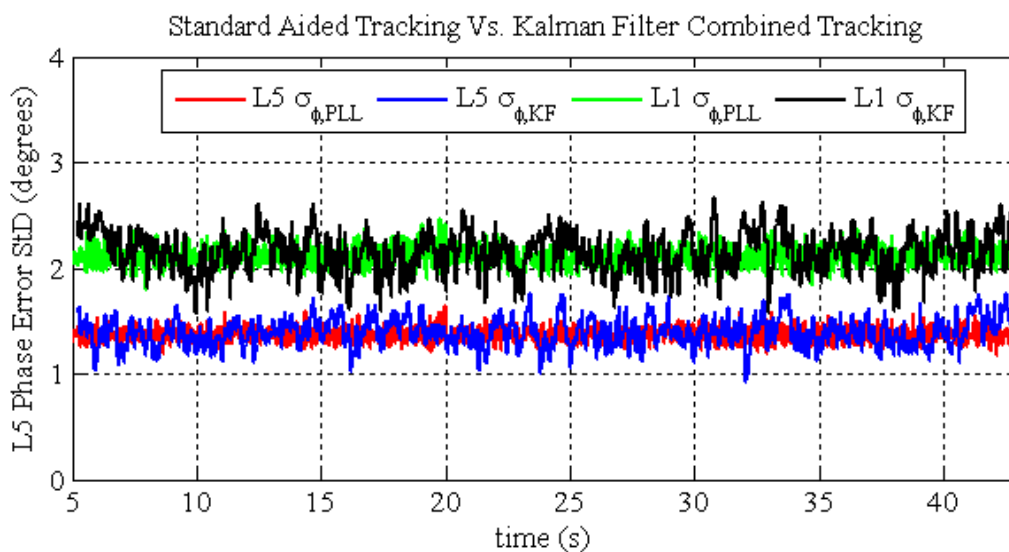


Figure 5-42: Carrier phase error: strong signal-combined tracking

Using the standard aided tracking loops and the combined Kalman filter, the PLI of the L1 signal is calculated as shown in Figure 5-43. The L5 signal uses a separate (unaided) PLL tracking loop, so it is not shown in this comparison.

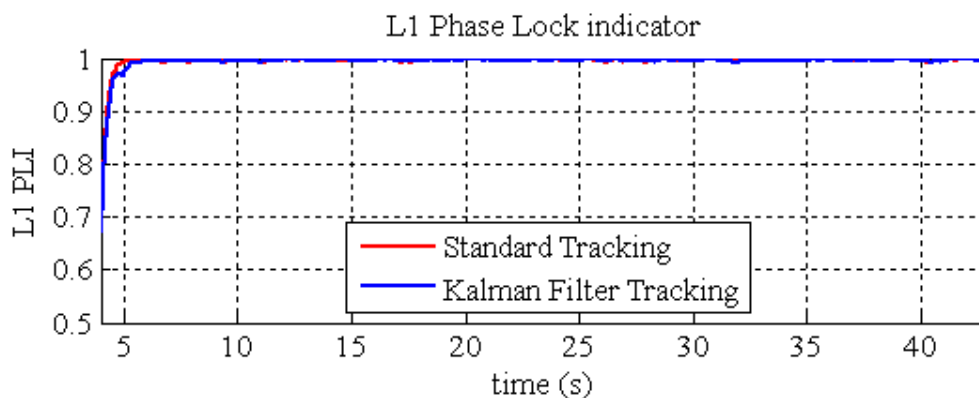


Figure 5-43: L1 PLI: strong signal-combined tracking

5.3.2 Equivalent Bandwidth Calculation Steps

Figure 5-44 summarizes the steps required to calculate the EKF equivalent bandwidth. First, set the acceleration PSD of the EKF, then run the EKF and calculate the mean of 1-sigma carrier phase error output of both the L1 and L5 signals. Next, set the dynamic stress in the PLL to be the same value as the acceleration PSD, and the threshold of the PLL to be the value of the mean calculated in the first step. Using these two parameters, calculate the equivalent bandwidth. Finally, using the equivalent bandwidth in the standard PLL, calculate the 1-sigma carrier phase error, which is then compared to that of the EKF.

To that end the methodology used to calculate the equivalent bandwidth of the EKF has been illustrated. It should be noted though even with the two loops designed to have similar steady state response, they will still have different transient response. The next

sections show the application of that method to two sets of scenarios: first, the dynamic vehicle discussed in Section 5.1.3.2, followed by a scenario assuming the received signal is suffering from continuously decreasing power levels to evaluate the sensitivity of both approaches.

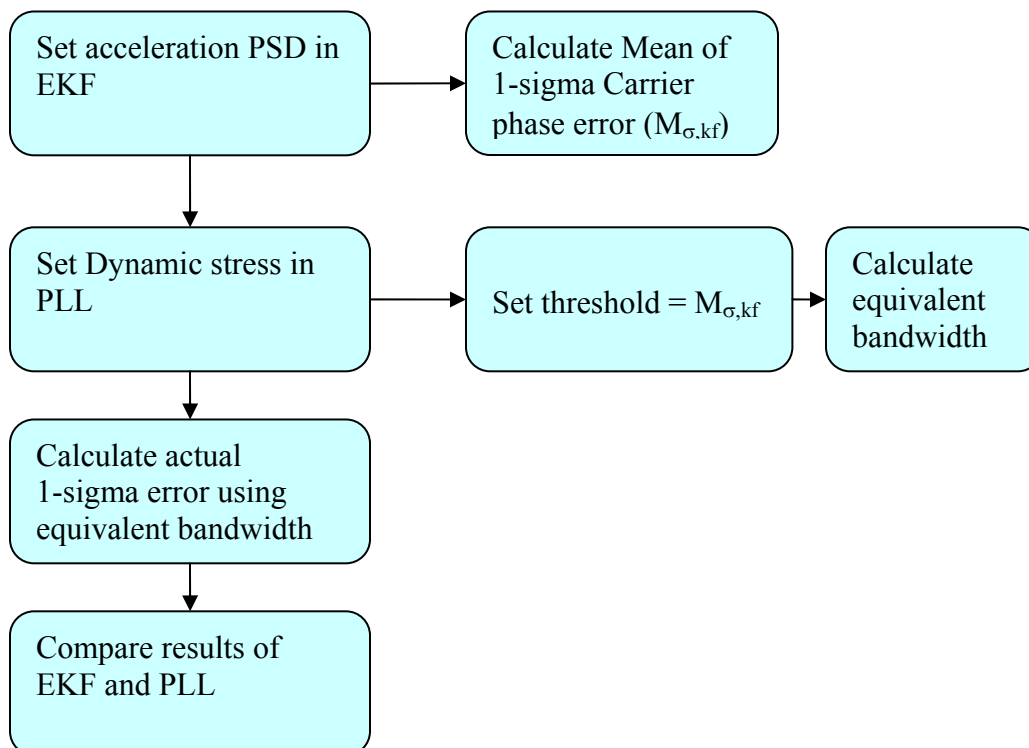


Figure 5-44: EKF equivalent bandwidth calculation

5.3.3 Motion

The method used to calculate the equivalent bandwidth has been verified using a strong signal for a static user. However, the difference between the Kalman filter tracking loops and the standard PLL tracking loops is of interest in real scenarios, e.g. dynamic vehicle, weak signals, etc. The scenario used here is simulating a dynamic vehicle, moving with varying speed, as described in Section 5.1.3.2.

5.3.3.1 Separate EKF versus Separate Tracking Loops

Following the same steps, Figure 5-45 shows the equivalent bandwidth, followed by the 1-sigma carrier phase errors in Figure 5-46.

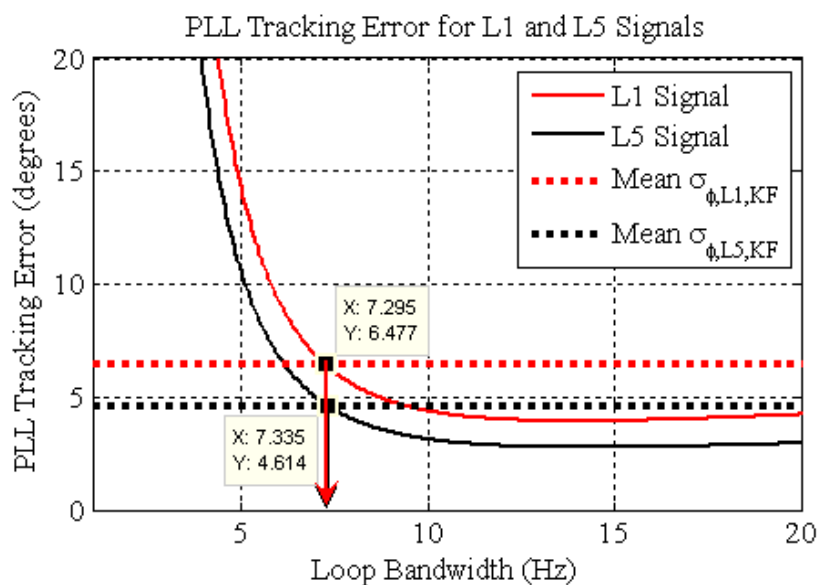


Figure 5-45: PLL tracking errors for L1 and L5 signals: moving vehicle-separate tracking

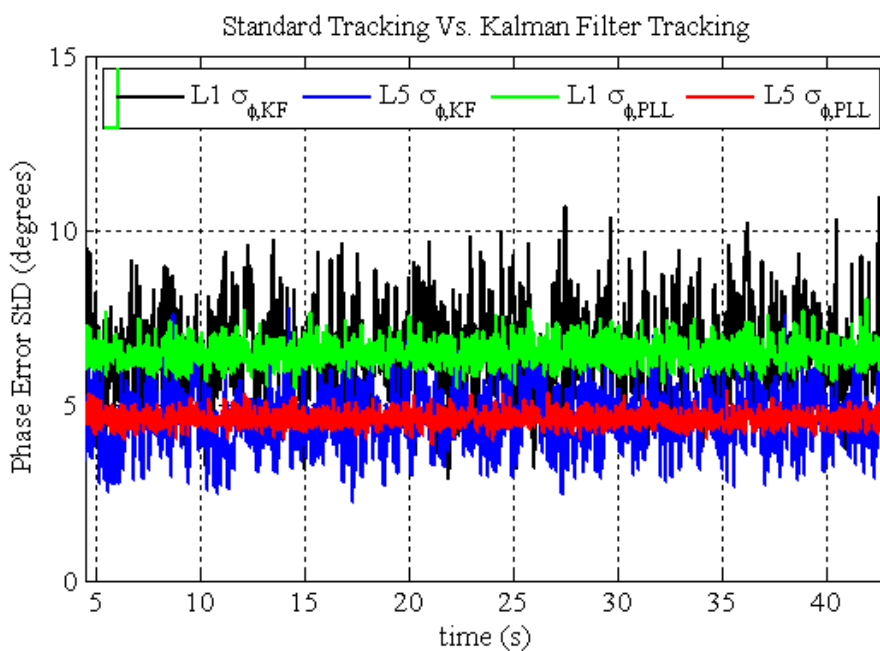


Figure 5-46: Phase error: moving vehicle-separate tracking

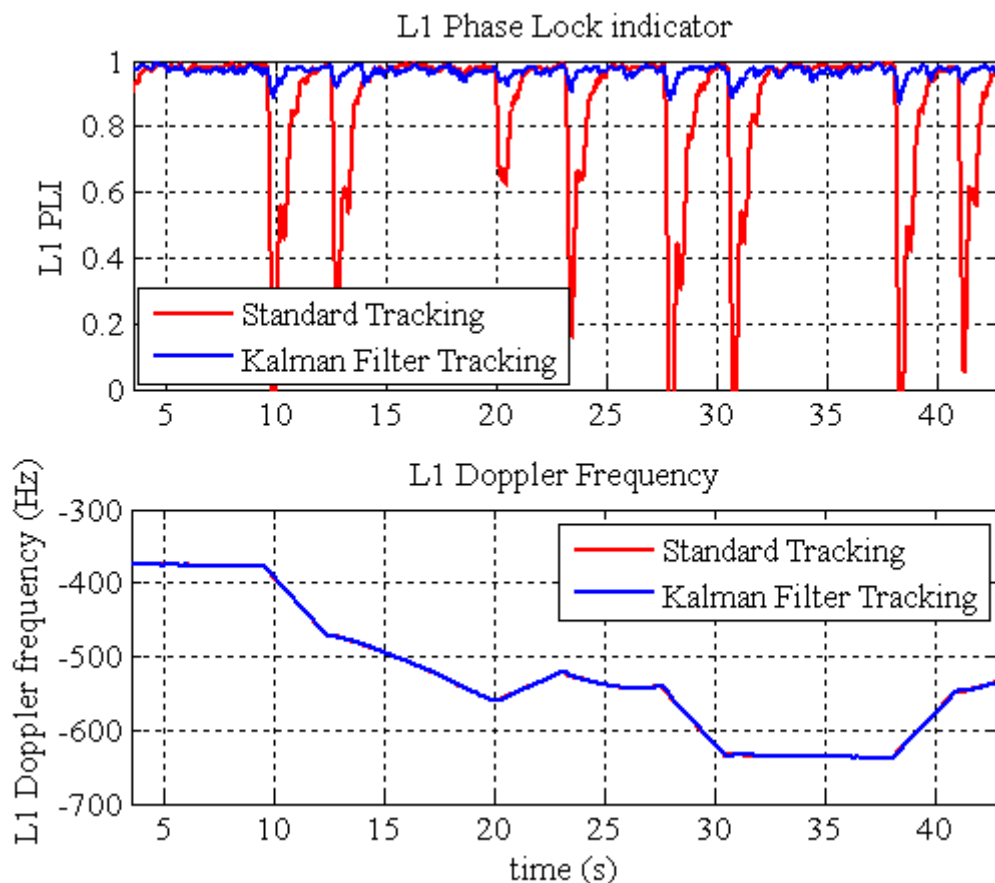


Figure 5-47: L1 PLI and Doppler frequency: moving vehicle-separate tracking

In the static user case, a strong agreement has been observed between the Kalman filter tracking loop and the equivalent PLL; however when motion is introduced, the equivalent PLL shows deviation from the Kalman filter. The Kalman filter adapts its bandwidth according to changes in the signal power, which points out its second advantage, whereas the PLL assumes a deterministic signal with pre-known dynamics and uses a fixed bandwidth which results in degraded performance when the signal suffers unpredicted dynamics. The L1 PLI illustrates these results as shown in Figure 5-47. The standard PLL shows lower PLI in instances where the vehicle changes its speed, and that is reflected in

the Doppler frequency shown in the same figure. The L5 PLI shows the same results as the L1 as shown in Figure 5-48.

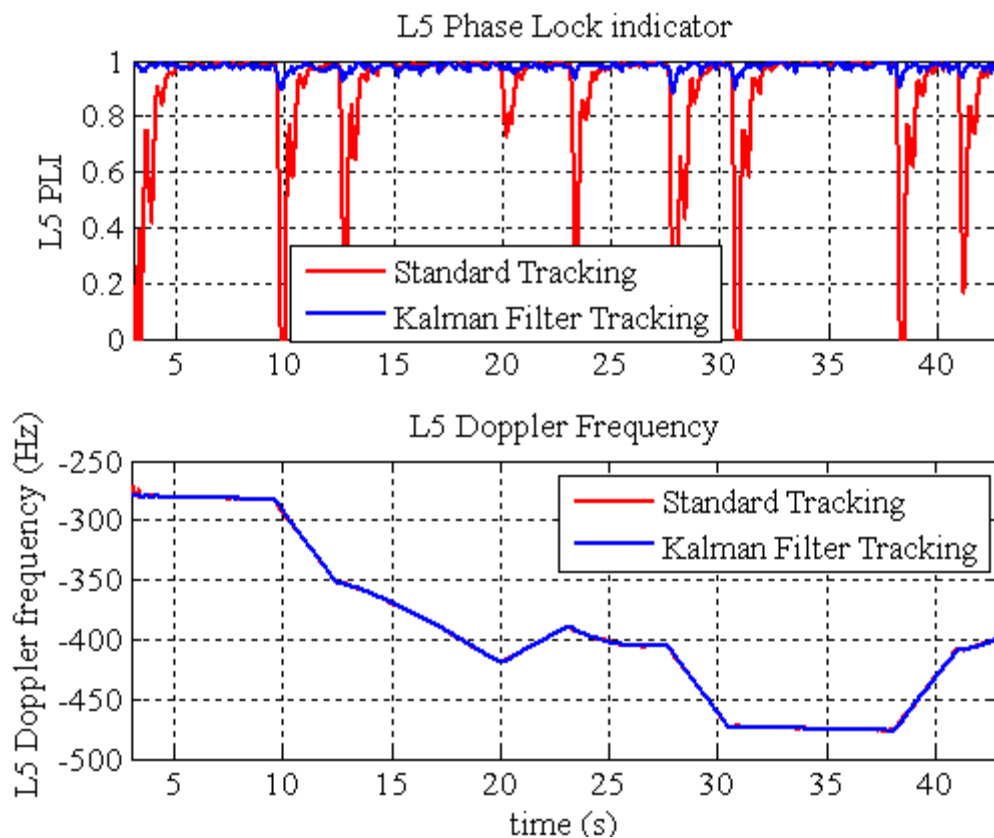


Figure 5-48: L5 PLI and Doppler frequency: moving vehicle-separate tracking

5.3.3.2 Combined EKF versus Aided Tracking Loops

For the combined case, the aided L1 PLL shows even lower PLI, due to the contribution of the L5 PLL since it is using the equivalent bandwidth in its loop filter. That is clearly illustrated in Figure 5-49, where the L5 PLI is affecting the aided L1 PLI.

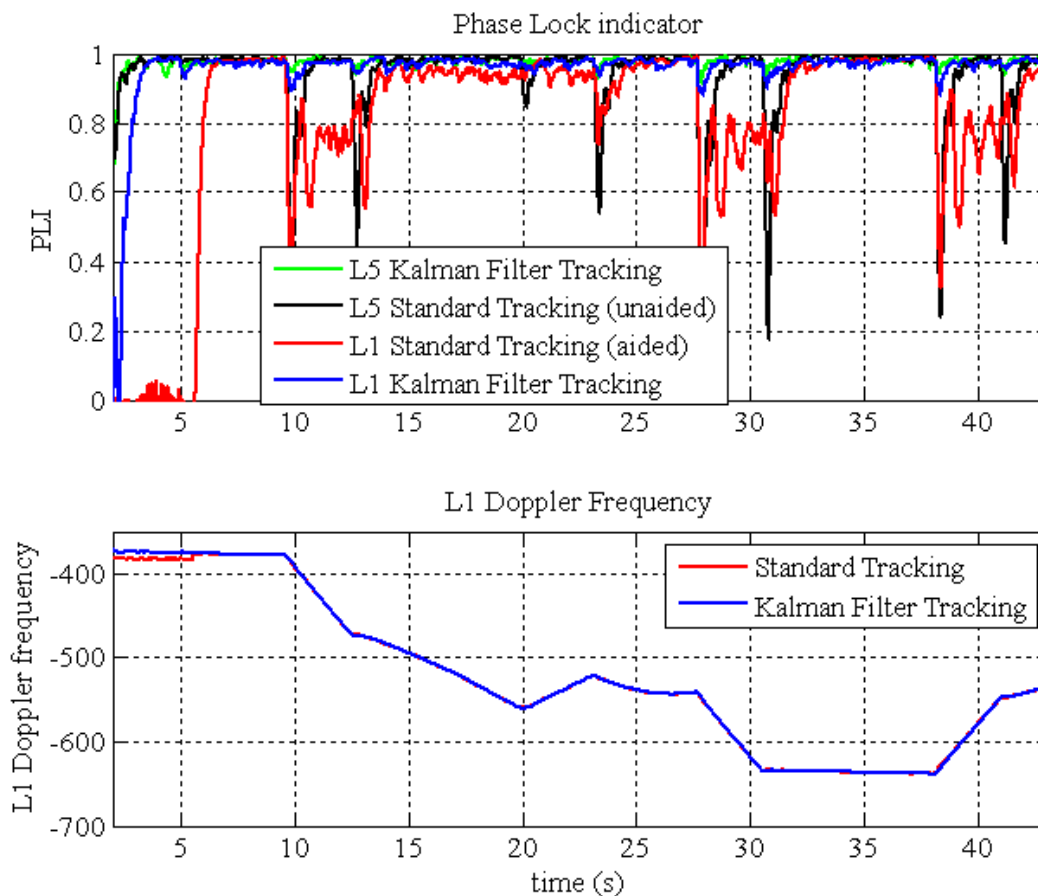


Figure 5-49: L1 PLI and Doppler frequency: moving vehicle-combined tracking

The equivalent bandwidth used in the L5 PLL is calculated as shown in Figure 5-50, followed by that of the L1 PLL in Figure 5-51 and the results of the 1-sigma carrier phase errors in Figure 5-52.

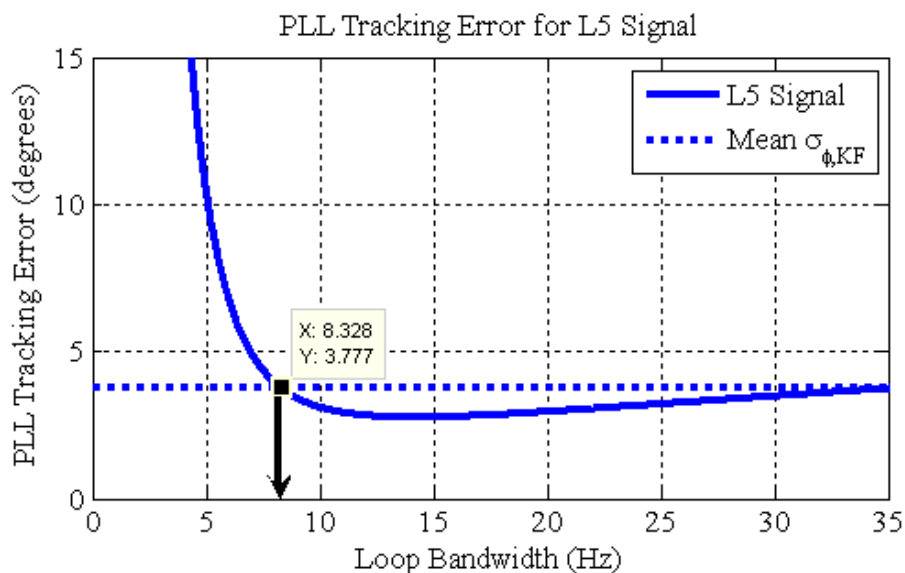


Figure 5-50: PLL tracking errors for L5 signal: moving vehicle-combined tracking

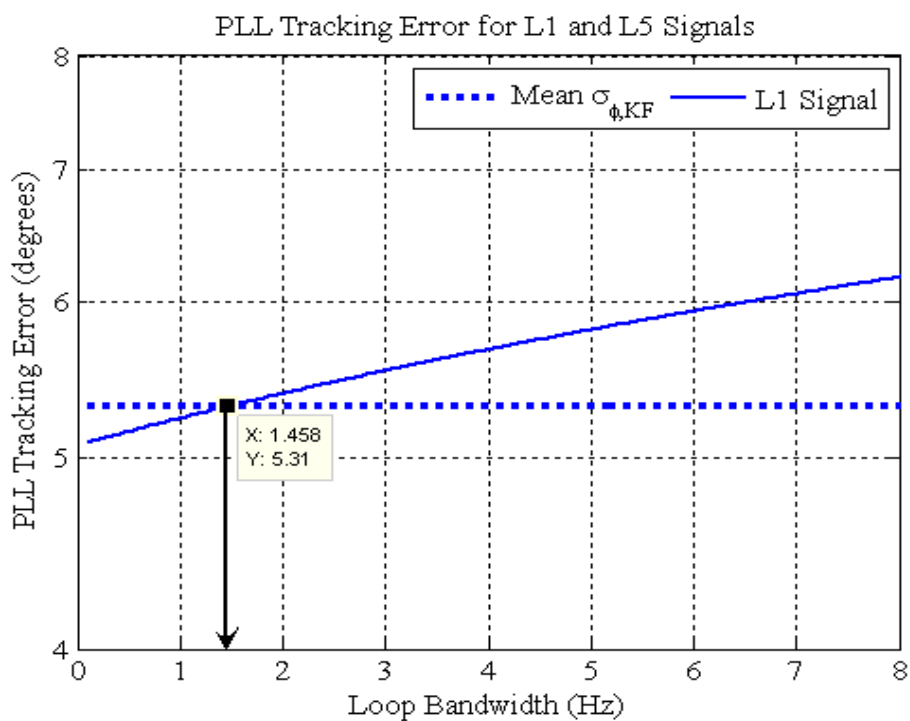


Figure 5-51: PLL tracking errors for L1 signal: moving vehicle-combined tracking

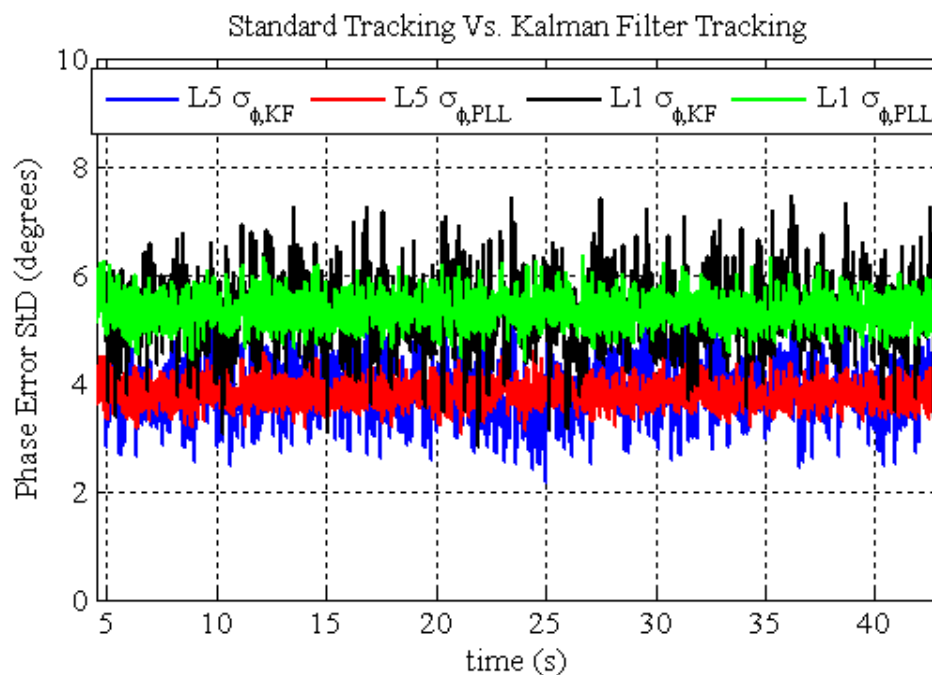


Figure 5-52: Carrier phase error: moving vehicle-combined tracking

5.3.4 Sensitivity Analysis

The third attempt to evaluate and compare the two tracking approaches is by simulating a signal for a static user that suffers from a continuous decrease in its power levels by a rate of 0.5 dB per second. Figure 5-53 shows the carrier to noise ratio calculated from the software receiver.

Figure 5-54 shows the equivalent bandwidth calculation for the separate case. It is interesting to note that these calculations are based on the mean of the 1-sigma carrier phase error of the Kalman filter, which is continuously increasing due to the decrease of the C/N_0 as shown in Figure 5-55. That is why the PLL is showing more error at the start of the scenario and less at the end; it is on the average the same as that of the Kalman filter. This figure also emphasises the second advantage of the EKF: it adapts its

bandwidth to changes in scenario (most particularly changes in C/No) whereas the standard tracking is a fixed bandwidth approach.

Figure 5-56 shows the equivalent bandwidth calculation for the combined case for both signals, and the associated 1-sigma carrier phase error in Figure 5-57.

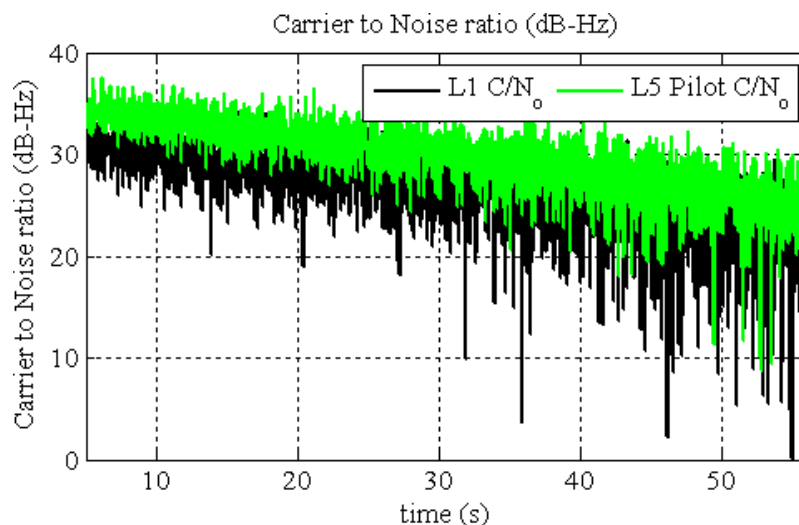


Figure 5-53: Carrier to noise ratio-sensitivity analysis

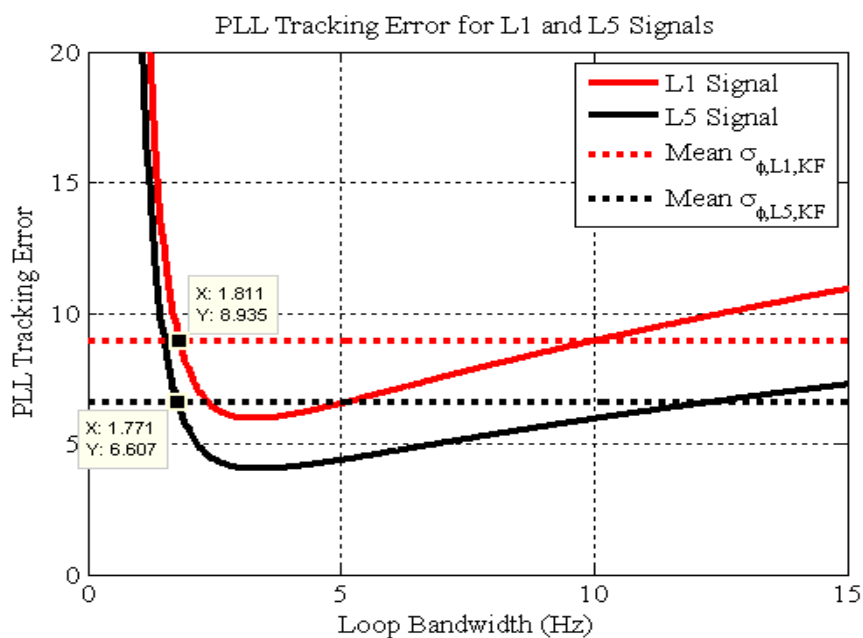


Figure 5-54: PLL tracking errors for L1 and L5 signals: sensitivity analysis-separate tracking

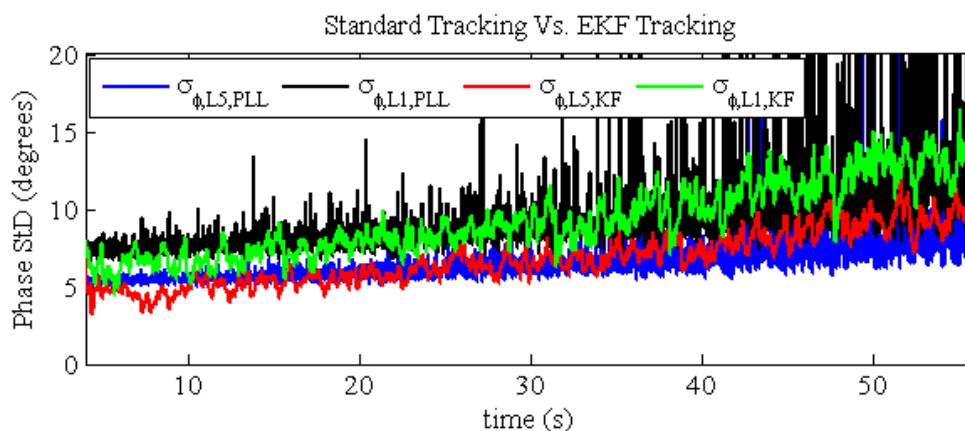


Figure 5-55: Phase error: sensitivity analysis-separate tracking

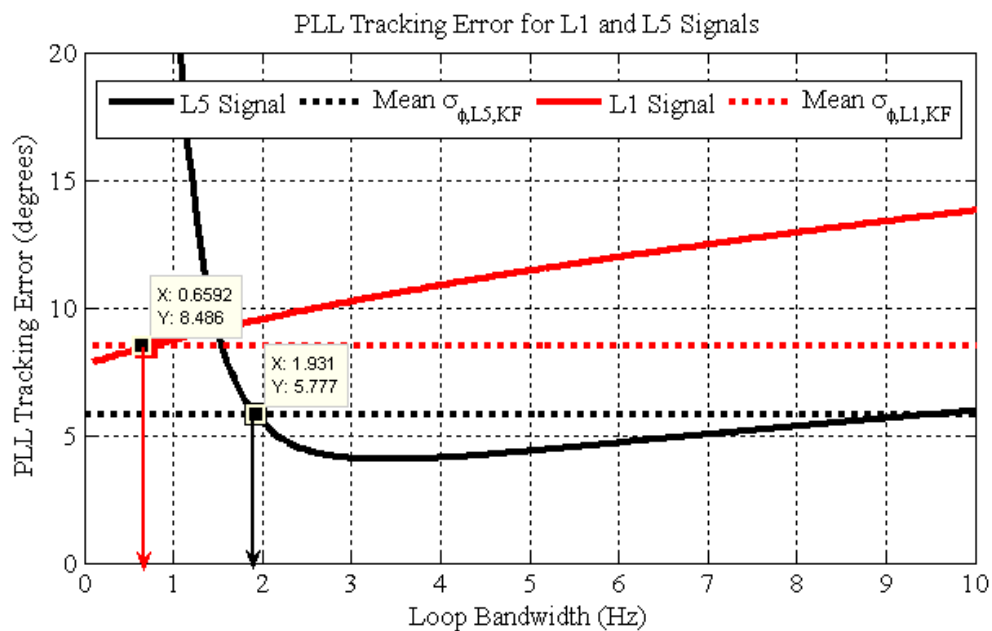


Figure 5-56: PLL tracking errors for L1 and L5 signals: sensitivity analysis-combined tracking

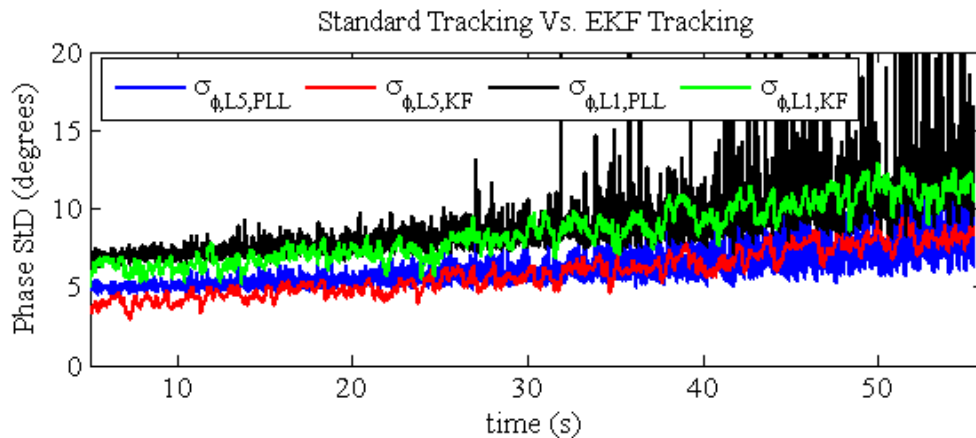


Figure 5-57 Phase error: sensitivity analysis-combined tracking

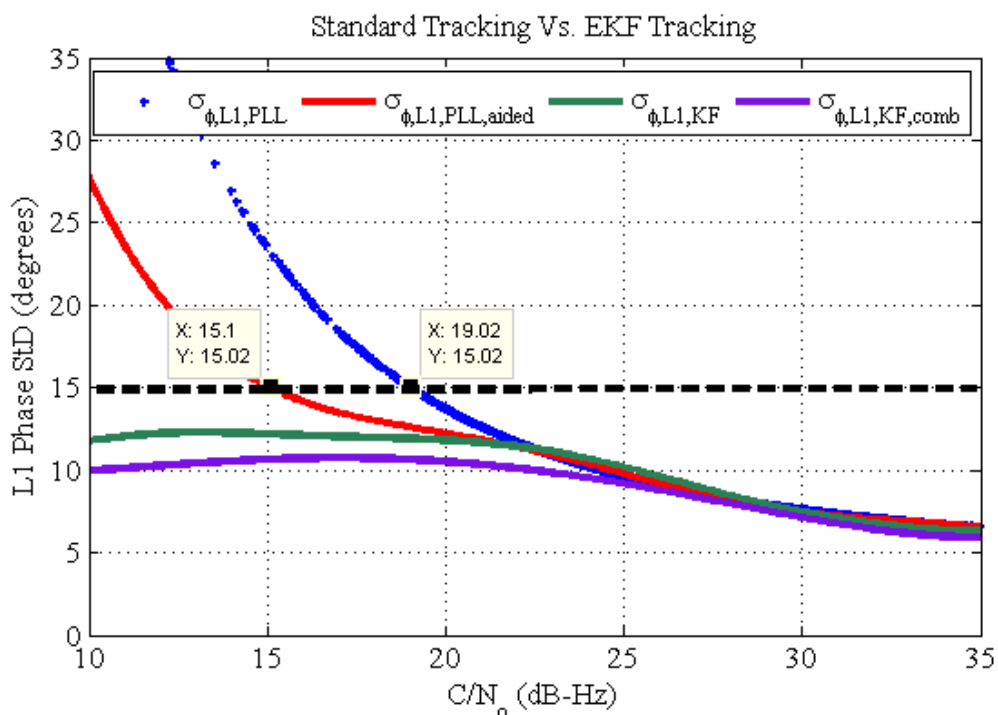


Figure 5-58: L1 Phase error versus carrier to noise ratio

Figure 5-58 shows the 1-sigma carrier phase error for the L1 signal using the four approaches, namely separate PLL, aided PLL, separate Kalman filter and combined Kalman filter. At high to moderate values of C/N_0 , the four methods are giving almost the

same error. However, they start to deviate at lower C/N_0 . The separate PLL crossed the 15° rule of thumb threshold at a C/N_0 value of 19 dB-Hz, followed by the aided PLL at 15 dB-Hz, which is an increase of 4 dB. The separate Kalman filter also shows deviation from the combined Kalman filter at lower C/N_0 . However, both filters did not cross the threshold even at low C/N_0 .

Figure 5-59 shows the 1-sigma carrier phase error for the L5 signal using separate PLL, separate Kalman filter and combined Kalman filter. At high to moderate values of C/N_0 , the three methods are giving almost the same error. The separate PLL started to deviate from the Kalman filter at lower C/N_0 values and crossed the 30° rule of thumb threshold at a C/N_0 value of 12 dB-Hz. The separate Kalman filter also shows deviation from the combined Kalman filter at lower C/N_0 . However, similar to the L1 signal, both filters did not cross the threshold even at low C/N_0 values.

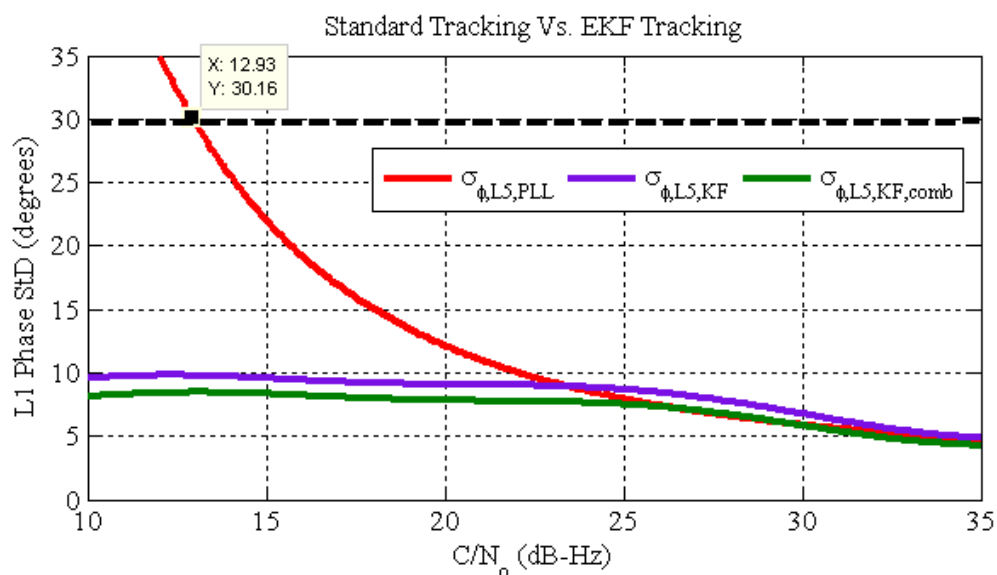


Figure 5-59: L1 Phase error versus carrier to noise ratio

5.4 Summary

The chapter presented a detailed performance evaluation for the aided tracking loops and the combined Kalman filter tracking loops. First a derivation of the aided PLL tracking loops was presented, followed by a theoretical and experimental evaluation which demonstrated the benefit of aiding the L1 PLL with the L5 Doppler frequency.

The chapter then proceeded to the Kalman filter, where a comparison of the tracking performance was made between the separate and the combined Kalman filters in two different scenarios. The combined Kalman filter has demonstrated its advantage over the separate Kalman filter for both signals. The benefits of using the data and pilot channels were also verified; they further enhanced the tracking performance of the two signals and this was shown with the phase and frequency lock indicators, and Kalman filter statistics.

Finally a method to compare the two approaches was described based on experimentally finding the equivalent bandwidth of the Kalman filter and plugging it into the standard PLL. The Kalman filter showed an improvement in the transient response of the tracking loop compared to the standard PLL. Also, the filter showed better adaptation to different signal dynamics. A sensitivity analysis showed that the aided PLL increased the L1 tracking sensitivity by 4 dB over the separate PLL. Moreover, the combined Kalman filter was shown to provide a lower 1-sigma carrier phase error compared to the separate Kalman filter even at lower C/N_0 values.

Chapter Six: CONCLUSIONS AND RECOMMENDATIONS

A detailed study of the combination possibilities of the L1 C/A code and L5 signals has been presented in this thesis. This chapter discusses the main conclusions derived from the thesis, followed by recommendations for future work that can complement its work.

6.1 Conclusions

The objectives of the thesis listed in Chapter 1 included:

- i. Aiding using standard tracking loops
- ii. Combination using Kalman- filter tracking
- iii. Combination of L1 data, L5 data and L5 pilot channels
- iv. Developing a methodology to compare the standard PLL and Kalman filter based tracking loops

The thesis had fulfilled these objectives, whereby a complete combined Kalman filter model has been developed and evaluated. Also, aided tracking loops were implemented and assessed. Finally, an experimental method of comparing these two approaches was presented. The conclusions from each are expanded below.

6.1.1 Aiding Using Standard Tracking Loops

The aided L1 PLL was the first approach investigated in the thesis. It was a direct implementation, however only the L1 signal could benefit from it. Taking that into consideration, the results shown lead to the following conclusions:

- ✓ The aided L1 PLL outperforms the separate L1 PLL. Lower loop filter bandwidth can be used in the case of the aided PLL, leading to a decrease in the level of noise of the loop.
- ✓ With a bandwidth as low as 0.1 Hz, the aided L1 PLL could track a signal with a C/N_0 of 21.5 dB-Hz under 0.01 g/s jerk, whereas the unaided L1 could not track the same signal, even with using 10 times larger bandwidth.
- ✓ The aided PLL increased the L1 tracking sensitivity by 4 dB over the separate PLL.

Standard loop aiding can therefore lead to improvements in L1 signal tracking, both in terms of thermal noise performance and tracking sensitivity. There is, however, no benefit to L5 tracking.

6.1.2 Combination Using Kalman-Filter Tracking

A complete Kalman filter model was designed and implemented to combine the tracking information of the two signals. The analysis and simulations shown in Chapter 5 lead to the following conclusions:

- ✓ The combined Kalman filter had proved its advantage over the separate Kalman filter for the both signals. That was apparent in the improvement in the phase and frequency lock indicators, root mean squares and standard deviations of the estimated carrier phase errors of both the L1 and L5 signals achieved using the combined Kalman filter.
- ✓ The combined Kalman filter was shown to provide a lower 1-sigma carrier phase error compared to the separate Kalman filter even at lower C/N_0 .

Thus the combined Kalman filter tracking provides superior thermal noise and tracking performance to separate Kalman filter tracking.

6.1.3 Combination of L1 Data, L5 Data and L5 Pilot Channels

The benefits of using the three available channels were shown in the thesis. The following conclusion can be extracted from the simulations shown in the thesis:

- ✓ For the aided L1 tracking, combining the total power of the L5 signal led to enhanced L1 phase tracking performance, as seen by an increase in the PLI.
- ✓ For the combined Kalman filter, combining the total power of the L5 signal reduced the L1 carrier phase error by approximately 40% when using both the data and pilot channels as opposed to using only the pilot channel.
- ✓ For the L5 signal, combining the data and pilot channels was beneficial in most cases. However, combining these two channels with the L1 signal is only beneficial when the L1 estimates are good, e.g., in the car dynamics scenario. When the L1 estimates were noisy, e.g. due to multipath, the benefits from combining these two channels with the L1 signal start to diminish.

Consequently, combining the data and pilot channels of the L5 signal with the L1 signal leads to improvements in L1 signal tracking, both in terms of thermal noise and tracking performance. However, the L1 signal combination with the data and pilot channels is only beneficial to the L5 signal in cases where the L1 estimates are good enough, otherwise that combination doesn't have any benefit to the L5 signal.

6.1.4 Developing a Methodology to Compare the Standard PLL and Kalman Filter Based Tracking Loops

A methodology to compare the two approaches had been developed and presented. The Kalman filter showed an improvement over the standard PLL tracking loops in three main aspects:

- ✓ The transient response of the tracking loop: That was noticed in the faster adaptation to the change of bandwidth when the tracking loop was switching from the FLL to the Kalman filter based tracking, as compared to the standard tracking loop's slower adaptation when switching to PLL.
- ✓ The adaptation to different signal dynamics: The Kalman filter was adapting its bandwidth according to changes in the signal dynamics, whereas the PLL assumed a deterministic signal with pre-known dynamics and uses a fixed bandwidth. That was also apparent in the sensitivity analysis scenario, where again the Kalman filter was using the calculated noise power to weigh the measurements and the estimated states, resulting in a bandwidth that is adaptive to the signal's C/N_0 .
- ✓ The improved sensitivity of the tracking loop, which was noticed when standard tracking loops crossed the 15° and 30° rule of thumb tracking thresholds, contrary to the Kalman filter which did not cross these thresholds even at low C/N_0 values (down to 10 dB-Hz).

6.2 Recommendations for Future Work

Following these conclusions, this section lists the limitations of the research presented in the thesis and provides recommendations for future work.

- i. The methodology presented for comparing the performance of the standard PLL and Kalman filter based tracking loops is based on an experimental approach. An analytical model of the equivalent PLL would help to solidify the approach provided.
- ii. The developed Kalman filter made use of both L1 and L5 correlator outputs. These two signals however have different behaviour towards the ionospheric errors. This was accounted for in the process noise term which was responsible for any deviations between the L1 and L5 signals due to the ionospheric errors, and the results verified the validity of this approach. However, it would be interesting to discuss the possibility of including the ionospheric error in the Kalman filter.
- iii. The simulations and the test scenarios shown in the thesis were limited to the car dynamics. Testing the developed algorithms on higher order dynamics would give a better assessment of the overall tracking performance.
- iv. The thesis is concerned with the combination at the tracking level and the improvement in the tracking performance; however an evaluation of the impact of the combined tracking on the positioning level remains important to study.
- v. Finally, although the GPS signal simulator used herein emulates the signal transmitted by GPS satellites, it would be valuable to test the proposed algorithms on real data. The use of real data would allow testing of the developed algorithms shown in the thesis in various environments. Appendix B showed the problems with the test L5 payload transmitted from SVN 49. The first Block IIF-1 GPS satellite is scheduled for launch in May 2010, with full L5 capability (UNAVCO 2010).

References

- Bastide, F., O. Julien, C. Macabiau and B. Roturier (2002) “**Analysis of L5/E5 Acquisition, Tracking and Data Demodulation Thresholds**,” in Proceedings of the US Institute of Navigation GNSS, Portland, OR, USA, Sept. 24-27.
- Brown, R.G. and P.Y.C. Hwang (1992), *Introduction to Random Signals and Applied Kalman Filtering*, John Wiley & Sons, Inc., USA.
- Betz, J., C. Cahn, P. Dafesh, C. Hegarty, K. Hudnut, C. Jones, R. Keegan, K. Kovach, L. Lenahan, H. Ma, J. Rushanan, T. Stansell, C. Wang and S. Yi (2006) “**L1C Signal Design Options**,” in *Proceedings of ION NTM 2006*, Monterey, California, Pages 685-697
- Cahn, C., C. Wang, C. Hegarty, D. Sklar, H. Ma, J. Betz, J. Rushanan, K. Kovach, K. Hudnut, L. Lenahan, M. Blanco, P. Dafesh, R. Keegan, S. Yi, T. Stansell and V. Kasemsri (2007) *Enhancing the Future of Civil GPS: Overview of the L1C Signal*, InsideGNSS, Spring 2007.
- Conley, R., R. Cosentino, C. J. Hegarty, E. Kaplan, J. Leva, M. Hang and K. Dyke (2006) “**Satellite Signal Performance of Stand-Alone GPS**,” [Chapter 7] in *Understanding GPS Principles and Applications*, second edition, Artech House Mobile Communications Series, p. 301.
- Egziabher D.G, A. Razavi, P. Enge, J. Gautier, D. Akos, S. Pullen and B. Pervan (2003) “**Doppler Aided Tracking Loops for SRGPS Integrity Monitoring**,” in *Proceedings of ION GPS/GNSS 2003*, 9-12 September 2003, Portland, OR.
- Gao, G. X., L. Heng, D. DeLorenzo, S. Lo, D. Akos, A. Chen, T. Walter, P. Enge and B. Parkinson (2009) “**Modernization Milestone: Observing the First GPS Satellite with an L5 Payload**,” *Inside GNSS*, May/June 2009.
- Gelb, A. (1974), *Applied Optimal Estimation*, The M.I.T. Press.
- Gernot, C. (2009) *Development of Combined GPS L1/L2C Acquisition and Tracking Methods for Weak Signal Environments*, PhD Thesis, Department of Geomatics Engineering, the University of Calgary, Canada. (Available at <http://plan.geomatics.ucalgary.ca>)
- Goldstein, D. (2009) *GPS IIR-20 (SVN 49) Panel Discussion*, in the *ION GNSS 2009 Panel Discussions*, 22-25 September, Savannah, GA.

- GPS Navstar (1995) *Global Positioning System Standard Positioning Service Signal Specification: Annex A Standard Positioning Service Performance Specification*, GPS Navstar, 2nd Edition, June 2nd 1995.
- GPS World (2009) *L5 Signal Activation Anticipated for Friday*, <http://sidt.gpsworld.com/gpssid/Latest+News/L5-Signal-Activation-Anticipated-for-Thursday/ArticleStandard/Article/detail/591925?contextCategoryId=1385>, last visited on April 14th, 2009.
- Gunawardena, S., Z. Zhu and M. Braash (2009) “**First Look: Observing the GPS L5 Test Transmission from SVN49 Using Software Radio Processing**,” *Inside GNSS*, May/June 2009.
- Hegarty, C. and M. Tran (2003) “**Acquisition Algorithms for the GPS L5 Signal**,” in *proceedings of ION GPS/GNSS 2003*, 9-12 September 2003, Portland, OR.
- Hu, T., G. Lachapelle and R. Klukas (2005) “**Indoor GPS Signal Replication Using a Hardware Simulator**,” in *Proceedings of ION GNSS 2005*, Long Beach, CA, September 13-16, 2005.
- Ioannides, R. T., L. E. Aguado and G. Brodin (2006) “**Coherent Integration of Future GNSS Signals**,” in *Proceedings of the 19th International Technical Meeting of the Satellite Division of the Institute of Navigation ION GNSS 2006*, September 26 - 29, 2006, Fort Worth Convention Center, Fort Worth, Texas.
- Insigler, M. and B. Eissfeller (2002) “**PLL Tracking Performance in the Presence of Oscillator Phase Noise**,” *GPS Solutions*, Vol. 5, No. 4, pp. 45-57 (2002)
- IS-GPS-705 (2005) *Navstar GPS Space Segment/ User Segment L5 Interfaces*, ARINC Incorporated, 22nd September 2005.
- IS-GPS-200 (2006) *Interface Specification – Navstar GPS Space Segment/ Navigation User Interfaces*, ARINC Incorporated, Revision D, 7th March 2006.
- Julien, O. (2005) “**Carrier-Phase Tracking of Future Data/Pilot Signals**” in *Proceedings of GNSS 2005*, Session B1, Long Beach, CA, 13-16 September, The Institute of Navigation, Fairfax, VA, 12 pages.
- Kazemi, P. (2008) “**Optimum Digital Filters for GNSS Tracking Loops**,” in *Proceedings of ION GNSS08*, Savannah, GA, 16-19 Sep.
- Lachapelle, G.E. (2007) *Advanced GNSS Theory And Applications*, ENGO 625 Course Notes, Department of Geomatics Engineering, University of Calgary, Canada.

- Lachapelle, G., E. Cannon, R. Klukas, S. Singh, R. Watson P. Boulton, A. Read and K. Jones (2003) “**Hardware Simulator Models and Methodologies for Controlled Indoor Performance Assessment of High Sensitivity AGPS Receivers,**” in *Proceedings of GNSS 2003*, Graz, Australia, 22-25 April 2003.
- Langley, R. B. (2009) *Expert Advice: Cause Identified for Pseudorange Error from New GPS Satellite SVN49*, GPS World, July 13th 2009.
- Lee, D. (2002) “**Analysis of Jitter in Phase-Locked Loops,**” in *IEEE Transactions on Circuits and Systems-II: Analog and Digital Signal Processing*, Vol. 49, No. 11, November 2002.
- LOS ANGELES AIR FORCE BASE (2009) *Air Force Successfully Transmits an L5 Signal from GPS IIR-20 (M) Satellite*, last accessed on April, 10th, 2009. <http://www.losangeles.af.mil/news/story.asp?storyID=123144001,-> LOS ANGELES AIR FORCE BASE, California.
- Macabiau, C., L. Ries, F. Bastide, J-L. Issler (2003) “**GPS L5 Receiver Implementation Issues,**” in *Proceedings of the ION GPS/GNSS 2003*, Portland, OR, USA, 9-12 September 2003.
- McDonald, K. D. (2002) “**The Modernization of GPS: Plans, New Capabilities and the Future Relationship to Galileo,**” *Journal of Global Positioning Systems*, Vol. 1, No. 1-17.
- McDonald, K. D. and C. Hegarty (2000) “**Post-Modernization GPS Performance Capabilities,**” in *Proceedings of ION 56th Annual Meeting*, 26-28 June 2000, San Diego, California, USA (Institute of Navigation, Alexandria, Virginia), pp. 242-249.
- Megahed, D., C. O’Driscoll, and G. Lachapelle (2009) “**Combined L1/L5 Kalman Filter Based Tracking for Weak Signal Environments,**” *ATTI dell’Istituto Italiano di Navigazione*, No 189, July Issue, 45-56
- Meurer, M., S. Erker, S. Thöler, O. Montenbruck, A. Hauschild, and R. B. Langley (2009) *GPS L5 First Light: A Preliminary Analysis of SVN49’s Demonstration Signal*, GPS World, June 2009. http://www.gpsworld.com/gnss-system/gps-modernization/innovation-l5-signal-first-light-8661?page_id=4
- Misra P. and P. Enge (2001) “**GPS Measurements and Error Sources,**” [Chapter 4] in *Global Positioning System, Signals, Measurements and Performance*, Ganga-Jamuna Press.

- Mongrédien, C. (2008) *GPS L5 Software Development for High-Accuracy Applications*, PhD Thesis, published as UCGE Report No. 20268, Department of Geomatics Engineering, University of Calgary, Canada (Available at <http://plan.geomatics.ucalgary.ca>).
- NI PXI-5661 (2006) *2.7 GHz RF Vector Signal Analyzer with Digital Downconversion*, National Instruments Corporation (Available at http://www.ni.com/pdf/products/us/cat_vectorsignalanalyzer.pdf, last accessed December 2, 2009).
- O'Driscoll, C. and G. Lachapelle (2009) “**Comparison of Traditional and Kalman Filter Based Tracking Architectures**,” in *Proceedings of European Navigation Conference 2009*, Naples, Italy, May 3-6, 2009.
- Boulton, P., A. Read, G. MacGougan, R. Klukas, M.E. Cannon, G. Lachapelle (2002) “**Proposed Models and Methodologies for Verification Testing of AGPS-Equipped Cellular Mobile Phones in the Laboratory**,” in *Proceedings of the Institute of Navigation GPS2002*, Portland, OR, September 24-27, pp. 200-212.
- Petovello, M.G. and G. Lachapelle (2006) “**Comparison of Vector-Based Software Receiver Implementation with Applications to Ultra-Tight GPS/INS Integration**,” in *Proceedings of ION GNSS 2006*.
- Physics Laboratory (2010) *Time and Frequency from A to Z*, <http://tf.nist.gov/general/glossary.htm>, last accessed on February 11th, 2010, National Institute of Standards and Technology.
- Psiaki, M.L. and H. Jung (2002) “**Extended Kalman Filter Methods for Tracking Weak GPS Signals**,” in *Proceedings of ION GPS 2002*.
- Qaisar, S. (2009) “**Performance Analysis of Doppler Aided Tracking Loops in Modernized GPS Receivers**,” in *Proceedings of ION GNSS 2009*, 22-25 September, Savannah, GA.
- Ries, L., C. Macabiau, O. Nouvel, Q. Jeandel, W. Vigneau, V. Calmettes, and , JL. Issler (2002) “**A Software Receiver for GPS-IIIF L5 Signal**,” in *Proceedings of ION GPS 2002*, 24-27 September 2002, Portland, OR.
- Salem, D., C. O'Driscoll and G. Lachapelle (2009) “**Performance Evaluation of Combined L1/L5 Kalman Filter Based Tracking versus Standalone L1/L5 Tracking in Challenging Environments**,” accepted for publication in the *Journal of Global Positioning Systems*, December 2009.

- Spilker, J. J., and A. J. Van Dierendonck (1999) “**Proposed New Civil GPS Signal at 1176.45 MHz**,” in Proceedings of ION GPS 1999, 14-17 September, pp. 1717-1725, Nashville, TN.
- Spirent (2006) *Signal Generator Hardware User Manual*, Spirent Communications, issue 1-20, September 2006.
- Stephens S.A., and J. B. Thomas (1995) “**Controlled-Root Formulation for Digital Phase-Locked Loops**” in *IEEE Transactions on Aerospace and Electronic Systems*, Vol. 31, No. 1, pp. 78-95.
- U.S. Air Force (2006) **GPS Modernization Fact Sheet**, <http://pnt.gov/public/docs/2006/modernization.pdf>, last accessed October 27th, 2009.
- UNAVCO (2010) *Science & Technology - GNSS Modernization: GPS L2C / L5 / L1C*, http://facility.unavco.org/science_tech/gnss_modernization.html_modernization.html, last accessed February 8, 2010
- Van Dierendonck, A. J. (1996) “**GPS Receivers**,” [Chapter 8] in *Global Positioning System: Theory and Applications*, Progress in Astronautics and Aeronautics, Vol. 163, p. 329
- Van Dierendonck, A. J. and AJ Systems (2000) *Mathematical Challenges in GPS: New Opportunities Using New Civil Signals for Multipath Mitigation and Carrier Phase Ambiguity Resolution*, presented at IMA Workshop: Mathematical Challenges in Global Positioning (GPS), University of Minnesota, August 16-18, 2000
- Van Dierendonck, A. J. and J. J. Spilker (1999), “**Proposed civil GPS signal at 1176.45 MHz: In-phase/quadrature codes at 10.23 MHz chip rate**,” in *Proceedings of ION Annual Meeting (AM)*, Cambridge, MA, June 1999, pp. 761 – 770.
- Ward, P. W. and J. W. Betz (2006) “**Satellite Signal Characteristics**,” [Chapter 4] in *Understanding GPS Principles and Applications*, second edition, Artech House Mobile Communications Series, p. 113.
- Ward, P. W., J. W. Betz, and C. J. Hegarty (2006a) “**Satellite Signal Acquisition, Tracking and Data Demodulation**,” [Chapter 5] in *Understanding GPS Principles and Applications*, second edition, Artech House Mobile Communications Series, p. 153.

- Ward, P. W., J. W. Betz, and C. J. Hegarty (2006b) “**Interference, Multipath and Scintillation**,” [Chapter 6] in *Understanding GPS Principles and Applications*, second edition, Artech House Mobile Communications Series, p. 153.
- Watson, J. R. A. (2005) *High-Sensitivity GPS L1 Signal Analysis for Indoor Channel Modelling*, MSc Thesis, Department of Geomatics Engineering, University of Calgary, Canada. (Available at <http://plan.geomatics.ucalgary.ca>)
- Winkel, J. O. (2000) *Modeling and Simulating GNSS Signal Structures and Receivers*, PhD Thesis, Faculty of Civil Engineering and Surveying, University of the Bundeswehr Munich (Available at <http://137.193.200.177/ediss/winkel-jon/meta.html>, last accessed December 2, 2009).
- Yi, Q., C. Xiaowei, L. Mingquan and F. Zhenming (2009) **Steady-State Performance of Kalman Filter for DPLL**, in *Tsinghua Science And Technology*, pp. 470-473, Vol. 14, Number 4, August 2009.

APPENDIX A: DSICRETE COVARIANCE MATRIX

A.1. Separate Kalman Filter Tracking Q Matrix

$S_{am} \cdot T$	0	0	0	0
$= Q_{1,1}$	$S_{mp} \cdot T + \beta^2 \cdot S_f \cdot T$ $+ \frac{1}{3} \cdot T^3 \cdot \beta^2 \cdot S_g$ $+ \frac{1}{20} \cdot T^5 \cdot \beta^2 \cdot S_a$	$\beta \cdot S_f \cdot T$ $+ \frac{1}{3} \cdot T^3 \cdot \beta \cdot S_g$ $+ \frac{1}{20} \cdot T^5 \cdot \beta \cdot S_a$	$\frac{1}{2} \cdot T^2 \cdot \beta \cdot S_g$ $+ \frac{1}{8} \cdot T^4 \cdot \beta \cdot S_a$	$\frac{1}{6} \cdot T^3 \cdot \beta \cdot S_a$
$= Q_{1,2}$	$= Q_{2,2}$	$S_f \cdot T$ $+ \frac{1}{3} \cdot T^3 \cdot S_g$ $+ \frac{1}{20} \cdot T^5 \cdot S_a$	$\frac{1}{2} \cdot T^2 \cdot S_g$ $+ \frac{1}{8} \cdot T^4 \cdot S_a$	$\frac{1}{6} \cdot T^3 \cdot S_a$
$= Q_{1,3}$	$= Q_{2,3}$	$= Q_{2,3}$	$T \cdot S_g$ $+ \frac{1}{3} \cdot T^3 \cdot S_a$	$\frac{1}{2} \cdot T^2 \cdot S_a$
$= Q_{1,4}$	$= Q_{2,4}$	$= Q_{2,4}$	$= Q_{2,4}$	$T \cdot S_a$

where S_{am} : Amplitude power spectral density
 S_{mp} : Code power spectral density
 S_a : Carrier phase acceleration power spectral density

A.2. Combined Kalman Filter Tracking Q Matrix

$S_{am1} \cdot T$	0	0	0	0	0	0	0
$= Q_{0,1}$	$S_{mp1} \cdot T + \beta_1^2 \cdot SF^2 \cdot S_{f5} \cdot T$ $+ \frac{1}{3} \cdot T^3 \cdot \beta_1^2 \cdot SF^2 \cdot S_{g5}$ $+ \frac{1}{20} \cdot T^5 \cdot \beta_1^2 \cdot SF^2 \cdot S_{a5}$	$\beta_1 \cdot SF^2 \cdot S_{f5} \cdot T$ $+ \frac{1}{3} \cdot T^3 \cdot \beta_1 \cdot SF^2 \cdot S_{g5}$ $+ \frac{1}{20} \cdot T^5 \cdot \beta_1 \cdot SF^2 \cdot S_{a5}$	0	$\beta_1 \cdot SF \cdot S_{f5} \cdot \beta_5 \cdot T$ $+ \frac{1}{3} \cdot T^3 \cdot \beta_1 \cdot SF \cdot S_{g5} \cdot \beta_5$ $+ \frac{1}{20} \cdot T^5 \cdot \beta_1 \cdot SF \cdot S_{a5} \cdot \beta_5$	$\beta_1 \cdot SF \cdot S_{f5} \cdot T$ $+ \frac{1}{3} \cdot T^3 \cdot \beta_1 \cdot SF \cdot S_{g5}$ $+ \frac{1}{20} \cdot T^5 \cdot \beta_1 \cdot SF \cdot S_{a5}$	$\frac{1}{2} \cdot T^2 \cdot \beta_1 \cdot SF \cdot S_{g5}$ $+ \frac{1}{8} \cdot T^4 \cdot \beta_1 \cdot SF \cdot S_{a5}$	$\frac{1}{6} \cdot T^3 \cdot \beta_1 \cdot SF \cdot S_{a5}$
$= Q_{0,2}$	$= Q_{1,2}$	$S_{f1} \cdot T + SF^2 \cdot S_{f5} \cdot T$ $+ \frac{1}{3} \cdot T^3 \cdot SF^2 \cdot S_{g5}$ $+ \frac{1}{20} \cdot T^5 \cdot SF^2 \cdot S_{a5}$	0	$SF \cdot S_{f5} \cdot \beta_5 \cdot T$ $+ \frac{1}{3} \cdot T^3 \cdot SF \cdot S_{g5} \cdot \beta_5$ $+ \frac{1}{20} \cdot T^5 \cdot SF \cdot S_{a5} \cdot \beta_5$	$SF \cdot S_{f5} \cdot T$ $+ \frac{1}{3} \cdot T^3 \cdot SF \cdot S_{g5}$ $+ \frac{1}{20} \cdot T^5 \cdot SF \cdot S_{a5}$	$\frac{1}{2} \cdot T^2 \cdot SF \cdot S_{g5}$ $+ \frac{1}{8} \cdot T^4 \cdot SF \cdot S_{a5}$	$\frac{1}{6} \cdot T^3 \cdot SF \cdot S_{a5}$
$= Q_{0,3}$	$= Q_{1,3}$	$= Q_{2,3}$	$S_{am5} \cdot T$	0	0	0	0
$= Q_{0,4}$	$= Q_{1,4}$	$= Q_{2,4}$	$= Q_{3,4}$	$S_{mp5} \cdot T + \beta_5^2 \cdot S_{f5} \cdot T$ $+ \frac{1}{3} \cdot T^3 \cdot \beta_5^2 \cdot S_{g5}$ $+ \frac{1}{20} \cdot T^5 \cdot \beta_5^2 \cdot S_{a5}$	$\beta_5 \cdot S_{f5} \cdot T$ $+ \frac{1}{3} \cdot T^3 \cdot \beta_5 \cdot S_{g5}$ $+ \frac{1}{20} \cdot T^5 \cdot \beta_5 \cdot S_{a5}$	$\frac{1}{2} \cdot T^2 \cdot \beta_5 \cdot S_{g5}$ $+ \frac{1}{8} \cdot T^4 \cdot \beta_5 \cdot S_{a5}$	$\frac{1}{6} \cdot T^3 \cdot \beta_5 \cdot S_{a5}$
$= Q_{0,5}$	$= Q_{1,5}$	$= Q_{2,5}$	$= Q_{3,5}$	$= Q_{4,5}$	$S_{f5} \cdot T$ $+ \frac{1}{3} \cdot T^3 \cdot S_{g5}$ $+ \frac{1}{20} \cdot T^5 \cdot S_{a5}$	$\frac{1}{2} \cdot T^2 \cdot S_{g5}$ $+ \frac{1}{8} \cdot T^4 \cdot S_{a5}$	$\frac{1}{6} \cdot T^3 \cdot S_{a5}$
$= Q_{0,6}$	$= Q_{1,6}$	$= Q_{2,6}$	$= Q_{3,6}$	$= Q_{4,6}$	$= Q_{5,6}$	$T \cdot S_{g5}$ $+ \frac{1}{3} \cdot T^3 \cdot S_{a5}$	$\frac{1}{2} \cdot T^2 \cdot S_{a5}$
$= Q_{0,7}$	$= Q_{1,7}$	$= Q_{2,7}$	$= Q_{3,7}$	$= Q_{4,7}$	$= Q_{5,7}$	$= Q_{6,7}$	$T \cdot S_{a5}$

**APPENDIX B: INITIAL COMPARISON BETWEEN COMBINED KALMAN
FILTER AND SEPARATE STANDARD TRACKING LOOPS**

The first attempt to evaluate the proposed model for the L1/L5 combination is through comparing it to the separate tracking of each of the two signals using standard phase and delay lock loops (Megahed et al 2009). Only the L5 pilot channel is used for this comparison. In the standard tracking, the only parameters that have to be tuned are those of the loop filters including the coherent integration time (T), the loop filter bandwidth (B_n) and also the filter order used.

Table B-1: Standard tracking parameters

Phase Tracking			Code Tracking		
Signal	Parameter	Value	Signal	Parameter	Value
L1	T (ms)	20	L1	T (ms)	20
	B_n (Hz)	1		B_n (Hz)	1
	Order	3		Order	1
L5	T (ms)	20	L5	T (ms)	20
	B_n (Hz)	1		B_n (Hz)	1
	Order	3		Order	1

For a fairer comparison, the bandwidth of the standard loop filter has been adjusted to produce a similar measurement noise level as that of the Kalman filter. This is achieved by comparing the noise levels produced from the Kalman filter and the standard PLL and adjusting the bandwidth accordingly. When attempting to decrease the DLL bandwidth, a

significant bias was observed in the phase estimates of both signals, so the delay lock loop was kept at 1 Hz. The loop filter parameters used for the phase tracking loop are shown in Table B-1.

B.1. Sensitivity

The simulated scenario used is for a static user suffering from both ionospheric errors and power degradation. A strong signal has been simulated at the beginning of the data set to enable the acquisition and bit synchronization of the two signals. Degradation of the power is done gradually afterwards. For the L1 signal, a signal of -150 dBW is simulated at the beginning, then the power is decreased 2 dB each 2 s, to reach a minimum of -176 dBW, which is 16 dB below the nominal power.

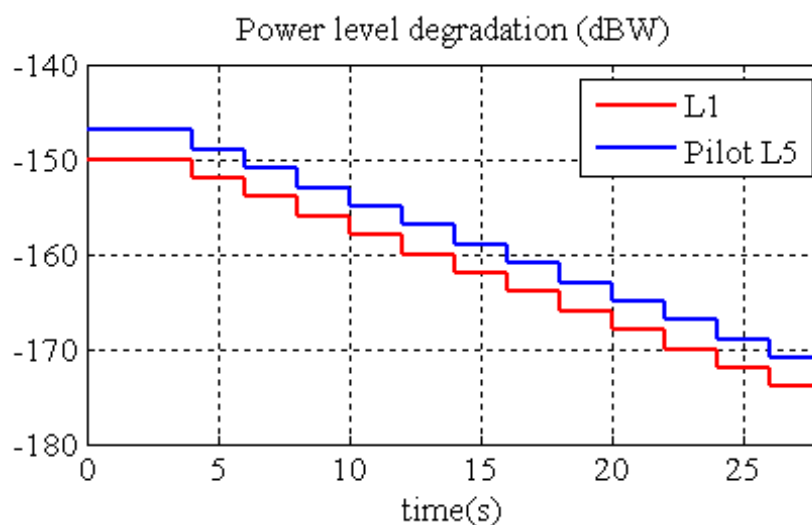


Figure B-1: Power level degradation

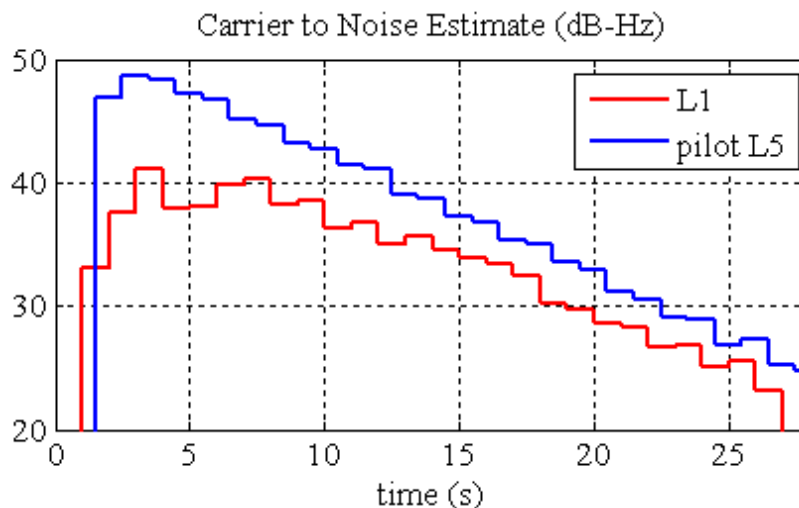


Figure B-2: Carrier to noise estimate

Figure B-1 shows the power levels simulated for each signal, and Figure B-2 shows the corresponding carrier to noise estimates from the software receiver. The two figures show a close match in the difference between the L1 and the L5 pilot power, and also in the estimated degradation. The results will be shown for one of the simulated PRNs- PRN 10.

B.2. Simulation Results

The first criteria in the comparison are the phase and frequency lock indicators. The upper part of Figure B-3 shows the PLI for four cases. The first is the PLI for standalone L1, the second is for the standalone L5, the third is for the L1 signal using the combined tracking, and the last one is for the L5 signal using the combined tracking. The lower part shows the FLI for the same cases. The phase and frequency lock indicators provide information about how well the signal is tracked both in phase and frequency. Both lock indicators also infer code lock.

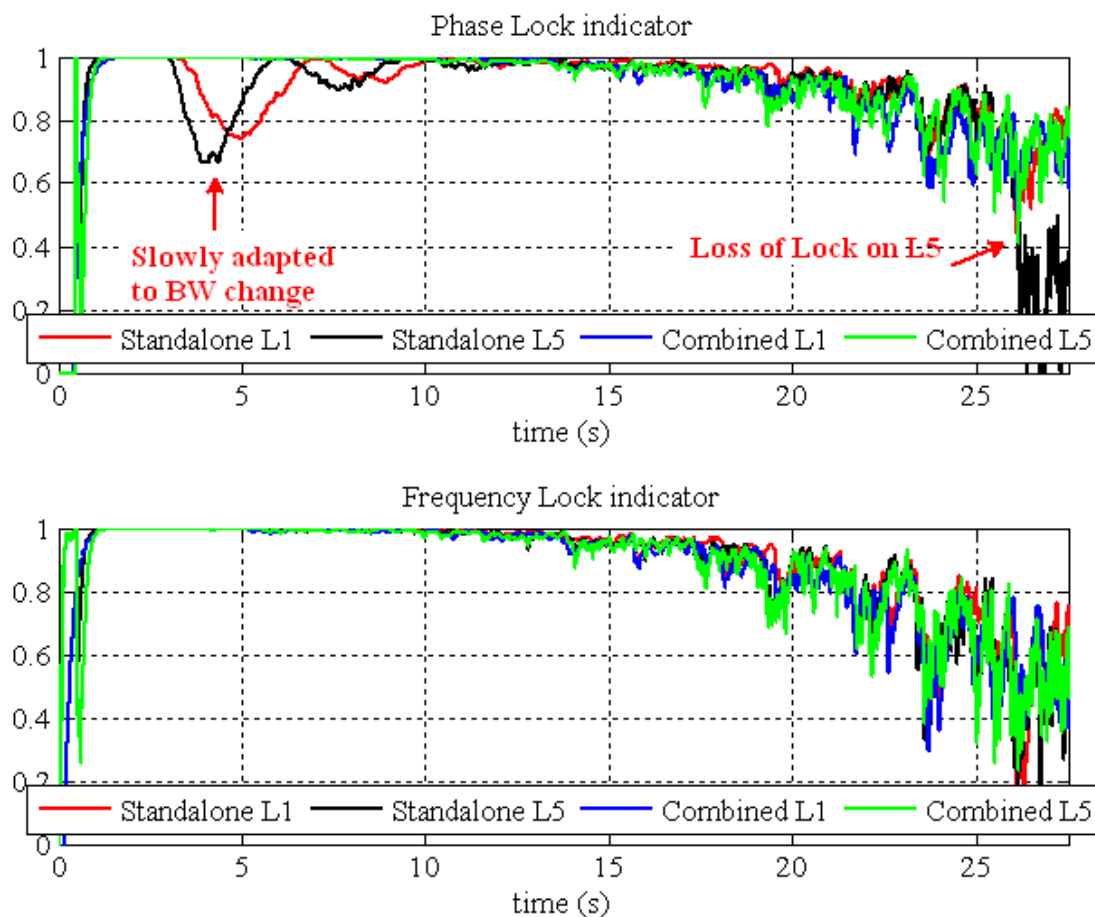


Figure B-3: Phase and frequency lock indicators

The first important result to point out in Figure B-3 is that when switching from frequency tracking to phase tracking using the standard loop filters, the loop filter adapted slowly to the change in the bandwidth, compared to the Kalman filter which did not suffer any difficulties when switching from frequency tracking. The Kalman filter eliminated the tradeoff between decreasing the bandwidth to have lower noise versus increasing the bandwidth to have higher dynamic response.

The second result is that up to the end of the simulation interval, the phase information was reserved in the case of the combined tracking. For the L5 case, as it is the one

suffering more from the ionospheric errors, the standalone tracking lost lock when the L5 pilot signal power was decreased beyond -169 dBW, whereas the in the combined case the L5 continued to lock till -173 dBW. So the combined tracking helped to increase the sensitivity by 4 dB for the L5 signal.

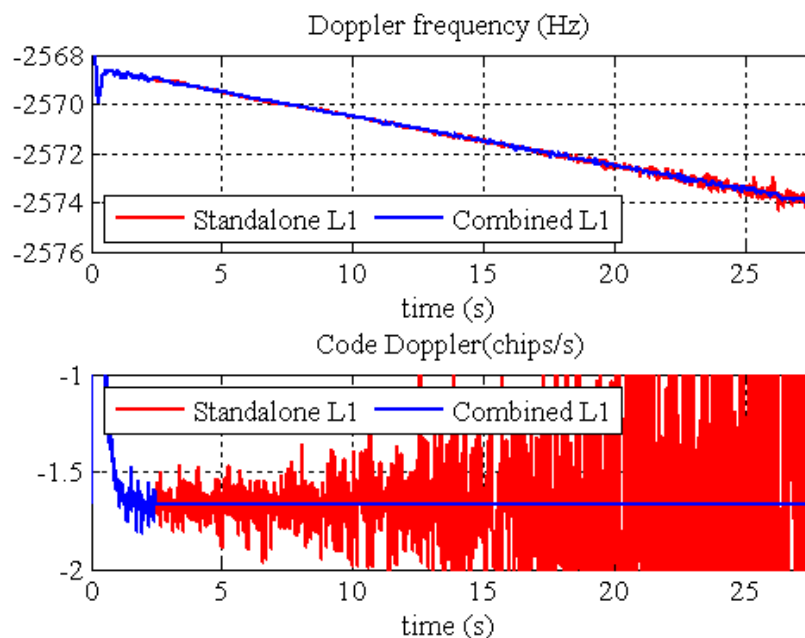


Figure B-4: L1 Doppler frequency, code Doppler

In Figure B-4 and Figure B-5, the Doppler frequency and the code Doppler of the same four cases are plotted. Note that the bandwidth of the PLL was adjusted to give the same noise levels as the Kalman filter case. The DLL on the other hand has more variations due to the bandwidth used as discussed before.

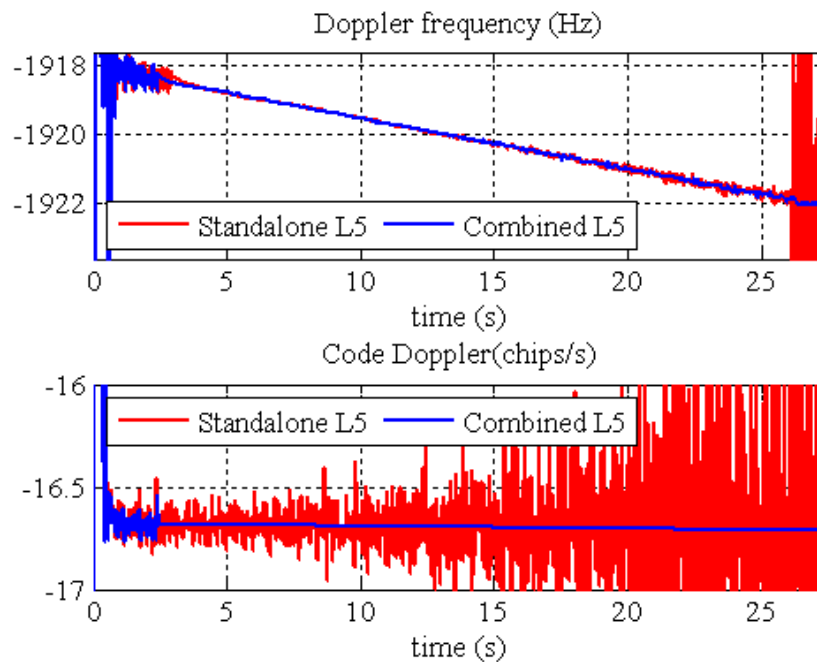


Figure B-5: L5 Doppler frequency, code Doppler

The next figures show the estimated eight states with their corresponding estimated standard deviations. Note that in Figure B-6, the effect of the L1 data bit transitions are totally eliminated verifying the bit estimation introduced in the Kalman filter.

Also note that for the eight states, the variances do not reach a steady-state value. This is due to the fact that during the simulations the signal power is continuously decreasing to evaluate weak signal performance, as is shown in the signal amplitude estimates in Figure B-6.

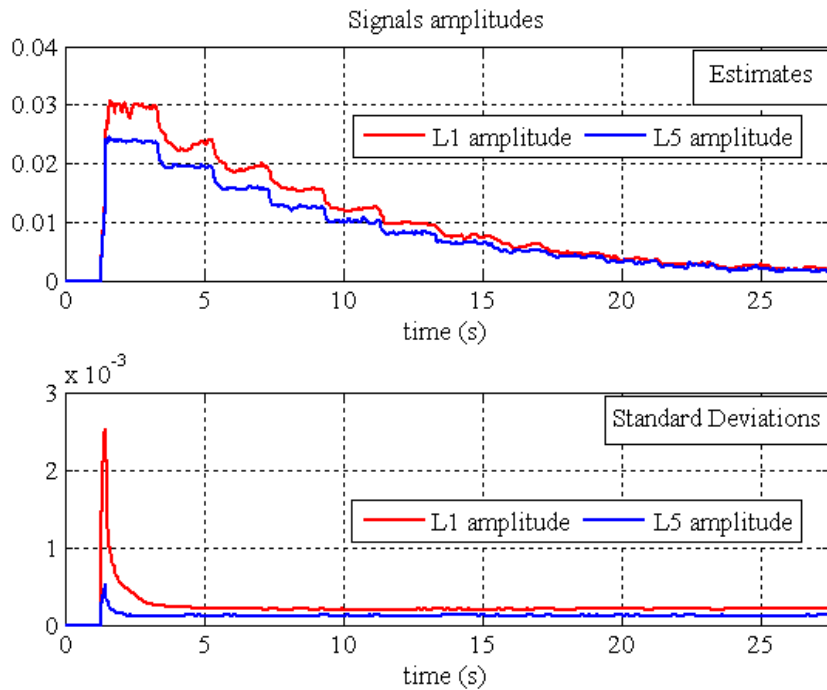


Figure B-6: L1 and L5 amplitudes

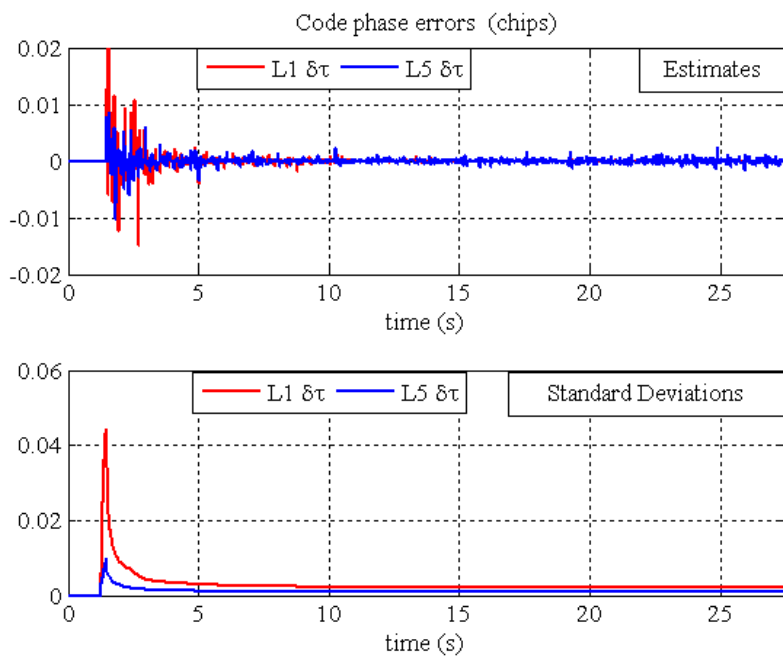


Figure B-7: L1 and L5 code phase errors

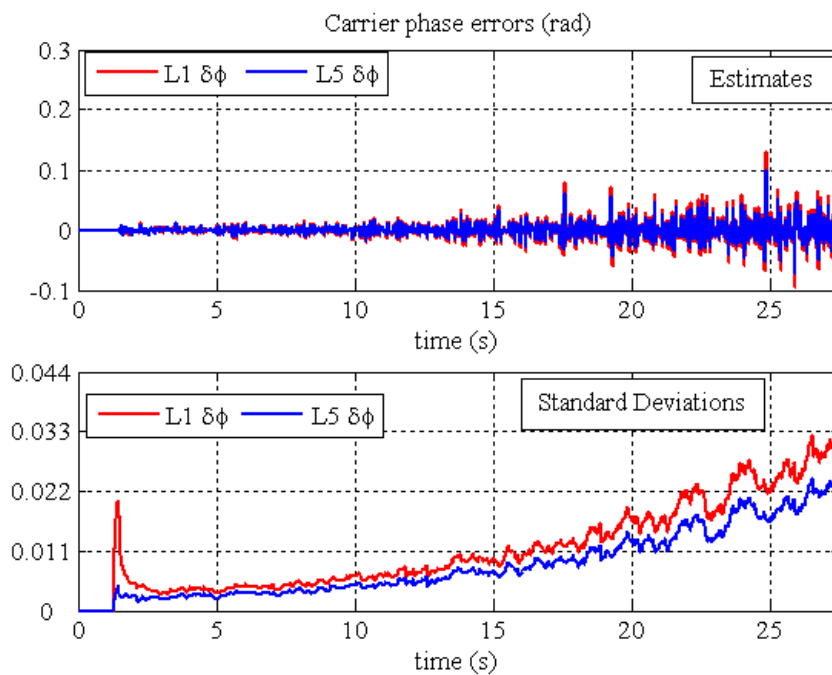


Figure B-8: L1 and L5 carrier phase errors

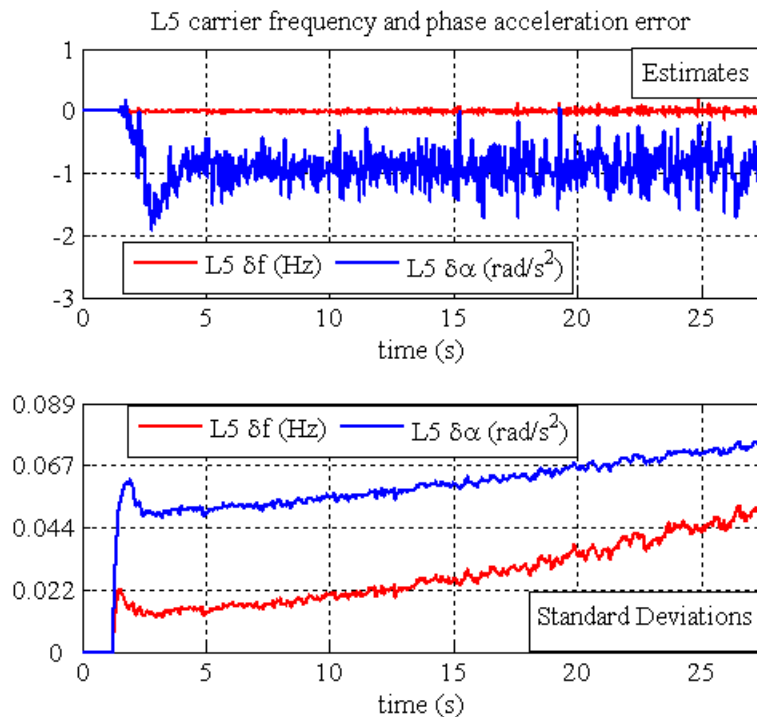


Figure B-9: L5 frequency and acceleration errors

APPENDIX C: SVN 49

SVN 49 was launched on March 24th 2009. However, several problems have been observed and identified with the data collected from that satellite, either from the L1, L2C or L5 signals. These problems are highlighted to explain why the real data were not used throughout the thesis.

C.1. L5 Demonstration Payload on SVN 49

The SVN 49 is transmitting a demo L5 payload, which was not intended to be operational, but was only intended to bring the L5 frequency into use. That was critical to enable the United States to meet the International Telecommunications Union (ITU) deadline for securing that RF band. That said, there were some deviations from the specifications of the IS-GPS-705 as follows (Gunawardena et al 2009):

- i. SVN 49 transmits only the dataless component.
- ii. It is hardwired to generate L5-Q PRN 63, whatever PRN assigned.
- iii. The transmitted power is lower than the minimum specifications.
- iv. The antenna gain pattern is not optimal for the L5 frequency.

Exciting as it was to have the first real data collected from that satellite, several papers (e.g. Meurer et al 2009, Gao et al 2009 and Gunawardena et al 2009) have been published to analyze that data. However, these papers pointed out several issues with the data collected as listed in the next section.

C.1.1. Problems

Other GPS signals, L1 and L2C, transmitted by SVN 49 started to show higher than usual pseudorange residuals. The typical errors have zero mean with peak to peak variation of two meters, but those calculated from SVN 49 have peak to peak variation of four meters. Moreover, when plotted against elevation, these errors are clearly showing elevation dependence. At 50° or 60° elevation, greater pseudorange residual errors are calculated, getting even higher with higher elevations as shown in Figure C-1.

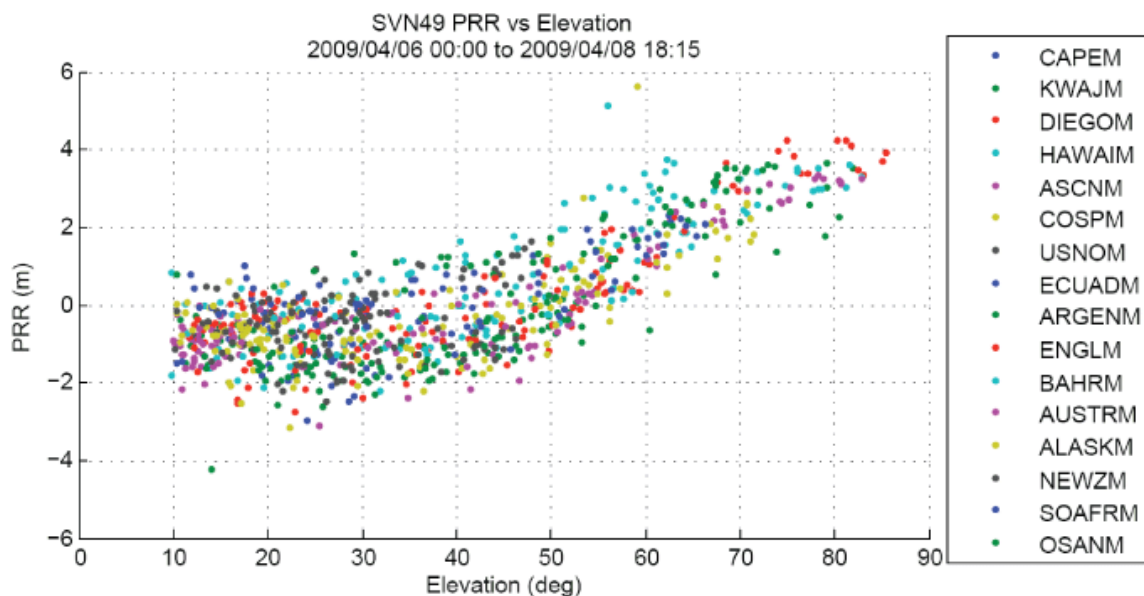


Figure C-1: SVN 49 pseudorange residuals versus elevation (Langley 2009)

C.1.2. Causes and Solutions

The distortion is caused when some of the L1 and L2C signals leaving the antenna port are reflecting off the L5 filter and transmitted through satellite antenna with a 30 nanoseconds delay. The results are characterized as a permanent static multipath signal, generated from within the satellite (Goldstein 2009).

Although there is no current fix for that problem, several alternatives for minimizing that error have been proposed. Solutions include:

- i. Placing the antenna phase offset 152 m above actual position, thus tricking the Kalman filter to think that the satellite is in different place.
- ii. Applying a pseudorange correction model in the Kalman filter by modelling the elevation-dependant pseudorange
- iii. Increasing the User Range Accuracy (URA) to allow the receivers to de-weight measurements from SVN 49.

C.2. SVN 49 Real Data Example

A sample data is collected on April 10th, 2009 at 6:07 am at a stationary open sky station. Even with the problems associated with that satellite, the combined Kalman filter is tested and the results are provided herein for illustration.

Figure C-2 shows the elevation of the satellite at the time of data collection. That is important to find out in order to know the exact difference in power between the L1 and the L5 pilot signal. The satellite was at a 64° elevation at the time of data collection.

Figure C-3 shows the elevation-dependant received power of the L5 signal (Meurer et al 2009). There is a difference of 18 dB between the low and high elevation angles for the L5 signal, where it is only 3 dB for the L1 and L2C signals. At the 64° elevation specified in Figure C-2, the difference of the received power is approximately 4.8 dB between the L1 and L5 signals. Figure C-4 shows the calculated C/N_0 at the software receiver, where approximately 5 dB difference is noticed.

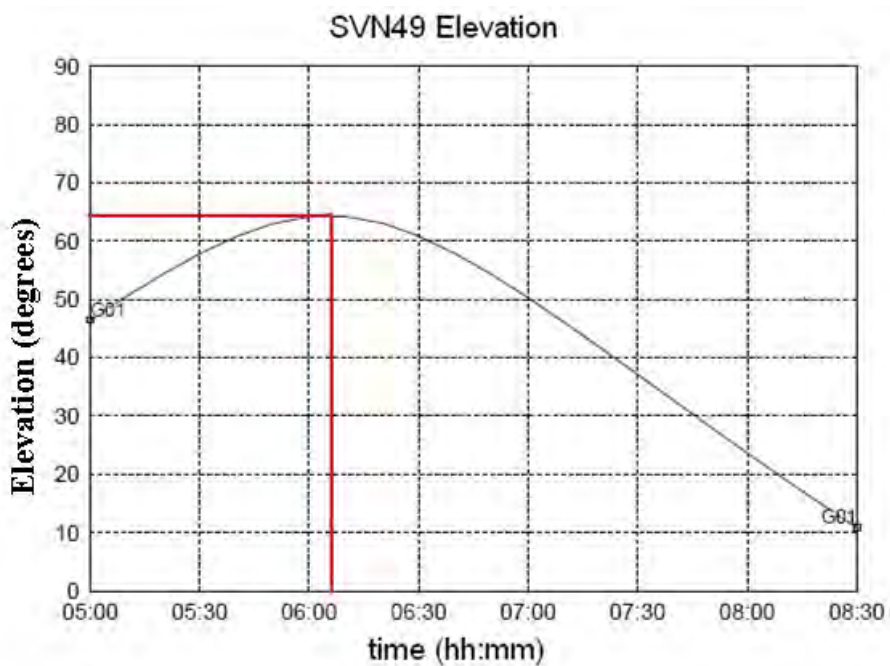


Figure C-2: SVN 49 elevation

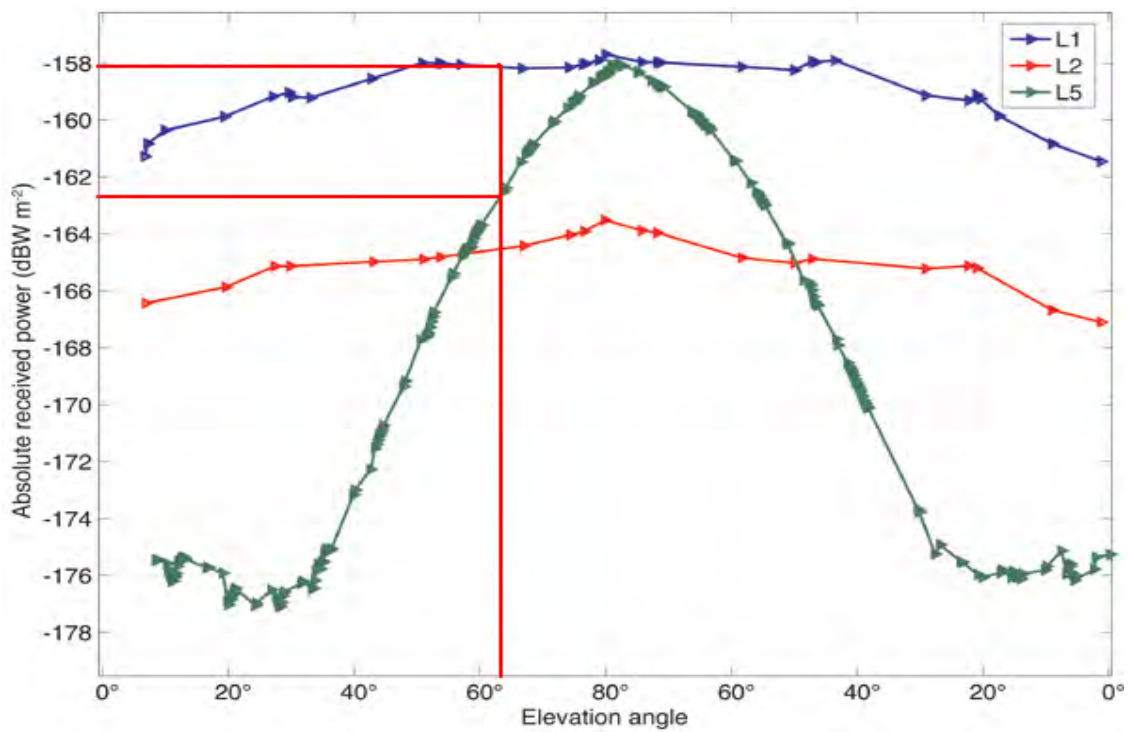


Figure C-3: SVN 49 received power versus elevation (Meurer et al 2009)

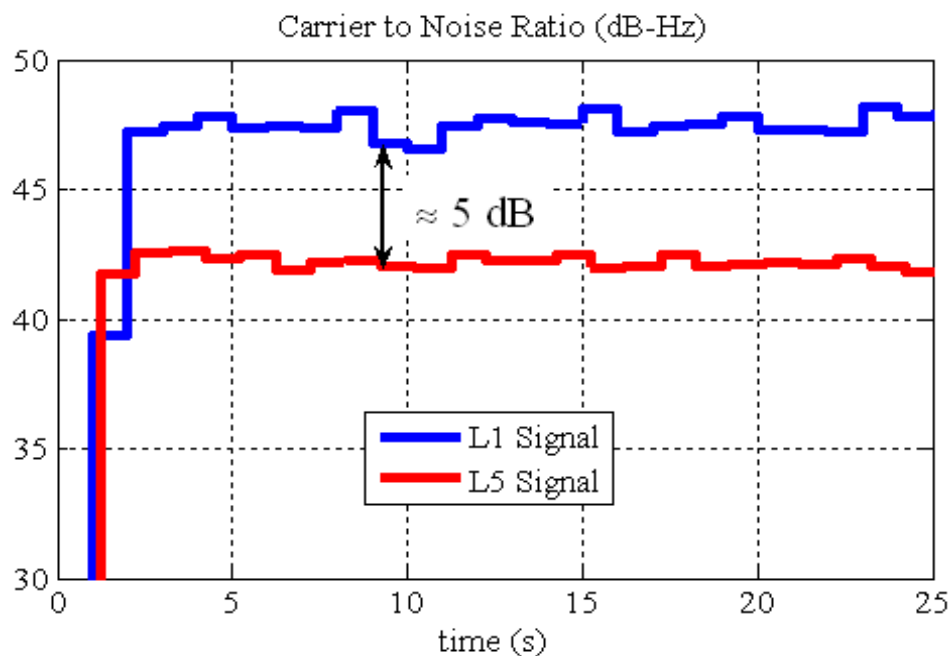


Figure C-4: Received C/N₀ for SVN 49

Given the current specifications of the transmitted L5 pilot channel, the L1 signal is the candidate chosen for driving the Kalman filter. The state space model of the combined Kalman filter is modified to be driven by the L1 signal LOS acceleration instead of that of the L5 signal.

Figure C-5 shows the PLI and FLI of the separate and combined L1 and L5 signals. Even though the L5 signal does not comply with the ICD characteristics, it is showing a significant improvement in both indicators when combined with the L1 signal, which proves the benefits achieved from the Kalman filter.

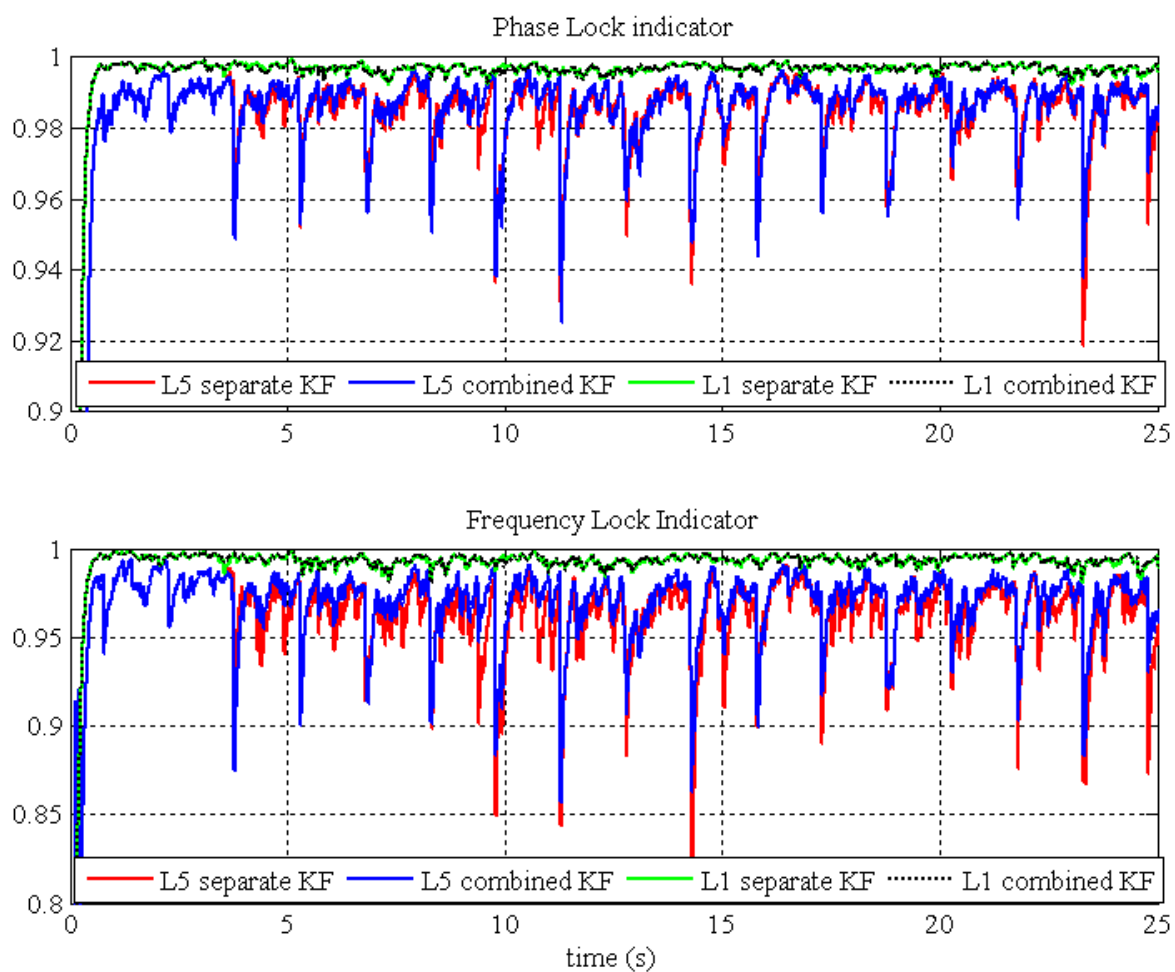


Figure C-5: PLI and FLI for L1 and L5 signals transmitted from SVN 49 using separate and combined KF

Figure C-5 is also showing a repetitive drop in the L5 PLI and FLI every 1.5 seconds. This drop has been reported also by Gao et al 2009, and indicates an unexplained periodic carrier scattering.